THE UNIVERSITY
of EDINBURGH

Epigenetic gene silencing by heterochromatin primes fungal resistance

Sito Torres-Garcia

Thesis presented for the degree of

Doctor of Philosophy

University of Edinburgh

2020

Thesis committee

Professor Robin Allshire

Wellcome Centre for Cell Biology, Institute of Cell Biology,
University of Edinburgh, Edinburgh, United Kingdom
Principal supervisor

Professor Sir Adrian Bird

Wellcome Centre for Cell Biology, Institute of Cell Biology,
University of Edinburgh, Edinburgh, United Kingdom
Second supervisor

Dr Patrick Heun

Wellcome Centre for Cell Biology, Institute of Cell Biology,
University of Edinburgh, Edinburgh, United Kingdom
Member

Dr Sinead Collins

Institute of Evolutionary Biology,
University of Edinburgh, Edinburgh, United Kingdom
Member

Professor Dame Caroline Dean

John Innes Centre, Norwich, United Kingdom
External examiner

Professor Martin Taylor

MRC Human Genetics Unit, MRC Institute of Genetics and Molecular Medicine,
University of Edinburgh, Edinburgh, United Kingdom
Internal examiner

Declaration of originality

This thesis is the result of my own work; the research presented herein is my own unless otherwise indicated. This work has not been submitted for any other degree or professional qualification. Note, many of the findings presented in this thesis have previously been published in the following research papers:

Torres-Garcia, S., Yaseen, I., Shukla, M., Audergon, P.N.C.B., White, S.A., Pidoux, A.L. & Allshire, R.C. (2020) **Epigenetic gene silencing by heterochromatin primes fungal resistance.** ***Nature*****.** 585 (7825), pp. 453–458.

PMID: 32908306. https://doi.org/10.1038/s41586-020-2706-x

Torres-Garcia, S., Di Pompeo, L., Eivers, L., Gaborieau, B., White, S.A., Pidoux, A.L., Kanigowska, P., Yaseen, I., Cai, Y. & Allshire, R.C. (2020) ***SpEDIT*****: A fast and efficient CRISPR/Cas9 method for the fission yeast.** ***Wellcome Open Research***. 5: 274.

PMID: 33313420. https://doi.org/10.12688/wellcomeopenres.16405.1

Sito Torres-Garcia,

Student number: s1616976

December 2020

Abstract

Genes embedded in H3 lysine 9 methylation (H3K9me)–dependent heterochromatin are transcriptionally silenced. In fission yeast, *Schizosaccharomyces pombe*, H3K9me-mediated heterochromatin can be transmitted through cell division provided the counteracting demethylase Epe1 is absent. Under certain conditions wild-type cells might utilize heterochromatin heritability to form epimutations, phenotypes mediated by unstable silencing rather than DNA changes. This study shows that resistant heterochromatin-dependent epimutants arise in threshold levels of caffeine. Unstable resistant isolates exhibit distinct heterochromatin islands, which reduce expression of underlying genes, some of which confer resistance when mutated. Targeting synthetic heterochromatin to implicated loci confirms that resistance results from heterochromatin-mediated silencing. The analyses presented here reveal that epigenetic processes promote phenotypic plasticity, allowing wild-type cells to adapt to non-favorable environments without altering their genotype. In some isolates, subsequent or co-occurring gene amplification events augment resistance. Caffeine impacts two anti-silencing factors: Epe1 levels are downregulated, reducing its chromatin association; and Mst2 histone acetyltransferase expression switches to a shortened isoform. Thus, heterochromatin-dependent epimutant formation provides a bet-hedging strategy that allows cells to remain genetically wild-type but adapt transiently to external insults. Unstable caffeine-resistant isolates show cross-resistance to antifungal agents, suggesting that related heterochromatin-dependent processes may contribute to antifungal drug resistance in plant and human pathogenic fungi.

Lay summary

Each year fungal diseases affect billions of people worldwide, causing an estimated 1.6 million deaths. The emergence of infections resistant to treatment is a growing issue, especially in patients with weakened immune systems such as those with HIV. Moreover, fungal diseases also result in the loss of up to a third of the planet's food crops annually, and overuse of agricultural fungicides is leading to increasing resistance in soil-borne fungi. Because few effective antifungal drugs exist, the rise of resistance challenges human health and food security. It is known that mutations in a fungus' DNA can result in antifungal drug resistance. In fact, current diagnostic techniques rely on sequencing of all of a fungus' DNA to detect such mutations. Using the yeast *Schizosaccharomyces pombe* as a fungal model organism, here I present evidence that fungi can also develop drug resistance without changes in their DNA. Treating yeast with caffeine to mimic the activity of antifungal drugs led to the identification of resistant isolates that had acquired distinctive chemical tags. The presence of such tags or epigenetic changes was found to cause resistance by inducing the packing of specific regions of the fungus' genome into a structure known as heterochromatin, which silence or inactivate underlying genes. Thus, this work uncovers that fungal cells can develop drug resistance by acquiring epigenetic changes that alter how their DNA is packaged, rather than by changing their DNA sequence, and suggests that many causes and cases of antifungal drug resistance could have been previously missed. Importantly, this research could provide insights into the development of new fungicides that specifically target fungal epigenetic changes to potentially aid the control of antifungal drug resistance in both clinical and agricultural settings.

Acknowledgements

First and foremost, I would like to thank my supervisor and mentor Prof. Robin Allshire for accepting me in his team, putting his trust in me, and offering me the freedom and resources to carry out the most stimulating research project I could have ever imagined. I am truly grateful for his continuous encouragement throughout these years, even at times when things were stuck, or results did not seem to provide clear answers. I felt more positive and optimistic each time I left his office. I am particularly thankful for remarkably entertaining karaoke duets, and above all, for countless Paul Hewson stories.

I am hugely indebted to the Darwin Trust of Edinburgh, especially to Prof. Jean Beggs, for awarding me a PhD studentship that supported me during my degree.

I would also like to thank my second supervisor Prof. Adrian Bird as well as thesis committee members Dr Patrick Heun and Dr Sinead Collins for their interest in my work and for sharing their expertise and opinion.

I am grateful to my colleagues in the Allshire lab who made this journey an overall enjoyable and fun experience. Special thanks to Alison, Sharon and Manu, without whom I wouldn't have even made it to my 10-week report. I am indebted to Alison for taking the time to proof-read and edit every single document I have produced in the last five years, for her invaluable wisdom, and for her support in times of need. Live long and prosper. I am thankful to Sharon for dropping whatever she was in the middle of any time I needed something, for believing in me, and for being the best damn lab DJ on planet Earth. I am obliged to Manu, the real Obi-Wan Kenobi, for being liable for any Biochemistry I may be familiar with, for his *Slowhand*-written protocols, and for always offering a seat when I sought his thoughts on things, even guitars.

I am grateful to Pauline, who taught me everything I needed in 2 weeks; to Robbie, for many Italo-Cuban lessons; to Tania, for her stories; to Dominik, for

doughnuts; and to Imtiyaz, for splitting the best band after the Beatles and sharing his results. To other past and current members of the Allshire lab: Ryan, Max, Pin, Puneet, Desi, Weifang, Nitobe, Andreas, Marcel and Becky; you made the lab a pleasant place to work in.

To my students: Baptiste, Lorenza and Luke, for withstanding me. You undoubtedly deserve a prize.

To Araceli and Eduardo, for giving me my first opportunity. To Tábata and Edgar, for teaching me well.

To Hans Zimmer, Howard Shore, John Williams, Pyotr Tchaikovsky, Kieran Hebden, Steven Wilson, Adam Jones and Keaton Henson, for the soundtrack.

To my friends Ana, Mariana, Pedro and Ignatius, for the good times, for keeping the loneliness at bay, but the Mediterranean at hand.

To Lucia, for showing up, for uncountable lockdown walks, and for keeping me fed and relatively sane as I wrote this thesis.

I must also acknowledge my exceptional family, especially Rafa, Conchi, Marina and Ceci for their constant support, for visiting me numerous times in Scotland, for coping with my unhealthy work habits, and for the unlimited supplies of *jamón* and *salchichón.*

To my siblings Belén, Nacho and Nico, for accepting I always had to travel back to Edinburgh soon. To my father, for demonstrating that hard work takes you anywhere.

To my grandmother Encarna, who passed away while I was writing this thesis; she would be happy to know I finally finished school.

Lastly, I dedicate this thesis to my first Biology teacher and probably the most capable researcher the world has ever missed. Words will never convey my full gratitude or pride, yet I'll do my best: *Thank you Mum!*

Contents

Abbreviations

5mC	5-methyl-cytosine
AHT	Anhydrotetracycline
AURORA-B	Aurora kinase B
bp	Base pair
BRCA1	Breast cancer type 1 susceptibility protein
CAF	Caffeine
CBP	CREB-binding protein
cdd	Chromodomain deleted
cDNA	Complementary deoxyribonucleic acid
ChIP	Chromatin immunoprecipitation
ChIP-seq	Chromatin immunoprecipitation coupled to high-throughput sequencing
cloNAT	Nourseothricin
CLRC	Clr4 complex
CLZ	Clotrimazole
dH_2O	Distilled water
DNA	Deoxyribonucleic acid
dNTP	Deoxynucleotide triphosphate
dsRNA	Double-stranded ribonucleic acid
DTT	Dithiothreitol
DUBs	Deubiquitinating enzymes
EDTA	Ethylene-diamine-tetra-acetic acid
FAD	Flavin adenine dinucleotide
FLZ	Fluconazole
FOA	5-fluoroorotic acid
G418	Geneticin
GFP	Green fluorescent protein
GNAT	Gcn5-related *N*-acetyltransferases
H3ac	Histone H3 acetylation
H3K27me	Histone H3 lysine 27 methylation

H3K9me	Histone H3 lysine 9 methylation
HAT	Histone acetyltransferase
HDAC	Histone deacetylase
Hyg	Hygromycin B
imr	Innermost repeats
JmjC	Jumonji C protein family
kb	Kilobase
kDa	Kilodalton
KDM	Lysine demethylase
KMT	Lysine methyltransferase
LB	Luria-Bertani / Lysogeny broth
Mb	Megabase
ME	Malt extract
mRNA	Messenger ribonucleic acid
MSK1/2	Mitogen- and stress-activated protein kinase 1/2
MST1	Mammalian STE20-like protein kinase 1
N-terminal	Amino terminal
nt	Nucleotide
ORF	Open reading frame
otr	Outer repeats
PBS	Phosphate buffered saline
PCR	Polymerase chain reaction
PEG	Polyethylene glycol
PMG	Pombe minimal glutamate
PRMTs	Protein arginine *N*-methyltransferases
qChIP	Chromatin immunoprecipitation coupled to quantitative PCR
RDRC	RNA-dependent RNA polymerase complex
RITS	RNA-induced initiation of transcriptional gene silencing
RNA	Ribonucleic acid
RNA-seq	Reverse transcription coupled to high-throughput sequencing
RNAi	RNA interference

RNAPII	RNA polymerase II
RNAPIII	RNA polymerase III
RT-qPCR	Reverse transcription coupled to quantitative PCR
SDS	Sodium dodecyl sulfate
Sir	Silent information regulator
siRNA	Small interfering RNA
SIRT	Sirtuin
SR	Stable resistant isolate
sRNA	Small RNA
Su(var)39	Suppressor of variegation 3–9
TBE	Tris borate EDTA
tetO	Tetracycline operator
TetR	Tetracycline repressor
TEZ	Tebuconazole
tRNA	Transfer ribonucleic acid
TSS	Transcription start site
Tween	Polyethylene glycol sorbitan monolaurate
UR	Unstable resistant isolate
wt	Wild-type
YES	Yeast extract plus supplements

‘To suppose that the evolution of the wonderfully adapted biological mechanisms has depended only on a selection out of a haphazard set of variations, each produced by blind chance, is like suggesting that if we went on throwing bricks together into heaps, we should eventually be able to choose ourselves the most desirable house.’

C. H. Waddington

Chapter 1: Introduction

1.1. Chromatin

1.1.1. Definition and function

The eukaryotic genome is compacted into the cell nucleus forming a nucleoprotein complex named chromatin. The fundamental unit of chromatin is the nucleosome, composed of 145-147 base pairs of genomic DNA wrapped around an octamer of histones. Originally articulated as the *chromatin subunit model* (Kornberg 1974), the nucleosomal organization of chromatin was first visualized by the X-ray crystal structure of the histone octamer–DNA particle (Luger et al. 1997). The standard octamer of histones consists of a tetramer of H3/H4 flanked by two separate H2A/H2B dimers (Figure 1.1). In many organisms, histone H1 binds and protects the linker DNA between nucleosomes, forming a full nucleosome or chromatosome, and stabilising higher-order chromatin structures (Kornberg & Thomas 1974; Kornberg & Lorch 1999). Nucleosomes are found every 200 ±40 bases and they form a characteristic 'beads on a string' structure visualised by electron microscopy (Olins & Olins 1974 and 2003).

Histones are predominantly globular except for their N-terminal tails, which are unstructured and enriched in basic residues (Figure 1.1). The primary function of chromatin is to allow the packaging of long genomic DNA molecules into the small nuclear compartment, organizing the genome into highly structured chromosomes and protecting DNA from degradation. Chromatin is dynamically adjusted and regulates gene expression to integrate regulatory cues that program appropriate cellular pathways (Kouzarides 2007; Allis & Jenuwein 2016).

1.1.2. Chromatin organization: euchromatin and heterochromatin

Chromatin is divided into two main functionally distinct domains with different DNA, RNA and protein composition. Euchromatin, initially described using light

microscopy as the nuclear region that displays low density staining, constitutes an open, accessible form of the chromatin and contains most actively expressed genes. On the other hand, heterochromatin, initially described as high-density staining regions, harbours less accessible and often transcriptionally silent genes, and is gene poor (Figure 1.2) (Bickmore & van Steensel 2013; Allis & Jenuwein 2016). More recently many specialized chromatin sub-domains have been characterized by their specific composition in terms of histone variants (see section 1.1.3.3); histone post-translational modifications (see section 1.1.3.5); or by their nuclear localisation or 3D organization (reviewed in Bonev & Cavalli 2016 and Zheng & Xie 2019).

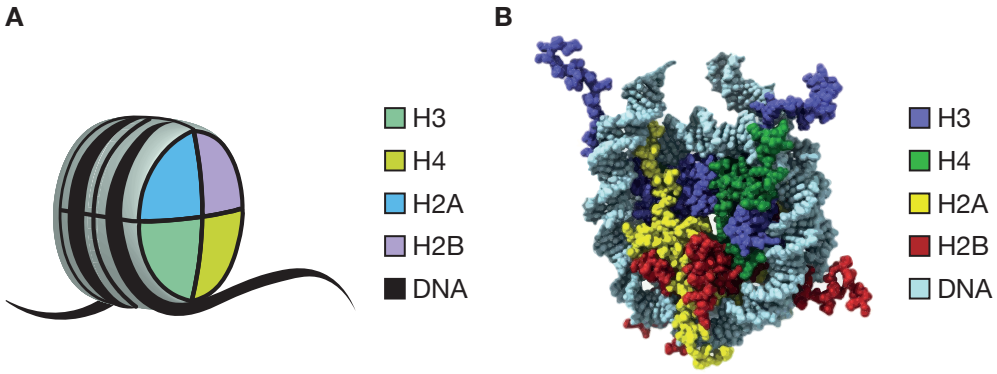

Figure 1.1. Nucleosome structure. Left. Schematic representation of the nucleosome. Right. Nucleosome disc view. Taken from Zhou et al. (2019); histone octamer structure from Davey et al. (2002); DNA structure from Schalch et al. (2005).

1.1.3. Regulation of chromatin organization and function

Chromatin composition and dynamics can be regulated by several processes, including timely assembly, positioning and remodelling of nucleosomes, or precise modifications of DNA and histones. These mechanisms function individually and in concert to modulate genome-wide topology and gene expression, thereby regulating cell differentiation, cell division, and tissue and organism development (Bannister & Kouzarides 2011; Valencia & Kadoch 2019).

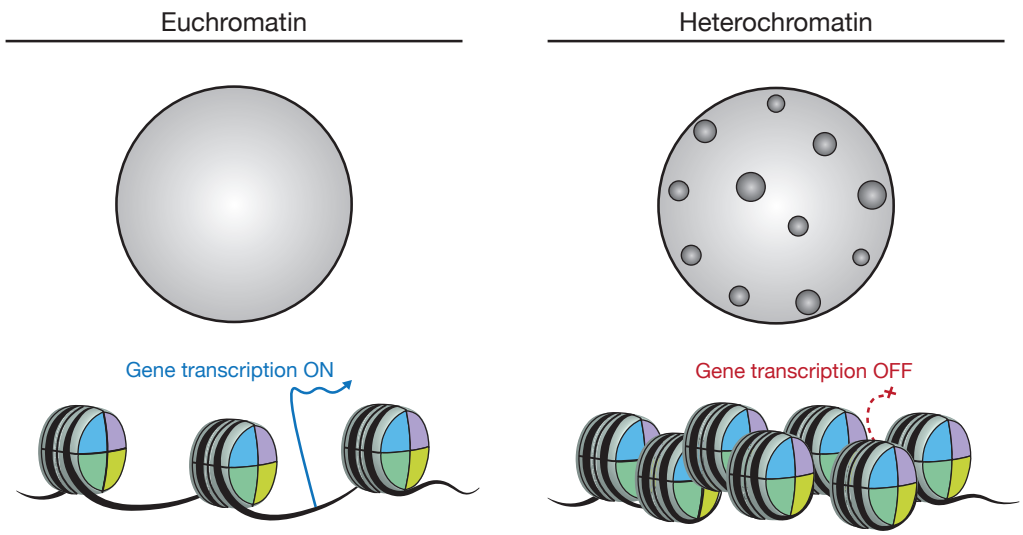

Figure 1.2. Euchromatin and Heterochromatin. Top. Cytologically visible ground states of active (euchromatic, left) and repressed (heterochromatic, right) chromatin. Schematic representation of two interphase nuclei from somatic cells: the left nucleus displays broad and decondensed staining of unique DNA sequences and the right nucleus shows the characteristic heterochromatic foci (grey dots) that are visualized by DAPI (4′,6-diamidino-2-phenylindole) staining of AT-rich repeat sequences. Bottom. Active and repressed chromatin states associated with gene activity (euchromatin, left) or gene repression (heterochromatin, right), respectively. Adapted from Allis & Jenuwein (2016).

1.1.3.1. Histone chaperones

Both parental and newly synthesised histones are (dis)assembled into nucleosomes with the aid of histone chaperone proteins (Tagami et al. 2004; Burgess & Zhang 2013; Gurard-Levin et al. 2014). Histone chaperones also help to shuttle newly synthesized histones from the cytoplasm to the nucleus (Campos et al. 2010; Burgess & Zhang 2013), and act as histone reservoirs regulating histone supply (Groth, Corpet, et al. 2007; Cook et al. 2011; Burgess & Zhang 2013).

Following DNA replication during S phase, nucleosomes are re-constituted in a process called replication-coupled nucleosome assembly (Groth, Corpet, et al. 2007). In addition, nucleosome assembly during gene transcription occurs throughout the cell cycle in a replication-independent manner (Burgess & Zhang 2013).

1.1.3.2. ATP-dependent chromatin remodelling complexes

ATP-dependent chromatin-remodelling complexes include enzymes that mediate the movement or ejection of histones to control proper nucleosome density and spacing (Ito et al. 1997), or to enable the binding of transcription factors to DNA (Tsukiyama et al. 1994). Remodellers also participate in creating specialized chromosomal regions where canonical histones are replaced by histone variants (Mizuguchi et al. 2004). Thus, genome-wide nucleosome occupancy and composition are tailored by specialized remodellers (Clapier et al. 2017).

All chromatin-remodelling complex subfamilies contain an ATPase–translocase 'motor' that utilises ATP to translocate DNA along the histone surface from a common location within the nucleosome (Clapier et al. 2017). Functional and phylogenetic analyses have classified all chromatin-remodelling ATPases within the RNA/DNA helicase superfamily 2, which can be divided into four subfamilies of chromatin-remodelling enzymes: imitation switch (ISWI), chromodomain helicase DNA-binding (CHD), switch/sucrose non-fermentable (SWI/SNF) and INO80, on the basis of the similarities and differences in their catalytic ATPases and associated subunits (Flaus et al. 2006; Clapier et al. 2017). Orphan remodellers, which do not belong to a subfamily (for example, Cockayne syndrome group B (CSB)) also exist (Woudstra et al. 2002), but their mechanism of action is poorly understood (Clapier et al. 2017).

1.1.3.3. Histone variants

Histone variants are characterized by a distinct protein sequence and a suite of designated chaperone systems and chromatin remodelling complexes that recognize amino acid differences among variants and regulate their localization in the genome (Martire & Banaszynski 2020). Whereas canonical histones are assembled into nucleosomes behind the replication fork to package newly synthesized DNA (Groth, Corpet, et al. 2007; Groth, Rocha, et al. 2007), histone variants are subject to dynamic exchange and are typically

incorporated throughout the cell cycle (Talbert & Henikoff 2017). Some histone variants are uniformly expressed, while others are tissue specific, with selective expression demonstrated in the male germ line (testes) and the brain (Wiedemann et al. 2010).

Histone variants replace core histones at specific genomic regions and therefore have the capacity to endow specific regions of chromatin with unique character and function in a regulated manner (Talbert & Henikoff 2017; Martire & Banaszynski 2020). For example, the incorporation of the centromeric H3 variant (known as CENP-A in vertebrates, Cse4 in yeast and CENH3 in plants) instead of H3 into a nucleosome forms the foundation of centromeric chromatin and is at the basis of kinetochore assembly (Earnshaw & Rothfield 1985; Allshire & Karpen 2008; Earnshaw 2015). Several H2A variants affect gene expression: H2A.Z and H2A.B are implicated in transcription initiation (Adam et al. 2001; Soboleva et al. 2011) whereas macroH2A in animals and H2A.W in plants seem to be associated with nucleosome immobility and transcriptional silencing (Ratnakumar et al. 2012; Yelagandula et al. 2014).

1.1.3.4. DNA methylation

DNA methylation is conserved in plants and mammals, and precise patterns of genomic DNA methylation are crucial for development (Goldberg et al. 2007; Valencia & Kadoch 2019). DNA methylation occurs at the position 5 of the cytosine ring (5-methylcytosine (5mC)) and is catalysed by conserved DNA methyltransferases using *S*-adenosyl-L-methionine (SAM) as the methyl donor (Law & Jacobsen 2010).

In mammals, nearly all DNA methylation occurs on cytosine residues of CpG dinucleotides. Regions of the genome that have a high density of CpGs are referred to as CpG islands (Bird et al. 1985), and DNA methylation of these islands correlates with transcriptional repression (Goll & Bestor 2005). Genomic patterns of cytosine methylation in mammals play a critical role in many cellular processes including silencing of repetitive and centromeric sequences; X chromosome inactivation in females; gene regulation and

chromatin organization during embryogenesis and gametogenesis; and imprinting (Surani et al. 2007; Goldberg et al. 2007).

In plants, DNA methylation occurs in all cytosine sequence contexts: CG, CHG and CHH (H represents A, T or C) (Zhang et al. 2006). In *Arabidopsis thaliana*, DNA methylation principally occurs in heterochromatin, which is enriched with transposable elements and other repetitive DNA sequences (Zhang et al. 2006). However, interspersed transposon-associated DNA methylation also exists in euchromatic chromosome arms. DNA methylation has a vital role in regulating transposon silencing, gene expression and chromosomal interactions. Moreover, DNA methylation contributes to proper plant development as well as plant responses to biotic and abiotic environmental stimuli (Law & Jacobsen 2010; Zhang et al. 2018).

In addition, the formation of heterochromatin in many organisms is facilitated in part by DNA methylation and its binding proteins, which can recruit additional factors that mediate the deposition of histone modifications characteristic of silent chromatin (Zaratiegui et al. 2007).

1.1.3.5. Histone post-translational modifications

Histones are post-translationally modified (Allfrey et al. 1964). Histone-modifying proteins mediate >200 distinct covalent post-translational modifications (PTMs) on histone globular domains or protruding histone tails that make contact with neighbouring nucleosomes (Figure 1.3) (Bannister & Kouzarides 2011; Valencia & Kadoch 2019). Histone PTMs can affect histone-DNA and histone-histone interactions to alter nucleosome dynamics and local chromatin compaction, promote recruitment of other chromatin bound proteins, and ultimately, modulate transcription (Figure 1.3) (Tessarz & Kouzarides 2014; Valencia & Kadoch 2019). Histone PTMs include acetylation, methylation, phosphorylation, ubiquitylation, sumoylation, ADP ribosylation, deamination and proline isomerization (Kouzarides 2007). More recently, additional modifications such as propionylation, butyrylation and crotonylation have been described (Tan et al. 2011; Lawrence et al. 2016).

A

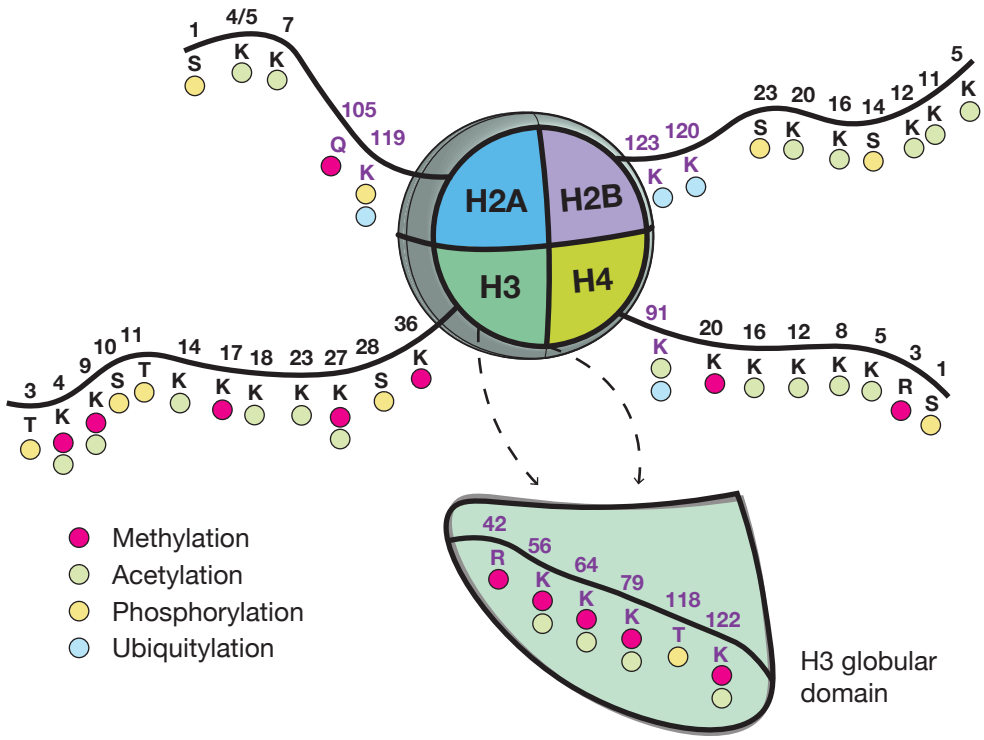

B

Chromatin modifications	Residues modified	Functions regulated
Acetylation	**K**-ac	Transcription, Repair, Replication,Condensation
Methylation (lysines)	**K**-me1/me2/me3	Transcription, Repair
Methylation (arginines)	**R**-me1/me2/me3	Transcription
Phosphorylation	**S**-ph **T**-ph	Transcription, Repair, Condensation
Ubiquitylation	**K**-ub	Transcription
Sumoylation	**K**-su	Transcription
ADP ribosylation	**E**-ar	Transcription
Deimination	**R** > **Cit**	Transcription
Proline Isomerization	**P-cis** > **P-trans**	Transcription

Figure 1.3. Histone post-translational modifications. A. Schematic showing post-translational modification of histone tails and histone globular domains (purple residues). The location of each amino acid and its modification is shown (K, lysine; R, arginine; S, serine; T, threonine). Colours indicate how each residue is modified (red, methylated; green, acetylated; yellow, phosphorylated; light blue, ubiquitylated). Adapted from Kouzarides (2007); Tessarz & Kouzarides (2014); Lawrence et al. (2016). **B.** Overview of different classes of modifications identified on histones. The functions that have been associated with each modification are shown. Taken from Kouzarides (2007).

1.1.3.5.1. Histone tail modifications

To date, the most-studied histone PTMs are those that occur on the N-terminal tail regions of histones that protrude from the nucleosome and are accessible on its surface (Luger et al. 1997; Kouzarides 2007). Some of the modifications on histone tails can directly affect the interactions between nucleosomes. For example, the addition of acetyl modifications to lysine 16 of histone H4 (H4K16ac) has been shown to reduce chromatin compaction and increase transcription both *in vitro* and *in vivo* (Shogren-Knaak et al. 2006; Akhtar & Becker 2000). Histone tail modifications can also do the opposite and increase DNA compaction; for example, H4K20 di- and tri-methylation (H4K20me2/3) have been shown to enhance *in vitro* chromatin condensation (Lu et al. 2008). However, these two modifications (H4K16ac and H4K20me2/3) are the only histone tail PTMs shown to have a direct effect on chromatin architecture *in vitro*, suggesting that this mode of action for histone tail modifications might not be the rule but rather the exception (Lawrence et al. 2016).

In general, histone tail modifications act indirectly and recruit effector proteins to activate downstream signalling or influence the recruitment of chromatin modifiers and transcription factors (Figure 1.4) (Brownell et al. 1996; Clements et al. 2003; Rea et al. 2000; Bannister et al. 2001; Wysocka et al. 2006).

Initial identification and characterization of histone tail modifications led to the idea that the nucleosome carries *epi*-genetic regulatory information (Turner 1993). The 'histone code hypothesis' (Strahl & Allis 2000) was put forward after the identification of the first histone tail modification-binding domain; the p300/CBP-associated factor (PCAF) bromodomain as an acetyl-lysine binding module for docking onto acetylated histones (Dhalluin et al. 1999) (Figure 1.4). This hypothesis proposed that combinatorial patterns of histone modifications specify distinct biological outcomes, in part by the recruitment of downstream effector proteins (named *readers* to match the analogy of *writers* and *erasers* for histone-modifying enzymes) or complexes in *trans*. The histone code hypothesis predicted that readers of other histone modifications would be identified. Indeed, many types of histone modification-binding modules have

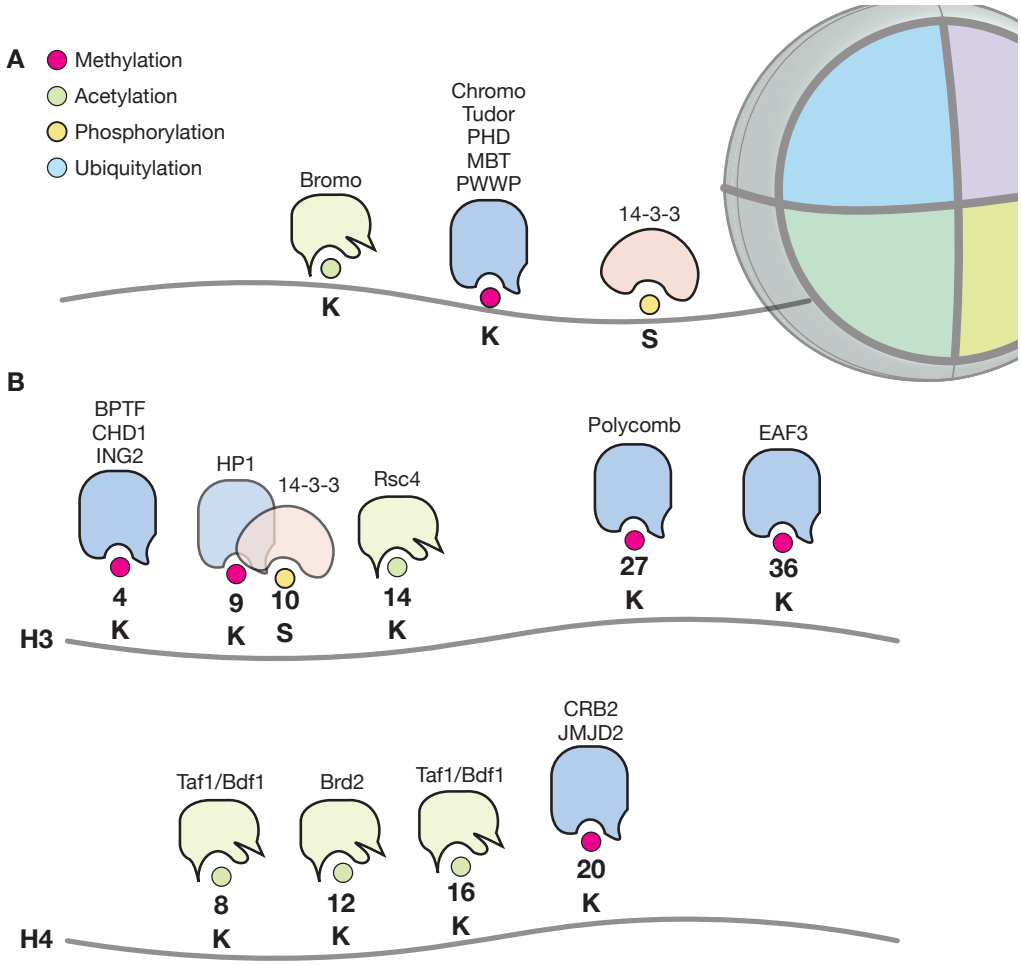

C

	Methylation	Acetylation	Phosphorylation	Ubiquitylation

Writers	**KMTs or PRMTs**	**HATs**	**Kinases**	**E3 ligases**
	Su(var)39	CBP/p300	AURORA-B	BRCA1
	KMT2A-D	MYST family		RING1A/B
	EZH2	GNAT family		BMI1
	DOT21L			
Erasers	**KDMs**	**HDACs**	**Phosphatases**	**DUBs**
	JmjC family	HDAC1-11	MSK1/2	MYSM1
	KDM1A	SIRT1-7	MST1	OTLD1
	KDM5A/B			
	KDM6A/B			

Figure 1.4. Recruitment of proteins to histone modifications. A. Domains used for recognition of acetylated lysines, methylated lysines or phosphorylates serines. **B.** Depicted are proteins containing histone modification-binding domains shown in **A** that associate preferentially with modified versions of histone H3 or histone H4. Adapted from Kouzarides (2007); Bannister & Kouzarides (2011); Tessarz & Kouzarides (2014). **C.** Common writers and erasers of histone modifications. Modified from Kouzarides (2007); Valencia & Kadoch (2019).

been discovered to date (for example, chromodomains, tudor domains and plant homeodomain (PHD) fingers) (Figure 1.4), and many of them have been characterised in detailed atomic resolution with their associated modified-histone ligands (Patel 2016). Such progress has resulted in recent extensions of the histone code hypothesis (Jenuwein & Allis 2001; Allis & Jenuwein 2016).

Distinct groups of *writers, readers* and *erasers* act together to impose particular histone modification patterns that define highly conserved chromatin states and play a role in crucial biological processes such as DNA replication or transcription (Figure 1.4) (Allis & Jenuwein 2016). For example, the nuclear histone acetyltransferase (HAT) p55 from *Tetrahymena thermophila* (ortholog to yeast Gcn5) was the first described transcriptional co-activator that acetylates the histone H3 amino-terminal tail (H3K14ac) (Brownell et al. 1996). The acetylated lysine provides a docking site for bromodomain-containing proteins (including p55) that bind to further stimulate nucleosome accessibility and transcriptional activity. Histone acetylation can be reversed by opposing histone deacetylases (HDACs), such as Rpd3, which often cause transcriptional repression (Taunton et al. 1996) (Figure 1.5). In contrast, the human histone lysine methyltransferase (KMT) SUV39H1 (orthologue of the *Drosophila melanogaster* Suppressor of variegation 39 (Su(var)39) and the *Schizosaccharomyces pombe* Cryptic loci regulator 4 (Clr4) proteins) methylates the histone H3 amino-terminal tail (H3K9me) (Rea et al. 2000). Tri-methylated H3K9 (H3K9me3) serves as a docking site for chromodomain-containing proteins (such as heterochromatin protein 1 (HP1) or SUV39H1 itself), which then impede nucleosome accessibility and induce gene repression (Bannister et al. 2001; Lachner et al. 2001). Histone methylation can be reversed by opposing histone demethylases (KDMs) (Shi et al. 2004; Tsukada et al. 2006) (Figure 1.5).

1.1.3.5.2. Histone core modifications

Besides histone tails, the central core (or globular) domains of histones, which together form the core of the nucleosome, also contain a large number of modification sites (see Figure 1.3) (Tessarz & Kouzarides 2014).

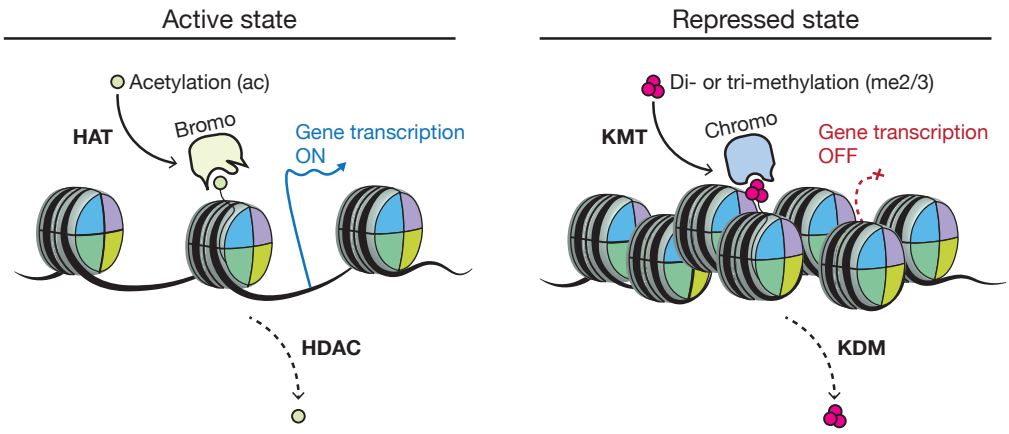

Figure 1.5. Chromatin *writers*, *readers* and *erasers*. Distinct groups of proteins act together to impose particular histone modifications patterns that define transcriptionally active (left) or repressed (right) chromatin states. Adapted from Allis & Jenuwein (2016).

Histone core modifications can affect histone-DNA interactions. For example, H3K56 acetylation, one of the first described core modifications (Xu et al. 2005; Masumoto et al. 2005), has been proposed to enhance the unwrapping of the DNA close to the nucleosome DNA entry-exit site (where H3K56 is located) to regulate chromatin at the higher order level (Simon et al. 2011). Moreover, it has been shown that acetylation of core residues H3K122 and H3K64 results in nucleosome destabilization and this positively correlates with transcriptional activation (Tessarz & Kouzarides 2014). In addition, asymmetric di-methylation of H3R42 results in transcriptional activation *in vitro* (Casadio et al. 2013) and mutation of H3R42 to Alanine (eliminating hydrogen bond potential) produces a hyper-transcription phenotype partially due to decreased H3 occupancy in *S. cerevisiae* (Hyland et al. 2011).

Histone core modifications have also been proposed to affect histone-histone interactions, albeit experimental evidence is limited. Methylation of H3K79, the first core modification identified within histone H3 (Ng et al. 2002), has been shown to correlate with active transcription in yeast and mammalian cells (Ng et al. 2003; Pokholok et al. 2005; Steger et al. 2008). This modification does not cause a major change in nucleosome structure, as revealed by structural analysis of nucleosome crystals harbouring H3K79me2. Instead, H3K79

methylation provokes a subtle reorientation of the region surrounding K79, which likely results in decreased interaction with histone H4 and the generation of a novel docking site on the nucleosome surface (Lu et al. 2008). Contrastingly, acetylation of H4K91 has been shown to decrease the association of H2A-H2B dimers with chromatin and this can lead to nucleosome instability (Ye et al. 2005). H4K91 is positioned within the H3-H4 tetramer – H2A-H2B dimer interface and a mutation mimicking the acetylated state leads to decondensed chromatin and loss of nucleosomal interaction (Ye et al. 2005).

1.1.3.5.3. Histone methylation

Histone methyltransferases (HMT) catalyse the addition of methyl groups to histone lysine or arginine residues using *S*-adenosyl-L-methionine (SAM or AdoMet) as a donor (Dillon et al. 2005). Histones can be mono-, di- or tri-methylated on lysine residues (Figure 1.6), and mono- or di-methylated on arginine residues (Qian & Zhou 2006). Methylation of histone lysine residues is catalysed by histone lysine methyltransferases (KMTs) containing a SET (Su(var)39, Enhancer of Zeste and Trithorax) catalytic domain similar to that of the *D. melanogaster* Su(var)39 proteins (Dillon et al. 2005; Qian & Zhou 2006). An exception to this rule is H3K79 methylation deposited by the histone KMT Dot1, which lacks a conserved SET domain (Ng et al. 2002). Notably, more than a hundred SET domain-containing proteins have been identified in humans (Qian & Zhou 2006).

KMTs are highly specific regarding their substrates. In fact, a single KMT usually methylates an individual histone residue and several different KMTs are in some cases required to catalyse mono-, di- and tri-methylation of a particular amino acid (see section 1.2.3 for examples). Methylated lysine residues can be bound by several protein domains such as chromo, tudor, PHD, malignant brain tumour (MBT), or Pro-Trp-Trp-Pro (PWWP) domains (Figure 1.4) (Bannister & Kouzarides 2011; Tessarz & Kouzarides 2014). Histone lysine methylation is associated with both transcriptional activation and transcriptional repression depending on which histone residue is modified.

H3K4, H3K36 and H3K79 methylation are generally found on actively transcribed regions, while H3K9, H3K27 and H4K20 methylation are usually associated with repressed chromatin (Bannister & Kouzarides 2011; Valencia & Kadoch 2019).

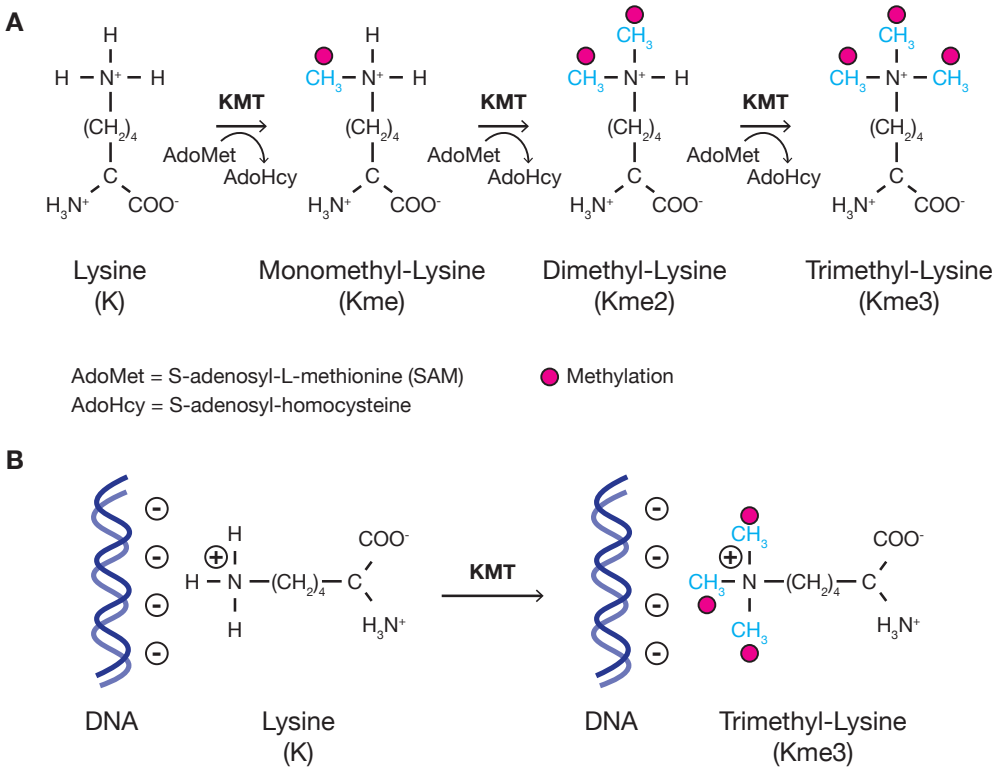

Figure 1.6. Lysine methylation. A. Methylation of lysine residues by lysine methyltransferases (KMTs) into mono-, di- or tri-methyl-lysine. Adapted from Zhang & Reinberg (2001). **B.** Histone lysine residues harbour a positive charge that can form a salt bridge with the negatively charged DNA backbone. Following lysine methylation by KMTs the charge of the lysine side chain is retained. Lysine methylation can then provide a docking platform for additional proteins (as shown in Figures 1.4 and 1.5). In addition, lysine methylation might affect histone-DNA binding. Adapted from Tessarz & Kouzarides (2014).

Histone methylation was originally thought to be a permanent mark that would remain on the amino acid residue until natural histone turnover or DNA replication replaces the modified histone with an unmodified one (Bannister et al. 2002). This notion came from early studies looking at the turnover of methyl groups in bulk histones. Such studies concluded that histone methylation is

not reversible since the half-life of histones and methyl-lysine residues within them are equal (Byvoet et al. 1972; Duerre & Lee 1974). However, subsequent studies suggested that active turnover of methyl groups exists but at a low level (Borun et al. 1972; Annunziato et al. 1995).

The first identified histone lysine demethylase (KDM) was lysine-specific demethylase 1 (LSD1), a nuclear flavin adenine dinucleotide (FAD)-dependent amino oxidase homologue (Shi et al. 2004). FAD-dependent amino oxidases were found to demethylate mono- and di-, but not tri-methylated lysines (Shi et al. 2004; Klose & Zhang 2007), raising the possibility that lysine tri-methylation could be a permanent histone mark. However, the identification of Jumonji domain-containing histone demethylase 1 (JHDM1), capable of removing mono-, di- and tri-methyl-lysine modifications in histones (Tsukada et al. 2006), led to the now established general view that all chromatin marks are probably reversible (Allis & Jenuwein 2016). JHDM1 was the first identified member of a novel second class of lysine demethylases: Fe(II) and α-ketoglutarate-dependent dioxygenases with catalytic modules known as Jumonji domains. This class of proteins promote demethylation via an oxidative reaction that relies on Fe(II) and α-ketoglutarate as cofactors (Bannister et al. 2002; Trewick et al. 2005; Trewick et al. 2007; Klose & Zhang 2007).

In addition, histone methylation can also be removed from chromatin via endopeptidase-mediated histone tail clipping, a process that leads to the removal of the histone N-terminal tail and hence the loss of all incorporated PTMs (Allis et al. 1980; Santos-Rosa et al. 2009).

1.2. Heterochromatin

1.2.1. Definition and function

Heterochromatin is a fundamental architectural feature of eukaryotic chromosomes that endows particular genomic regions with specific functional properties. Originally described as high-density staining regions within the nucleus (see Figure 1.2) (Heitz 1928), the term now generally refers to molecular subtypes of transcriptionally repressed chromatin domains (Allshire & Madhani 2018).

The link from those initial cytological observations to the current molecular definition came from experiments in *D. melanogaster* in which flies acquired a mutant (white) eye phenotype due to chromosome rearrangements that displaced the white eye gene from its original position to positions near heterochromatin, a phenomenon originally termed position-effect variegation (Muller 1930; Schultz 1936). It was found later that repetitive genomic regions, which displayed a distinct 'satellite' position in CsCl gradients due to their skewed base composition and density, colocalized with centromeric heterochromatin regions of metaphase chromosomes (Kit 1961), and with high-density chromatin at the nuclear periphery of interphase cells (Yasmineh & Yunis 1970; Rae & Franke 1972). The inability to detect satellite-derived RNA, and experiments in which the insertion of genes within centromeric sequences led to their transcriptional inactivation suggested that heterochromatin is transcriptionally inactive (Flamm et al. 1969).

Different subtypes of heterochromatin are characterized by particular combinations of DNA modifications and histone PTMs. The best-studied types of heterochromatin are marked by di- or tri-methylation of H3K9 (H3K9me2/3) or tri-methylation of H3K27 (H3K27me3). These histone marks can mediate the folding of chromatin and the recruitment of *readers* through their highly specific binding domains (Allshire & Madhani 2018). In some systems, histone methylation can be coupled with DNA methylation. For example, in mammals and plants, H3K9 methyltransferases can recruit 5mC DNA

methyltransferases so that these two repressive modifications reciprocally bolster each other to ensure that the DNA is rendered inaccessible (Tamaru & Selker 2001; Jackson et al. 2002; Lehnertz et al. 2003)

From a functional perspective, heterochromatin can be divided into three subtypes: constitutive, facultative and ectopic heterochromatin (Grewal & Jia 2007; Wang et al. 2016).

Constitutive heterochromatin preferentially assembles at repetitive elements and is concentrated at centromeres and telomeres in most eukaryotes. These major and permanent blocks of heterochromatin, defined by the presence of H3K9me2/3, are known to play a crucial role in nuclear organization, accurate chromosome segregation and genome integrity maintenance against transposable elements (Grewal & Jia 2007; Allshire & Madhani 2018).

Facultative heterochromatin is associated with a subset of genes only packaged into a repressed state in response to differentiation signals or environmental cues (Trojer & Reinberg 2007). Facultative heterochromatin can cover an entire chromosome (e.g. the inactive X chromosome in female mammals (Galupa & Heard 2018)), or be restricted to defined regulatory regions (e.g. *flowering locus C* (*FLC*) silencing in plants (Baulcombe & Dean 2014)). The most distinctive histone mark of facultative heterochromatin is H3K27me3. In addition, facultative heterochromatin is often enriched with H3K9me2/3, H4K20me3, H2AK119ub1, hypoacetylated histones and the histone variant macroH2A (Trojer & Reinberg 2007). For a full description, see section 1.2.2.

Ectopic heterochromatin, characterized by the atypical presence of H3K9me2/3 at euchromatic regions, has been shown to assemble upon removal of key anti-silencing factors (Trewick et al. 2007; Zofall et al. 2012; Wang et al. 2015; Sorida et al. 2019), or following genetic manipulations that introduce a nucleation signal at a euchromatic locus (Kagansky et al. 2009; Kowalik et al. 2015; Audergon et al. 2015; Ragunathan et al. 2015; Duempelmann et al. 2019). Recently it has been proposed that the assembly

of ectopic heterochromatin has adaptive potential because it can promote transcriptional silencing of genes under stress conditions (Wang et al. 2016; Sorida & Murakami 2020). However, experimental evidence is scarce and only observed in cells lacking crucial anti-silencing factors (Wang et al. 2015). For a full description, see section 1.4.1.

1.2.2. H3K27 methylation heterochromatin: facultative heterochromatin and the Polycomb system

Facultative heterochromatin refers to chromosomal domains packaged into a repressed state as a result of specific external signals or differentiation stages (Trojer & Reinberg 2007). H3K27 tri-methylation (H3K27me3) is widely considered the most distinctive hallmark of facultative heterochromatin (Trojer & Reinberg 2007; Schuettengruber et al. 2017). However, facultative heterochromatin domains can also show enrichment of or be exclusively mediated by H3K9me in some cases (Heard et al. 2001; Bastow et al. 2004; Wen et al. 2009; Hawkins et al. 2010; Soufi et al. 2012; Zofall et al. 2012; Zhu et al. 2013; Becker et al. 2016).

H3K27 methylation is deposited by the Polycomb repressive complex 2 (PRC2) catalytic subunit Enhancer of zeste (E(z)) in *D. melanogaster* (Cao et al. 2002; Müller et al. 2002; Czermin et al. 2002). Orthologues of E(z) are found in mammals (EZH1 and EZH2) and in plants (CLF, MEA and SWN), all of which share a highly conserved SET domain, responsible for catalytic activity (Müller & Verrijzer 2009). In addition, the PRC2 subunits Extra sex combs (Esc) in *D. melanogaster* and Embryonic ectoderm development (EED) in mammals (FIE in plants), recognize the H3K27me mark and allosterically activate E(z) or EZH2, respectively (Margueron et al. 2009). E(z) and Esc form the broadly conserved core PRC2 complex together with Suppressor of zeste (Su(z)12) (SUZ12 in mammals; FIS2, VRN2 and EMF2 in plants) and the CAF1 histone-binding protein Nurf55 (RBBP4/7 in mammals; MSI1/5 in plants). This complex is conserved in some fungi, including *Neurospora crassa*

and the yeast *Cryptococcus neoformans*, but not fission yeast *S. pombe*) (Kim & Sung 2014; Schuettengruber et al. 2017).

H3K27 methylation by PRC2 promotes binding of the PRC1 complex through its chromodomain-containing Polycomb (Pc) subunit (CBX2, CBX4, and CBX6–CBX8 in mammals) (Fischle et al. 2003). PRC1 complexes share a protein core that is conserved in animals and plants, but not in fungi (Kim & Sung 2014; Schuettengruber et al. 2017). The PRC1 core complex consists of a dRing protein (RING1A/B in mammals; AtRING1a-c in plants), which has E3 ubiquitin ligase activity that mediates H2AK119ub1; and the Polycomb group ring-finger domain protein Psc (PCGF1–PCGF6 in mammals; AtBMI1a-c in plants). This core is then specified by the presence of the above-mentioned chromodomain-containing Pc subunit, and a Polyhomeotic (Ph) protein (PHC1–PHC3 in mammals) which contains a sterile alpha motif (SAM) domain essential for Polycomb-mediated repression. To date, no apparent sequence homolog of either Pc or Ph is found in plants. However, Like heterochromatin protein (LHP1) has been proposed as the functional equivalent of Pc in *A. thaliana* (Sung et al. 2006; Mylne et al. 2006; Kim & Sung 2014).

Polycomb mutations in *D. melanogaster* were initially found to transform anterior embryonic segments into more posterior ones due to ectopic expression of Homeotic (Hox) genes (Lewis 1978). Subsequently, some Polycomb members have been linked to proliferation, senescence and cancer (van Lohuizen et al. 1991; Jacobs et al. 1999). Polycomb proteins therefore regulate a plethora of cellular processes, including X chromosome inactivation in female mammals, vernalization in flowering plants, genomic imprinting, cell cycle control and stem cell biology. Such functional diversity is achieved by a variety of Polycomb complexes that are assembled in a developmental stage- and cell-specific manner to alter chromatin at their target genes via histone-modifying or chromatin-remodelling activities (Schuettengruber et al. 2017).

PRC2 catalyses H3K27 mono-, di- and tri-methylation (H3K27me1/me2/me3). H3K27me1/me2 cover the large majority of the euchromatic genome, but

PRC2 is not detected in regions marked by H3K27me2, suggesting that its binding to these regions is transient (Ferrari et al. 2014; Lee et al. 2015). Early studies in *D. melanogaster* identified Polycomb response elements (PREs) as the DNA regulatory elements that recruit Polycomb factors to chromatin (Simon et al. 1993). PREs frequently contain DNA motifs for sequence-specific DNA-binding transcription factors, but these were found insufficient to recruit Polycomb on their own (Schuettengruber et al. 2017). In mammals, CpG islands facilitate targeting of Polycomb machinery, with Polycomb complexes 'sampling' chromatin in order to determine transcriptional states (Farcas et al. 2012).

Recently, it was shown that tethering KDM2B (an H3K36 demethylase that is also a subunit of a variant PRC1 complex) in mouse embryonic stem cells induces the recruitment of PRC1 complexes and the deposition of H2AK119ub1 to chromatin, which in turn promotes binding of PRC2 (Cooper et al. 2014; Blackledge et al. 2014). In addition, it has been reported that a non-canonical PRC1 complex (that contains the RING finger 3/5 (PCGF3/5)) initiates recruitment of both PRC1 and PRC2 to the inactive X chromosome via H2AK119ub1, demonstrating a function of H2AK119ub1 for the initiation of Polycomb domains in a physiological context (Almeida et al. 2017). The predominant view is that Polycomb complexes have relatively poor DNA sequence specificity, but they can be specifically recruited to selected regions by specific transcription factors, nascent RNAs, non-coding RNAs (ncRNAs), and chromatin modifications (Schuettengruber et al. 2017).

Paradigmatic models of Polycomb-mediated H3K27me3-dependent facultative heterochromatin include the inactivation of the X chromosome in female mammals and the cold-induced vernalization process in flowering plants.

In somatic nuclei of female eutherian mammals, one of the two X chromosomes is mostly silent and forms a cytologically detectable heterochromatic structure termed the Barr body (Figure 1.7A) (Barr & Bertram 1949; Ohno et al. 1959). This structure is formed during female development

through a process termed X-chromosome inactivation (XCI). At the molecular level, the noncoding RNA X-inactive-specific transcript (*Xist*), expressed exclusively from the X chromosome that will be inactivated, recruits the transcriptional repressor SPEN to enhancers and promoters of active genes. SPEN then recruits the gene-inactivating HDAC HDAC3, as well as the gene-silencing complexes NCoR/SMT and NuRD, to initiate XCI (Chu et al. 2015; Dossin et al. 2020). In addition, *Xist* also recruits PRC1 and PRC2 to the inactive X chromosome (Xi) (Plath et al. 2003; Silva et al. 2003; de Napoles et al. 2004). A 600-nucleotide sequence in mouse *Xist* RNA, *Xist* RNA Polycomb Interaction Domain (XR-PID), promotes PRC1 (PCGF3/5-PRC1) recruitment to Xi via the RNA-binding protein hnRNPK (Pintacuda et al. 2017). PRC1-mediated deposition of H2AK119ub1 on Xi promotes the recruitment of PRC2 and the formation of H3K27me3 heterochromatin (Almeida et al. 2017). PRC2 recruitment to Xi requires the PRC2 cofactor Jarid2 (the founding member of the Jumonji family of proteins), which can bind the PRC1-deposited H2AK119ub1 mark (Figure 1.7A) (da Rocha et al. 2014; Cooper et al. 2016). In addition, complete XCI also requires the deposition of DNA methylation and H3K9me (reviewed in Galupa & Heard 2018).

The phenomenon of vernalization, by which exposure to prolonged cold induces the chromatin-mediated silencing of the floral repressor *flowering locus C* (*FLC*), facilitates alignment of flowering with spring and the return of more favourable environmental conditions. This process ensures effective flower formation, pollination, and fruit set (Baulcombe & Dean 2014). In the absence of cold, *FLC* acts as a brake to flowering (Figure 1.7B). Cold induces up-regulation of antisense transcripts to *FLC* (collectively known as COOLAIR) (Swiezewski et al. 2009) and a plant homeodomain (PHD) protein called Vernalization insensitive 3 (VIN3) (Sung & Amasino 2004). COOLAIR facilitates *FLC* transcriptional silencing (Csorba et al. 2014). VIN3 associates with a homologous PHD protein, Vernalization 5 (VRN5), and a vernalization-specific PRC2 complex that includes VRN2 (a Su(z)12 homolog) (Gendall et al. 2001) to form the VIN3-VRN5-PRC2 complex (PHD-PRC2).

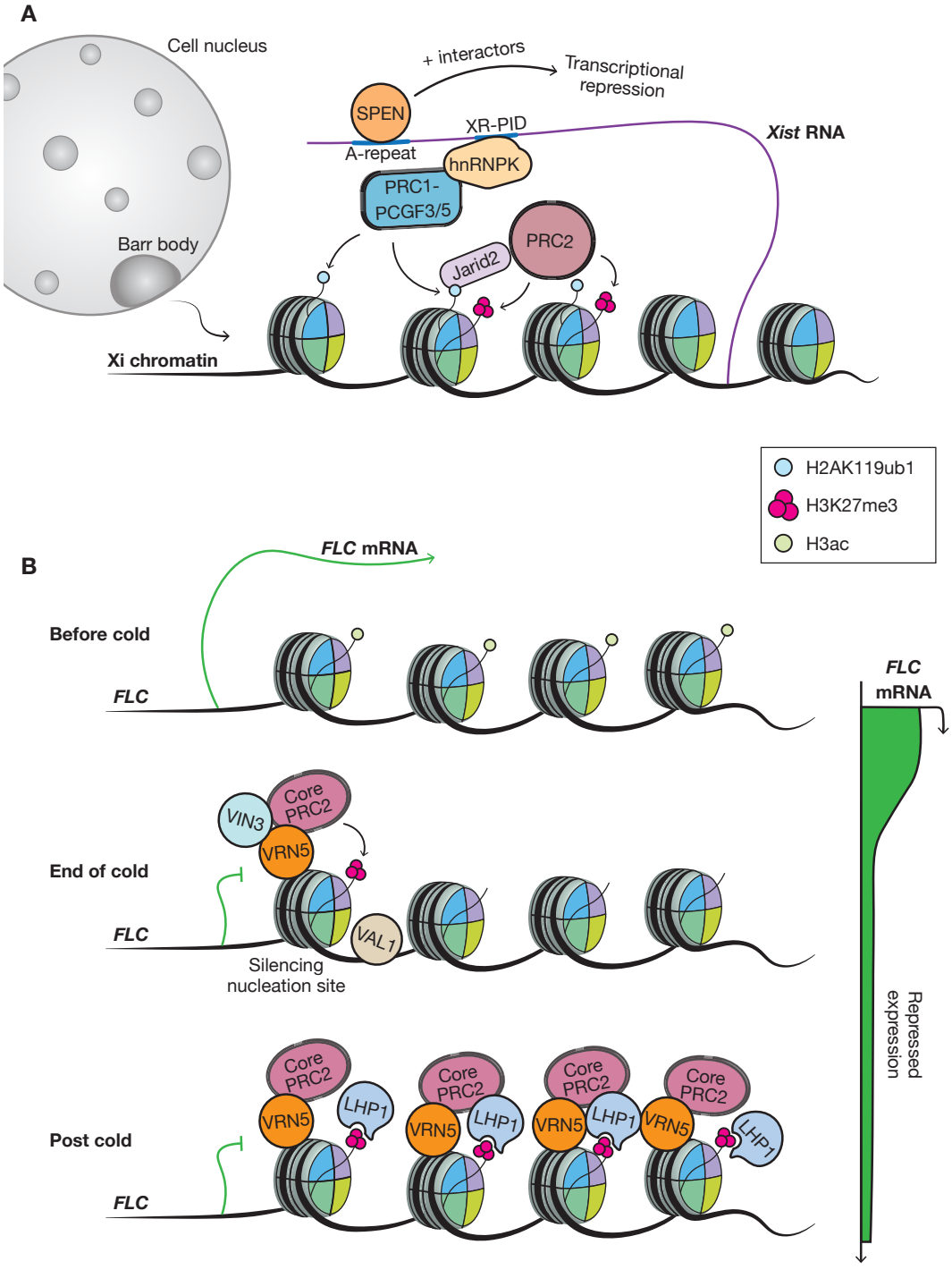

Figure 1.7. Classic models of Polycomb-mediated facultative heterochromatin. A. Schematic summary of X inactivation (Xi) in female mammals. **B.** Schematic summary of cold-induced gene silencing of the floral repressor *FLC*. LHP1, the *A. thaliana* homolog of metazoan HP1, is required to maintain the *FLC* repressed state. Interestingly, unlike in fission yeast, flies and mammalian cells, Arabidopsis LHP1 binds H3K27me3 rather than H3K9me3 (Mylne et al. 2006). Adapted from Baulcombe & Dean (2014).

The Viviparous/abscisic acid insensitive-like1 (VAL1) transcriptional repressor promotes recruitment of PHD-PRC2 to an intragenic nucleating region covering the first exon and part of the first intron of *FLC* (Qüesta et al. 2016). PHD-PRC2-mediated quantitative accumulation of H3K27me3 at the nucleation region during cold exposure, and over the whole locus after cold exposure (Yang et al. 2017), reflects a cell-autonomous switch affecting an increasing proportion of the cell population (Figure 1.7B) (Angel et al. 2011). Importantly, the chromatin state of the *FLC* locus is reset in every generation by the H3K27-specific demethylase ELF6, preventing transgenerational inheritance of previous exposures to cold (Crevillén et al. 2014). It was originally thought that variation in this silencing mechanism exclusively underpinned the adaptation of plants to climates with different winters. However, it was recently shown that autumnal *FLC* expression, rather than silencing alone, is the major variable conferred by the distinct Arabidopsis *FLC* haplotypes (Hepworth et al. 2020).

1.2.3. H3K9 methylation heterochromatin

Histone H3K9 methylation forms the major blocks of heterochromatin in cells and constitutes the defining molecular feature of constitutive heterochromatin in many eukaryotes (Allshire & Madhani 2018). H3K9 methylation is catalysed by SET domain-containing KMTs orthologues of the *D. melanogaster* Su(var)39 and *S. pombe* Clr4 proteins (Eissenberg et al. 1990; Tschiersch et al. 1994; Rea et al. 2000). Orthologues of Su(var)39 and Clr4 are found in mammals (SUV39H1 and SUV39H2) (Rea et al. 2000), and in plants (SUVH1-9) (Baumbusch et al. 2001; Jackson et al. 2002).

The Clr4 protein, the sole H3K9 methyltransferase encoded by the *S. pombe* genome, is responsible for mono-, di- and tri-methylation of H3K9 (H3K9me1/me2/me3) (Ivanova et al. 1998; Zhang et al. 2008). In more complex eukaryotes, several H3K9 KMTs collaborate to methylate H3K9. In humans, the G9a-GLP complex mostly directs mono- and di-methylation of H3K9 (Tachibana et al. 2001; Tachibana et al. 2005), SUV39H1/H2 mediate

H3K9 di- and tri-methylation (Rea et al. 2000), and SetDB1 tri-methylates H3K9 (Matsui et al. 2010). Su(var)39 orthologues are highly conserved, as illustrated by the fact that human SUV39H1 can partially rescue the silencing defect of a *D. melanogaster su(var)39* null mutant (Schotta et al. 2002).

H3K9 mono-, di- and tri- methylation are enriched over specific genomic regions in which they have been proposed to exert distinct regulatory function (Barski et al. 2007). In human cells, H3K9me1 is found at promoters and 5' UTR of active genes (Barski et al. 2007). H3K9me2 and H3K9me3 are the *bona fide* hallmarks of heterochromatin (Allshire & Madhani 2018). H3K9me2/me3 are highly enriched over constitutively repressed genomic regions including centromeres and subtelomeres of fission yeast, mammalian cells and flies (Cam et al. 2005; Barski et al. 2007; Yasuhara & Wakimoto 2008). However, in mammalian cells, the distributions of H3K9me2 and H3K9me3 do not totally overlap. Large organised chromatin K9 modifications (LOCKs) are extended facultative domains of H3K9me2 that are highly conserved between human and mouse. Interestingly, not all H3K9me2 LOCKs, which are differentiation specific, show enrichment of H3K9me3, suggesting that H3K9me2 LOCKs and not H3K9me3 domains might contribute to phenotypic plasticity during mammalian development (Wen et al. 2009).

In fission yeast, H3K9me2 and H3K9me3 overlap almost completely over heterochromatin regions, but H3K9me2 was found to be more predominant than H3K9me3 in heterochromatic nucleosomes (Al-Sady et al. 2013). Recently, an elegant study revealed that H3K9me2 and H3K9me3 have different roles in heterochromatin gene silencing (Jih et al. 2017). Centromeric H3K9me2 domains were shown to be transcriptionally permissive and contain modifications associated with euchromatic transcription. This allows RNA interference (RNAi)-mediated co-transcriptional gene silencing at centromeric DNA repeats (see section 1.2.3.1.2). On the other hand, H3K9me3 domains were found to be transcriptionally silent. The two H3K9me states can recruit reader proteins with different efficiencies, which explains their distinct downstream silencing effects (Jih et al. 2017).

H3K9 methylation is recognised by the chromodomain proteins Heterochromatin protein 1a and b (HP1a and HP1b) in *D. melanogaster* and their *S. pombe* orthologues Swi6 and Chromodomain-containing protein 2 (Chp2) (HP1α, HP1β and HP1γ in mammalian cells) (Figure 1.8) (Bannister et al. 2001; Lachner et al. 2001; Klar & Bonaduce 1991; Lorentz et al. 1994; Allshire et al. 1995; Thon & Verhein-Hansen 2000). HP1 proteins contain the above-mentioned chromodomain, an unstructured hinge region and a chromoshadow domain (Figure 1.8). Chromoshadow domain dimerization through its PxVxL motif allows HP1 dimerization and constitutes a binding platform for additional effector proteins, many of which contain a PxVxL motif (Cowieson et al. 2000; Brasher et al. 2000; Smothers & Henikoff 2000; Richart et al. 2012). For example, the *S. pombe* chromodomain proteins Swi6 and Chp2 recruit the Snf2/HDAC-containing repressor (SHREC) HDAC complex and the Clr6 HDAC complex to remove acetylation, thus allowing H3K9 methylation (Motamedi et al. 2008; Fischer et al. 2009). Moreover, Swi6 dimerization through its chromoshadow domain enables two dimers of Swi6 to bind a single H3K9me nucleosome, providing 'sticky ends' that enable Swi6 to bridge two nucleosomes and allow the spreading of heterochromatin (Canzio et al. 2011; Canzio et al. 2013).

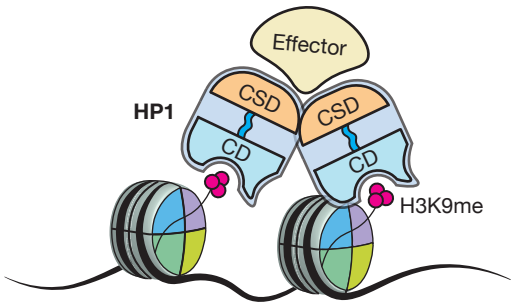

Figure 1.8. The H3K9me reader HP1. The chromodomain (CD) of HP1 specifically binds H3K9me. Chromoshadow domain (CSD) dimerization forms a platform that enables binding of additional effector proteins. Note that an HP1 dimer could also bind two K9-methylated H3 tails of a single nucleosome. Adapted from Allshire & Madhani (2018).

Different HP1 proteins exhibit different localisation patterns and functions. For example, *S. pombe* Swi6 and mammalian HP1α are critical regulators of DNA replication at centromeric heterochromatin (Chen et al. 2008; Quivy et al. 2008). In euchromatic regions, mammalian HP1α and HP1β are recruited to repress gene promoters, while HP1γ associates with the coding regions of actively transcribed genes. In addition, it has been shown that re-localization of mammalian HP1β helps establish a repair-competent chromatin environment following DNA damage (Vakoc et al. 2005).

HP1 can associate directly with the H3K9 KMT Su(var)39 in *D. melanogaster*, *S. pombe* (Swi6-Clr4) and mammalian cells (HP1-SUV39H1), and this interaction is functionally relevant for the spreading and maintenance of H3K9 methylation (Yamamoto & Sonoda 2003; Haldar et al. 2011). Importantly, Su(var)39 and its orthologues (Clr4 and SUV39H1) contain an N-terminal chromodomain in addition to the catalytic C-terminal SET domain (Rea et al. 2000). This enables Su(var)39 enzymes to bind the same modification that they deposit, and thus coupling *reader* and *writer* modules in the same protein.

1.2.3.1. Heterochromatin establishment

Heterochromatin establishment requires chromatin modifiers to be recruited to a nucleation site through specific signals. Such signals vary depending on the biological system or the type of heterochromatin being established (Grewal & Jia 2007).

The first system in which the molecular mechanisms of heterochromatin silencing were dissected was the budding yeast *Saccharomyces cerevisiae.* Notably, unlike in *S. pombe* or more complex eukaryotes*, S. cerevisiae* heterochromatin domains do not depend on H3K9 methylation but rely completely on histone deacetylation and the silent information regulator (SIR) group of proteins (Kueng et al. 2013). In this non-canonical heterochromatin system, restricted to *S. cerevisiae* and its relatives, silencer elements are recognized by sequence-specific DNA-binding proteins that then recruit four SIR proteins: Sir1, Sir2, Sir3 and Sir4. H4K16 deacetylation by the Sir2 HDAC

(*eraser*) enables Sir3 (*reader*) to bind nucleosomes through its bromo-adjacent homology (BAH) domain (Onishi et al. 2007). This allows further cycles of SIR protein recruitment to form silent chromatin domains (Kueng et al. 2013; Hanson & Wolfe 2017).

1.2.3.1.1. RNAi-mediated heterochromatin establishment

Heterochromatin domains are considered transcriptionally silent. However, a low level of transcription occurs in heterochromatin regions and this is required for H3K9 methylation-dependent heterochromatin establishment in several organisms. Low-level transcription of non-coding RNAs (ncRNAs) from constitutive heterochromatic loci is tightly regulated and occurs predominantly during DNA replication (S phase), when heterochromatin regions become accessible (Lu & Gilbert 2007; Chen et al. 2008; Kloc et al. 2008). ncRNAs can be processed into small RNAs such as PIWI-interacting RNAs (piRNAs) or small interfering RNAs (siRNAs) that are then loaded into an Argonaute (AGO) protein. Small RNA-AGO complexes act as heterochromatin nucleation signals and recruit silencing factors through base pairing (Holoch & Moazed 2015; Martienssen & Moazed 2015; Allshire & Madhani 2018). Molecular mechanisms that trigger gene silencing by combining small RNAs with an AGO protein are broadly referred as RNA interference (RNAi). Note that the term RNAi was originally used to exclusively describe post-transcriptional silencing that is mediated by exogenous double-stranded RNA (dsRNA) in *Caenorhabditis elegans* (Fire et al. 1998). The finding that small RNAs can also trigger gene silencing at the chromatin level led to the expanded and currently accepted definition of the term (Volpe et al. 2002).

piRNA-mediated heterochromatin establishment

piRNAs are 23 to 29-nucleotide small RNAs generated through a process known as ‘the ping-pong cycle’, initially described in the *D. melanogaster* germ line (Brennecke et al. 2007; Gunawardane et al. 2007) (reviewed in Castel & Martienssen 2013). piRNAs target transposon transcripts in animal germ lines. In *D. melanogaster* ovaries, piRNAs silence transposons in oocytes, somatic

follicle cells and germline nurse cells via transposon transcript degradation and deposition of H3K9 methylation (Malone et al. 2009; Wang & Elgin 2011). In mice, the piRNA pathway is required in the male germ line to silence transposons through DNA methylation during early development (Aravin et al. 2007; Aravin et al. 2008; Watanabe et al. 2011; Zoch et al. 2020). Although no evidence of the ping-pong cycle has been observed in the worm *C. elegans*, a class of small RNAs termed 21U that associates with the PIWI family protein PRG-1 has been shown to transcriptionally silence transposons in the germline through H3K9 methylation (Ruby et al. 2006; Das et al. 2008; Ashe et al. 2012).

siRNA-mediated heterochromatin establishment

Processing of non-coding double-stranded RNAs (dsRNAs) into siRNAs has been proposed to occur in the nucleus of *S. pombe* and *D. melanogaster,* in the nucleolus of *A. thaliana*, and in the cytoplasm of *C. elegans* (Figure 1.9) (Castel & Martienssen 2013). dsRNAs can be produced by convergent transcription, complementary transcripts, structured loci or RNA-directed RNA polymerase complex (RDRC) activity. Dicer, an RNase III class ribonuclease, processes dsRNAs and generates 21 to 24-nucleotide complementary duplexes or siRNAs (Hamilton & Baulcombe 1999; Bernstein et al. 2001), that are loaded into an Argonaute protein (Liu et al. 2004). Argonaute-mediated cleavage and release of the siRNA-duplex passenger strand leave a single-stranded siRNA stably incorporated, where it acts as a guide for transcript degradation through base-pairing interactions with complementary target sequences (Figure 1.9) (Irvine et al. 2006; Buker et al. 2007; Martienssen & Moazed 2015). Argonaute-associated siRNAs can target nascent transcript to mediate heterochromatin establishment in a process known as transcriptional gene silencing (TGS) or RNAi-mediated heterochromatin establishment. In addition, Argonaute-associated siRNAs can also trigger the degradation of messenger RNA (mRNAs) post-transcriptionally in a process named post-transcriptional gene silencing (PTGS) (White & Allshire 2008; Martienssen & Moazed 2015). A similar pathway generates micro RNAs (miRNAs) through a series of related steps, but unlike siRNAs, that can target transcriptional

silencing, miRNAs predominantly cause translational repression of homologous genes in a developmental stage-specific manner (reviewed in Elgin & Reuter 2013).

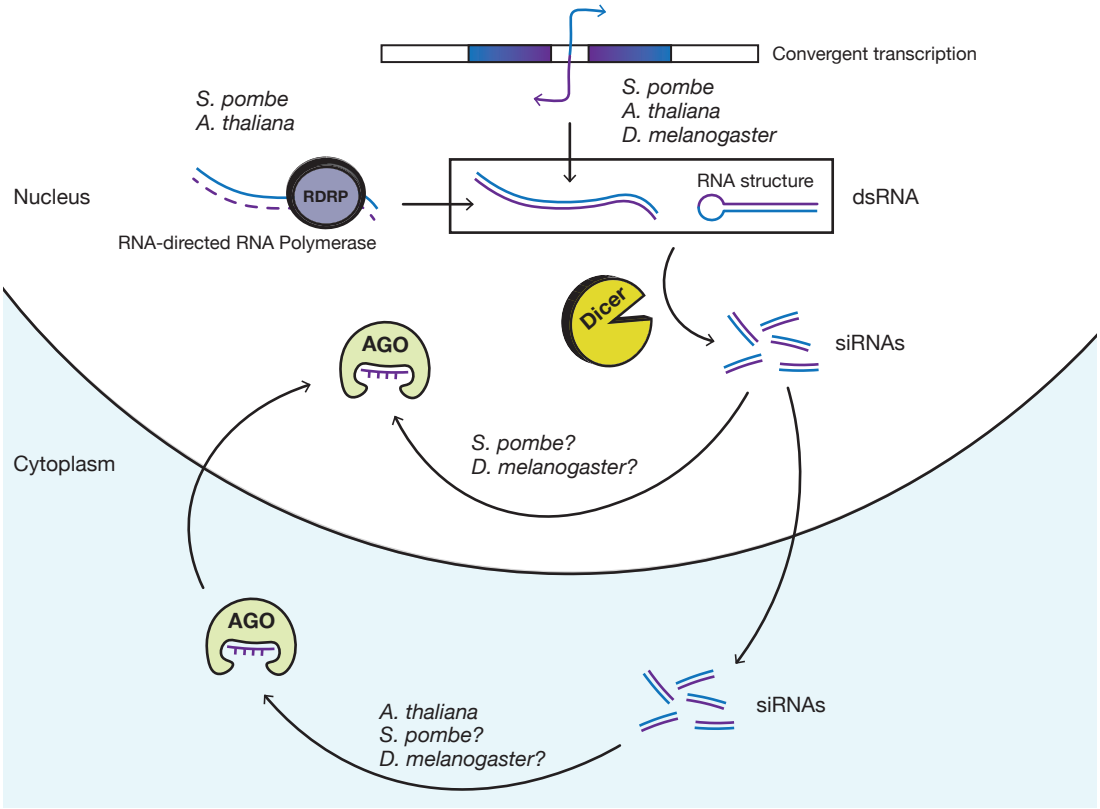

Figure 1.9. Biogenesis of small interfering RNAs (siRNAs). Double-stranded RNA (dsRNA) can be produced by convergent transcription, complementary transcripts, structured loci or (in *S. pombe* and *A. thaliana*) RNA-directed RNA polymerase complex (RDRC) activity. Dicer proteins generate siRNAs that are loaded into an Argonaute protein (AGO). In *A. thaliana*, siRNAs are transported to the cytoplasm, where they are loaded into AGO and then imported back into the nucleus. In *S. pombe* and *D. melanogaster*, the specific cellular location at which AGO loading occurs is unclear. siRNA biogenesis in *C. elegans* occurs in the cytoplasm (not shown). Adapted from Castel & Martienssen (2013).

1.2.3.1.2. RNAi-mediated heterochromatin establishment in *S. pombe*

Fission yeast *S. pombe* has provided crucial insights into the establishment of siRNA/RNAi-mediated heterochromatin domains. Heterochromatin assembly in *S. pombe* depends on a single H3K9 KMT: the Su(var)39 orthologue Clr4

protein (Zhang et al. 2008), responsible for mono-, di- and tri-methylation of H3K9. Heterochromatin is not essential for cell survival in *S. pombe*, however the absence of centromeric heterochromatin domains leads to chromosome segregation defects (Allshire et al. 1995; Bernard et al. 2001). Importantly, *S. pombe* lacks both DNA methylation (5mC) and Polycomb-deposited H3K27 methylation (Allshire & Ekwall 2015). This facilitates the investigation of factors directly involved in the establishment of H3K9 heterochromatin.

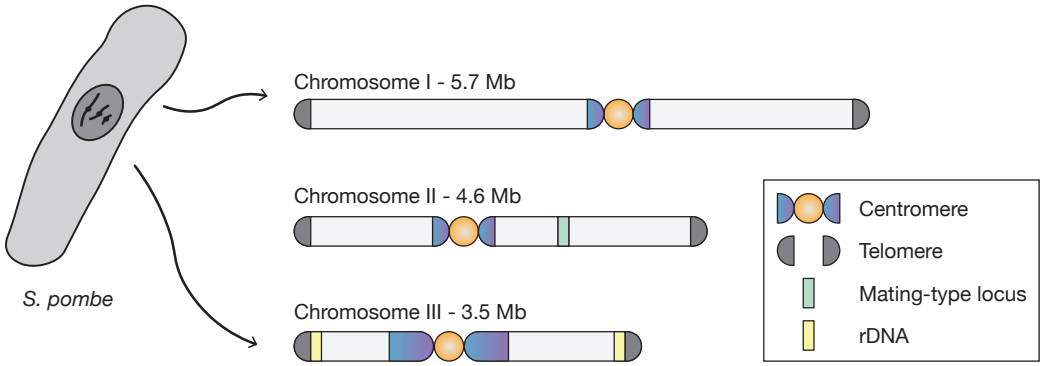

Figure 1.10. *S. pombe* chromosomes. Schematic representation of *S. pombe* chromosomes. Chromosomes are depicted displaying domains of constitutive heterochromatin at centromeres, telomeres, mating-type locus (*mat2/3*) and rDNA regions. Adapted from Allshire & Ekwall (2015).

At *S. pombe* centromeres, RNA polymerase II (RNAPII) convergently transcribes heterochromatin repeats during S phase (Djupedal et al. 2005; Chen et al. 2008; Kloc et al. 2008). Pericentromeric repeats, the major source of siRNAs in fission yeast, consist of *dg* and *dh* sequences, and *dg/dh*-related repeats can also be found within subtelomeric repeats and between the *mat2* and *mat3* genes at the silent mating type locus (Figure 1.10) (Grewal & Klar 1997; Kanoh et al. 2005). dsRNAs resulting from convergent *dg/dh* transcription are processed by Dicer (Dcr1) into siRNAs (Colmenares et al. 2007). siRNAs are then loaded into Argonaute (Ago1) where they direct the targeting of homologous nascent repeat transcripts and recruit silencing factors (Kato et al. 2005; Djupedal et al. 2005; Bühler et al. 2006; Irvine et al.

2006). In addition, it has been proposed that Dicer-independent small RNAs that originate from the degradation of abundant transcripts, termed primal small RNAs (priRNAs), also associate with Argonaute and might target nascent transcripts in a way similar to siRNAs (Halic & Moazed 2010).

Ago1 is part of the RNA-induced initiation of transcriptional gene silencing (RITS) complex (Verdel et al. 2004) which comprises three subunits: Ago1, targeting complex subunit 3 (Tas3) and the chromodomain-containing protein Chp1 that stabilises RITS to heterochromatin through its chromodomain (Sadaie et al 2004; Partridge et al. 2000). RITS associates with two complexes: the RNA-dependent RNA polymerase complex (RDRC) (Motamedi et al. 2004), via the Essential for RNA silencing (Ers1) protein (Rougemaille et al. 2008); and the Clr4 complex (CLRC) (Zhang et al. 2008), via the siRNA to chromatin (Stc1) protein (Bayne et al. 2010). RDRC uses RNAPII centromeric transcripts as templates for synthesis of dsRNA, thereby amplifying siRNA production (Motamedi et al. 2004; Sugiyama et al. 2005). RITS-mediated recruitment of the CLRC complex via the Stc1 protein to chromatin allows Clr4 to deposit H3K9 methylation and the establishment of heterochromatin (Figure 1.11) (Hall et al. 2002; Volpe et al. 2002; Bayne et al. 2010).

The RDRC complex is composed of the RNA-dependent polymerase 1 (Rdp1), a putative RNA helicase (Hrr1) and a polyA polymerase (Cid12) (Motamedi et al. 2004; Sugiyama et al. 2005). Cid12 was found to interact with several splicing factors that are required for processing of centromeric transcripts into siRNAs (Bayne et al. 2008). In addition, RDRC interacts with Dicer, coupling dsRNA production with siRNA generation (Colmenares et al. 2007).

The CLRC complex consists of the H3K9 KMT Clr4, the cullin scaffold protein Cul4, the WD repeat protein Rik1, the RING box protein Rbx1, and the WD repeat subunits Raf1 and Raf2 (Partridge et al. 2002; Jia et al. 2005; Horn et al. 2005; Hong et al. 2005; Buscaino et al. 2012; White et al. 2014). The SET catalytic domain of Clr4 has been shown to methylate H3K9 *in vitro*, but association of Clr4 with other CLRC components is necessary for H3K9 *in vivo*

(Rea et al. 2000; Zhang et al. 2008). Cul4, Rik1, Raf1 and Raf2 form a multisubunit E3 enzyme (Cul4-Rik1$^{Raf1/Raf2}$), related to the cullin-RING finger family of ubiquitin ligases Cul4-Dbd1^{DCAF}. Indeed, ubiquitin ligase activity of CLRC has been demonstrated *in vitro* (Horn et al. 2005), and *in vivo* (Oya et al. 2019). Notably, CLRC-mediated H3K14 ubiquitylation was shown to promote H3K9 methylation by Clr4 (Oya et al. 2019), suggesting that CLRC ubiquitin ligase activity is intimately linked to the assembly of H3K9me. Moreover, Cul4 is also part of the canonical Cul4-Ddb1^{Cdt2} E3 complex, which promotes ubiquitylation and degradation of the boundary factor Enhancer of position effect 1 (Epe1) (Braun et al. 2011).

CLRC promotes heterochromatin formation mainly through the methyltransferase activity of Clr4 but it also participates in siRNA production. Interestingly, H3K9me-deposition and siRNA-production activities of CLRC can be uncoupled. Tethering Rik1 to a euchromatic locus results in siRNA-mediated silencing at the target locus independently of H3K9 methylation and in the absence of other CLRC components (Gerace et al. 2010). In addition, mutations in Raf1 lead to its dissociation from CLRC and the abolishment of H3K9 methylation without affecting siRNA production (Buscaino et al. 2012).

Interactions among RITS, RDRC and CLRC allow the generation of a positive feedback loop that ensures the establishment of heterochromatin domains through siRNA production and H3K9 methylation (Figure 1.11).

In addition to CLRC-mediated H3K9me deposition, transcriptional silencing at heterochromatin regions requires histone deacetylation by HDACs. Three complexes with HDAC activities contribute to the formation of heterochromatin regions in *S. pombe*: The Snf2/HDAC-containing repressor complex (SHREC), the Clr6 HDAC complex and the Sir2 HDAC (Sugiyama et al. 2007; Nakayama et al. 2003; Buscaino et al. 2013). SHREC is recruited to heterochromatin by the chromodomain proteins Swi6 and Chp2. SHREC contains the H3K14 HDAC Clr3, whose absence results in a partial loss of heterochromatin-dependent silencing (Sugiyama et al. 2007).

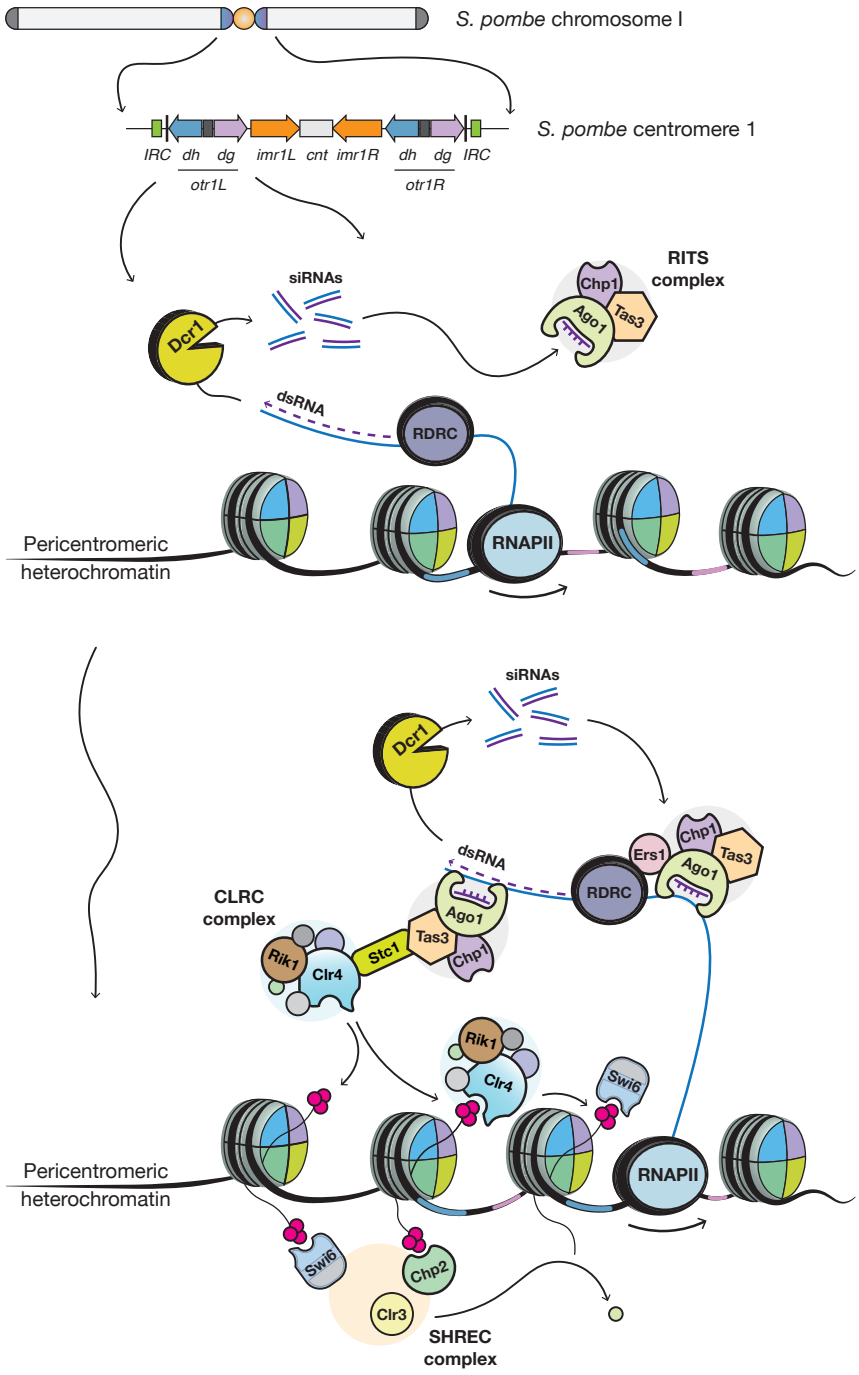

Figure 1.11. RNAi-mediated heterochromatin establishment at fission yeast centromeres. Transcription of pericentromeric repeats generates dsRNAs that are processed into siRNAs by Dicer (Dcr1). siRNAs loaded into the Argonaute (Ago1)-containing RITS complex target a nascent transcript by base-pairing interactions. RITS recruits RDRC and CLRC. RDRC generates more dsRNA, leading to additional siRNA production. RITS recruits CLRC to chromatin via the adaptor protein Stc1. Clr4-mediated deposition of H3K9me leads to binding of chromodomain proteins Swi6, Chp2, Chp1 and Clr4 itself. Swi6 and Chp2 recruit the SHREC complex containing the Clr3 HDAC, which promotes histone deacetylation. Interactions among RITS, RDRC and CLRC allow the generation of a positive feedback loop that ensures the establishment of heterochromatin domains through siRNA production and H3K9 methylation. Small red circles, H3K9me. Small green circle, H3ac.

The Clr6 HDAC is essential (Grewal et al. 1998). Clr6 prevents accumulation of *dg/dh* repeat transcripts via its H3K9 deacetylase activity (Nakayama et al. 2003; Nicolas et al. 2007), and Clr6 mutants exhibit silencing defects at centromeric repeats and at the mating type locus (Grewal et al. 1998). The Sir2 HDAC deacetylates H3K9ac, H3K14ac, H3K4ac and H4K16ac *in vitro* (Alper et al. 2013). Sir2 has been proposed to act upstream of Clr4 to establish H3K9 methylation *in vivo*. Indeed, loss of Sir2 causes increased levels of H3K9ac that prevent H3K9 methylation at heterochromatin loci, and this results in moderate silencing defects at centromeric and subtelomeric heterochromatin regions (Shankaranarayana et al. 2003; Alper et al. 2013; Buscaino et al. 2013). Even though single deletions of Clr3 or Sir2 do not display a severe defect in centromeric heterochromatin, the combined removal of Clr3 and Sir2 provokes the loss of heterochromatin from centromeric repeats (Alper et al. 2013; Buscaino et al. 2013).

1.2.3.1.3. RNAi-independent heterochromatin establishment in *S. pombe*

Additional mechanisms that include RNA-processing and DNA-binding factors act in parallel or independently of siRNAs/RNAi to target the H3K9 methylation machinery to heterochromatin regions of fission yeast including centromeres, facultative heterochromatin loci, telomeres or the silent mating-type locus.

At the centromere, cells lacking RNAi components show silencing defects due to the absence of siRNAs and decreased deposition of H3K9 methylation (Volpe et al. 2002). Loss of Mlo3, a protein related to mRNA quality control and export factors, causes severe reduction in the levels of centromeric siRNAs, but this has no major effect on H3K9me deposition or heterochromatin silencing (Zhang et al. 2011). Interestingly, in the absence of RNAi components (and hence siRNAs), loss of Mlo3 restores centromeric H3K9me heterochromatin and silencing, likely due to the accumulation of repeat-transcripts which restores Rik1 enrichment at repeats (Reyes-Turcu et al. 2011).

RNA-processing factors have also been shown to play a role in the assembly of H3K9me-mediated facultative heterochromatin in fission yeast. During vegetative growth, transcripts of meiotic genes that contain a determinant of selective removal (DSR) motif are degraded by the nuclear exosome to prevent incidence of untimely meiosis (Harigaya et al. 2006). DSR motifs are bound by the Mmi1 protein. Mmi1 forms a complex with Enhancer of rudimentary homolog (Erh1) called Erh1-Mmi1 complex (EMC) (Sugiyama et al. 2016). EMC associates with the exosome-associated 3'-to-5' exonuclease Rrp6; the canonical poly(A) polymerase Pla1; the poly(A)-binding protein Pab2; and the zinc-finger protein Red1, which is essential for elimination of meiotic mRNAs and forms a complex with Mtl1 (Mtl1-Red1, MTREC) (Houseley et al. 2006; Yamanaka et al. 2010; Sugiyama & Sugioka-Sugiyama 2011; Lee et al. 2013).

EMC-mediated DSR transcript recognition has two outcomes: it triggers mRNA degradation via the exosome complex (Harigaya et al. 2006); and it promotes RNAi-independent heterochromatin island formation at loci harbouring DSR-containing meiotic genes via the interaction of MTREC with Clr4 (Zofall et al. 2012). Importantly, loss of Clr4 does not result in up-regulation of DSR-containing transcripts, indicating that the transcriptional control of meiotic genes is predominantly exerted by the nuclear exosome and not by heterochromatin formation (Egan et al. 2014). Indeed, H3K9me levels at most DSR-containing heterochromatin islands are close to background in wild-type cells (Zofall et al. 2012; Wang et al. 2015; Sorida et al. 2019). Thus, EMC-MTREC interactions facilitate the assembly of facultative heterochromatin islands that coat meiotic genes silenced by the nuclear exosome. In addition, EMC also interacts with the CCR4-NOT complex to promote RNAi-dependent heterochromatin assembly at heterochromatin domains (HOODs) including retrotransposons and genes containing cryptic introns (Yamanaka et al. 2013). However, detection of siRNAs and H3K9me at HOODs is solely observed in the absence of nuclear exosome components, indicating that in wild-type cells these loci are silenced exclusively by exosome function and not by heterochromatin assembly (Yamanaka et al. 2013).

Heterochromatin establishment in fission yeast can also be triggered by DNA-binding factors. Telomeres of most eukaryotes assemble heterochromatin (Allshire & Madhani 2018). In *S. pombe*, telomeric heterochromatin extends 45-75 kb away from chromosome ends (see Figure 1.10) (Allshire & Ekwall 2015). Telomeric heterochromatin prevents recombination between telomeric repeats (Cooper et al. 1998; Nimmo et al. 1998). Assembly of telomeric heterochromatin involves two redundant pathways. First, subtelomeric regions of chromosome I and II harbour *dg/dh*-related *tlh* elements that trigger RNAi to promote RITS-CLRC recruitment to telomeres and Clr4-mediated deposition of H3K9 methylation in a process similar to that observed at centromeres (Volpe et al. 2002). Second, the telomere-repeat-binding protein Taz1 recruits CLRC to the telomere via the shelterin subunit Ccq1 and establishes Swi6 heterochromatin independently of RNAi (Cooper et al. 1997; Kanoh et al. 2005; Wang et al. 2016). Loss of H3K9me and Swi6 enrichment at telomeres is observed only in cells lacking components from both RNAi and Taz1 pathways, indicating that they act redundantly (Kanoh et al. 2005). Recently, Taz1 has also been shown to promote assembly of H3K9 methylation at a subset of the above-mentioned facultative heterochromatin islands. Taz1-dependent heterochromatin islands do not coat DSR-containing meiotic genes but include chromosome-internal sites containing late replication origins (Zofall et al. 2016).

In addition, at the silent mating-type locus, *dg/dh*-related *cenH* repeats mediate RNAi-dependent H3K9me deposition and heterochromatin formation (Hall et al. 2002). However, RNAi mutants can still assemble heterochromatin over this locus, albeit at a low efficiency. It was shown that two ATF/CREB transcription factors, Atf1 and Pcr1, bind to specific recognition sequences adjacent to *cenH* and mediate recruitment of Clr4 and Swi6, therefore acting in a parallel mechanism to the RNAi pathway for heterochromatin nucleation. Loss of either Atf1 or Pcr1 in combination with RNAi mutants results in failure to nucleate heterochromatin assembly at the mating-type locus (Jia et al. 2004). Interestingly, ATF/CREB transcription factors are involved in cellular responses to environmental stresses (Takeda et al. 1995; Watanabe &

Yamamoto 1996), suggesting that these factors might modify chromatin structure as part of a programmed response to unfavourable external conditions.

1.2.3.2. Heterochromatin spreading

Once established at a particular locus, heterochromatin domains can spread in *cis* in a manner that is largely independent of the underlying DNA sequence. This phenomenon is illustrated by the classic example of position-effect variegation in *D. melanogaster*, where euchromatic genes juxtaposed with heterochromatin due to chromosome rearrangements are transcriptionally silenced (see section 1.2.1) (Schultz 1936; Tartof et al. 1984). The degree of repression caused by position effect variegation depends on the stochasticity of heterochromatin spreading and the availability of heterochromatin components (Hecht et al. 1996). Similarly, insertion of a reporter gene within centromeric heterochromatin in fission yeast results in genetically identical cells mosaic for its expression (Allshire et al. 1994).

Heterochromatin spreading requires coupling of *writer-reader* function to form positive feedback loops that extend heterochromatin domains (Figure 1.12). Mutations in the chromodomain of Clr4 allow H3K9me deposition but impede heterochromatin spreading (Zhang et al. 2008). Spreading also requires the recruitment of HDACs (Yamada et al. 2005; Buscaino et al. 2013). In addition, single-cell reporter analysis has revealed that heterochromatin spreading requires several cell divisions following nucleation and does not always occur in a linear fashion (Obersriebnig et al. 2016).

It is crucial that heterochromatin spreading is controlled and restricted to prevent erroneous and potentially deleterious gene silencing. Several mechanisms have been reported that stop heterochromatin from spreading into euchromatic regions, including generation of nucleosome-depleted regions by binding of proteins; processes that promote nucleosome turnover; recruitment of readers with anti-silencing activity; and recruitment of anti-silencing factors by ongoing transcription (Figure 1.12).

tRNAs serve as heterochromatin-spreading barriers in many organisms (Donze et al. 1999; Raab et al. 2012). The insulation function of tRNAs appears to depend on binding sites for the RNA polymerase III transcription factor complex TFIIIC. Indeed, genomic loci that contain TFIIIC sites are highly accessible and have large nucleosome-free regions that may impede the crossing of *writer-reader* machineries (Figure 1.12) (Noma et al. 2006; Scott et al. 2007).

Heterochromatin regions in *S. pombe* are characterized by low nucleosome turnover (Aygün et al. 2013; Svensson et al. 2015). Low turnover of nucleosomes assembled in heterochromatin requires the HDAC Clr3 (Aygün et al. 2013). Moreover, the anti-silencing factor and putative H3K9 demethylase Epe1, a JmjC domain chromatin-associated protein (Ayoub et al. 2003), has been proposed to counteract heterochromatic silencing by promoting nucleosome turnover (Aygün et al. 2013), albeit this effect might be indirect. Epe1 also acts in parallel to boundary elements, as loss of both Epe1 and TFIIIC sites flanking the mating-type locus provokes substantial heterochromatin spreading and slow cell growth (Garcia et al. 2015). Paradoxically, Epe1 is recruited to heterochromatin by the chromodomain protein and *reader* Swi6 (Zofall & Grewal 2006; Trewick et al. 2007). Within heterochromatin domains, Epe1 is degraded through the action of the Cul4-Ddb1^{Cdt2} ubiquitin ligase, whose activity is limited to the interior of heterochromatin domains and absent from their edges (Braun et al. 2011). This mechanism restricts heterochromatin spreading from constitutive heterochromatic loci (Figure 1.12).

Heterochromatin spreading is also restricted by chromatin modifications associated with euchromatin. For example, histone PTMs associated with active transcription such as methylation of H3K36 or acetylation of H3K14 have an anti-silencing role at SIR-dependent heterochromatin in *S. cerevisiae* and H3K9me-dependent heterochromatin in *S. pombe,* respectively (Figure 1.12) (Tompa & Madhani 2007; Wang et al. 2015). Interestingly, the combined loss of anti-silencing factors that prevent heterochromatin spreading leads to

severe growth defects. Cells lacking the putative H3K9 demethylase Epe1 and the H3K14 acetyltransferase Mst2 display extensive ectopic heterochromatin assembly at euchromatic loci and markedly slow growth (Wang et al. 2015). Importantly, ectopic heterochromatic formation is not restricted to regions flanking constitutive heterochromatin but also occurs at isolated active loci, suggesting that in wild-type conditions key anti-silencing factors block the assembly of H3K9me at heterochromatin-prone euchromatic regions (Wang et al. 2015).

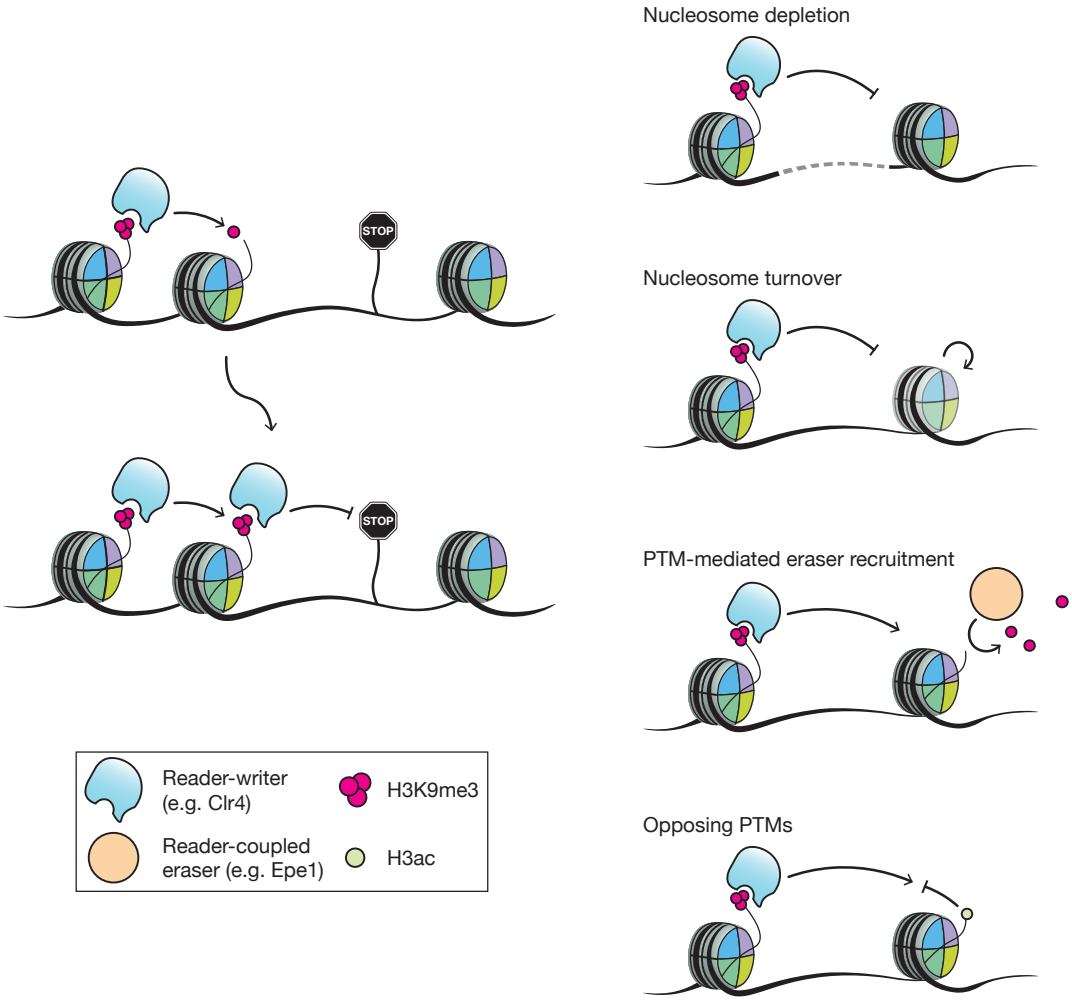

Figure 1.12. Heterochromatin spreading is restrained. Left. Heterochromatin spreading mediated by coupling of *reader-writer* function. Iterative cycles result in the formation of extensive heterochromatin domains. The *STOP* sign represents mechanisms that restrict heterochromatin spreading, which are shown on right panel. Right. A series of mechanisms known to impede heterochromatin expansion. Adapted from Allshire & Madhani (2018).

1.2.3.3. Heterochromatin maintenance

Upon DNA replication, nucleosome occupancy on the newly synthesized DNA molecules is reinstated with new nucleosomes assembled from free histones (see section 1.1.3.1). As parental H3-H4 tetramers are in general randomly distributed to sister chromatids during DNA synthesis (Petryk et al. 2018), any heterochromatin-associated histone PTM such as H3K9me is consequently diluted by half upon replication (Figure 1.13). *Reader*-mediated recruitment of *writers* (*reader-writer* coupling) may allow pre-established but diluted heterochromatin states to be fully restored in naïve, newly assembled nucleosomes (Figure 1.13). Consistent with this notion, some factors required to establish heterochromatin are not necessary for its maintenance. In *S. pombe*, RNAi is required for establishing H3K9me-dependent heterochromatin at centromeres (see section 1.2.3.1.2). In the absence of RNAi components, no H3K9me can be established at centromeric repeats when the H3K9 KMT Clr4 is re-introduced into cells lacking Clr4 (Sadaie et al. 2004). Likewise, H3K9me does not assemble on a repeat-containing mini-chromosome when transformed into cells lacking RNAi factors (Folco et al. 2008). However, once centromeric heterochromatin is established, deletion of some RNAi components (e.g. Argonaute) only leads to partial but not complete loss of H3K9me from this locus (Volpe et al. 2002), albeit transcriptional silencing is defective. Moreover, this partial loss of H3K9me has been proposed to be the result of defective replication-coupled RNAPII release in RNAi mutants and not due to reduced H3K9me re-deposition *per se* (Zaratiegui et al. 2011). In addition, in *D. melanogaster*, piRNA-mediated silencing of transposable elements is established during early stages of development. The Argonaute-related piRNA component PIWI is required for heterochromatin establishment, but its loss during later larval stages has no impact on silencing (Gu & Elgin 2013). This indicates that, similar to the case in fission yeast, some components required for piRNA-mediated heterochromatin establishment can be dispensable for subsequent heterochromatin maintenance.

Together these pieces of evidence suggest that *reader-writer* coupling might be sufficient to maintain a pre-established heterochromatin state in the absence of the nucleation signal. Because *reader-writer* coupling is independent of the underlying DNA sequence, it has been proposed that the maintenance of heterochromatin domains might be truly *epi*-genetic.

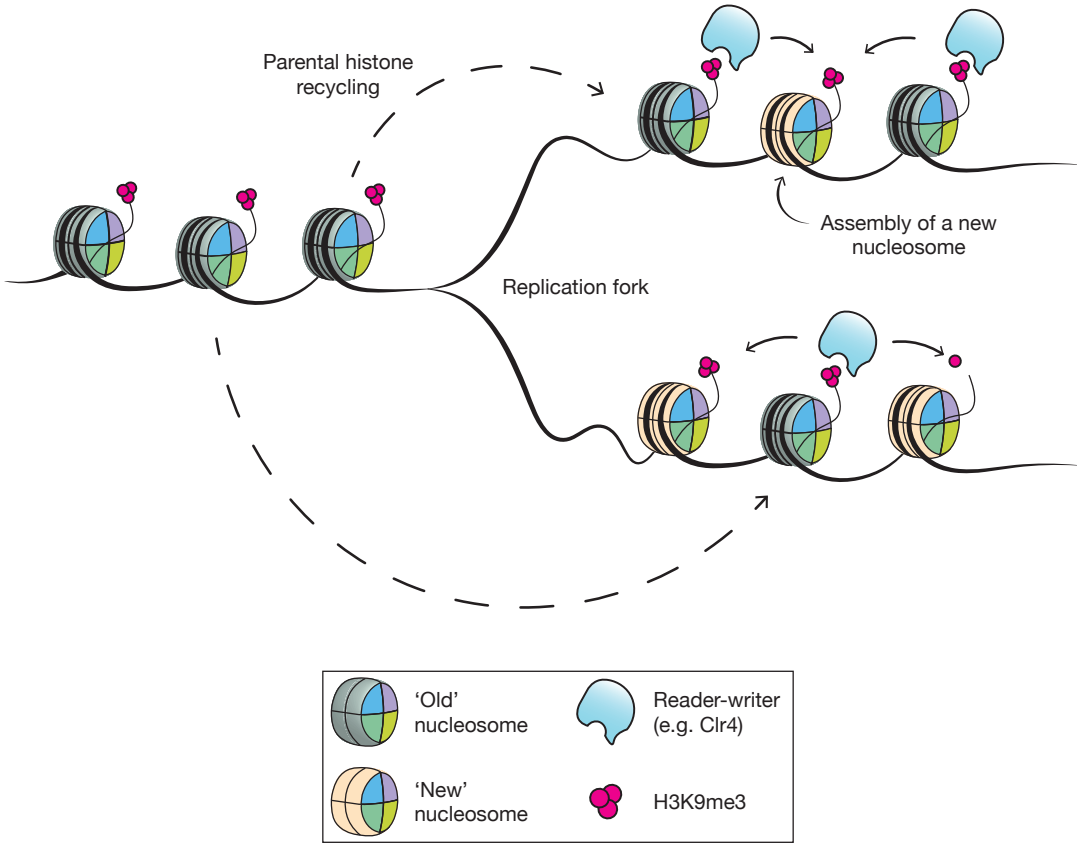

Figure 1.13. Heterochromatin maintenance through DNA replication. During S phase, parental 'old' H3-H4 tetramers are randomly transmitted to either of the two newly synthesized DNA molecules and thus the number of nucleosomes bearing a histone PTM such as H3K9me is diluted by half compared with the parental chromatin. Coupling of *reader-writer* function should enable transmission of H3K9me from old nucleosomes to newly assembled nucleosomes, consequently restoring PTM levels and full chromatin domains on both progeny cells upon cell division. Adapted from Allshire & Madhani (2018).

1.3. Epigenetic maintenance of heterochromatin domains

1.3.1. What is epigenetics?

Conrad Waddington coined the term *epigenetics* in the 1940s to refer to "the branch of biology that studies the causal interactions between genes and their products which bring the phenotype into being" (Waddington 1942). Robin Holliday redefined the term, formulating the concept of *epimutation* for the first time to describe "heritable changes in gene function that do not involve a change in DNA sequence" (Jeggo & Holliday 1986; Holliday 2006). Mark Ptashne modified the latter definition to add that such heritable and DNA sequence-independent changes in gene expression should "persist in the absence of the initiation signal" (Ptashne 2007).

Subsequently, Adrian Bird suggested a broader definition of epigenetics as "the structural adaptation of chromosomal regions so as to register, signal or perpetuate altered activity states" (Bird 2007). Bird excluded heritability as part of the definition because it is challenging to specify how many generations of inheritance might be necessary to satisfy the requirement. The definition also excludes *trans*-acting elements such as prions despite the fact that they can drive distinct phenotypes and be inherited to daughter cells (Patino et al. 1996; Harvey et al. 2020). Importantly, Bird's definition implies that epigenetic marks are responsive, not proactive. Under this definition epigenetic systems would not initiate a change of state at a particular locus but would only register a change already imposed by other events. For example, transcriptional activation via sequence-specified DNA-binding factors recruits histone acetyltransferases that adapt a promoter region for transcription through histone modification and recruitment of additional proteins. This definition portrays epigenetic mechanisms as tightly regulated marionettes at the mercy of DNA sequence-controlled events. In this thesis it will be investigated whether epimutations, defined here as heritable changes in gene expression that occur independently of changes in DNA sequence, can also have a distinctly proactive role in determining a cellular phenotype.

1.3.2. Inheritance of epigenetic changes

Whether epigenetic changes can be inherited from cell to cell and to the next generation has been a matter of discussion for decades (Heard & Martienssen 2014). It is now widely accepted that epigenetic changes such as facultative heterochromatin domains can be transmitted mitotically. For example, the inactivation of the X chromosome in female mammals is stably maintained from cell to cell in a process that involves, as previously described (see section 1.2.2), the deposition of H3K27me, but also H3K9me and DNA methylation (Galupa & Heard 2018). Silencing of the *FLC* repressor in flowering plants constitutes a similar example, as once established, the repressed state of this locus can be propagated to daughter cells during the winter months (see section 1.2.2). It is important to state that in the above-mentioned natural processes, constant nucleation events or coupling to DNA methylation might ensure the replenishment of histone marks upon DNA replication. Therefore, it is unclear whether in those scenarios the mitotic transmission of epigenetic changes can be exclusively mediated by histone *reader-writer* coupling.

Transgenerational inheritance of epigenetic changes, however, appears to be restricted in most cases. Many plants and animals undergo epigenetic "reprogramming" steps in the germline and/or at early stages of embryonic development, resulting in the nearly-total loss of chromatin modifications such as histone PTMs or DNA methylation (Feng et al. 2010). These erasing events prevent the inheritance of most changes acquired during lifetime and impede the transmission of potentially deleterious epimutations to the offspring (Heard & Martienssen 2014). Nevertheless, although rare, evidence of transgenerational epigenetic inheritance exists in plants and animals. For example, in naturally occurring epimutants of the toadflax *Linaria vulgaris*, the *Lcyc* gene is extensively methylated (DNA 5mC). Hypermethylation leads to *Lcyc* transcriptional silencing, which results in the fundamental symmetry of the flower changed from bilateral to radial (Cubas et al. 1999). *Lcyc* hypermethylation is heritable, though occasionally reverts to an unmethylated state. Similarly, in *A. thaliana*, hypermethylated (DNA 5mC) and

transcriptionally silent epialleles of the flower development gene *SUPERMAN*, known as *clark kent*, are stable during many generations, yet they can revert to an unmethylated and active state at a frequency of ~3% per generation (Jacobsen 1997). Moreover, analyses of *A. thaliana* transposon expression and DNA methylation patterns in pollen grains and in the embryo, respectively, suggest that even though genome-wide decreases in DNA methylation occur during male and female gametogenesis, this does not seem to be as extensive as in mammalian cells (Law & Jacobsen 2010). Still, transgenerational inheritance of most epigenetic changes in plants is restricted, especially inheritance of changes mediated by histone PTMs. For example, H3K27me deposited at the *FLC* locus upon cold exposure is extensively removed during gametophyte development, resulting in *FLC* reactivation in the seed. Thus, flowering is inhibited by reactivated *FLC* until the next-generation plants encounter cold weather (Choi et al. 2009; Crevillén et al. 2014).

In mammalian cells, reprogramming occurs in the germline and during pre-implantation development. Reprogramming causes the extensive removal of DNA methylation by both active and passive demethylation (Mayer et al. 2000; Smith et al. 2014). Loss of DNA methylation is also associated with the loss of H3K9me and H3K27me. However, some regions in mammalian genomes are protected during DNA demethylation, such as imprinted loci and repetitive DNA sequences. Genomic imprinting is a phenomenon that causes some genes to be expressed according to their parental origin. A classic example of genomic imprinting is the *agouti* locus in the mouse, which exhibits parental origin effects imposed by the DNA methylation state of a neighbouring *IAP* retroviral element (Morgan et al. 1999). DNA methylation on the *IAP* promoter correlates with silencing of the *agouti* gene and this leads to mice displaying a brown pseudo-*agouti* coat colour (in contrast to yellow coat in unmethylated, *agouti*-expressing mice). The paternal *agouti* state does not influence the methylation levels of *agouti* in the offspring. However, in the female germ line, incomplete erasure of DNA methylation at this locus results in offspring preferentially displaying the maternal *agouti* state (Morgan et al. 1999).

Together these findings have suggested over the years that epigenetic changes that depend on DNA methylation can be inherited transgenerationally in plants and animals, albeit transmission is generally restricted and has been shown to occur only in few rare loci.

1.3.3. H3K9 methylation is a heritable epigenetic mark

The mechanism that maintains DNA methylation (5mC) domains following DNA replication and cell division is well documented (Holliday & Pugh 1975). Upon replication of a CpG dinucleotide, the CpG on a nascent strand is initially unmethylated. Maintenance DNA (5mC)-methyltransferase 1 (DNMT1) associates with the replisome, recognises 5mC in CpG dinucleotides and adds a methyl group to the cytosine in the CpG of the complementary strand (Law & Jacobsen 2010). In systems in which both 5mC and H3K9me are present, these modifications can reinforce each other. For example, in *A. thaliana*, H3K9me deposition by the H3K9 KMT Kryptonite recruits the DNA methyltransferase Chromomethylase 3 (CMT3) through LHP1 (Jackson et al. 2002). In the filamentous fungus *Neurospora crassa*, the DNA methyltransferase Defective in methylation 2 (DIM2) is recruited to H3K9me nucleosomes via HP1 (Freitag et al. 2004), and reciprocally, DNA methylation can recruit the H3K9 KMT DIM5 (Tamaru & Selker 2001). In mammalian cells, synthetic H3K9me heterochromatin domains have been shown to temporarily persist in the absence of the nucleating signal. However, a potential role for DNA methylation in such maintenance mechanism has not been ruled out (Amabile et al. 2016; Bintu et al. 2016). Given that 5mC is stably heritable through DNA replication, it is challenging to discern, in those systems where 5mC and H3K9me co-exist, whether histone *reader-writer* coupling mechanisms can solely mediate the maintenance of H3K9me, or it is coupling to 5mC that mediates its inheritance.

S. pombe lacks detectable DNA methylation (Antequera et al. 1984; Wilkinson et al. 1995; Capuano et al. 2014), and thus DNA 5mC cannot participate in a hypothetical H3K9me inheritance mechanism in this organism. Established

H3K9me heterochromatin domains can be stably maintained and inherited at the silent mating-type locus of fission yeast, but this depends on specific DNA-binding factors (Hall et al. 2002; Wang & Moazed 2017), as in the case of Polycomb-mediated H3K27me domains in other organisms (Berry et al. 2015; Laprell et al. 2017; Coleman & Struhl 2017). Therefore, H3K9me heterochromatin maintenance at the *S. pombe* mating-type locus does not constitute a truly epigenetic mechanism mediated by histone *reader-writer* coupling.

Fusing Clr4, the sole H3K9 KMT in fission yeast, to the DNA-binding domain of the Gal4 protein (GBD) or the Tet repressor ($TetR^{off}$) allows the generation of synthetic heterochromatin domains at cognate binding sites placed at euchromatic loci, resulting in gene silencing (Kagansky et al. 2009; Audergon et al. 2015; Ragunathan et al. 2015). TetR-Clr4 tethering can be released by addition of the small molecule anhydrotetracycline (AHT). This set-up allowed the idea that synthetic heterochromatin and gene silencing generated at a neutral euchromatic locus could be maintained by endogenous Clr4 through cell division to be directly tested (Figure 1.14). Using this system, it was found that synthetic heterochromatin is rapidly lost from tethering domains upon Clr4 release (Audergon et al. 2015; Ragunathan et al. 2015). H3K9me removal still occurred when the cell cycle was arrested, indicating that the erasing process is active and not due to passive dilution of H3-H4 tetramers during DNA replication. Importantly, cells lacking the putative H3K9 demethylase Epe1 can stably maintain synthetic H3K9me through multiple cell divisions and even through meiosis following Clr4 release (Figure 1.14) (Audergon et al. 2015; Ragunathan et al. 2015). Therefore, H3K9 methylation can be inherited and affect phenotype through a histone *reader-writer* coupling mechanism, but only in the absence of Epe1.

This finding raises the question of why Epe1 activity does not also remove H3K9me at constitutive heterochromatin domains. As mentioned above, Epe1 activity is restricted at centromeric heterochromatin through Cul4-$Ddb1^{Cdt2}$-mediated poly-ubiquitylation (Braun et al. 2011). It is therefore possible that

synthetic heterochromatin domains lack specific signals required to trigger Epe1 degradation and consequently high levels of H3K9me cannot accumulate at these artificial domains. Alternatively, the stable maintenance of heterochromatin at constitutive domains might depend on constant nucleation events mainly mediated by RNAi but also by other complementary mechanisms (as proposed for RNA-processing or DNA-binding factors, see section 1.2.3.1.3).

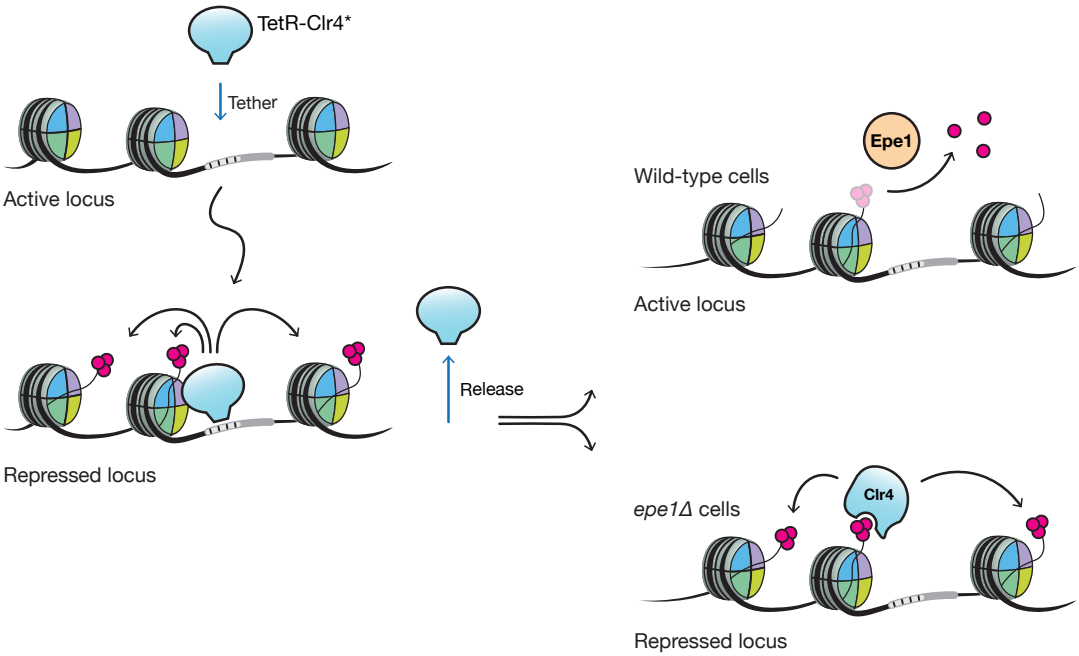

Figure 1.14. Restricted epigenetic inheritance of H3K9 methylation. TetR-Clr4*-mediated synthetic heterochromatin is actively removed following release of TetR-Clr4* by the putative H3K9 demethylase Epe1. In the absence of Epe1 (*epe1Δ*), H3K9me is not actively removed, and the presence of endogenous Clr4 and chromodomain proteins Swi6 and Chp2 (not shown) allow the methylation of newly deposited nucleosomes (Audergon et al. 2015; Ragunathan et al. 2015). The use of an engineered chromodomain-deficient version of Clr4 (Clr4*) leads to more efficient silencing at the ectopic locus as TetR-Clr4* cannot be recruited to constitutive, H3K9me-rich heterochromatin regions, and ensures that TetR-Clr4* is unable to propagate H3K9me once it is deposited (Kagansky et al. 2009).

The spatial location of heterochromatin regions has also been proposed to play a major role in the maintenance of H3K9me domains. Heterochromatin is enriched within the perinuclear zone (Bickmore & van Steensel 2013; van Steensel & Belmont 2017), and synthetic tethering of loci to the nuclear periphery promotes gene silencing in yeast and mammalian cells (Andrulis et al. 1998; Robson et al. 2016). In fission yeast, it has recently been suggested that positioning heterochromatin at the nuclear periphery suppresses histone turnover to promote epigenetic inheritance (Holla et al. 2020). Heterochromatin is connected to the nuclear periphery via Swi6 association with the RNA processing complex RIXC, that in turns binds the nuclear rim protein Amo1. Cells lacking Amo1 or harbouring mutations in Rix1, a component of RIXC, fail to maintain synthetic heterochromatin domains even in the absence of Epe1 (Holla et al. 2020). In line with a role of nuclear organisation in the maintenance of heterochromatin domains, recent studies have shown that H3K9me regions display properties of phase-separated liquids due to HP1-mediated liquid-liquid phase separation (Strom et al. 2017; Larson et al. 2017; Sanulli et al. 2019). Proteinaceous liquid droplets can form more efficiently when HP1 is phosphorylated, suggesting potential for regulation *in vivo*. For example, constitutive heterochromatin regions might be confined to HP1/Swi6-mediated droplets that physically restrain the access of key anti-silencing factors, therefore promoting the stable maintenance of heterochromatin.

1.4. Adaptive epigenetic changes as a means of survival

Changes in DNA sequence (mutations) that drive evolution are slow and nearly irreversible, and thus not ideal for a population to survive in a rapidly changing environment (Heard & Martienssen 2014). Epimutations have been proposed to enable 'soft inheritance', resulting in the formation of different phenotypes that enable adaptation to fluctuating environments (Richards 2006). This bet-hedging strategy would allow cells to adapt transiently to insults while remaining genetically wild-type, and thus the reversal of epimutations when selective pressures are relaxed (de Jong et al. 2011; Klironomos et al. 2013). Furthermore, theoretical models and simulations predict that epigenetic variation has the potential to affect the rate and outcomes of adaptation (Klironomos et al. 2013; Kronholm & Collins 2015), and that when epigenetic variation and genetic variation are both acted on by natural selection, adapted phenotypes can appear long before genetic changes do (Klironomos et al. 2013). In fact, Waddington (1942, 1953 and 1956) already proposed that epigenetic variation might have a role as a bridge towards genetic end points by facilitating genetic assimilation of characters.

Evidence of heritable epigenetic variegation among isogenic organisms has been reported, as discussed in section 1.3.2 for flower symmetry determination in *L. vulgaris* or the mouse *agouti* locus. In addition, recent studies suggest that epigenetic variation can respond to the environment and certain traits acquired by an organism during its lifetime may be transmitted to the next generation via epigenetic changes, though the underlying mechanism is not always clear. For example, in rats, diet-induced paternal obesity was proposed to program β-cell 'dysfunction' in female offspring through DNA methylation (Ng et al. 2010). Moreover, in mice, individuals exposed to odour-induced fear gave rise to F1 and F2 offspring that are more sensitive to the same odour (Dias & Ressler 2014). The increased sensitivity in F1 individuals correlated with DNA hypomethylation of the gene encoding the odour-responsive receptor. However, whether the decreased methylation levels at this locus caused any changes at the transcriptional level was not investigated. In plants,

a recent study using *A. thaliana* has proposed that hyperosmotic stress-induced DNA methylation changes at epigenetically labile sites in the genome are associated with adaptive phenotypic stress responses. These changes can be transmitted transgenerationally through the female lineage, resulting in a maternal short-term stress memory (Wibowo et al. 2016). Nonetheless, although these environment-triggered epigenetic changes can be inherited, it is certainly unclear whether such changes have a causative role in establishing the claimed adaptive phenotypes or merely constitute a consequence of upstream changes.

Contrastingly, several reports have provided convincing evidence for transgenerational inheritance of environmental information mediated by small RNAs. In *C. elegans*, it has been shown that starvation can induce transgenerational inheritance of small RNAs that affect longevity in subsequent generations (Rechavi et al. 2014), and that siRNAs generated in response to a viral infection can be transmitted to progeny (Rechavi et al. 2011). Moreover, in the human fungal pathogen *Mucor circinelloides*, siRNAs can mediate the formation of an adaptive epimutation that drives resistance to the drug tacrolimus by silencing the *fkbA* gene (Calo et al. 2014). Silencing is reversible and requires canonical RNAi components. However, whether *fkbA*-targeting siRNAs can be transmitted to the progeny upon meiosis or whether silencing requires additional chromatin factors in addition to RNAi is unknown. Interestingly, *M. circinelloides* isolates from human or other animal hosts form siRNA-mediated tacrolimus-resistant epimutants with a higher frequency than lab strains, suggesting that host-pathogen interactions may promote the emergence of plastic epigenetic responses (Calo et al. 2017).

In addition, environmental stress can also cause heritable epigenetic changes in heterochromatin domains. Specifically, heat shock results in loss of H3K9me2 over constitutive heterochromatin regions in *D. melanogaster* and decreased H3K9me3 over an inserted transgene in *C. elegans* (Seong et al. 2011; Klosin et al. 2017). Both of these effects can be transmitted to

subsequent generations, but whether these changes are truly adaptive is far from clear (Heard & Martienssen 2014; Cavalli & Heard 2019).

1.4.1. Can ectopic heterochromatin formation drive fungal resistance?

In *S. pombe,* synthetic H3K9me heterochromatin domains can be epigenetically inherited in the absence of the putative H3K9 demethylase Epe1 (Audergon et al. 2015; Ragunathan et al. 2015). In addition, ectopic heterochromatin formation has been detected in the absence of key anti-silencing factors including Epe1 or the H3K14 acetyltransferase Mst2 (Zofall et al. 2012; Wang et al. 2015; Parsa et al. 2018; Sorida et al. 2019). The absence of Epe1 alone results in increased H3K9me levels at facultative heterochromatin islands that assemble over DSR-containing meiotic genes or Taz1-bound loci (Zofall et al. 2012; Zofall et al. 2016; Sorida et al. 2019). Combining Epe1 loss with increased RNAPII pausing (by generating mutations in the elongation factor TFIIS), results in the assembly of additional pause-induced heterochromatic regions (PIERs) at euchromatic loci (Parsa et al. 2018).

The combined loss of Epe1 and Mst2 leads to widespread ectopic heterochromatin assembly at euchromatic regions and cells displaying markedly severe growth defects (Wang et al. 2015). Remarkably, *epe1Δmst2Δ* cells, although initially sick, rapidly adapt to the uncontrolled formation of ectopic heterochromatin by assembling H3K9me over the *clr4* locus, thus down-regulating the levels of the Clr4 H3K9 KMT to restrict heterochromatin formation in the genome (Figure 1.15). Strikingly, if the *clr4* locus is genetically manipulated to not assemble H3K9me, cells were found to establish heterochromatin over *rik1*$^{+}$, which encodes another subunit of the Clr4-containing CLRC methyltransferase complex (Wang et al. 2015). These findings demonstrate that ectopic heterochromatin formation has the potential to mediate adaptation to stress in *S. pombe*, at least in mutant cells lacking Epe1 and Mst2.

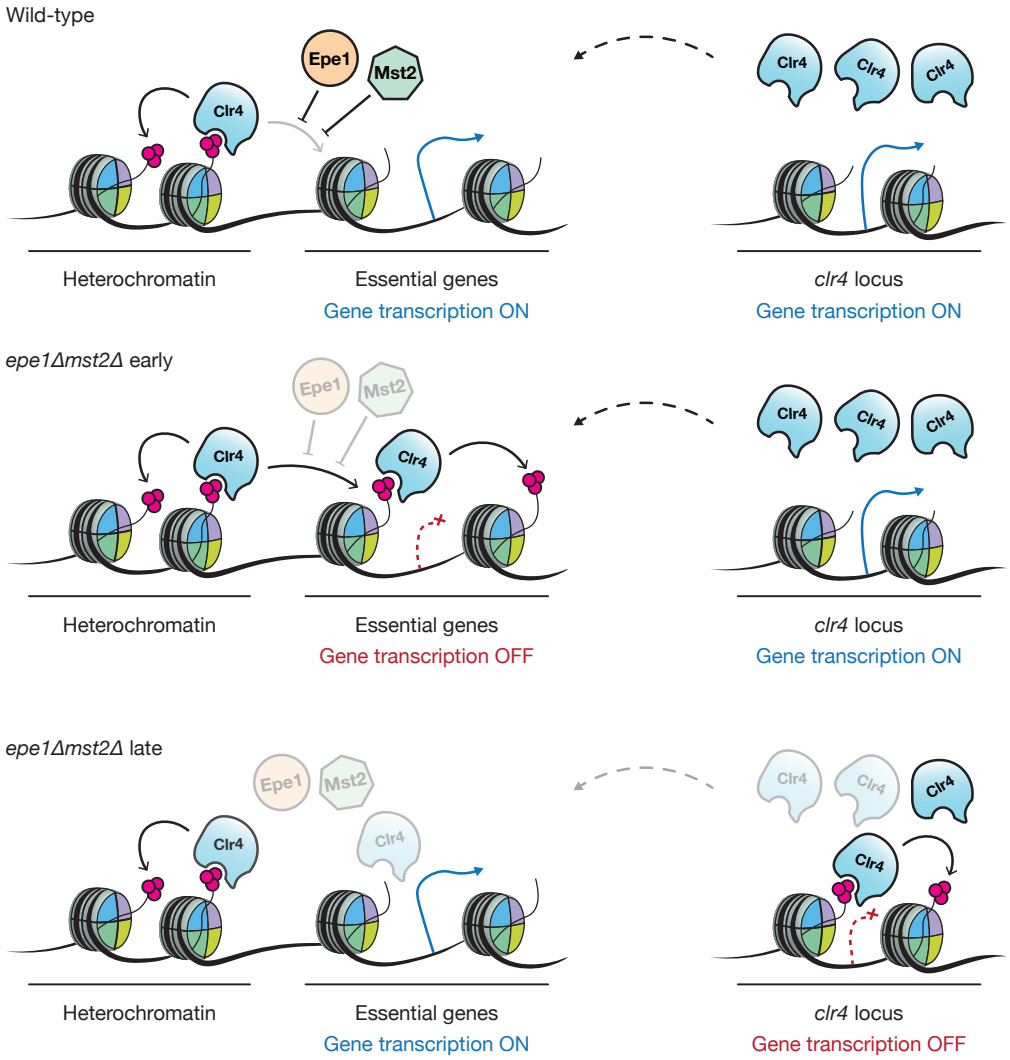

Figure 1.15. Rapid epigenetic adaptation to uncontrolled heterochromatin spreading. Loss of key anti-silencing factors Epe1 and Mst2 results in uncontrolled heterochromatin spreading over essential genes, leading to severe growth defects. Subsequently, cells assemble ectopic heterochromatin at the *clr4* locus to reduce Clr4 levels, establishing an equilibrium that maintains heterochromatin at constitutive locations but minimises heterochromatin spreading over euchromatic loci (Wang et al. 2015).

The ectopic formation of heterochromatin has also been suggested to mediate survival during quiescence in wild-type fission yeast cells. Cellular quiescence (G0) is a ubiquitous stress response through which cells enter reversible dormancy and acquire distinct properties such as resistance to stress and reduced metabolism (Pardee 1974). Joh et al. (2016) reported that as cells enter G0, their survival and global gene expression program become

increasingly dependent on the Clr4 H3K9 methyltransferase and RNAi proteins. G0 entry was shown to result in RNAi-dependent H3K9 methylation of several euchromatic pockets. However, the reported increase in H3K9me levels at ectopic heterochromatin domains is minimal. Moreover, a related study in which similar experiments were performed did not report the presence of ectopic H3K9me at euchromatic loci in G0 cells, nor the emergence of Ago1-associated siRNAs from similar euchromatic regions (Roche et al. 2016).

Lastly, a recent study has proposed that the assembly of ectopic heterochromatin contributes to an adaptive response that regulates gene expression patterns at a low temperature in wild-type *S. pombe* cells (Gallagher et al. 2018). Transcriptional up-regulation of mRNAs during growth at 18°C (optimal growth temperature is 25-32°C) provides feedback to prevent their uncontrolled expression through ectopic heterochromatin assembly. Cells grown at 18°C form novel heterochromatin islands, which require prior mRNA up-regulation for assembly, suggesting that mRNAs recruit Clr4 in *cis* to buffer against uncontrolled expression. Notably, even though cold-induced heterochromatin islands preferentially mapped to stress-responsive genes, cells lacking the H3K9 methyltransferase Clr4 do not exhibit increased cold sensitivity. These results argue against a major role of ectopic heterochromatin assembly in promoting a cold-tolerant phenotype. However, the assembly of ectopic heterochromatin domains following cold treatment in wild-type fission yeast cells suggests that stress- and drug-responsive pathways might control key heterochromatin components to promote cellular plasticity upon external insults.

1.4.1.1. Fungal drug resistance

Worldwide emergence of resistance to antifungal drugs challenges human health and food security. Currently, crop-destroying fungi account for perennial yield losses of ~20% world-wide, with a further 10% loss post-harvest (Fisher et al. 2018). In addition, fungal effects on human health are on the rise, especially in immunocompromised patients. Indeed, global mortality rate for fungal diseases now exceeds that for malaria or breast cancer and is

comparable to those for tuberculosis and HIV (Brown et al. 2012). A limited number of antifungal drugs exists, and resistance is rendering these increasingly ineffective. The most widely used class of fungicides is the azoles, which block biosynthesis of ergosterol, an essential component of fungal plasma membranes. Azoles act in fungi through direct binding to sterol 14-α-demethylase (CYP51, Erg11), a member of the cytochrome P450 superfamily. Azoles are the dominant chemicals in the treatment of fungal infections in crops, livestock and humans (Fisher et al. 2018). Azole resistance can emerge from mutations in the *erg11* coding region that alter the azole-targeting site (Leroux et al. 2007). Resistance can also emerge from mutations in the *erg11* promoter that lead to its transcriptional up-regulation (Hamamoto et al. 2000). Furthermore, structural genome plasticity can also result in resistance, with chromosome arm duplications or extrachromosomal circular DNA formation leading to efflux pump up-regulation and reduced intracellular drug accumulation (Selmecki et al. 2006; Hull et al. 2017; Hull et al. 2019)

1.4.1.2. Drug resistance in *S. pombe*

S. pombe constitutes an ideal system for studying fungal drug resistance because it is amenable to genetic manipulations and shares conserved similarities with some pathogenic fungi. For example, similar to the case in fungal pathogens, *erg11*$^{+}$ overexpression leads to azole resistance in *S. pombe* (Zhang et al. 2015).

Drug treatment triggers the induction of cellular stress pathways which are hardwired to promote cell adaptation and survival upon exposure to diverse external insults. Mitogen-activated protein kinase (MAPK) constitute a large conserved family of proteins that connect cell-surface receptors to critical regulatory targets within the cell. MAPKs are activated through a series of upstream events and ultimately induce the expression of stress-response genes to coordinate different cellular processes that promote stress resistance. The basic architecture of a MAPK pathway consists of three sequentially acting kinases: MAPK kinase kinases (MAPKKKs) phosphorylate

and activate MAPK kinases (MAPKKs), which in turn phosphorylate and activate MAPKs (Morrison 2012).

In *S. pombe*, three distinct MAPK pathways have been identified to date: the stress-activated protein kinase (SAPK) (Sty1) pathway (Shiozaki & Russell 1995), the cell integrity (Pmk1) pathway (Toda et al. 1996), and the pheromone signalling (Spk1) pathway (Toda et al. 1991). The Sty1 and Pmk1 pathways share regulatory links (e.g. the Pyp1, Pyp2 and Ptc1 protein phosphatases) as well as the same downstream target: the ATF/CREB transcription factor Atf1 (Figure 1.16) (Wilkinson et al. 1996; Shiozaki & Russell 1996).

Sty1 activation by the dual phosphorylation of a threonine and a tyrosine residue leads to its translocation to the nucleus. Nuclear Sty1 phosphorylates Atf1, which then binds to a conserved DNA sequence known as the c-AMP responsive element (CRE) to promote transcription of stress-response genes (Chen et al. 2003). Atf1 can form a heterodimer with another ATF/CREB transcription factor, Pcr1, with which it shares many overlapping (CRE) binding sites. Atf1/Pcr1 binding promotes transcriptional activation, but also triggers the recruitment of additional factors, as illustrated for RNAi-independent heterochromatin establishment at the *S. pombe* mating-type locus (see section 1.2.3.1.3). The Sty1 pathway plays a vital role in cell survival under many and diverse stress conditions including oxidative, osmotic, heat and metal stress (Papadakis & Workman 2015). Importantly, the Sty1 pathway is also activated upon exposure to azoles or the drug caffeine (Calvo et al. 2009; Hu et al. 2015).

1.4.1.3. Caffeine resistance in *S. pombe*

The methylxanthine derivative caffeine is one of the most widely used drugs in the world and is available in many mediums for human consumption. This adenosine antagonist provides active psychostimulant action to coffee drinkers by blocking of adenosine receptors which may potentiate dopaminergic neurotransmission (Fulton et al. 2018; Cornelis 2019).

In addition, caffeine is a very well-studied analogue of purine bases that has been involved in a variety of cellular processes in eukaryotic cells, including plants, mammals and fungi (Calvo et al. 2009). Caffeine has shown a wide array of toxic biological effects that interfere with DNA repair, recombination pathways and the cell cycle. For example, in *S. cerevisiae*, caffeine has been reported to affect cell cycle progression as well as cell morphology and integrity (Sutton et al. 1991; Costigan et al. 1992). In *S. pombe*, caffeine has been demonstrated to inhibit DNA repair mechanisms (Gentner & Werner 1975; Osman & McCready 1998), to interfere with both meiotic and UV-induced mitotic recombination (Loprieno et al. 1974; Fabre 1972), and to override the replication checkpoint (Kumagai et al. 1998; Wang et al. 1999). Furthermore, caffeine is known to be an inhibitor of cAMP phosphodiesterase in different eukaryotic cell types (Butcher & Sutherland 1962).

Mechanisms that lead to caffeine resistance in *S. pombe* have been extensively described through traditional genetic studies but also via genome-wide identification of genes required for caffeine tolerance or resistance (Calvo et al. 2009). Caffeine resistance in *S. pombe* can result from mutations that lead to over-expression or modification of a target molecule. Moreover, amplification of repair activities has also been shown to improve survival. Alternatively, cells with reduced import or increased export of the drug also display resistance (Calvo et al. 2009). Exposure to caffeine leads to the activation of the Sty1 stress pathway. Moreover, components of both the Sty1 and Pmk1 stress pathways are required for *S. pombe* tolerance to caffeine, and hyperactivation of either pathway leads to caffeine resistance (Figure 1.16) (Calvo et al. 2009). In addition to the Sty1 and Pmk1 pathways, caffeine tolerance in *S. pombe* requires components of the Pap1-dependent pathway. In fact, all of the initially isolated caffeine-resistant mutants of *S. pombe* are connected to Pap1 function (Figure 1.16) (Kumada et al. 1996; Benkö et al. 1997; Benkö et al. 1998; Benkö et al. 2004).

Pap1 is an AP1-like transcription factor with cytosolic localization prior to stress. In non-stress conditions, reduced Pap1 is constantly exported to the

cytoplasm by the nuclear export factor Crm1 and its cofactor Hba1 (Fornerod et al. 1997; Castillo et al. 2003). Stress conditions trigger the oxidation and conformational change of Pap1, which lead to its dissociation with Crm1-Hba1 and its fast accumulation in the nucleus. Nuclear Pap1 causes the activation of an adaptive transcriptional response (Quinn et al. 2002; Vivancos et al. 2004), including up-regulation of the major efflux transporter Bfr1 (Toone et al. 1998). Intriguingly, caffeine treatment does not lead to Pap1 oxidation/activation (Calvo et al. 2009). However, nuclear Pap1 is required for caffeine tolerance (Calvo et al. 2009), and constitutive nuclear localization of Pap1 confers caffeine resistance (Castillo et al. 2003), mainly through up-regulation of Bfr1 (Calvo et al. 2009).

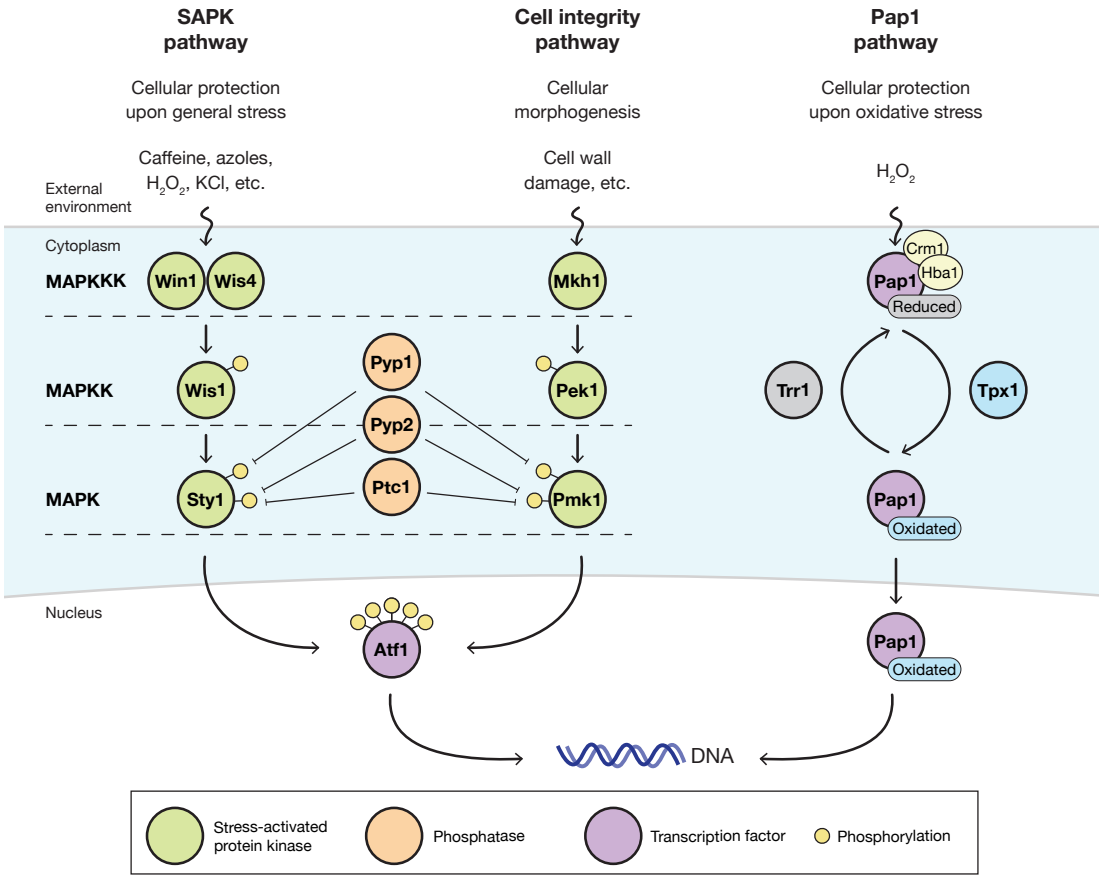

Figure 1.16. Stress pathways required for caffeine tolerance in *S. pombe.* Schematic depiction of key components of the Sty1, Pmk1 and Pap1 stress pathways. Constitutive activation of these pathways through mutation leads to caffeine resistance. Only the Sty1 pathway is activated upon caffeine treatment in wild-type cells (Calvo et al. 2009).

1.5. Aims of this study

Epimutations are potentially adaptive if inherited across generations and might even respond to environmental challenges, yet experimental evidence is scarce. In the fungal model *S. pombe* H3K9me heterochromatin can be epigenetically inherited by a *reader-writer* coupling mechanism and has been observed to arise stochastically at various loci, albeit only in the absence of key anti-silencing factors or specific growth conditions. Thus, it is unknown whether the ectopic formation of heterochromatin can drive the formation of adaptive epimutations in wild-type cells.

The purine analogue caffeine constitutes a well-studied drug and a comprehensive catalogue of fission yeast genes whose deletion confers caffeine resistance is available. I hypothesize that wild-type fission yeast cells might utilize heterochromatin plasticity to form reversible epimutations that drive caffeine resistance through gene silencing in the absence of genetic mutations. Therefore, in this thesis I aim to:

- Identify heterochromatin-dependent epimutants resistant to caffeine.
- Explore the role of adaptive epigenetic changes in facilitating ensuing genetic changes.
- Investigate the mechanisms through which heterochromatin pathways buffer external insults to promote cellular plasticity and adaptation.

Chapter 2: Materials and methods

2.1. Standard techniques and growth conditions

2.1.1. Bacterial protocols

2.1.1.1. Bacterial growth conditions and media

Single *Escherichia coli* colonies were grown in Lysogeny broth (Luria-Bertani, LB) medium (Bertani 1951) at 37°C.

LB medium: 1% w/v Bacto tryptone, 0.5% w/v Bacto yeast extract, 170 mM NaCl. 15 g/L Bacto agar for LB/agar plates.

For plasmid selection, cultures were grown in LB medium containing 50 µg/mL carbenicillin.

2.1.1.2. Bacterial transformation

Approximately 1 to 5 ng of plasmid DNA was transformed into 25 µL of NEB 5-alpha Competent *E. coli* (High Efficiency) (New England Biolabs). DNA and cells were mixed in incubated on ice for 30 min, heat shocked in a water bath at 42°C for 30 sec and left on ice for 5 min before addition of 475 µL of SOC medium. Cells were then grown for 1 hour at 37°C with shaking and plated onto LB medium containing 50 µg/mL carbenicillin.

SOC medium: 2% Tryptone, 0.5% Yeast Extract, 10 mM NaCl, 2.5 mM KCl, 10 mM MgCl2, 10 mM MgSO4, 20 mM glucose.

2.1.1.3. Plasmid isolation (miniprep)

Single bacterial colonies were grown in 5 mL of LB medium plus 50 µg/mL carbenicillin at 37°C overnight. Cells were harvested and miniprep was performed using the Monarch Plasmid Miniprep Kit (New England Biolabs) according to manufacturer's instructions. Plasmid DNA was eluted from

columns using NEB DNA Elution Buffer (10 mM Tris, 0.1 mM EDTA, pH 8.5) and stored at -20°C.

2.1.2. Fission yeast protocols

2.1.2.1. Fission yeast growth conditions and media

Fission yeast *Schizosaccharomyces pombe* was grown at 25°C or 32°C in YES (Yeast Extract plus Supplements) or PMG (Pombe Minimal Glutamate) media.

Wild type haploid strains will grow with the following generation times when in log phase:

YES medium. 25°C: 3 hrs; 32°C: 2 hrs 10 min.

PMG medium. 25°C: 4 hrs, 32°C: 2hrs 30 min.

YES: 0.5% w/v yeast extract, 3% w/v glucose, 225 mg/L supplements (adenine, histidine, leucine, uracil, and lysine hydrochloride), and 20 g/L agar for YES/agar plates.

PMG: 14.7 mM potassium hydrogen phthalate, 15.5 mM Na_2HPO_4, 3.75 g/L L-glutamic acid (monosodium salt), 2% w/v glucose, 20 mL/L 50x salt stock, 1 mL/L 1,000x vitamin stock, 0.1 mL/L 10,000x mineral stock, required supplements, and 20 g/L agar for PMG/agar plates.

Supplement stocks: 5 g/L 50x adenine, 10 g/L 100x arginine, 10 g/L 100x histidine, 10 g/L 100x leucine, 2 g/L 20x uracil.

50x Salt Stock: 260 mM $MgCl_2.6H_2O$, 4.99 mM $CaCl_2.2H_2O$, 670 mM KCl, 14.1 mM Na_2SO_4.

1,000x Vitamin Stock: 4.20 mM pantothenic acid, 81.2 mM nicotinic acid, 55.5 mM inositol, 40.8 mM biotin.

10,000x Mineral Stock: 80.9 mM boric acid, 23.7 mM $MnSO_4$, 13.9 mM $ZnSO_4.7H_2O$, 7.40 mM $FeCl_2.6H_2O$, 2.47 mM molybdic acid, 6.02 mM KI, 1.60 mM $CuSO_4.5H_2O$, 47.6 mM citric acid.

Drugs and additional supplements

Caffeine (CAF) (Sigma, C0750): final concentration of 16 mM unless stated otherwise.

Hydrogen peroxide (H_2O_2) (Sigma, H1009): final concentration of 1 mM.

Clotrimazole (CLZ) (Sigma, C6019): final concentration of 0.29 µM.

Tebuconazole (TEZ) (Sigma, 32013): final concentration of 1.6 µM.

Fluconazole (FLZ) (Sigma, PHR1160): final concentration of 0.6 mM.

Fluoroorotic acid (FOA) (Melford Laboratories): final concentration of 1 g/500mL.

Nourseothricin (cloNAT) (Werner BioAgents): final concentration of 0.1 mg/mL.

Geneticin (G418) (Gibco): final concentration of 0.1 mg/mL.

Hygromycin B (Hyg) (Duchefa Biochemie): final concentration of 0.1 mg/mL.

Anhydrotetracycline hydrochloride (AHT) (Sigma): 10 µM final. 20 mM stock in DMSO was kept at -20°C. Before addition to the medium, 250 µL of this concentrated stock was added into 5 mL of DMSO and then added to 500 mL of medium. To release TetR-Clr4*, cells were grown in the presence of 10 µM AHT for 2 days.

2.1.2.2. *S. pombe* transformation

2.1.2.2.1. Standard transformation of *S. pombe* cells by electroporation

50 mL cultures were grown to log phase ($5x10^6$ to $1x10^7$ cells per mL) and harvested at 3500 x g for 2 min. Cells were then washed three times in 10 mL of 1.2 M ice-cold sorbitol and resuspended in 500 µL of 1.2 M ice-cold sorbitol. 200 µL cells were added to 1 µg of linear DNA in an ice-cold electroporation cuvette. Cells were pulsed using a Gene Pulser II electroporation system (Bio-Rad) with *S. pombe* settings: 2.25 kV, 200 Ω and 25 µF. Immediately following pulse, cells were rapidly mixed with 500 µL of 1.2 M ice-cold sorbitol. For auxotrophic markers, cells were directly plated on selective media. For antibiotic markers, cells were grown overnight in 10 mL of non-selective YES medium before plating on selection. Plates were incubated inverted at 32°C for 3-5 days.

2.1.2.2.2. Transformation of *S. pombe* cells by electroporation for CRISPR/Cas9 genome editing

50 mL cultures were grown to log phase ($5x10^6$ to $1x10^7$ cells per mL) in YES media and harvested at 3500 x g for 2 min. Cells were resuspended in 5 mL of pre-transformation buffer (25 mM DTT, 0.6 M sorbitol, 20 mM HEPES, pH 7.6) and incubated at 32°C for 10 min. Cells were then washed three times in 10 mL of 1.2 M ice-cold sorbitol and resuspended in 500 µL of 1.2 M ice-cold sorbitol. 200 µL cells were added to 200 ng of empty or sgRNA-loaded pLSB or pMZ379 plasmid DNA and 500-1000 ng of HR template DNA (when applicable) in an ice-cold electroporation cuvette. Cells were pulsed using a Gene Pulser II electroporation system (Bio-Rad) with *S. pombe* settings: 2.25 kV, 200 Ω and 25 µF. Immediately following pulse, cells were rapidly mixed with 500 µL of 1.2 M ice-cold sorbitol. Cells were grown overnight in 10 mL of non-selective YES medium before plating on selection (YES plus cloNAT, YES plus G418 or YES plus hygromycin depending on pLSB version used). Plates were incubated at 32°C for 3-5 days.

2.1.2.2.3. Transformation of cryopreserved G1-synchronized *S. pombe* cells by lithium acetate/PEG for CRISPR/Cas9 genome editing

Competent cryopreserved G1-synchronized *S. pombe* cells were prepared as described in Rodríguez-López et al. (2016). Wild-type cells were grown to a concentration of $1x10^7$ cells per mL in EMM media and harvested at 3500 x g for 2 min. Cells were then resuspended in EMM-N and incubated for 2 hrs at 25ºC until cells were of a small round morphology. Following three washes with ice-cold H_2O, cells were resuspended in 2 mL of ice-cold 30% glycerol, 0.1 M lithium acetate (pH 4.9) and 50 µL aliquots were made and stored at -80°C until further usage.

Competent cryopreserved G1-synchronized *S. pombe* cells were transformed using the lithium acetate/PEG method (Sabatinos & Forsburg 2010), as described in Rodríguez-López et al. (2016). Aliquots of cryopreserved, G1-synchronised cells were thawed at 40°C for 2 min. 200 ng of empty or sgRNA-loaded pLSB or pMZ379 plasmid DNA, 500-1000 ng of HR template DNA (when applicable) and 145 µL of 50% PEG 4000 were added to the cells and mixed thoroughly. Note that herring sperm DNA was omitted due to concerns regarding the erroneous integration of these fragments at the targeted loci as described in Longmuir et al. (2019). Cells were then resuspended in 1 mL of EMM-N and incubated for 16 hrs at room temperature. Following incubation, cells were resuspended in 500 µL H_2O and plated onto YES plus cloNAT media. Plates were incubated at 32°C for 3-5 days.

2.1.2.3. *S. pombe* mating and crosses

Crosses were performed on malt extract (ME) medium in order to starve cells of nitrogen and induce mating/sporulation. A similar amount of cells from two strains of opposite mating types (h^+/h^-) were mixed together and incubated for two days at 25°C. The presence of asci containing four spores was assessed by light microscopy. Asci were then resuspended in 300 µL of 1:10 diluted glusulase and incubated at 36°C for 24 hrs. Glusulase digests asci wall and vegetative cells so that only spores remain alive. 5 mL dH_2O was then added

and 2 µL, 5 µL, 10 µL and 40 µL were plated onto YES or PMG agar plates with appropriate selection and incubated for 3-5 days at 32°C.

ME agar plates: 30 g/L malt extract (OXOID), plus supplements, 20 g/L agar.

2.1.2.4. Serial dilution assays

Equal amounts of cells were serially diluted five-fold and then spotted using a custom-made pin onto appropriate media. Cells were grown at 32°C for 3-6 days and then plates were scanned.

2.1.2.5. Unstable caffeine resistance screening

16 mM caffeine was found to be the minimum inhibitory concentration (MIC) for wild-type (*972 h*$^{-}$, Allshire lab strain number 143) *S. pombe* cells on YES plates (see section 3.2). 10^5 wild-type log phase cells were plated onto 16 mM caffeine YES (+CAF) plates and incubated at 32°C. Caffeine-resistant colonies that formed after 7 days were picked and patched to +CAF plates. After 4 days of growth, isolates were frozen (4 days +CAF). 4 days +CAF isolates were re-patched and grown on: 1) non-selective YES plates for 2 days (4 days +CAF, 2 days -CAF) and 14 days (4 days +CAF, 14 days -CAF) and then frozen; 2) +CAF plates for 3 days (7 days +CAF) and 16 days (20 days +CAF) and then frozen. To maintain isolates in a dividing state up to the last time point, isolates were re-patched every 2 days when growing on -CAF plates and every 3 days when growing on +CAF plates.

2.1.2.6. Assessing mutations at the *ade6* and *ura4* loci

Colonies harbouring mutations at the target genes *ade6*$^{+}$ or *ura4*$^{+}$ were identified through a replica-plating assay. cloNAT-resistant colonies were individually picked from YES plus cloNAT plates, re-streaked onto YES plates without selection and incubated at 32°C for two days. Isolates were then replica-plated onto the following plates: YES, YES 1/10 adenine (to examine *ade6*$^{+}$ mutations), PMG minus uracil and PMG plus 5-fluoroorotic acid (to

examine *ura4*$^+$ mutations). Plates were incubated at 32°C for two-four days and then visually examined.

2.2. DNA protocols

2.2.1. Restriction enzyme digestions

Approximately 400 ng of plasmid were digested with 4 U of enzyme for 1 hr at 37°C in the following reaction:

Reagent	*Volume*
H_2O	21.3 µL
CutSmart buffer (or appropriate)	2.5 µL
Plasmid	1 µL
Restriction enzyme	0.2 µL

2.2.2. PCR reaction

2.2.2.1. *Taq* PCR reaction

DNA amplification using *Taq* polymerase (Roche) was used for PCR reactions that do not require precise amplification.

Reagent	*Volume*
H_2O	11 µL
10x *Taq* buffer	2 µL
dNTPs (10 mM stock)	0.5 µL
$MgCl_2$	1 µL
Primer F + Primer R (100 µM stock)	0.2 µL + 0.2 µL
Taq enzyme	0.1 µL
Template	1 ng DNA or 5 µL SPZed cells

Program	
1x	94°C for 4 min
29x	94°C for 30 sec
	55°C for 30 sec
	72°C for 1 min
1x	72°C for 5 min

2.2.2.2. *Pfx* PCR reaction

DNA amplification using *Pfx* polymerase (Invitrogen) was used for PCR reactions that require precise amplification.

Reagent	*Volume*
H_2O	11.7 µL
10x *Pfx* buffer	4 µL
dNTPs (10 mM stock)	0.6 µL
$MgSO_4$	0.4 µL
Enhancer	2 µL
Primer F + Primer R (100 µM stock)	0.1 µL + 0.1 µL
Pfx enzyme	0.1 µL
Template	1 µL genomic prep or 5 ng plasmid
Program	
1x	94°C for 4 min
35x	94°C for 15 sec
	55°C for 30 sec
	68°C for 1 min per kb
1x	68°C for 5 min

2.2.2.3. *Phusion* PCR reaction

DNA amplification using *Phusion* polymerase (New England Biolabs) was used for building DNA constructs that consist of multiple fragments generated by *Pfx* PCR reaction.

Reagent	*Volume*
H_2O	Up to 25 µL
5x *Phusion* buffer	5 µL
dNTPs (10 mM stock)	0.5 µL
Phusion enzyme	0.25 µL
Template	200 ng total DNA in 1:3:1 molar ratio
Program	
1x	98°C for 30 sec
14x	98°C for 15 sec
	58°C for 5 min
	72°C for 1 min
1x	72°C for 5 min

Use 0.5 µL of this PCR product for the next round of PCR (below):

Reagent	*Volume*
H_2O	37.5 µL
5x *Phusion* HF buffer	10 µL
dNTPs (10 mM stock)	1 µL
Primer F + Primer R (100 µM stock)	0.25 µL + 0.25 µL
Phusion enzyme	0.5 µL
Template	0.5 µL from reaction above
Program	
1x	98°C for 30 sec
34x	98°C for 30 sec
	55°C for 30 sec
	72°C for 30 sec per kb
1x	72°C for 7 min

2.2.3. Agarose gel electrophoresis

Agarose gel electrophoresis was used to analyse the size of DNA fragments. Agarose was dissolved in 1x TBE (55 g boric acid, 9.3 g EDTA, 108 g Trizma base) to make an appropriate percentage gel usually between 0.8 and 1.5% agarose. Ethidium bromide at 0.03 µg/mL (Sigma) was added to the agarose gel. Orange G loading buffer (30% glycerol; 0.25% orange G) was added to the DNA samples before loading the gel. After migration, DNA was visualized by UV using a transilluminator.

2.2.4. PCR reaction purification and gel extraction

PCR reactions were purified using Monarch PCR Cleanup Kit (New England Biolabs) and Monarch DNA Gel Extraction Kit (New England Biolabs) according to manufacturer's instructions. DNA fragments were eluted in 15-20 µL of Elution Buffer or TE. Depending on the application, DNA was quantified using a NanoDrop ND-2000c spectrophotometer (Thermo Scientific) or a Qubit fluorometer (Life Technologies) according to manufacturers' instructions.

2.2.5. Gibson Assembly

All Gibson Assembly primers were designed using SnapGene so that following PCR, 40 bp homology between adjacent fragments would be generated. Fragments were prepared by *Pfx* PCR reaction. Fragment concentrations were measured using a Qubit fluorometer (Life Technologies), and Gibson assembly was set up in a 1:3 (vector:insert) molar ratio, using 75 ng vector DNA.

The DNA mixture was added to 10 µl Gibson Assembly Mix (New England Biolabs) in a 20 µL reaction and incubated for 30 min at 50°C. 2 µl Gibson Assembly product was transformed into 50 µl of NEB 5-alpha Competent *E. coli* (High Efficiency) (New England Biolabs).

2.2.6. Sanger sequencing

BigDye Terminator Cycle sequencing kit (Applied Biosystems – Thermo Scientific) was used in the following sequencing reaction.

Reagent	*Volume*
H_2O	Up to 10 µL
Template	20 ng linear DNA 150-300 ng plasmid DNA
Primer (3.2 µM)	1 µL
Big Dye Mix	2 µL
PCR program	
1x	95°C for 5 min
25x	95°C for 30 sec 55°C for 15 sec 64°C for 4 min

2.2.7. *S. pombe* colony PCR

A small amount of fission yeast cells (~1 x 10^4 cells) was incubated in 10 µL of SPZ buffer (1.2 M sorbitol, 100 mM sodium phosphate, 2.5 mg/mL Zymolyase 100T (AMS Biotechnology)) at 37°C for approximately 1 hr. 40 µL H_2O was

added to the cells and 5 µL of the extract was used as a *Taq* or *Pfx* PCR template.

2.2.8. Genomic DNA preparation from *S. pombe*

10 ml of culture was harvested at 3500 x g for 2 minutes. The pellet was resuspended in 250 µl of DNA buffer (0.1 M Tris pH 8; 0.1 M NaCl; 1 mM EDTA; 1% SDS) and 250 µl of phenol. Cells were then mechanically lysed using acid-washed glass beads (Sigma). The DNA was isolated by phenol/chloroform extraction and ethanol precipitated. 1/10 volume of sodium acetate (3 M, pH 5.2) was added followed by 2.5x to 3x volume of 100% ethanol. The sample was incubated on ice for 15 min and harvested at 4°C for 30 min at 14000 x g. The DNA pellet was rinsed with 70% ethanol followed by 15 min centrifugation. The pellet was resuspended in 50 µl TE. DNA was quantified using a NanoDrop ND-2000c spectrophotometer (Thermo Scientific) and stored at -20°C.

2.2.9. Construction of TetR-Clr4* and *4xtetO* tethering sites

For *pDUAL-adh21-TetR-2xFLAG-Clr4-CDΔ* (abbreviated as TetR-Clr4*), the *nmt81* promoter of *pDUAL-nmt81-TetR-2xFLAG-Clr4-CDΔ* (Audergon et al. 2015), was replaced by the *adh21* promoter (pRAD21, gift from Y. Watanabe, (Yamagishi et al. 2008)) by Gibson Assembly. The resulting plasmid was digested by *Not*I and integrated at *leu1*$^{+}$.

4xtetO binding sites constructs were built by amplifying two 200-bp fragments with flanking sequence homology to the integration site from wild-type fission yeast genomic DNA and one *4xtetO* fragment from the *bw5_6+4xtetO* plasmid (containing *4xtetO* binding sites) using *Pfx* PCR reaction. Subsequently, a *Phusion* PCR reaction was performed to join the three fragments together and the PCR product was gel extracted from an agarose gel. Constructs were Sanger sequenced to confirm no mutations had been generated during the cloning process. Oligonucleotides used are listed in Appendix III. *4xtetO*

binding sites constructs were inserted at specific genomic loci using the *SpEDIT* CRISPR/Cas9 genome editing system (described below).

2.2.10. CRISPR/Cas9-mediated genome engineering using the *SpEDIT* system

The *SpEDIT* CRISPR/Cas9 genome editing system for *S. pombe* was developed as part of this thesis with the support of three MSc students: Baptiste Gaborieau, Lorenza di Pompeo and Luke Eivers. See Appendix I for a detailed description of the *SpEDIT* system, including development, validation and full protocol.

Briefly, the *SpEDIT* system uses a synthesised Cas9 sequence codon-optimised for *S. pombe* expressed from the medium strength *adh15* promoter. *SpEDIT* exhibits a flexible modular design where the sgRNA is fused to the 3' end of the self-cleaving hepatitis delta virus (HDV) ribozyme, allowing expression of the sgRNA cassette to be driven by RNA polymerase III from a tRNA gene sequence. Lastly, the inclusion of sites for the *Bsa*I type IIS restriction enzyme flanking a GFP placeholder enables one-step Golden Gate mediated replacement of GFP with synthesized sgRNAs for expression. Both sgRNA and Cas9 modules are expressed from a single plasmid (pLSB), which is available in three versions that use cloNAT (*natMX6*), G418 (*kanMX6*) or hygromycin (*hphMX6*) selectable markers, respectively.

The following strains were constructed by CRISPR/Cas9-mediated genome editing using the *SpEDIT* system: *pap1-N424STOP*, *clr5-Q264STOP meu27-S100Y*, *LocusPX:cup1-3xDSR*, *cup1-TT*, *cup1-L73G*, *cup1-F99G*, *cup1-GFP, 3xFLAG–epe1, epe1Δ* and strains carrying *4xtetO* insertions.

Oligonucleotides used to construct sgRNA-loaded pLSB plasmids and homologous recombination (HR) donor templates are indicated in Appendix III. sgRNA and HR template sequences are indicated in Appendix IV.

For pLSB-NAT construction, the Cas9 gene and the strong *adh1* promoter present in pMZ379 (plasmid generated by Mikel Zaratiegui and provided by

Jürg Bähler (Rodríguez-López et al. 2016)), were replaced by a Cas9 gene codon-optimised for *S. pombe* (custom synthesised, Gen9) and the medium strength *adh15* promoter (from pRAD15, gift from Yoshi Watanabe), respectively, via Gibson assembly. Next, the rrk1/HHR sgRNA cassette present in pMZ379 was replaced by the tDNA/HDV sgRNA cassette (custom synthesised, Gen9) via Gibson Assembly. *Bsa*I sites flanking the GFP placeholder in the tDNA/HDV sgRNA cassette were then introduced using Q5 Site-Directed Mutagenesis Kit (New England Biolabs).

To construct pLSB versions with *kanMX6* (pLSB-Kan, G418 resistance) or *hphMX6* (pLSB-Hyg, hygromycin resistance) selectable markers, the *natMX6* gene from pLSB-NAT was replaced by the *kanMX6 or hphMX6* genes from *pFA6a-kanMX6* (Bähler et al. 1998) or *pFA6a-hphMX6* (Hentges et al. 2005) plasmids, respectively, by Gibson assembly.

2.2.11. Extrachromosomal circular DNA diagnostic PCRs

ChIP-input DNA samples were used as template for PCR with *Taq* polymerase (Roche) according to manufacturer's instructions. Two types of PCR were performed: control PCR for loci present on endogenous chromosome III (expected to be present in wild-type, UR-2 (7 days +CAF) and UR-4 and circle-specific PCRs specific for putative extrachromosomal circles predicted to be present in UR-2 (7 days +CAF) or UR-4. For wild-type and UR-2 (7 days +CAF): control primers were located on either on side of 5S rRNA.24 (primers A (forward), B (reverse); see Appendix III) and 5S rRNA.26 (primers C, D); circle-specific primers were located on either side of a predicted junction between 5S rRNA.24 and 5S rRNA.26 (primers C and B). For wild-type and UR-4: control primers were located on either on side of LTR3 (primers E, F) and or LTR27 (primers G, H); circle-specific primers were located on either side of a predicted junction between LTR3 and LTR27 (primers G and F). For some locations, more than one forward and/or reverse primer was used, for instance: forward primers C1, C2 with reverse primers D1, D2. PCR products were electrophoresed on 2% agarose gels containing ethidium bromide.

2.3. RNA protocols

2.3.1. RNA extraction

10 mL of culture in log phase was harvested and total RNA was extracted using the Monarch Total RNA Miniprep Kit (New England Biolabs) according to the manufacturer's instructions. 10 µg of RNA was treated with Turbo DNase (Invitrogen) and incubated at 37°C for 1 hr to remove contaminating DNA. Depending on the application, RNA was quantified using a NanoDrop ND-2000c spectrophotometer (Thermo Scientific) or a Qubit fluorometer (Life Technologies) according to manufacturers' instructions.

2.3.2. Quantitative reverse-transcriptase PCR (RT-qPCR)

The relative abundance of specific RNA transcripts was quantified by RT-qPCR. Complementary DNA (cDNA) synthesis was performed on 1 µg of DNase treated RNA using LunaScript RT Supermix Kit (New England Biolabs) according to manufacturer's instructions. The LunaScript RT Supermix contains random hexamers, oligo-dT primers, and the Luna Reverse Transcriptase.

Negative controls lacking the reverse transcriptase enzyme (-RT control) were included alongside all RT-qPCR experiments to confirm no DNA was present in the sample before cDNA synthesis. cDNAs were diluted 1/20 with H_2O. Quantitative analysis was performed by qPCR using a LightCycler qPCR instrument (Roche) in 96- or 384-well plates (for a qPCR program see section 2.4.2.1). All transcript levels were calculated by normalizing the product of interest to an internal reference gene mRNA: the highly transcribed housekeeping gene actin: *act1*$^+$; and expressed relative to levels detected in wild-type cells.

Oligonucleotides used for RT-qPCR are listed in Appendix III. qRT-PCR histograms represent three biological replicates; error bars correspond to the standard deviation. *P<0.05 (t test).

2.3.3. Small RNA extraction

50 mL of log phase cells were collected and processed using the mirVana miRNA Isolation kit (Invitrogen) according to manufacturer's instructions to obtain small RNA < 200 nt. Resulting small RNA was treated with the TURBO DNA-free DNase Kit (Thermo Scientific), which allows the removal of the enzyme and divalent cations post-digestion *in tube* and therefore minimises sample loss.

2.4. Protein protocols

2.4.1. Protein extraction and western blot

10^8 log phase cells were harvested at 3500 x g and washed twice in PBS (127 mM NaCl, 2.7 mM KCl, 8mM Na_2HPO_4, 2 mM KH_2PO_4, pH 7.4). Cells were transferred to round-bottomed screw-cap tubes and lysed by bead beating using acid washed glass beads (Sigma) in sample buffer (50 mM Tris pH 6.8, 2% SDS, 2 mM EDTA, 0.03% bromophenol blue 10% glycerol) supplemented with 5 µM PMSF (Thermo Scientific), protease inhibitors (Roche) and 25 µM TCEP (Sigma). 500 µL of sample buffer was used for 10^8 cells. The supernatant was clarified and boiled at 90°C for 3 min. 10 µL of protein was then loaded on NuPAGE 4-12% Bis-Tris gels (Life Technologies). Gels were run at 200 V in 1x NuPAGE MOPS buffer (Life Technologies). Proteins were transferred to a nitrocellulose membrane in 1x transfer buffer (Life Technologies) supplemented with 5% methanol using a XCell Blot Module (Invitrogen) for 1 hr at 20 V.

Membranes were stained with Ponceau red (Sigma) to confirm transfer and blocked for 1 hr at room temperature in PBS + 0.1% tween + 5% milk. Membranes were incubated for 1 hr at room temperature with primary antibody in blocking solution (PBS + 0.1% tween + 5% milk) and then washed thrice (10 min, room temperature) with PBS + 0.1% tween. Membranes were then incubated for 1 hr at room temperature with secondary antibody in PBS + 0.1% tween, washed thrice (10 min, room temperature) with PBS + 0.1% tween and

once (10 min, room temperature) with PBS. Proteins of interest were detected by luminescence using an Enhanced Chemi-Luminescence kit (Amersham).

Antibodies used for western analyses: anti-FLAG-HRP (Sigma, A8591), anti-Myc (Cell Signalling, 9B11), anti-alpha-tubulin (gift from Keith Gull (Woods et al. 1989)), goat anti-mouse (Sigma, A4416), anti-Bip1 (Pidoux & Armstrong 1993), goat anti-rabbit (Sigma, A6154), anti-Cdc11 (gift from Ken Sawin), donkey anti-sheep (Abcam, ab6900) and anti-GFP (Invitrogen, A11122).

2.4.2. Chromatin immunoprecipitation (ChIP)

2.4.2.1. Quantitative ChIP-qPCR (qChIP)

$2.5x10^8$ cells were grown to log phase in non-selective medium and fixed for 15 min at room temperature in 1% paraformaldehyde (Sigma). Cells were washed twice in ice-cold PBS and then stored at -80°C. Cell pellets were resuspended in 350 µL of ice-cold lysis buffer (140 mM NaCl, 50 mM HEPES-KOH pH 7.5, 1 mM EDTA, 1% Triton-X100, 0.1% sodium deoxycholate) supplemented with 1 mM PMSF (Thermo Scientific) and protease inhibitors (Roche). 500 µL of acid washed glass beads were added to the samples in order to mechanically break the cells by bead beating (two pulses of 1 min each, with resting on ice in between). The lysate was recovered and the chromatin sheared by sonication using a Bioruptor (Diagenode) for 20 min, 30 sec ON/OFF cycles (HIGH setting) in order to obtain chromatin fragments of approximately 300 to 900 bp. The lysate was centrifuged for 20 min at 17,000 x g and the supernatant was transferred to fresh tubes. 10 µL of sample was retained as input control and 290 µL used for immunoprecipitation. 25 µL of pre-washed protein G Dynabeads (Invitrogen) and 1 µL of anti-H3K9me2 monoclonal antibody (m5.1.1, a kind gift by Takeshi Urano) or 2 µL of anti-GFP polyclonal antibody (Invitrogen) were added to the lysates and immunoprecipitation was performed on a rotating wheel overnight at 4°C. Samples were washed briefly in lysis buffer, 10 min in lysis buffer containing 0.5 M NaCl, 10 min in wash buffer (10 mM Tris-HCl pH 8, 0.25 M lithium chloride, 0.5% NP-40, 1 mM EDTA, 0.5% sodium deoxycholate) and briefly in

TE buffer (10 mM Tris-HCl pH 8, 1 mM EDTA). 100 µL of 10% Chelex resin (BioRad) was added to each input and IP sample and samples were boiled for 12 min at 100°C to extract the DNA. Samples were then incubated for 45 min at 55°C with 2.5 µL of proteinase K (10 mg/mL). Proteinase K was inactivated by boiling the samples at 100°C for 10 min. Samples were then recovered in fresh tubes and analysed by qPCR. qPCRs were performed in 96- or 384-well plates (Roche) with 10 µL of PCR reaction per well. Input DNA was diluted 1/100 and IP DNA was diluted 1/20 in H_2O for qPCR.

Reagent	*Volume*
H_2O	1.9 µL
LightCycler 480 SYBR Green Master Mix (Roche)	5 µL
Primer F + Primer R (100 µM stock)	0.05 µL each
Template DNA	3 µL

PCR program	
1x	95°C for 2 min
45x	95°C for 20 sec
	55°C for 20 sec
	72°C for 20 sec

Data were analysed using the LightCycler 480 Software (Roche). All ChIP enrichments were calculated as % DNA immunoprecipitated at the locus of interest relative to the corresponding input samples and normalized to % DNA immunoprecipitated at *act1*$^+$ locus. Histograms represent data averaged over three biological replicates. Error bars represent standard deviations from three biological replicates. For spike-in qChIPs, an equal number (~20%) of *Schizosaccharomyces octosporus* cells (H3K9me2 qChIP) (as described in Tong et al. 2019) or Sgo1-GFP *Saccharomyces cerevisiae* cells (GFP qChIP) (a gift from Adele Marston) were added to initial *S. pombe* pellets.

2.4.2.2. ChIP-seq

A modified ChIP protocol was used for ChIP-seq. $7.5x10^8$ cells were grown to log phase in non-selective medium and fixed for 15 min at room temperature in 1% paraformaldehyde (Sigma). Cells were washed twice in ice-cold PBS

and then stored at -80°C. Cell pellets were resuspended in 650 µL of ice-cold lysis buffer (140 mM NaCl, 50 mM HEPES-KOH pH 7.5, 1 mM EDTA, 1% Triton-X100, 0.1% sodium deoxycholate) supplemented with 1 mM PMSF (Thermo Scientific) and protease inhibitors (Roche). 500 µL of acid washed glass beads were added to the samples in order to mechanically break the cells by bead beating (four pulses of 1 min each, with resting on ice in between). The insoluble chromatin fraction was pelleted by centrifugation at 6000 x g for 8 min and washed with 1 mL lysis buffer before resuspension in 300 µL lysis buffer containing 0.2% SDS. Chromatin was sheared by sonication using a Bioruptor (Diagenode) for 30 min, 30 sec ON/OFF cycles (HIGH setting) in order to obtain fragments of approximately 150 bp. 900 µL of lysis buffer (no SDS) were added and samples clarified by centrifugation at 17,000 x g for 20 min. 15 µL of supernatant were retained as input control and the rest (approximately 1100 µL) used for immunoprecipitation.

75 µL of pre-washed protein G Dynabeads (Invitrogen) and 6 µL of anti-H3K9me2 monoclonal antibody (m5.1.1, a kind gift by Takeshi Urano) were added to the samples and immunoprecipitation was performed on a rotating wheel overnight at 4°C. Samples were washed in lysis buffer for 10 min, twice for 8 min in lysis buffer containing 0.5 M NaCl, twice for 8 min in wash buffer (10 mM Tris-HCl pH 8, 0.25 M lithium chloride, 0.5% NP-40, 1 mM EDTA, 0.5% sodium deoxycholate) and once for 10 min in TE buffer (10 mM Tris-HCl pH 8, 1 mM EDTA). Washed beads and input samples were resuspended in ChIP elution buffer (10 mM Tris pH 8.0, 300 mM NaCl, 5 mM EDTA, 1% SDS) and incubated at 65°C overnight with shaking to reverse crosslinks. Samples were then treated with 2 µL of DNase-free RNase (Roche, 0.5 µg/µL) at 37°C with shaking for 1 hr and with 20 µL of proteinase K (10 mg/mL) at 55°C with shaking for 2 hrs. Immunoprecipitated DNA was recovered using QIAquick PCR Purification Kit (Qiagen). Optimal enrichment was assessed by qPCR as described in section 2.4.2.1 above using primers for control loci.

2.5. Library construction

2.5.1. RNA-seq library construction

Total RNA was extracted using the Monarch Total RNA Miniprep Kit (New England Biolabs) and treated with TURBO DNase (Invitrogen) as indicated in section 2.3.1. rRNA was removed using the Ribo-Zero Gold rRNA removal kit (Yeast) (Illumina). RT-qPCR control experiments confirmed that >95% of rRNA was removed using this methodology. rRNA depleted RNA was analysed using a 2100 Bioanalyzer instrument (Agilent Technologies) to confirm RNA Integrity Number (RIN) was above 7. 100 ng of RNA was used for strand-specific library construction using NEBNext Ultra II Directional RNA Library Prep Kit for Illumina (New England Biolabs) following manufacturer's instructions. Directionality was achieved by the addition of deoxyuridine-trisphosphate (dUTP) during second strand synthesis step and subsequent cleavage of the uridine-containing strand by treatment of the sample with Uracil DNA Glycosylase. Libraries were quantified using a Qubit fluorometer (Life Technologies) and fragment size distribution was analysed using a 2100 Bioanalyzer instrument (Agilent Technologies) according to manufacturer's instructions. Libraries were then pooled and sequenced on an Illumina NextSeq system platform (Genome Facility, Western General Hospital, Edinburgh) by 75-bp paired-end sequencing.

2.5.2. Small RNA-seq library construction

Small RNAs (sRNAs) were extracted using the mirVana Isolation kit (Invitrogen) and treated with TURBO DNase (Invitrogen) as indicated in section 2.3.3. Isolated sRNAs were quantified using a Qubit fluorometer (Life Technologies) and analysed using a 2100 Bioanalyzer instrument (Agilent Technologies) to confirm optimal sample integrity. 100 ng of sRNAs was taken to construct libraries using NEBNext Multiplex Small RNA Library Prep Set for Illumina (New England Biolabs) according to manufacturer's instructions. After PCR amplification, gel size selection was performed using 6% Novex TBE PAGE gels (Life Technologies) and Costar Spin-X Centrifuge Tube

Filters (Sigma). Libraries were quantified using a Qubit fluorometer (Life Technologies) and fragment size distribution was analysed using a 2100 Bioanalyzer instrument (Agilent Technologies) according to manufacturer's instructions. Libraries were then pooled and sequenced on an Illumina NextSeq system platform (Genome Facility, Western General Hospital, Edinburgh) by 50-bp single-end sequencing.

2.5.3. ChIP-seq library construction

Illumina-compatible ChIP-seq libraries were prepared as described in Tong et al. (2019). Libraries were prepared with 1-5 ng of ChIP or 10 ng of input DNA. DNA was subjected to blunting and phosphorylation using Blunt Enzyme Mix (New England Biolabs, E1201), at room temperature for 45 min (see blunting reaction below). Ampure XP (Beckman) beads equilibrated to room temperature were used in a 1.6:1 ratio to samples (80 µl of beads mixed to 50 µl of sample), to purify fragments >100 bp onto beads. According to the standard Ampure XP protocol, beads were incubated with samples for 10 min, collected on a magnet for 5 min, washed twice with 250 µl of 80% EtOH and dried for 5 min. DNA was eluted from beads by resuspending beads in 30 µl nuclease-free water (Ambion) for 5 min, beads were then collected on a magnet for 5 minutes and the supernatant was transferred to a fresh tube. Next, a dA-tailing reaction was carried out using Klenow (exo-) (New England Biolabs, M0212) at 37°C for 30 minutes (see dA-tailing reaction below). The enzyme was heat-inactivated for 5 minutes at 75°C and the reaction was cooled on ice for 5 minutes. Using the dA overhangs, NEXTflex (Bioo Scientific) barcoded adapters were ligated to the fragments, using Quick Ligase (New England Biolabs, M2200) for 25 minutes at room temperature (see adapter ligation reaction below). Excess adapters were cleared by two sequential rounds of 1:1 Ampure XP purification (as detailed above) first with 70 µl beads, then with 50 µl. DNA was eluted in 30 µl water, and 10 µl was used for *Phusion* PCR amplification (see *Phusion* PCR reaction below). Following PCR, large DNA fragments were firstly cleared by a 0.65x purification (32.85 µl of Ampure XP beads added to 50 µl sample), a ratio that

binds >300 bp fragments on beads. Following the binding, beads were collected and the supernatant containing the fragments of interest (<300 bp) was transferred to a fresh tube. The 80 µl supernatant was mixed with 55 µl of beads, resulting in 1:1.6 purification that binds fragments >100 bp onto beads. Beads were eluted in 50 µl water and subjected to a final 1:1 Ampure XP purification. Finally, amplified libraries were eluted in 30 µl water. Libraries were quantified using a Qubit fluorometer (Life Technologies) and fragment size distribution was analysed using a 2100 Bioanalyzer instrument (Agilent Technologies) according to manufacturer's instructions. Libraries were then pooled to allow multiplexing and sequenced on an Illumina HiSeq2000 system (Edinburgh Genomics), Illumina NextSeq system (Genome Facility, Western General Hospital, Edinburgh) or Illumina MiniSeq system (Allshire Lab) by 75-bp paired-end sequencing.

Blunting reaction

Reagent	*Volume*
DNA	1-5 ng IP DNA or 10 ng input DNA
10x Blunting buffer	5 µl
1 mM dNTPs	5 µl
Blunt Enzyme Mix	1 µl
H_2O	up to 50 µl

dA-tailing reaction

Reagent	*Volume*
DNA	27.7 µl
NEB buffer 2	3.3 µl
10 mM dATP	1 µl
Klenow (exo-)	1 µl

Adapter ligation reaction

Reagent	*Volume*
DNA	33 µl
2x Quick ligase buffer	35 µl
0.5 µM adapters	1 µl
Quick ligase	1 µl

Phusion PCR reaction

Reagent	*Volume*
DNA	10 µl
1 mM dNTPs	10 µl
5x *Phusion* HF buffer	10 µl
PCR primer mix (12.5 µM each)	2 µl
DMSO	1.5 µL
Phusion polymerase	0.5 µL
H_2O	up to 50 µl

2.6. In-house MiniSeq sequencing

The molarity of ChIP-seq NGS libraries was calculated from the Qubit concentration measurements and the average fragment size from the 2100 Bioanalyzer results. All libraries were diluted to 1 nM in Qiagen EB buffer, and samples sequenced on the same sequencing cartridge were pooled together in a 1:4 (input:IP) ratio, in ~50 µl volume. 5 µl of pooled library was denatured with 5 µl 0.1 N NaOH at room temperature for 5 minutes, after which the reaction was stopped by the addition of 5 µl Tris-HCl pH 7.0. Denatured libraries were diluted with 985 µl hybridisation buffer (Illumina, supplied with the MiniSeq sequencing cartridge), and 150 µl of the pooled libraries was further diluted by addition of 350 µl hybridisation buffer. The resulting 500 µl 1.5 pM library was loaded on a thawed sequencing cartridge (Illumina, FC-420-1002) and sequenced on an Illumina MiniSeq instrument in paired-end mode, with read 1 and read 2 each being 76 bp long.

2.7. Bioinformatics

2.7.1. ChIP-seq analysis

Approximately 6-10 million 75 bp paired-end reads were produced for each sample. Raw reads were then de-multiplexed and trimmed using Trimmomatic (v0.35) (Bolger et al. 2014) to remove adapter contamination and regions of poor sequencing quality. Trimmed reads were aligned to the *S. pombe* reference genome (*972h*$^{-}$*,* ASM294v2.20) using Bowtie2 (v2.3.3) (Langmead & Salzberg 2012). Resulting bam files were processed using Samtools (v1.3.1)

(Li et al. 2009) and picard-tools (v2.1.0) (http://broadinstitute.github.io/picard) for sorting, removing duplicates and indexing. Coverage bigwig files were generated by BamCoverage (deepTools v2.0) and ratios IP/input were calculated using BamCompare (deepTools v2.0) (Ramírez et al. 2016) in SES mode for normalisation (Diaz et al. 2012). Peaks were called using MACS2 (Zhang et al. 2008) in PE mode and broad peak calling (broad-cutoff = 0.05). Region-specific H3K9me2 enrichment plots were generated using the Sushi R package (v1.22) (Phanstiel et al. 2014). Heatmaps were generated using computeMatrix and plotHeatmap (deepTools v2.0) (Ramírez et al. 2016).

2.7.2. SNP and indel calling

SNPs and indels were called as described in Jeffares et al. (2015). Trimmed reads were mapped to the *S. pombe* reference genome (*972h*$^{-}$, ASM294v2.20) using Bowtie2 (v2.3.3) (Langmead & Salzberg 2012). GATK (McKenna et al. 2010; Van der Auwera et al. 2013) was used for base quality score recalibration. SNPs and indels were called with GATK HaplotypeCaller (McKenna et al. 2010; Van der Auwera et al. 2013) and filtered using custom parameters. Functional effect of variants was determined using Variant Effect Predictor (McLaren et al. 2016).

2.7.3. Copy number variation analysis

Copy number variation was determined using CNVkit (Talevich et al. 2016) in Whole-Genome Sequencing (-wgs) mode. Wild-type ChIP-seq input bam files were used as reference.

2.7.4. Code availability

The complete Workflow Description Language (WDL) pipeline script used for ChIP-seq and variation analyses is available at:

https://github.com/SitoTorres/Torres-Garcia-et-al.-2019

2.7.5. RNA-seq analysis

Adapter-trimmed reads were aligned to the *S. pombe* reference genome (*972h-,* ASM294v2.20) using STAR (v2.2.1) (Dobin et al. 2013) and processed using Samtools (v1.3.1) (Li et al. 2009). Coverage bigwig files were generated by BamCoverage (deepTools v2.0) (Ramírez et al. 2016). Differential expression was analysed using the Bioconductor Rsamtools (v2.0.3), GenomicFeatures (v1.36.4) (Lawrence et al. 2013) and DESeq2 (v.1.24) (Love et al. 2014) R libraries. Log2 fold changes were shrunk using the apeglm method (Zhu et al. 2019) and a MA-plot was generated using R. Genes with an adjusted *p* value below 0.01 are shown in red.

2.7.6. Small RNA-seq analysis

Raw reads were then de-multiplexed and processed using Cutadapt (v1.17) to remove adapter contamination and discard reads shorter than 19 nucleotides or longer than 25 nucleotides. Coverage plots were generated using SCRAM (Fletcher et al. 2018).

2.8. Data availability

Sequencing data generated in this thesis have been submitted to GEO under accession number: GSE138436.

2.9. Cytology (Performed by Dr. Alison Pidoux)

S. pombe cultures were fixed before processing for immunofluorescence as described (Tong et al. 2019). Briefly, cells in YES culture were fixed with 3.7% formaldehyde (Sigma, F8775) for 30 min, followed by cell wall digestion with Zymolyase-100T (AMS Biotechnology) in PEMS buffer (100 mM PIPES pH 7, 1 mM EDTA, 1 mM $MgCl_2$, 1.2 M sorbitol). After permeabilization with Triton-X100, cells were washed, blocked in PEMBAL (PEM containing 1% BSA, 0.1% sodium azide, 100 mM lysine hydrochloride). Rabbit anti-GFP (Invitrogen, A11122) was used in PEMBAL at 1:500 dilution, and Alexa 488-coupled chicken-anti-rabbit secondary antibody (Invitrogen, A21441) at 1:1000 dilution.

Arg11-mCherry fluorescence survived fixation and no antibodies were used for localisation. Cells were stained with DAPI and mounted in Vectashield. Microscopy was performed with a Zeiss Imaging 2 microscope (Zeiss) using a 100x 1.4NA Plan-Apochromat objective, Prior filter wheel, illumination by HBO100 mercury bulb. Image acquisition with a Photometrics Prime sCMOS camera (Photometrics, https://www.photometrics.com) was controlled using Metamorph software (Universal Imaging Corporation). Exposures were 3000 ms for FITC/Alexa-488 channel (Cup1-GFP/Alexa 488), 500 ms for TRITC channel (Arg11-mCherry) and 100 ms for DAPI. For display of images, maximum intensity was determined for e.g. Cup1-GFP staining in Cup1-GFP Arg11-mCherry strain (B4909) and this maximum was applied for scaling of all B4909 and B4912 (expresses only Arg11-mCherry) images. FITC and TRITC channels were scaled in this way; DAPI images were autoscaled.

Chapter 3: Identification of heterochromatin-dependent epimutants resistant to caffeine

3.1. Introduction

Genes embedded in H3K9 methylation-dependent heterochromatin are transcriptionally silenced (Bannister et al. 2001; Lachner et al. 2001; Allshire & Madhani 2018). In the fungal model organism *S. pombe*, H3K9me heterochromatin can be epigenetically inherited by a *reader-writer* coupling mechanism provided the counteracting putative H3K9 demethylase Epe1 is absent (Zhang et al. 2008; Audergon et al. 2015; Ragunathan et al. 2015). H3K9me heterochromatin has been observed to arise ectopically at various loci in the absence of key anti-silencing factors such as Epe1 (Zofall et al. 2012; Wang et al. 2015; Parsa et al. 2018; Sorida et al. 2019), or the H3K14 acetyltransferase Mst2 (Wang et al. 2015). Ectopic islands of H3K9me have also been detected in wild-type cells grown at low temperature (Gallagher et al. 2018), but whether these cold-induced heterochromatin islands have adaptive potential is unknown.

It is possible that upon exposure to a lethal insult wild-type cells might utilize heterochromatin plasticity to form epimutations, which could drive an adaptive resistant phenotype through heterochromatic gene silencing in the absence of DNA changes. Epimutations, unlike genetic mutations, are predicted to be unstable (Jeggo & Holliday 1986; Oey & Whitelaw 2014), resulting in gradual loss of resistance following growth without the insult. To test this possibility, the well-studied purine analogue caffeine was chosen as insult because deletion of many genes with a variety of cellular roles confers caffeine resistance (Calvo et al. 2009), thereby increasing the chance of obtaining epimutations. Furthermore, many caffeine-resistant mutants display a multidrug resistance phenotype (Benkö et al. 1998; Carobbio et al. 2001; Castillo et al. 2003), suggesting that potential caffeine-resistant epimutants might also exhibit resistance to additional toxic compounds. In this chapter, I investigated whether wild-type fission yeast cells can acquire an unstable

caffeine-resistant phenotype through the formation of adaptive heterochromatin-mediated epimutations.

3.2. Screening strategy for the identification of unstable caffeine-resistant isolates

Epimutations have been proposed to enable 'soft inheritance', resulting in the formation of distinct phenotypes that enable initial adaptation to challenging and fluctuating environments (Richards 2006). It was surmised that unstable epimutants would occur more frequently at moderate caffeine concentrations that prevent most cells from growing rather than at high stringency selection used in conventional screens for genetic caffeine-resistant mutants (Benkö et al. 1997; Calvo et al. 2009). Genetic screens for caffeine resistance have traditionally been performed using rich medium (yeast extract, YE) plates containing 20 mM or higher caffeine concentrations (30 mM caffeine in initial caffeine resistance screens (Benkö et al. 1997; Benkö et al. 1998)), and caffeine has been shown to inhibit the growth of wild-type *S. pombe* cells at concentrations starting from 15 mM in YE (Calvo et al. 2009). However, similar amounts of caffeine might have different effects depending on the particular laboratory strain, medium recipe, or purity of the compound.

To determine the minimum inhibitory concentration (MIC) of caffeine for the specific wild-type fission yeast laboratory strain that will be used throughout this thesis, a lethal concentration test was performed. Log phase 972 h^- wild-type fission yeast cells (Leupold 1949; Fantes & Hoffman 2016) were serially diluted and spotted on rich medium (yeast extract plus supplements, YES) plates containing 10, 12, 14, 15, or 16 mM caffeine (Figure 3.1). Results showed that cell growth is moderately impaired in the presence of 14-15 mM caffeine and abolished on plates containing 16 mM caffeine. Therefore, 16 mM was identified as the minimum inhibitory concentration of caffeine for 972 h^- wild-type fission yeast cells on rich medium (YES) plates (referred to as +CAF medium from here on).

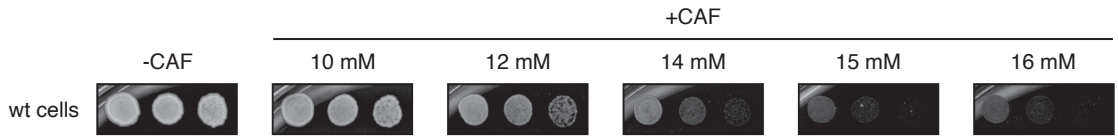

Figure 3.1. Exposure to 16 mM caffeine abolishes the growth of wild-type fission yeast. Growth of wild-type fission yeast cells in the presence of caffeine. 972 h^- wild-type (wt) fission yeast cells were serially diluted and spotted on rich medium (yeast extract plus supplements, YES) plates containing 10, 12, 14, 15, or 16 mM caffeine (+CAF).

To screen for unstable caffeine-resistant isolates, caffeine-resistant colonies that had grown 7 days after plating wild-type cells on +CAF medium were picked, propagated in the presence of caffeine for 4 days, and then frozen (4 days +CAF, initial isolates) (Figure 3.2A). Subsequently, initial isolates were successively propagated in the absence of caffeine (-CAF medium) for 2 and 14 days, and then frozen (4 days +CAF, 2 or 14 days -CAF) (Figure 3.2A and Methods section 2.1.2.5). Cells from the same initial isolate but frozen at different stages (4 days +CAF, 4 days +CAF 2 days -CAF, and 4 days +CAF 14 days -CAF) were then serially diluted and spotted on -CAF and +CAF medium to assess resistance to caffeine. Unstable caffeine-resistant isolates (potential epimutants) are expected to lose resistance to caffeine after 14 days (approximately 140 cell divisions) of non-selective growth whereas stable isolates (potential mutants) are predicted to maintain caffeine resistance indefinitely (Figure 3.2B). Caffeine resistance at the 4 days +CAF 2 days -CAF stage was assessed in order to detect and discard isolates exhibiting an overly unstable phenotype that would prevent any further manipulations (Figure 3.2B).

As other secondary events might also occur upon prolonged growth on caffeine, consecutive aliquots of each initial isolate were frozen after continued growth on caffeine for 3 days (7 days +CAF) and 16 days (20 days +CAF) (Figure 3.2A and Methods section 2.1.2.5). This provided a time series, permitting detection and separation of potential initiating and subsequent secondary events.

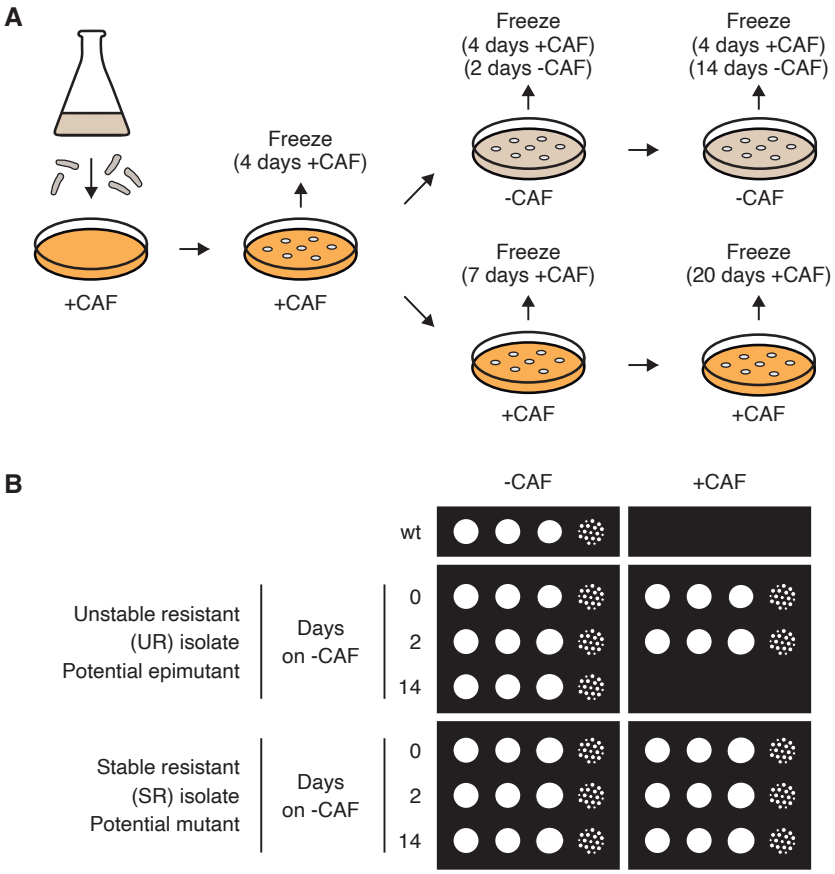

Figure 3.2. Screening strategy for the identification of unstable caffeine-resistant isolates. A. Wild-type (wt) *S. pombe* cells were plated on 16 mM caffeine-containing (+CAF) medium. Caffeine-resistant colonies were picked, propagated on +CAF medium for 4 days and then frozen (4 days +CAF, initial isolates). Subsequently, initial isolates were successively propagated on non-selective (-CAF) medium for 2 and 14 days or on +CAF medium for a total of 7 and 20 days, and then frozen (see Methods section 2.1.2.5 for further details). **B.** Schematic depiction of predicted scenarios. Assessment of resistance to caffeine by serial dilution on -CAF and +CAF plates after growth on -CAF medium for 2 and 14 days. Unstable (UR) caffeine-resistant isolates (potential epimutants) are expected to lose resistance to caffeine after 14 days of non-selective growth, whereas stable (SR) caffeine-resistant isolates (potential mutants) are expected to maintain caffeine resistance indefinitely.

3.3. Results

3.3.1. Identification of unstable caffeine-resistant isolates

To identify unstable caffeine-resistant isolates, three independent screens were performed. After plating a total of 1.61 x 10^6 wild-type cells on +CAF plates, 825 caffeine-resistant colonies were obtained (approximately 1 resistant colony per 2000 plated cells), and 176 were arbitrarily taken for further processing using the screening strategy detailed above (see section 3.2). Additional caffeine-resistant colonies obtained here were not further processed due to time and logistical constraints. Re-challenging 176 isolates with caffeine revealed that 23% lost their caffeine resistance after 14 days of non-selective growth (denoted 'unstable resistant' isolates, UR) whereas 13% remained caffeine resistant (denoted 'stable resistant' isolates, SR). 64% of isolates did not display a clear reproducible resistant phenotype (denoted 'unclear') (Figure 3.3).

To determine whether the loss of resistance in unstable isolates occurs abruptly or progressively over time, isolates UR-1, UR-2, SR-1 and SR-2 were propagated in the absence of caffeine for 2, 4, 8, 12 and 16 days. Re-exposing isolates to caffeine showed that caffeine resistance is lost progressively over time in unstable isolates whereas it is stably maintained for at least 16 days (approximately 160 cell divisions) in stable isolates (Figure 3.4). Moreover, results revealed that independent unstable isolates can display different levels of instability. Indeed, caffeine resistance is lost in UR-1 cells following 8 days of non-selective growth, whereas a clear loss of resistance is only observed in UR-2 cells after 12 days of growth in the absence of caffeine (Figure 3.4).

These results indicate that the proposed screening strategy enables the identification of unstable caffeine-resistant isolates. In unstable isolates, caffeine resistance reverts progressively over time to a wild-type caffeine-sensitive phenotype. The reversibility of this phenotype suggests that resistance might be mediated via epigenetic processes, such as the formation of ectopic H3K9me heterochromatin.

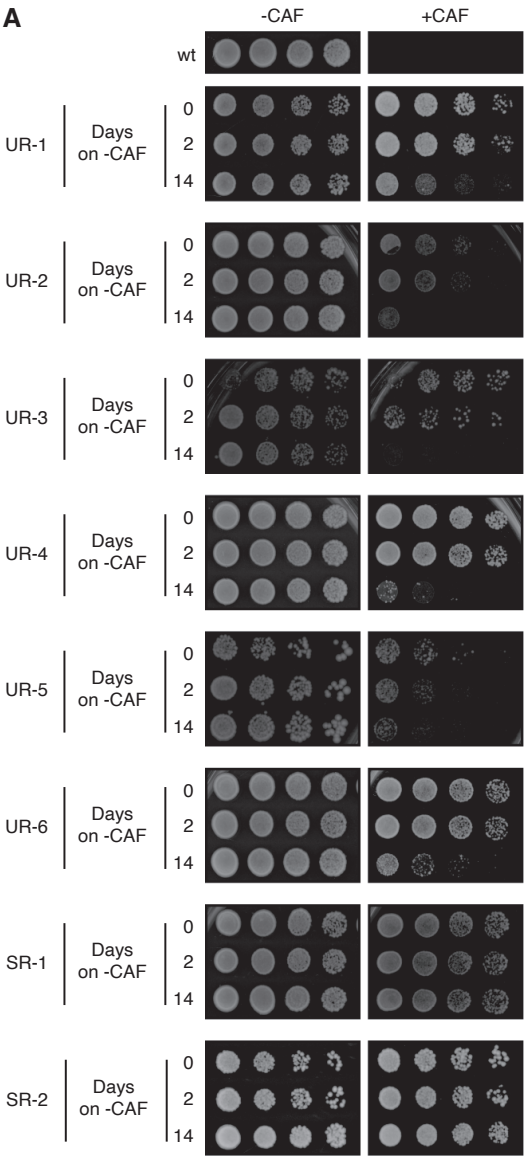

B

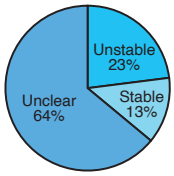

Screen	Plated cells	Resistant isolates	Analyzed isolates	Unstable (UR)	Stable (SR)	Unclear
1	1.2×10^5	87	48	19%	8%	73%
2	6.4×10^5	367	47	21%	29%	49%
3	8.5×10^5	371	81	26%	6%	68%

Figure 3.3. Identification of unstable caffeine-resistant isolates. A. Unstable (UR) and stable (SR) caffeine-resistant isolates were identified using the screening strategy described in Figure 3.2. After growth on non-selective medium for 2 and 14 days, caffeine-resistant isolates were serially diluted and spotted on -CAF and +CAF media to assess resistance to caffeine. Isolates taken for further analyses are shown. **B.** Frequencies of unstable and stable caffeine-resistant isolates obtained from three independent screens. 64% of isolates did not display a clear phenotype (unclear).

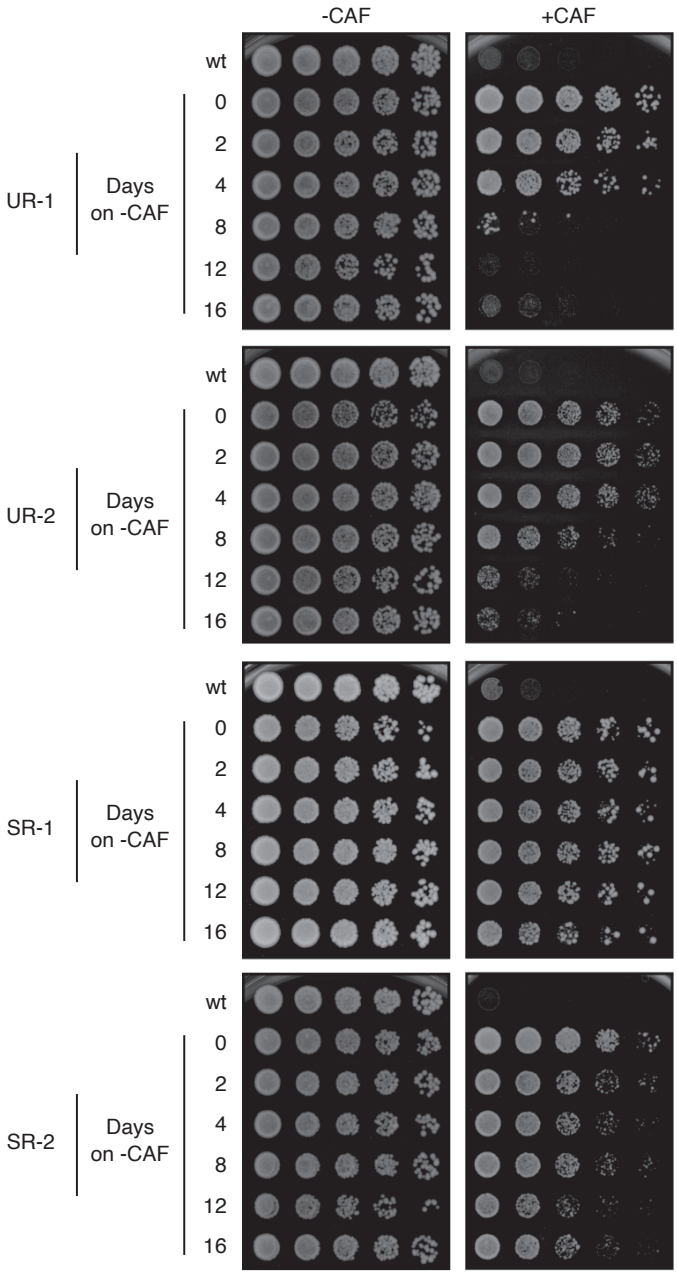

Figure 3.4. Caffeine resistance is lost progressively in unstable isolates but maintained in stable isolates. After growth in the absence of caffeine for 2, 4, 8, 12 and 16 days, unstable caffeine-resistant isolates (UR-1 and UR-2) and stable caffeine-resistant isolates (SR-1 and SR-2) were serially diluted and spotted on -CAF and +CAF media to assess resistance to caffeine.

3.3.2. Caffeine resistance depends on the Clr4 H3K9 methyltransferase in unstable caffeine-resistant isolates

The *S. pombe* genome contains a single H3K9 methyltransferase, the Su(var)39 orthologue Clr4 (Wood et al. 2002). Clr4 is responsible for all methylation on H3K9 (Ivanova et al. 1998; Rea et al. 2000), and deletion of *clr4*$^{+}$ results in genome-wide loss of H3K9 heterochromatin (Cam et al. 2005).

To test whether caffeine resistance in unstable isolates requires heterochromatin, the *clr4*$^{+}$ gene was deleted in isolates UR-1 and UR-2. In addition, *clr4*$^{+}$ was also deleted in stable isolates SR-1 and SR-2 to exclude a general requirement for Clr4/heterochromatin in caffeine resistance (Figure 3.5). Standard gene deletion in *S. pombe* entails transformation of cells with a construct that includes the desired deletion alongside a selectable marker. The DNA construct integrates in the genome via flanking regions that target the genomic locus of interest. The complete deletion protocol requires cells to be grown in the absence of caffeine for approximately 7 days (see Methods section 2.1.2.2.1). Thus, to determine whether a hypothetical loss of resistance in unstable isolates following deletion of *clr4*$^{+}$ is due to H3K9 methyltransferase loss and not due to prolonged growth in the absence of caffeine, an unlinked intergenic locus was deleted in a parallel transformation performed alongside.

Results revealed that deletion of *clr4*$^{+}$ (*clr4Δ*) from resistant isolates resulted in loss of caffeine resistance in unstable, but not stable isolates, whereas deletion of the control locus (control*Δ*) had no impact (Figure 3.5). Because Clr4 is the sole H3K9 methyltransferase in *S. pombe*, these results indicate that caffeine resistance in unstable isolates is dependent on heterochromatin.

3.3.3. A mutation in *pap1*$^{+}$ confers caffeine resistance in the stable isolate SR-1

Genetic mutations in genes with a variety of cellular roles are known to confer caffeine resistance in *S. pombe* (Calvo et al. 2009). Because mutations are

virtually irreversible, caffeine-resistant mutants are expected to maintain resistance indefinitely.

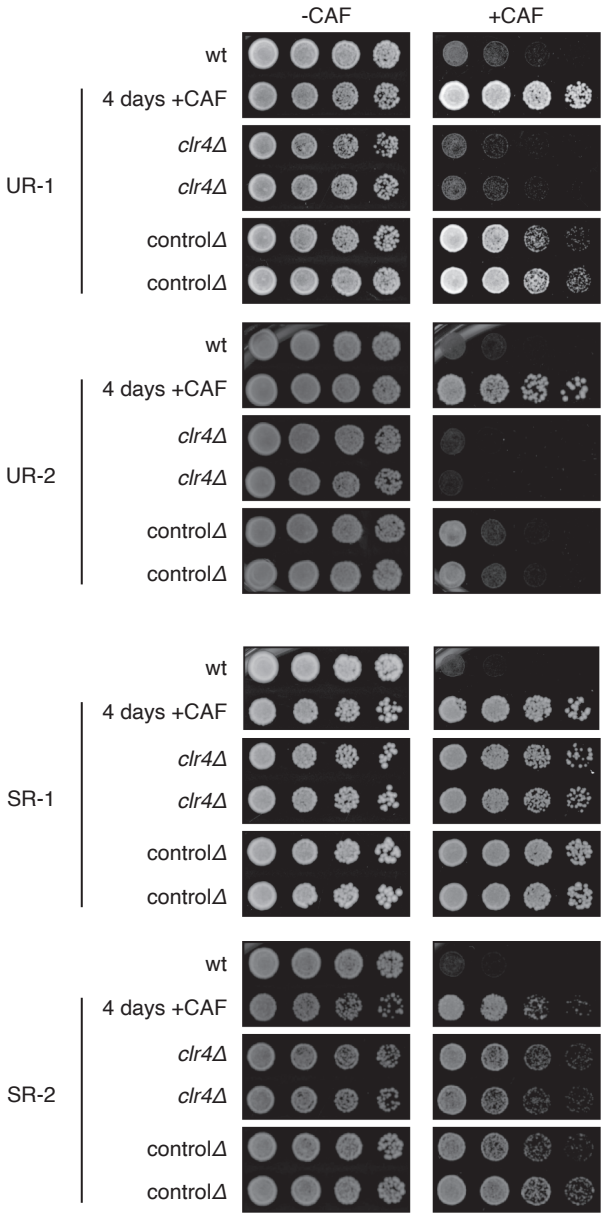

Figure 3.5. Caffeine resistance depends on the Clr4 H3K9 methyltransferase in unstable caffeine-resistant isolates. *clr4*$^{+}$ or an unlinked intergenic region was deleted (denoted *clr4Δ* and control*Δ*, respectively) in unstable (UR-1 and UR-2) and stable (SR-1 and SR-2) caffeine-resistant isolates and caffeine resistance was assessed.

Stable isolates maintain resistance to caffeine for at least 16 days (approximately 160 cell divisions) (Figure 3.4). To confirm that changes in DNA sequence underlie this stable phenotype, whole genome sequencing (WGS) was performed on the stable isolate SR-1. Sequence analysis uncovered a 7-nucleotide insertion in *pap1*$^{+}$ predicted to produce a truncated Pap1 transcription factor (Pap1-N424STOP) in SR-1 cells (Figure 3.6). Pap1-N424STOP lacks the Pap1 nuclear export signal (NES), required for Crm1-Hba1-mediated Pap1 nuclear export in non-stress conditions (Kudo et al. 1999). Cells harbouring alleles that disrupt the Pap1 NES are known to display caffeine resistance due to constitutive nuclear accumulation of Pap1 and resulting expression of stress-response genes (Benkö et al. 2004).

To corroborate that the identified mutation in *pap1*$^{+}$ is sufficient to drive caffeine resistance, the 7-nucleotide insertion identified in SR-1 cells was introduced into the *pap1*$^{+}$ gene of wild-type cells using the *SpEDIT* CRISPR/Cas9 genome editing system developed as part of this thesis (see Methods section 2.2.10 and Appendix I). Results showed that Pap1-N424STOP cells are caffeine resistant (Figure 3.6). Thus, the stable caffeine-resistant phenotype of SR-1 cells is mediated by a genetic mutation.

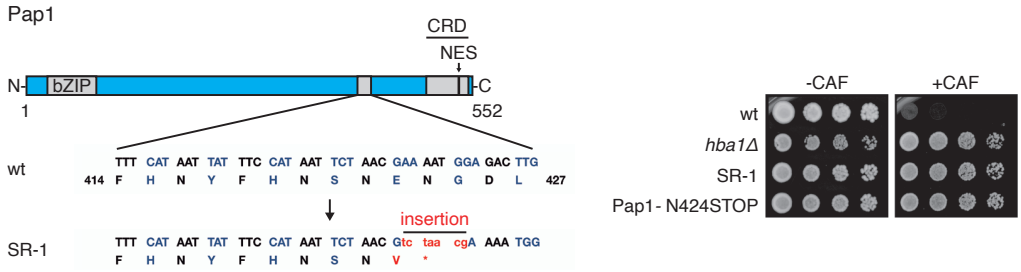

Figure 3.6. A mutation in *pap1*$^{+}$ confers caffeine resistance in the stable isolate SR-1
Left. Whole genome sequencing of the stable isolate SR-1 revealed a 7-nucleotide insertion in *pap1*$^{+}$. The insertion results in a truncated Pap1 protein (Pap1-N424STOP) that lacks the nuclear export signal (NES). CRD, cysteine-rich domain. Right. Pap1-N424STOP is resistant to caffeine. The 7-nucleotide insertion identified in SR-1 was introduced into the *pap1*$^{+}$ gene of wild-type cells (Pap1-N424STOP) and caffeine resistance assessed. *hba1Δ* (Castillo et al. 2003) and SR-1 cells were used as positive controls.

3.3.4. Unstable caffeine-resistant isolates do not harbour genetic mutations known to confer caffeine resistance

Unstable isolates exhibit a reversible caffeine-resistant phenotype that requires heterochromatin, suggesting that resistance might be mediated by epigenetic changes rather than genetic mutations. Indeed, WGS of 30 unstable isolates revealed no genetic changes (SNPs or indels) in coding sequences involved in caffeine resistance (Table 3.1), and 15 of 30 isolates had no detectable changes in coding sequences compared to wild-type (Table 3.1). An adaptive heterochromatin-dependent response could also arise following genetic disruption of key heterochromatin regulators (Wang et al. 2015), however no genetic changes were found in genes encoding major anti-silencing regulators or heterochromatin components (Table 3.1).

Surprisingly, isolates UR-1, UR-3, UR-5 and UR-7 harbour identical mutations in *clr5*$^{+}$ and *meu27*$^{+}$ (Clr5-Q264STOP and Meu27-S100Y). In addition, the same missense mutation in *sdo1*$^{+}$ (Sdo1-R11C) was found in UR-2 and UR19, whereas a matching synonymous mutation in *SPCC777.02*$^{+}$ (SPCC777.02-R120R/AGA>AGG) was detected in UR-17 and UR-18 (Table 3.1). None of these genes have previously been involved in caffeine resistance, suggesting that these changes might only reflect rare genetic variability among cells in the population. However, because Clr5-Q264STOP and Meu27-S100Y were identified in 4 independent unstable isolates, a potential role for these changes in mediating the observed caffeine-resistant phenotype was investigated.

To test whether cells harbouring Clr5-Q264STOP and Meu27-S100Y exhibit caffeine resistance or form more caffeine-resistant colonies than wild-type cells, the Clr5-Q264STOP and Meu27-S100Y mutations were both introduced into the *clr5*$^{+}$ and *meu27*$^{+}$ genes of wild-type cells using the *SpEDIT* CRISPR/Cas9 genome editing system (see Methods section 2.2.10) (Figure 3.7). The resulting Clr5-Q264STOP Meu27-S100Y cells did not form more caffeine-resistant colonies than wild-type cells nor did they display resistance to caffeine (Figure 3.7). Thus, Clr5-Q264STOP and Meu27-S100Y do not directly contribute to the caffeine-resistant phenotype in UR isolates.

Table 3.1. Genetic changes (SNPs, indels) found in unstable (UR) caffeine-resistant isolates. None of the genes below are known to be involved in caffeine resistance. SNP, single nucleotide polymorphism. Indel, small insertion or deletion.

Isolate	SNPs or indels in coding sequences
UR-1	Clr5-Q264STOP / Meu27-S100Y
UR-2	Sdo1-R11C
UR-3	Clr5-Q264STOP / Meu27-S100Y
UR-4	-
UR-5	Clr5-Q264STOP / Meu27-S100Y
UR-6	-
UR-7	Clr5-Q264STOP / Meu27-S100Y
UR-8	-
UR-9	-
UR-10	Cob1-F318L
UR-11	-
UR-12	-
UR-13	-
UR-14	Npp-W300STOP / SPBC16H5.13-S1011L
UR-15	-
UR-16	-
UR-17	SPCC777.02-R120R
UR-18	SPCC777.02-R120R
UR-19	Sdo1-R11C
UR-20	-
UR-21	-
UR-22	-
UR-23	Pch1-Q234STOP
UR-24	-
UR-25	-
UR-26	SPBC1271.08c-A133A
UR-27	SPCC4B3.13-A229V
UR-28	Mug72-N116S
UR-29	Mug72-N116S
UR-30	-

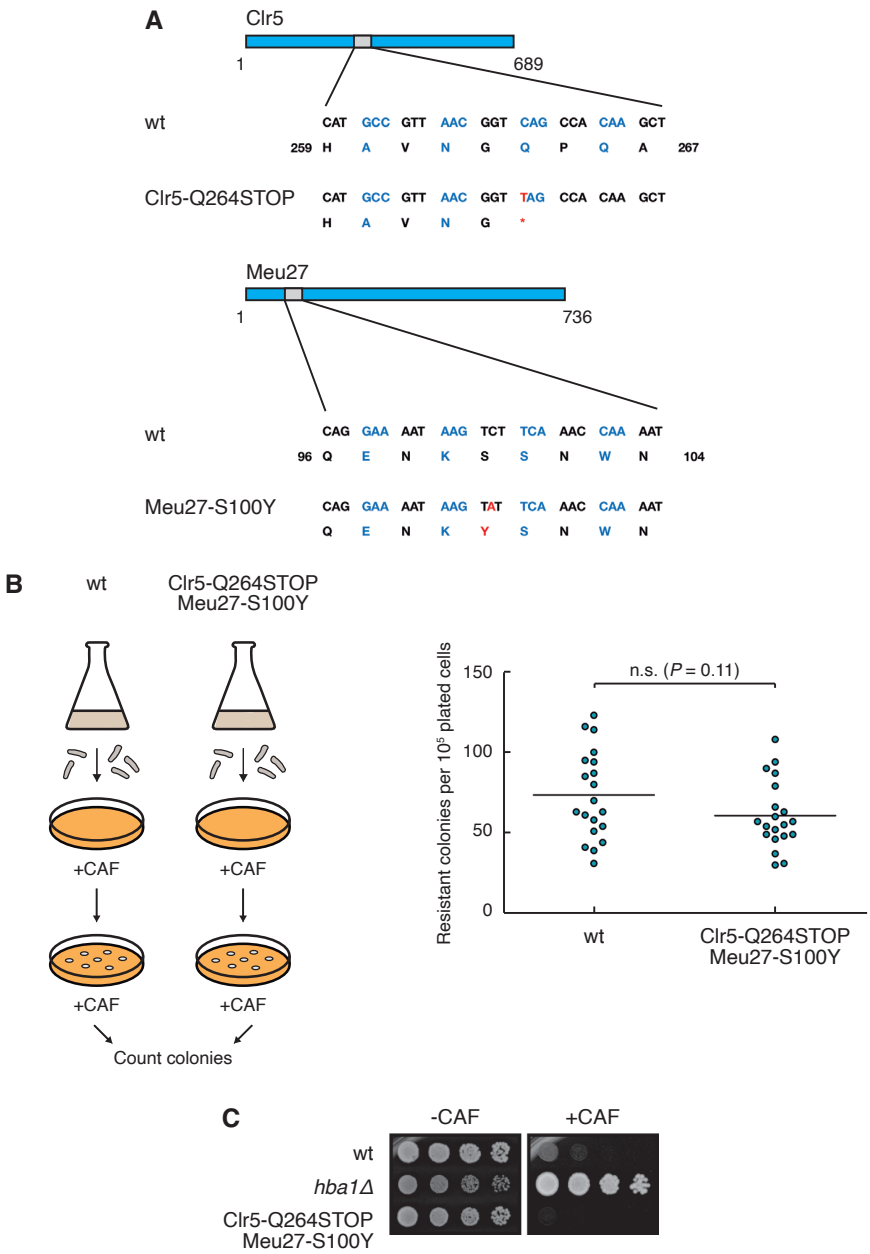

Figure 3.7. Genetic changes (Clr5-Q264STOP Meu27-S100Y) found in 4 of 30 unstable isolates do not contribute to the caffeine-resistant phenotype. A. Whole genome sequencing of the unstable isolates UR-1/3/5/7 revealed a single nucleotide polymorphism (SNP) in *clr5*$^{+}$ (Clr5-Q264STOP) and in *meu27*$^{+}$ (Meu27-S100Y). **B.** Left. Schematic of experiment to determine whether Clr5-Q264STOP Meu27-S100Y cells form more caffeine-resistant colonies than wild-type cells. Wild-type (wt) and Clr5-Q264STOP Meu27-S100Y cells were plated on +CAF media (10^5 cells per plate, 20 plates per strain, technical replicates). Caffeine-resistant colonies were counted after 7 days. Right. Clr5-Q264STOP Meu27-S100Y form a similar number of caffeine-resistant colonies to wt cells. *P* value from a two-tailed Student's *t* test is indicated (*P*=0.1051). **C.** Clr5-Q264STOP Meu27-S100Y cells are not resistant to caffeine. Clr5-Q264STOP Meu27-S100Y cells were serially diluted and spotted on -CAF and +CAF plates to assess caffeine resistance. *hba1Δ* cells served as positive control.

3.3.5. Ectopic islands of H3K9me are detected in unstable caffeine-resistant isolates

Unstable caffeine-resistant isolates do not harbour genetic mutations known to confer caffeine resistance yet depend on heterochromatin for resistance, suggesting that ectopic heterochromatin islands that drive an adaptive resistant phenotype could have assembled in these isolates. To investigate this possibility, chromatin immunoprecipitation coupled to high-throughput sequencing (ChIP-seq) was performed on isolates to assess levels of H3K9me2 across the genome. Note that isolates were grown in non-selective medium (for approximately 15 cell divisions) prior to ChIP experiments in order to prevent the generation of secondary changes that might occur after prolonged growth on caffeine. ChIP-seq for H3K9me2 on SR-1 revealed no changes in heterochromatin distribution (not shown), suggesting that the identified *pap1*$^{+}$ mutation (Pap1-N424STOP, Figure 3.6) alone is responsible for caffeine resistance in this stable isolate. ChIP-seq for H3K9me2 on unstable isolates revealed an altered heterochromatin distribution (Figure 3.8 and Table 3.2). UR-1 exhibited a novel H3K9me2 island over the *hba1* locus, whereas UR-2 to UR-6 exhibited H3K9me2 islands over the *ncRNA.394*, *ppr4*, *grt1*, *fio1*, and *mbx2* loci, respectively (Figure 3.8 and Table 3.2).

Deletion of *hba1*$^{+}$, encoding a nuclear export factor that acts together with Crm1 to shuttle NES-containing substrates to the cytoplasm (Benkö et al. 1998; Castillo et al. 2003), is known to confer caffeine resistance (Castillo et al. 2003). Loss of Hba1 leads to the constitutive nuclear localization of Pap1 and consequently expression of stress-response genes, similar to the effect of Pap1-N424STOP (Castillo et al. 2003). The formation of an ectopic heterochromatin island coating the *hba1* locus in UR-1 suggests that caffeine-induced heterochromatin islands may drive caffeine resistance by silencing underlying genes, partially mimicking a deletion phenotype. Consistent with this hypothesis, RT-qPCR analysis revealed reduced expression of genes underlying the observed novel heterochromatin island at the *hba1* locus (Figure 3.9).

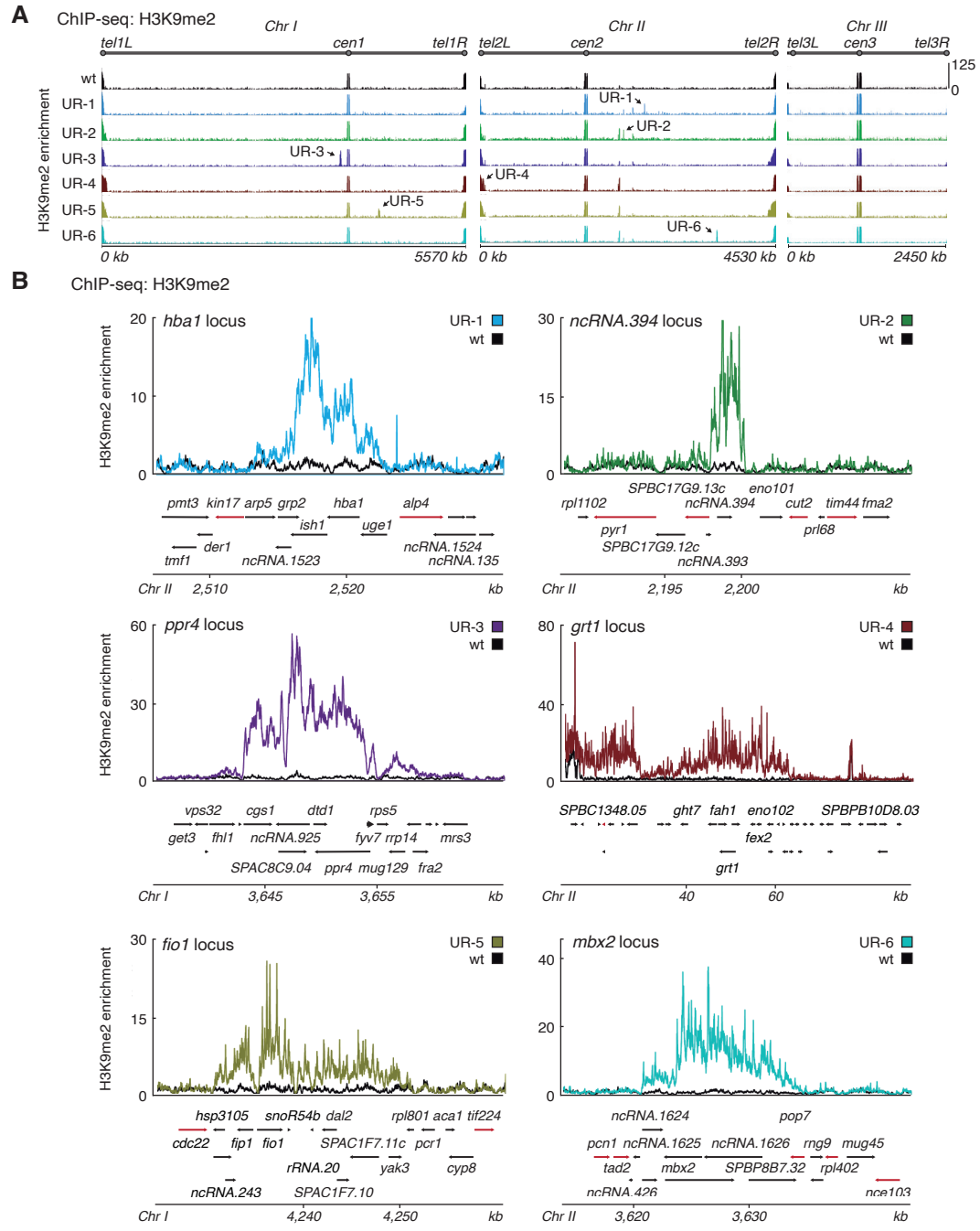

Figure 3.8. Ectopic islands of heterochromatin are detected in unstable caffeine-resistant isolates. A. Genome-wide H3K9me2 ChIP-seq enrichment in unstable (UR) caffeine-resistant isolates and wild-type (wt). Data are represented as relative fold enrichment over input. **B.** H3K9me2 ChIP-seq enrichment at ectopic heterochromatin islands in individual isolates. Data are represented as relative fold enrichment over input and compared to levels in wild-type (wt) cells. Relevant genes within and flanking ectopic heterochromatin islands are indicated. Red arrows indicate essential genes.

Table 3.2. Epigenetic (H3K9me2 islands) and genetic (SNPs, indels, as in Table 3.1) changes found in unstable (UR) caffeine-resistant isolates.

Isolate	Ectopic heterochromatin location		SNPs or indels in coding sequences
	ncRNA.394	**other loci**	
UR-1		✓ (*hba1*)	Clr5-Q264STOP / Meu27-S100Y
UR-2	✓		Sdo1-R11C
UR-3		✓ (*ppr4*)	Clr5-Q264STOP / Meu27-S100Y
UR-4		✓ (*grt1*)	-
UR-5		✓ (*fio1*)	Clr5-Q264STOP / Meu27-S100Y
UR-6		✓ (*mbx2*)	-
UR-7		✓ (*ppr4*)	Clr5-Q264STOP / Meu27-S100Y
UR-8	✓		-
UR-9	✓		-
UR-10	✓		Cob1-F318L
UR-11	✓		-
UR-12	✓		-
UR-13	✓		-
UR-14	✓		Npp-W300STOP / SPBC16H5.13-S1011L
UR-15	✓		-
UR-16	✓		-
UR-17	✓		SPCC777.02-R120R
UR-18	✓		SPCC777.02-R120R
UR-19	✓		Sdo1-R11C
UR-20	✓		-
UR-21	✓		-
UR-22	✓		-
UR-23	✓		Pch1-Q234STOP
UR-24	✓		-
UR-25	✓		-
UR-26	✓		SPBC1271.08c-A133A
UR-27	✓		SPCC4B3.13-A229V
UR-28	✓		Mug72-N116S
UR-29	✓		Mug72-N116S
UR-30	✓		-

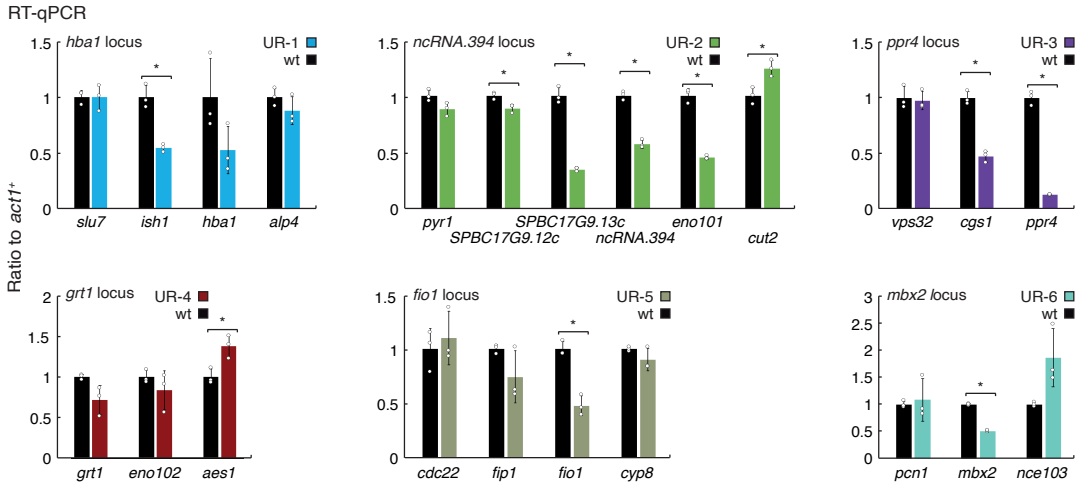

Figure 3.9. Genes coated in H3K9me are down-regulated in unstable caffeine-resistant isolates. Gene transcript levels within and flanking ectopic heterochromatin islands in individual isolates. See Figure 3.8. Data are mean ± s.d. from three biological replicates. **P*<0.05 (two-tailed Student's *t* test).

The *ncRNA.394*, *ppr4*, *grt1, fio1* and *mbx2* loci, which display H3K9me2 islands in unstable resistant isolates (Figure 3.8), have not previously been implicated in caffeine resistance. Interestingly, ChIP-seq and quantitative qChIP analyses revealed that 24 of 30 unstable isolates exhibited an ectopic heterochromatin island over the *ncRNA.394* locus (Figure 3.8, Table 3.2 and Figure 3.10A-B), and reduction in transcript levels from *ncRNA.394* and adjacent genes was also detected (Figure 3.9 and 3.10C), suggesting that transcriptional silencing within this region might mediate caffeine resistance. *ncRNA.394* was previously identified as a Taz1-dependent facultative heterochromatin island that gains H3K9me2 in the absence of the counteracting demethylase Epe1 (Zofall et al. 2012; Zofall et al. 2016). Indeed, ChIP-seq and qChIP analyses performed here failed to detect H3K9me2 over *ncRNA.394* in untreated wild-type cells (Figure 3.8 and 3.10A-B).

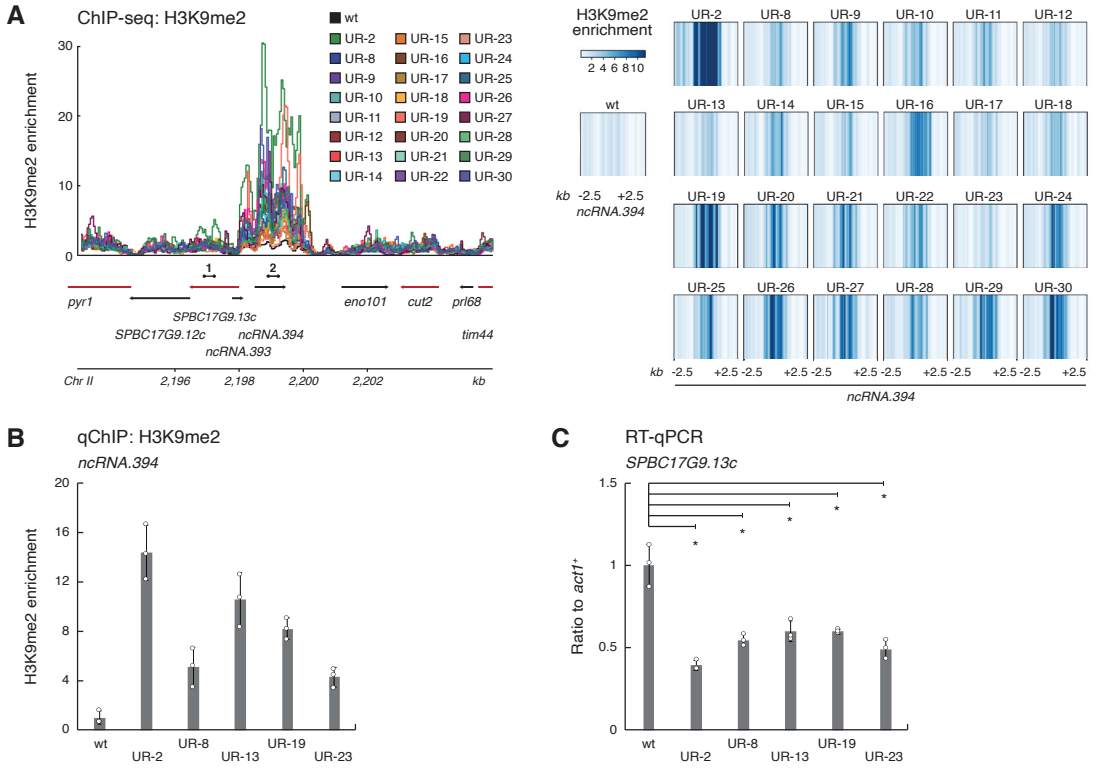

Figure 3.10. 24 of 30 unstable caffeine-resistant isolates display an ectopic heterochromatin island over the *ncRNA.394* locus. A. H3K9me ChIP-seq enrichment at the *ncRNA.394* locus in individual unstable (UR) caffeine-resistant isolates (left, coverage tracks; right, heatmaps). Data are represented as relative fold enrichment over input and compared to levels in wild-type cells. Relevant genes within and flanking ectopic heterochromatin islands are indicated. Red arrows indicate essential genes. Dumbbells indicate oligonucleotides used in **B** and **C**. **B.** Quantitative chromatin immunoprecipitation (qChIP) of H3K9me2 levels on *ncRNA.394* in individual isolates. Data are mean ± s.d. from three biological replicates. Oligonucleotides used are indicated in **A** (*ncRNA.394*, primer pair 2). **C.** *SPBC17G9.13c*$^{+}$ gene transcript levels in individual isolates. Data are mean ± s.d. from three biological replicates. Oligonucleotides used are indicated in **A** (*SPBC17G9.13c*$^{+}$, primer pair 1). **P*<0.05 (two tailed Student's *t* test).

3.3.6. RNAi contributes to caffeine resistance in the unstable isolate UR-2

RNAi is required to maintain intact domains of constitutive H3K9me heterochromatin at centromeric repeats in *S. pombe* (Volpe et al. 2002). However, facultative heterochromatin islands that gain H3K9me2 in the absence of Epe1, including *ncRNA.394,* were shown to persist in the absence of RNAi components (Zofall et al. 2012). To investigate whether the RNAi pathway is required for caffeine resistance in isolates that exhibit an ectopic heterochromatin island over the *ncRNA.394* locus, key RNAi components were deleted in the unstable isolate UR-2, which exhibits the highest H3K9me2 levels over *ncRNA.394* (Figure 3.10A-B). Deletion of *dcr1*$^+$ or *ago1*$^+$ from UR-2 cells resulted in loss of caffeine resistance (Figure 3.11A), suggesting that the caffeine-resistant phenotype of isolates that assemble ectopic H3K9me at the *ncRNA.394* locus requires RNAi. Consistent with this observation, total small RNA-seq analysis performed on UR-2 cells detected the generation of small interfering RNAs (siRNAs) at the ectopic *ncRNA.394* heterochromatin island (Figure 3.11B). Together, these results indicate that ectopic heterochromatin formation over the *ncRNA.394* locus is the most commonly detected epigenetic change in unstable caffeine-resistant isolates. Notably, ectopic H3K9me2 levels observed at this locus are dramatically increased relative to those detected in untreated wild-type cells and, at least in UR-2, are accompanied by generation of siRNAs, a hallmark of RNAi-associated heterochromatin.

3.3.7. Mutations in *clr5*$^+$/*meu27*$^+$ do not alter heterochromatin distribution

As discussed above, UR-1, UR-3, UR-5 and UR-7 harbour mutations in *clr5*$^+$ and *meu27*$^+$ (Clr5-Q264STOP and Meu27-S100Y) (Table 3.2). While Clr5-Q264STOP and Meu27-S100Y were shown not to mediate caffeine resistance directly (Figure 3.7), it is conceivable that these changes could facilitate the formation of ectopic heterochromatin in UR isolates. To test if Clr5-Q264STOP Meu27-S100Y cells display an altered heterochromatin distribution compared to wild-type cells or assemble ectopic heterochromatin islands at euchromatic

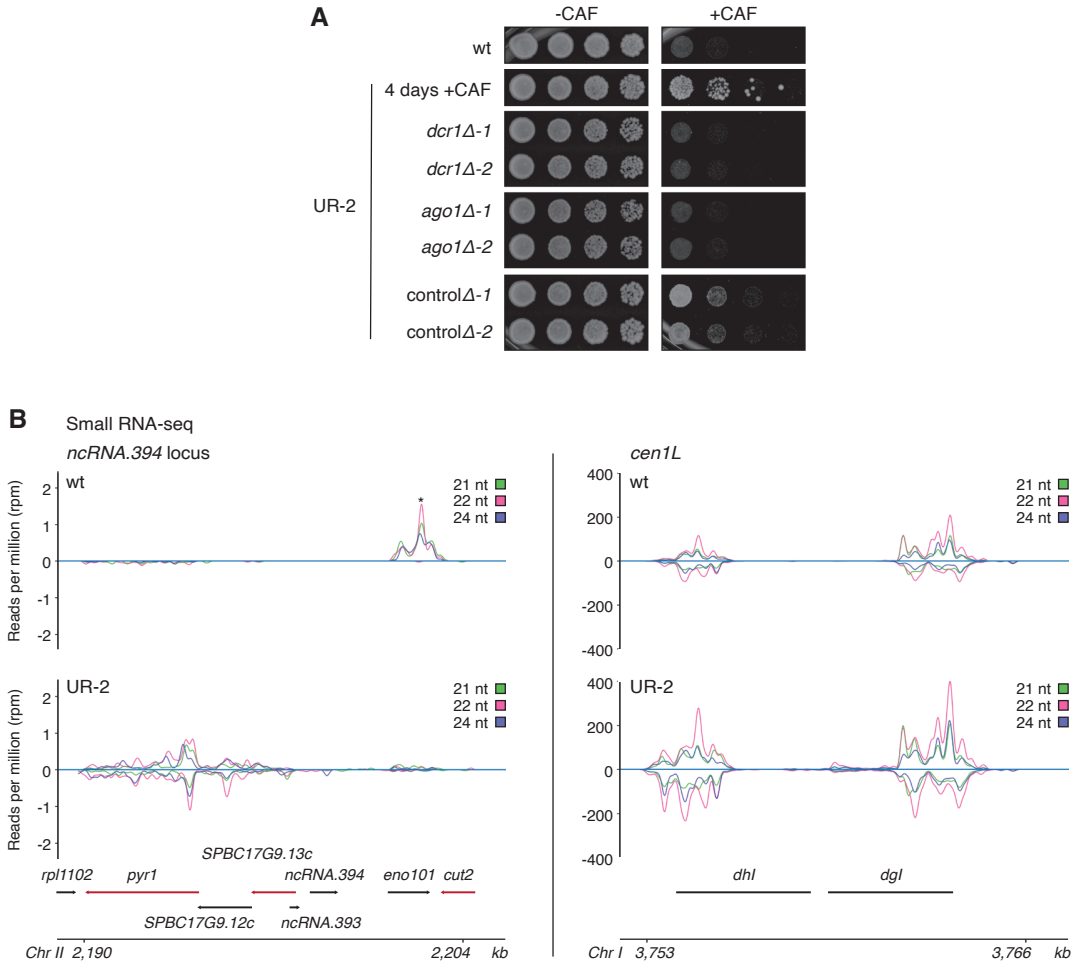

Figure 3.11. Caffeine resistance in UR-2 cells requires RNAi. A. *dcr1*$^{+}$ (*dcr1Δ*), *ago1*$^{+}$ (*ago1Δ*) or an unlinked intergenic region (control*Δ*) were deleted in UR-2 cells. **B.** Small interfering RNA generation at the ectopic *ncRNA.394* heterochromatin island. Left. Small RNA sequencing detects siRNAs (21-24 nucleotides) homologous to the ectopic heterochromatin island over *ncRNA.394* in UR-2 cells compared to wild-type (wt) cells. Right. siRNAs mapping to pericentromeric *dgI/dhI* repeats (*cen1L*) of chromosome I shown as control. *Transcripts mapping to the highly expressed gene *eno101*$^{+}$ in euchromatic wild-type conditions (note these are unidirectional RNAs and not siRNAs).

loci, as observed in cells lacking key anti-silencing factors (Zofall et al. 2012; Wang et al. 2015), ChIP-seq for H3K9me2 was performed on untreated Clr5-Q264STOP Meu27-S100Y cells (Figure 3.12).

Genome-wide ChIP-seq analyses showed that Clr5-Q264STOP Meu27-S100Y cells do not form ectopic heterochromatin at euchromatic loci (Figure 3.12A). Furthermore, Clr5-Q264STOP Meu27-S100Y cells do not exhibit

increased levels of H3K9me2 at facultative heterochromatin islands known to accumulate H3K9me2 in the absence of key anti-silencing factors such as Epe1 (Zofall et al. 2012; Wang et al. 2015; Sorida et al. 2019) (Figure 3.12B). These results indicate that Clr5-Q264STOP and Meu27-S100Y do not facilitate the formation of ectopic heterochromatin in UR isolates.

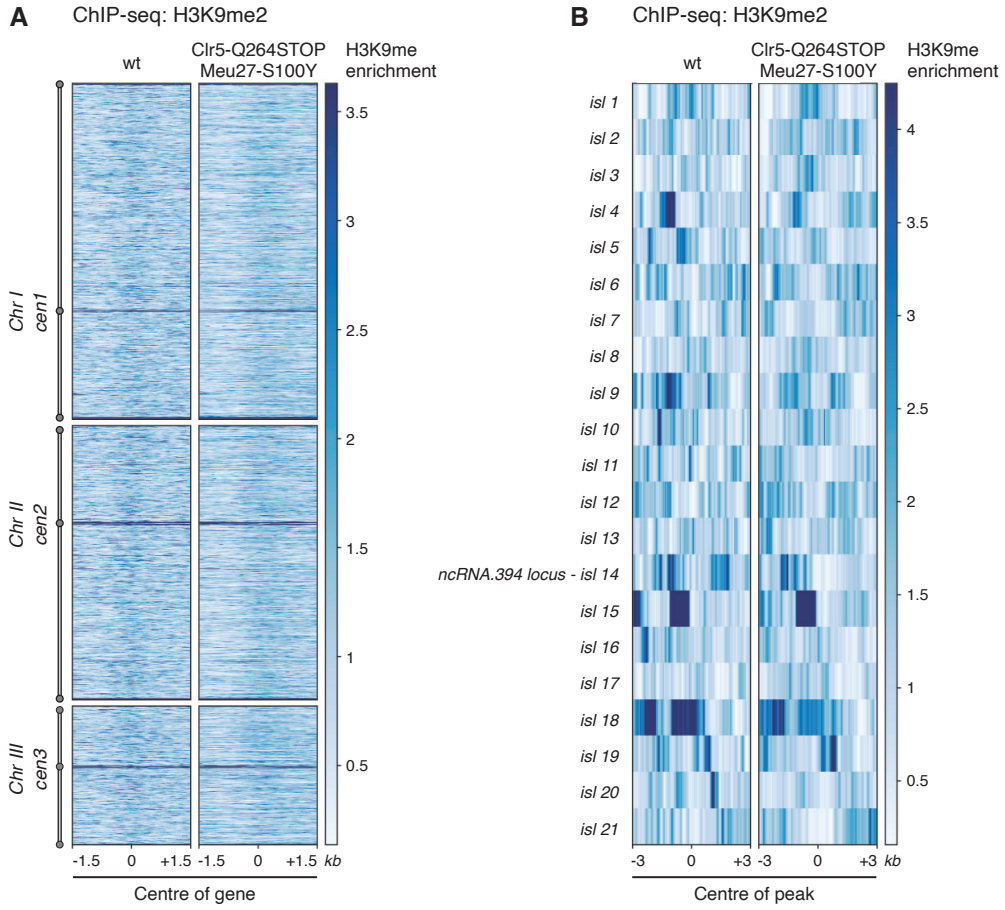

Figure 3.12. Genetic changes (Clr5-Q264STOP Meu27-S100Y) found in 4 of 30 unstable isolates do not cause the formation of ectopic heterochromatin. A. Genome-wide H3K9me2 ChIP-seq enrichment in wild-type (wt) and Clr5-Q264STOP Meu27-S100Y cells. Data are represented as relative fold enrichment over input and compared to levels in wild-type cells. **B.** H3K9me2 ChIP-seq enrichment at known facultative heterochromatin islands (detected in *epe1Δ* cells (Zofall et al. 2012)) in wt and Clr5-Q264STOP Meu27-S100Y cells. Data are represented as relative fold enrichment over input and compared to levels in wild-type cells.

3.4. Discussion

In this chapter, the identification of *S. pombe* isolates that display unstable resistance to the purine-analogue caffeine is reported (Figure 3.2 and 3.3). In unstable resistant isolates, caffeine resistance is progressively lost following growth on non-selective, caffeine-free medium (Figure 3.4). Notably, the unstable caffeine-resistant phenotype depends on Clr4, the sole H3K9 methyltransferase in fission yeast (Figure 3.5), indicating that caffeine resistance in unstable isolates requires heterochromatin.

Heterochromatin integrity is not a general requisite for caffeine tolerance, as deletion of core heterochromatin components does not lead to caffeine sensitivity (Calvo et al. 2009). Furthermore, deletion of *clr4*$^{+}$ in stable isolates has no impact on the caffeine-resistant phenotype, indicating that heterochromatin is also not a general requirement for caffeine resistance. Indeed, a mutation in *pap1*$^{+}$ (Pap1-N424STOP) was found to drive caffeine resistance in a heterochromatin-independent manner in the stable isolate SR-1 (Figure 3.5 and 3.6).

WGS of unstable caffeine-resistant isolates revealed that 15 of 30 had no genetic changes (SNPs or indels) in coding regions of the genome compared to wild-type (Table 3.1). Genetic changes detected in a proportion of unstable caffeine resistant isolates (Clr5-Q264STOP and Meu27-S100Y, 4 of 30 isolates) were found to have no impact on caffeine resistance (Figure 3.7). Clr5 has been proposed to mediate H3K9me-independent gene silencing at the mating-type locus of fission yeast via recognition of a *REIII* element adjacent to *cenH* repeats and recruitment of histone deacetylases (Hansen et al. 2011). Importantly, 972 *h*$^{-}$ wild-type cells used in this thesis lack both *cenH* repeats and *REIII* sequences at the mating-type locus and thus silencing (through either H3K9me or histone deacetylation) does not occur at this region (Leupold 1949; Wood et al. 2002; Fantes & Hoffman 2016). Nevertheless, a potential role for Clr5-Q264STOP in facilitating the formation of ectopic heterochromatin was investigated (Figure 3.12). Genome-wide ChIP-seq analysis showed that Clr5-Q264STOP Meu27-S100Y cells do not form ectopic heterochromatin at

euchromatic loci, nor do they accumulate higher H3K9me2 levels at facultative heterochromatin islands than those observed in wild-type cells (Figure 3.12). These results suggest that infrequent genetic changes found in unstable isolates might merely represent rare genetic variability among cells in a wild-type population.

H3K9me2 ChIP-seq analysis of unstable isolates revealed the presence of distinct, ectopic islands of heterochromatin (Figure 3.8 and Table 3.2), and reduced transcript levels of genes coated in ectopic H3K9me2 were detected (Figure 3.9), suggesting that heterochromatin-mediated transcriptional silencing at these loci might mediate caffeine resistance.

Deletion of *hba1*$^{+}$ confers caffeine resistance (Castillo et al. 2003; also shown here as positive control in Figure 3.6). Thus, it is likely that heterochromatin-mediated silencing of *hba1*$^{+}$ drives caffeine resistance in UR-1 cells. However, none of the genes located within the other detected ectopic heterochromatin islands have previously been associated with caffeine resistance (Figure 3.8 and Table 3.2) (Calvo et al. 2009).

The *ncRNA.394* heterochromatin island was detected in 24 of 30 unstable isolates (UR-2 and UR-8 to UR-30) (Figure 3.8 and 3.10A-B), 13 of which do not harbour genetic changes (SNPs or indels) in coding regions of the genome compared to wild-type (Table 3.2). Moreover, in UR-2 cells, caffeine resistance requires RNAi and siRNAs were detected at the *ncRNA.394* locus (Figure 3.11), indicating that ectopic heterochromatin islands display features of *bona fide* heterochromatin (Allshire & Madhani 2018). At the *ncRNA.394* locus, *ncRNA.393* and *ncRNA.394* are expressed at very low levels in untreated cells (Marguerat et al. 2012), yet their transcript levels are reduced even further in unstable isolates that assemble H3K9me over this locus (Figure 3.9, not shown for *ncRNA.393*). Nonetheless, because non-coding RNAs are known to exert diverse cellular functions, including the establishment of drug tolerance in fission yeast (Ard et al. 2014), a potential role of these reduced non-coding transcripts in driving caffeine resistance cannot be excluded. In

addition, the *ncRNA.394* heterochromatin island also coats the promoter of *SPBC17G9.13c*$^{+}$, a conserved fungal gene essential for cell growth whose function remains uncharacterized (Figure 3.8 and 3.10A) (Kim et al. 2010; Rhind et al. 2011; Hayles et al. 2013). Because cells lacking *SPBC17G9.13c*$^{+}$ are inviable, a genome-wide deletion screen such as that conducted to detect caffeine resistance (Calvo et al. 2009) would not include this gene among their candidates. Thus, whether the observed transcriptional down-regulation of *SPBC17G9.13c*$^{+}$ is sufficient to confer caffeine resistance in unstable isolates is unknown.

At the *ppr4* locus, *ppr4*$^{+}$ encodes a mitochondrial translational activator (Kühl et al. 2011). Deletion of several genes encoding mitochondrial proteins results in caffeine resistance (Calvo et al. 2009; Paulo et al. 2014), suggesting that reduced transcript levels of *ppr4*$^{+}$ might facilitate the caffeine-resistant phenotype of UR-3 and UR-7 cells. Alternatively, transcriptional down-regulation of *cgs1*$^{+}$, located upstream of *ppr4*$^{+}$, could activate the cAMP-dependent protein kinase catalytic subunit Pka1, as observed in *cgs1Δ* cells (DeVoti et al. 1991). Caffeine-mediated inhibition of cAMP phosphodiesterase leads to increased levels of intracellular cAMP (Butcher & Sutherland 1962), which may then be utilised by Pka1 to phosphorylate several cellular targets (Yu et al. 1994), and ultimately drive caffeine resistance. Consistent with this idea, *cgs1Δ* cells exhibit resistance to toxic levels of calcium (Matsuo & Kawamukai 2017).

The ectopic heterochromatin island that forms over the *grt1* locus comprises 60 kb in size and includes 22 genes. This large island size hinders the identification of potential candidate genes whose transcriptional down-regulation might confer resistance. Deletion of *grt1*$^{+}$ does not result in caffeine resistance (Yamada et al. 2000). However, many uncharacterized transmembrane transporters are located within this locus, as is common in subtelomeric regions of fission yeast (Tashiro et al. 2017). It is thus conceivable that heterochromatin-mediated silencing of one or multiple

transmembrane transporters in this region might lead to reduced drug import and ultimately caffeine resistance in UR-4 cells. In line with this hypothesis, decreasing intracellular levels of caffeine, albeit through increased drug export, has been shown to provoke the acquisition of a caffeine-resistant phenotype (Nagao et al. 1995; Arioka et al. 1998).

At the *fio1* locus, *fio1*$^{+}$ and *fip1*$^{+}$ encode subunits of an iron transmembrane transporter (Labbe et al. 1999), and loss of Fio1 has been shown to result in decreased ferrous iron import (Askwith & Kaplan 1997). Therefore, it is possible that transcriptional down-regulation of *fio1*$^{+}$ and/or *fip1*$^{+}$ might lead to reduced caffeine ingression and ultimately caffeine resistance in UR-5 cells.

Lastly, at the *mbx2* locus, *mbx2*$^{+}$ encodes a MADS-box transcription factor known to activate the expression of *gsf2*$^{+}$, a flocculin that induces non-sexual flocculation, in response to nitrogen limitation (Matsuzawa et al. 2012). Genome-wide Mbx2 ChIP-chip analysis has identified a potential consensus DNA binding sequence, but none of the genes detected as Mbx2 targets have been directly implicated in caffeine resistance (Kwon et al. 2012). It is therefore challenging to predict if reduced transcript levels of *mbx2*$^{+}$ might be the cause of caffeine resistance in UR-6 cells. Alternatively, transcriptional down-regulation of *ncRNA.426*, *ncRNA.1624*, *ncRNA.1625*, *ncRNA.1626* or the dubious gene *SPBP8B7.32*$^{+}$*,* also located within the *mbx2* heterochromatin island*,* may contribute to the caffeine-resistant phenotype in these cells.

Notably, ectopic heterochromatin islands that assemble at the *hba1*, *ncRNA.394*, *fio1* and *mbx2* loci are flanked by essential genes, suggesting that the uncontrolled spreading of heterochromatin can be suppressed by the deleterious effect of silencing essential genes that might not be required for resistance. However, it is unclear what elements or factors may act to create heterochromatin boundaries at the *ppr4* or *grt1* islands. Interestingly, deletion

of *vps32*$^{+}$, flanking the *ppr4* locus, leads to caffeine sensitivity (Calvo et al. 2009), suggesting that heterochromatin-mediated transcriptional down-regulation of *vps32*$^{+}$ might have a detrimental effect on the caffeine-resistant phenotype of UR-3 cells and thus function as a selected boundary.

Note that the *ncRNA.394*, *ppr4* and *mbx2* loci have been described before as facultative heterochromatin islands that gain H3K9me2 in the absence of Epe1 (Zofall et al. 2012, islands *14*, *4* and *16*, respectively). Indeed, ChIP-seq analyses performed here failed to detect significant levels of H3K9me2 over the *ncRNA.394*, *ppr4* or *mbx2* loci in untreated wild-type cells (Figure 3.8). Importantly, the formation of ectopic heterochromatin islands at these loci in caffeine-resistant isolates suggests that Epe1 function might be impaired upon caffeine treatment.

Together, the results presented here demonstrate that ectopic islands of heterochromatin are formed in unstable caffeine-resistant isolates that arise in the presence of lethal levels of caffeine. In the next chapter, it will be investigated whether the ectopic heterochromatin islands described here have adaptive potential and thus are sufficient to drive caffeine resistance in wild-type cells.

Chapter 4: Forced assembly of synthetic heterochromatin at the identified UR loci is sufficient to drive caffeine resistance in wild-type cells

4.1. Introduction

Unstable caffeine-resistant (UR) isolates that arise following exposure to a lethal dose of caffeine form ectopic heterochromatin islands at euchromatic loci. Resistance in unstable isolates requires heterochromatin, and genes coated in ectopic H3K9me are transcriptionally down-regulated, suggesting that heterochromatin silencing at these loci drives caffeine resistance. Intriguingly, however, only one of the identified ectopic heterochromatin islands contains a gene known to confer caffeine resistance when deleted. Genetic changes detected in a fraction of unstable isolates were found to have no direct role in mediating resistance. Still, it is conceivable that these rare mutations could indirectly facilitate the acquisition of an unstable caffeine-resistant phenotype. It is thus paramount to test whether the formation of ectopic heterochromatin islands at the identified UR loci is sufficient, in the absence of other factors, to drive caffeine resistance in wild-type cells.

Several reports have shown that tethering chromatin modifiers to ectopic locations in the genome can alter the chromatin landscape (Lustig et al. 1996; Hansen et al. 2008; Kagansky et al. 2009; Hathaway et al. 2012; Audergon et al. 2015; Ragunathan et al. 2015; Bintu et al. 2016). In *S. pombe*, expression of the Clr4 H3K9 methyltransferase fused to the Tet repressor ($TetR^{off}$) protein allows tethering of Clr4 activity to *tet* operator (*tetO*) sites inserted at the *ura4* locus (Audergon et al. 2015; Ragunathan et al. 2015). The $TetR^{off}$-2xFLAG-Clr4-cdd fusion protein (abbreviated TetR-Clr4*, as described in Audergon et al. 2015), lacks the Clr4 chromodomain, known to bind H3K9me2/3 (Zhang et al. 2008). The use of an engineered chromodomain-deficient version of Clr4 leads to more efficient silencing at an ectopic locus as TetR-Clr4* cannot be

recruited to constitutive, H3K9me-rich heterochromatin regions, and also ensures that TetR-Clr4* is unable to propagate H3K9me once it is deposited (Kagansky et al. 2009).

TetR^{off} binds *tetO* sites with high affinity in the absence of anhydrotetracycline (AHT) (Gossen et al. 1995; Urlinger et al. 2000; Erler et al. 2006). Addition of AHT changes the conformation of TetR^{off} resulting in its dissociation from *tetO* sites. Therefore, this system enables the inducible removal of TetR-Clr4* from tethering sites upon AHT addition.

Tethering TetR-Clr4* to the *ura4* locus leads to the establishment of a synthetic heterochromatin domain that spreads over a 10 kb region surrounding the tethering sites. TetR-Clr4*-induced synthetic heterochromatin is characterized by enrichment of H3K9me2, recruitment of the chromodomain protein Swi6, and silencing of underlying genes, which occurs independently of RNAi (Audergon et al. 2015). In wild-type cells, the release of tethered TetR-Clr4* results in the rapid and active removal of H3K9me and all associated heterochromatin features from tethering sites. However, inactivation of the putative H3K9 demethylase Epe1 allows H3K9me and silent chromatin maintenance at tethering sites through many mitotic divisions, and transgenerationally through meiosis, after release of tethered TetR-Clr4* (Audergon et al. 2015; Ragunathan et al. 2015). H3K9 methylation maintenance depends on endogenous Clr4, able to propagate H3K9me following replication due to its previously described *reader-writer* coupling mechanism (Zhang et al. 2008; Audergon et al. 2015; Ragunathan et al. 2015).

Therefore, in wild-type cells, the TetR-Clr4* tethering system can be utilised to generate reversible, synthetic domains of heterochromatin at *tetO* sites placed at theoretically any genomic location. In this chapter, TetR-Clr4* tethering was used to investigate whether forced synthetic heterochromatin formation at the previously identified UR loci is sufficient to drive caffeine resistance in wild-type cells.

4.2. Results

4.2.1. Forced synthetic heterochromatin at the *hba1, ncRNA.394* or *mbx2* loci is sufficient to drive caffeine resistance in wild-type cells

To test directly if ectopic heterochromatin formation at the identified loci can drive caffeine resistance in the absence of additional changes, the TetR-Clr4* tethering system was utilised to generate synthetic heterochromatin domains at the *hba1, ncRNA.394,* or *mbx2* loci in wild-type cells. The *hba1* locus was selected because deletion of *hba1*$^+$ is known to confer caffeine resistance (Castillo et al. 2003). Hence, *hba1*$^+$ is a clear candidate gene at this locus whose transcriptional down-regulation is expected to mediate caffeine resistance.

The *ncRNA.394* locus was investigated because ectopic heterochromatin formation over this region was frequent. Indeed, 24 of the 30 unstable caffeine-resistant isolates analysed exhibited a heterochromatin island over *ncRNA.394.* Importantly, high H3K9me2 levels over *ncRNA.394* were not detected in unstable isolates that exhibited heterochromatin islands elsewhere, suggesting that heterochromatin formation at *ncRNA.394* does not merely constitute a trivial consequence of caffeine exposure. Moreover, *ncRNA.394* island formation leads to transcriptional down-regulation of *SPBC17G9.13c*$^+$, an uncharacterized gene required for cell growth (Kim et al. 2010; Hayles et al. 2013). It was therefore reasoned that silencing of an essential gene would only occur if heterochromatin formation at such a locus provided a fitness advantage upon insult exposure.

Lastly, the *mbx2* locus was chosen because it was challenging to predict which gene within this region could be responsible for mediating a caffeine-resistant phenotype. Because *mbx2*$^+$ encodes a transcription factor known to activate a target gene in response to nitrogen limitation (Matsuzawa et al. 2012), it is conceivable that reduced *mbx2*$^+$ levels could also lead to an adaptive phenotypic response upon caffeine treatment. It was thus important to test if

heterochromatin formation at this locus could drive a caffeine-resistant phenotype before any further functional dissection was performed.

To construct strains that form ectopic heterochromatin at the *hba1*, *ncRNA.394, mbx2,* or (control) *ura4* loci, *tetO* binding sites (*4xtetO*) were inserted upstream of *hba1, ncRNA.394*, *mbx2* or *ura4* using the *SpEDIT* CRISPR/Cas9 genome editing system (see section 2.2.9 and 2.2.10 in Methods). Strains harbouring *tetO* sites and constitutively expressing TetR-Clr4* were grown in the absence of AHT to force assembly of synthetic heterochromatin upon recruitment to these loci. Subsequently, cells were challenged with caffeine and in parallel subjected to qChIP analysis to determine H3K9me2 levels at the corresponding tethering sites. Results showed that combining *tetO* with TetR-Clr4* in the absence of AHT (-AHT) resulted in a novel H3K9me2 domain at each locus. Remarkably, the formation of synthetic heterochromatin domains at the *hba1, ncRNA.394,* or *mbx2* loci rendered cells resistant to caffeine (Figure 4.1, 4.2 and 4.3). Moreover, AHT-mediated release of TetR-Clr4* from *tetO* sites (+AHT) resulted in the loss of H3K9me2 from these loci and cells returning to a caffeine-sensitive phenotype (Figure 4.1, 4.2 and 4.3). These results indicate that heterochromatin-mediated silencing at the *hba1, ncRNA.394* or *mbx2* loci results in caffeine resistance.

At the *hba1* locus, deletion of *hba1*$^{+}$ confers caffeine resistance (Castillo et al. 2003), whereas deletion of *ish1*$^{+}$, downstream of *hba1*$^{+}$, has no effect (Taricani et al. 2002). Thus, it was concluded that heterochromatin-mediated silencing of *hba1*$^{+}$ drives resistance at the *hba1* ectopic heterochromatin island. However, further investigation is required to determine which of the genes present at the *ncRNA.394* or *mbx2* loci mediates caffeine resistance when silenced via H3K9me heterochromatin.

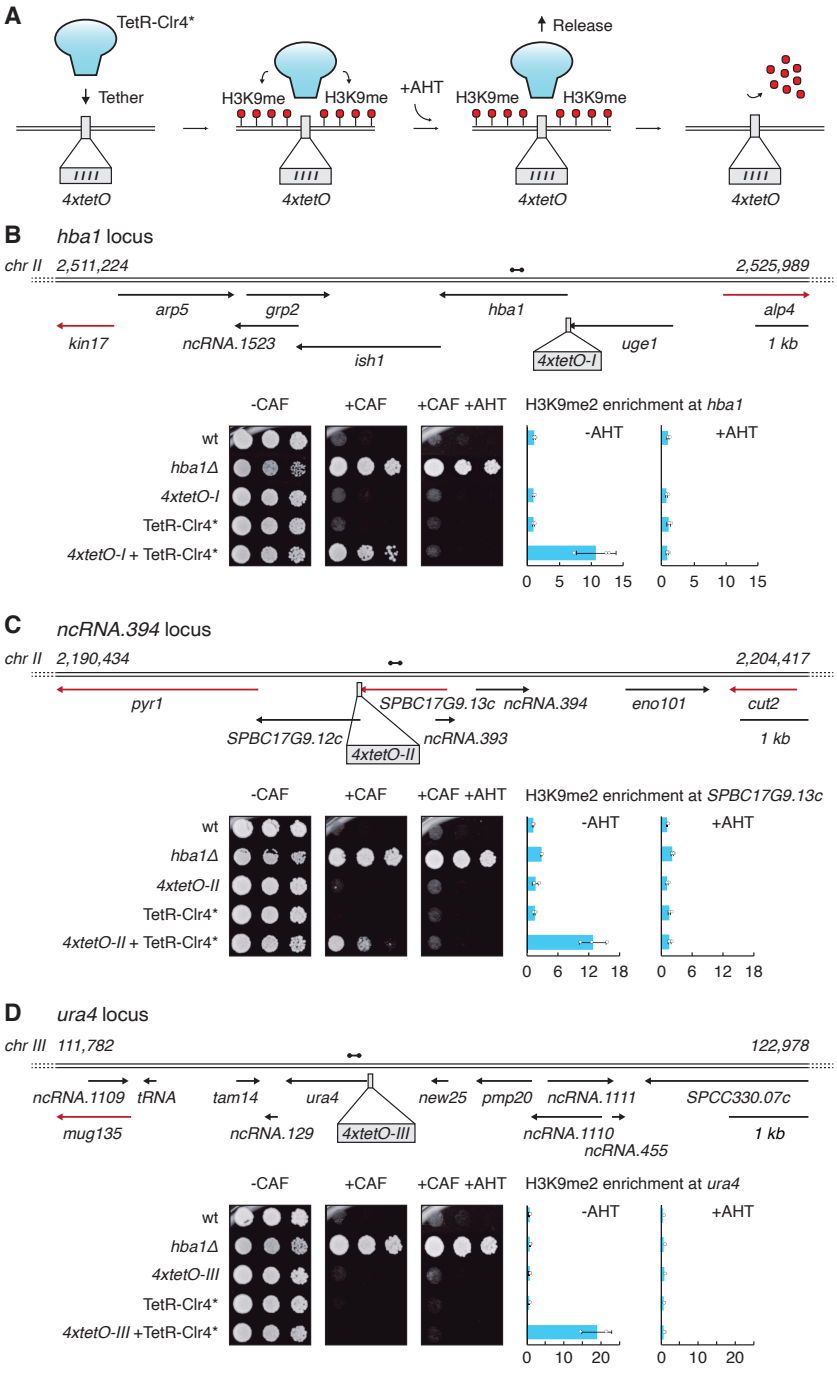

Figure 4.1. Forced assembly of synthetic heterochromatin at the *hba1* or *ncRNA.394* loci is sufficient to drive caffeine resistance in wild-type cells. A. Diagram illustrating TetR-Clr4*-mediated H3K9me deposition at *4xtetO* binding sites. Addition of anhydrotetracycline (+AHT) releases TetR-Clr4* from *4xtetO* sites resulting in removal of H3K9me. **B-D.** Wild-type cells harbouring *4xtetO* binding sites at the *hba1* or *ncRNA.394* loci (or *ura4* as control) and expressing TetR-Clr4* were assessed for caffeine resistance in the absence (-) or presence (+) of AHT. Quantitative chromatin immunoprecipitation (qChIP) of H3K9me2 levels on *hba1* (**B**), *SPBC17G9.13c* (**C**) and *ura4* (**D**) loci. Data are mean ± s.d. from three biological replicates. Dumbbells indicate oligonucleotides used. Red arrows indicate essential genes. *hba1Δ* cells served as positive control. Note *hba1* is not present in *hba1Δ*.

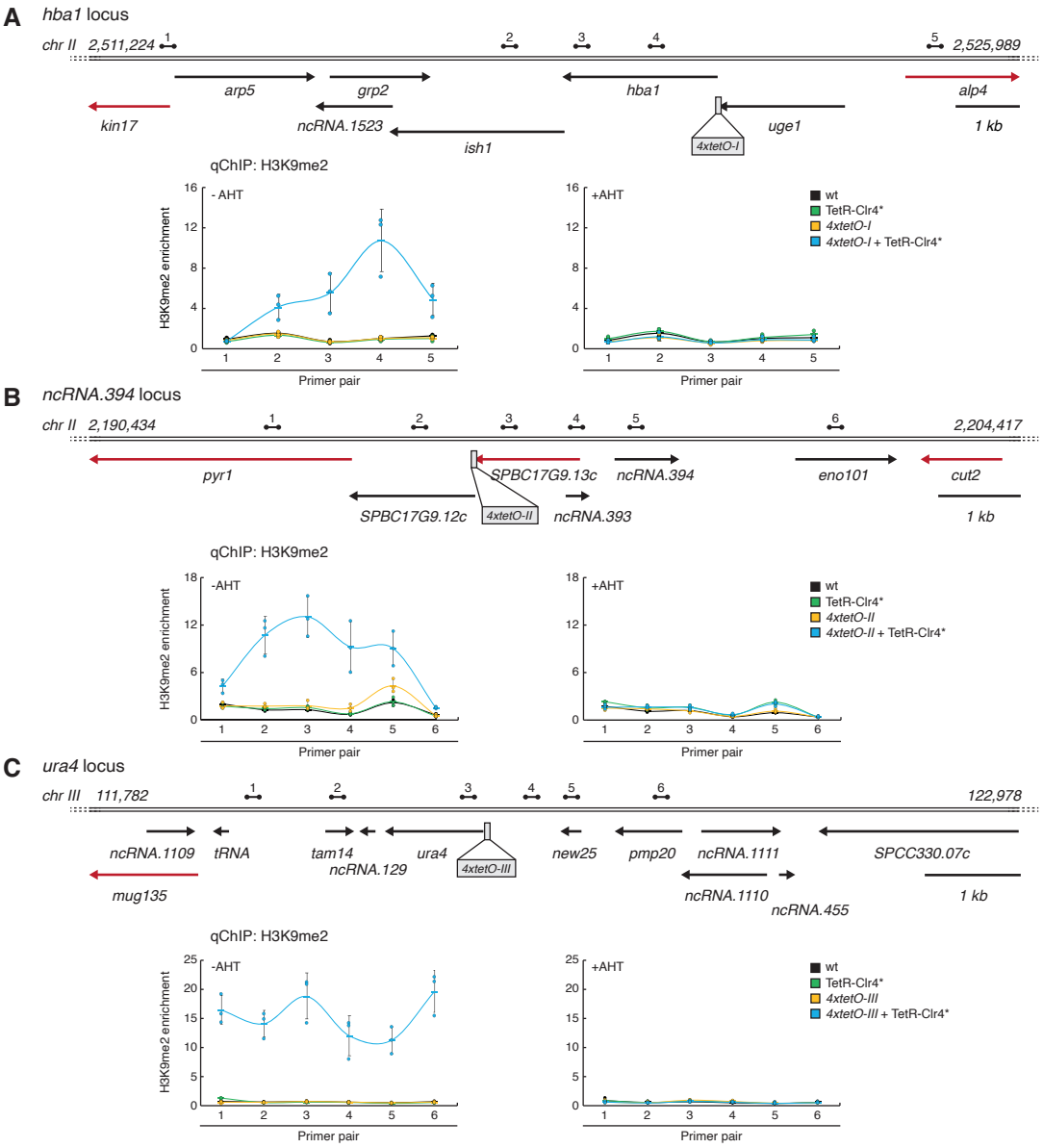

Figure 4.2. Forced assembly of synthetic heterochromatin at the *hba1* or *ncRNA.394* loci is sufficient to drive caffeine resistance in wild-type cells. A-C. Quantitative chromatin immunoprecipitation (qChIP) of H3K9me2 levels in wild-type cells harbouring *4xtetO* binding sites at the identified ectopic heterochromatin loci (or *ura4* as control) and expressing TetR-Clr4* in the absence (-) or presence (+) of AHT. **A.** *hba1* locus. **B.** *ncRNA.394* locus. **C.** *ura4* locus. Data are mean ± s.d. from three biological replicates. Dumbbells indicate oligonucleotides used. Red arrows indicate essential genes.

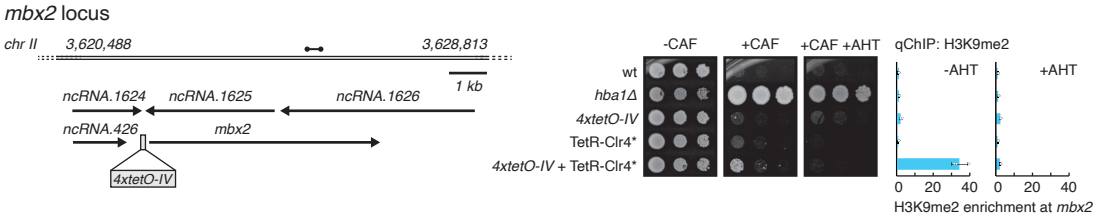

Figure 4.3. Forced assembly of synthetic heterochromatin at the *mbx2* locus is sufficient to drive caffeine resistance in wild-type cells. Wild-type cells harbouring *4xtetO* binding sites at the *mbx2* locus and expressing TetR-Clr4* were assessed for caffeine resistance in the absence (-) or presence (+) of AHT. qChIP of H3K9me2 levels on the *mbx2* locus. Data are mean ± s.d. from three biological replicates. Dumbbell indicates oligonucleotides used. *hba1Δ* cells served as positive control.

4.2.2. Decreased *cup1*$^{+}$ (*SPBC17G9.13c*$^{+}$) transcript levels or Cup1 LYR-domain mutation results in caffeine resistance

Heterochromatin formation at the *ncRNA.394* locus is sufficient to drive caffeine resistance in wild-type cells (Figure 4.1 and 4.2). To determine which gene within the *ncRNA.394* locus causes caffeine resistance, firstly, a classical knock-out approach was taken. Single deletion of *ncRNA393* or *ncRNA.394*, the only genes entirely coated in H3K9me2 in unstable isolates (Chapter 3, Figure 3.10A), did not result in caffeine resistance (Figure 4.4), indicating that the individual loss of these transcripts has no effect on the resistant phenotype.

It is possible that the *ncRNA.394* heterochromatin island that forms in unstable isolates expands over nearby genes when cells are grown under selective pressure. To investigate this possibility, UR-2 cells were grown in +CAF medium overnight and H3K9me2 levels at the *ncRNA.394* locus were assessed by qChIP. Growth in the presence of caffeine extended this heterochromatin island to include the upstream genes *SPBC17G9.13c*$^{+}$ and *SPBC17G9.12c*$^{+}$, whereas prolonged non-selective growth without caffeine resulted in loss of H3K9me2 over the complete *ncRNA.394* locus (Figure 4.5).

Deletion of *SPBC17G9.12c*$^{+}$ or the downstream gene *eno101*$^{+}$ did not result in caffeine resistance (Figure 4.4). *SPBC17G9.13c*$^{+}$ is essential for viability, precluding testing a deletion mutant for the resistance phenotype.

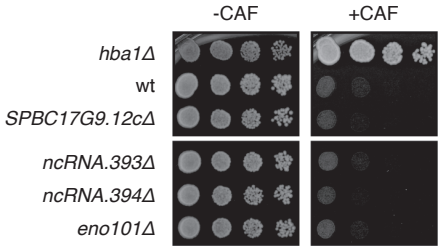

Figure 4.4. Deletion of *ncRNA.394* or non-essential adjacent genes does not result in caffeine resistance. Upon single deletion of *ncRNA.394* or non-essential adjacent genes, cells were serially diluted and spotted on -CAF and +CAF plates to assess resistance to caffeine. *hba1Δ* cells served as positive control.

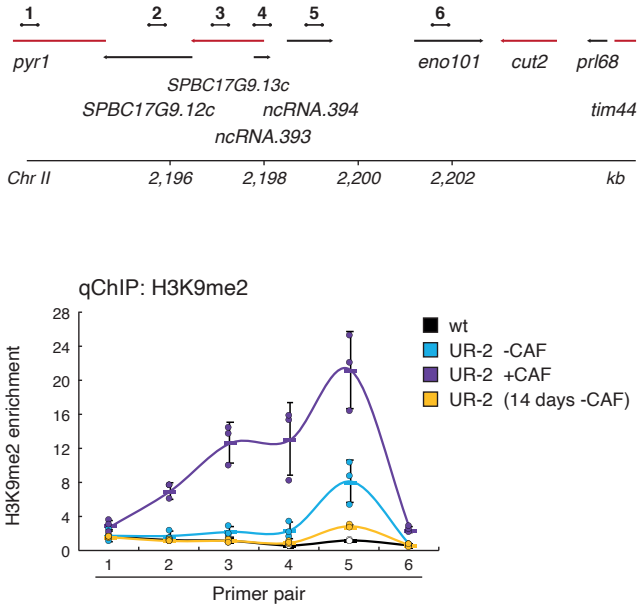

Figure 4.5. The ectopic heterochromatin island over *ncRNA.394* expands when cells are grown under selection. qChIP of H3K9me2 levels at the *ncRNA.394* locus in UR-2 cells. UR-2 cells were grown in the absence (-CAF) or presence (+CAF) of caffeine overnight or in the absence of caffeine for 14 days (14 days -CAF). Primer pairs used are indicated as dumbbells in diagram on top. Data are mean ± s.d. from three biological replicates.

TetR-Clr4* tethering close to *SPBC17G9.13c*$^{+}$ resulted in caffeine resistance (Figure 4.1C). Furthermore, additional tethering experiments performed on strains harbouring *tetO* sites at different positions within the *ncRNA.394* locus revealed that H3K9me2 levels over *SPBC17G9.13c* positively correlate with resistance to caffeine (Figure 4.6). Thus, reduced expression of *SPBC17G9.13c*$^{+}$ upstream of *ncRNA.394* may be responsible for caffeine resistance at this locus. Indeed, all caffeine-resistant cells that form synthetically mediated or naturally occurring heterochromatin islands at the *ncRNA.394* locus were found to exhibit reduced transcript levels of *SPBC17G9.13c*$^{+}$ (Figure 4.7 and Chapter 3, Figure 3.9 and 3.10C).

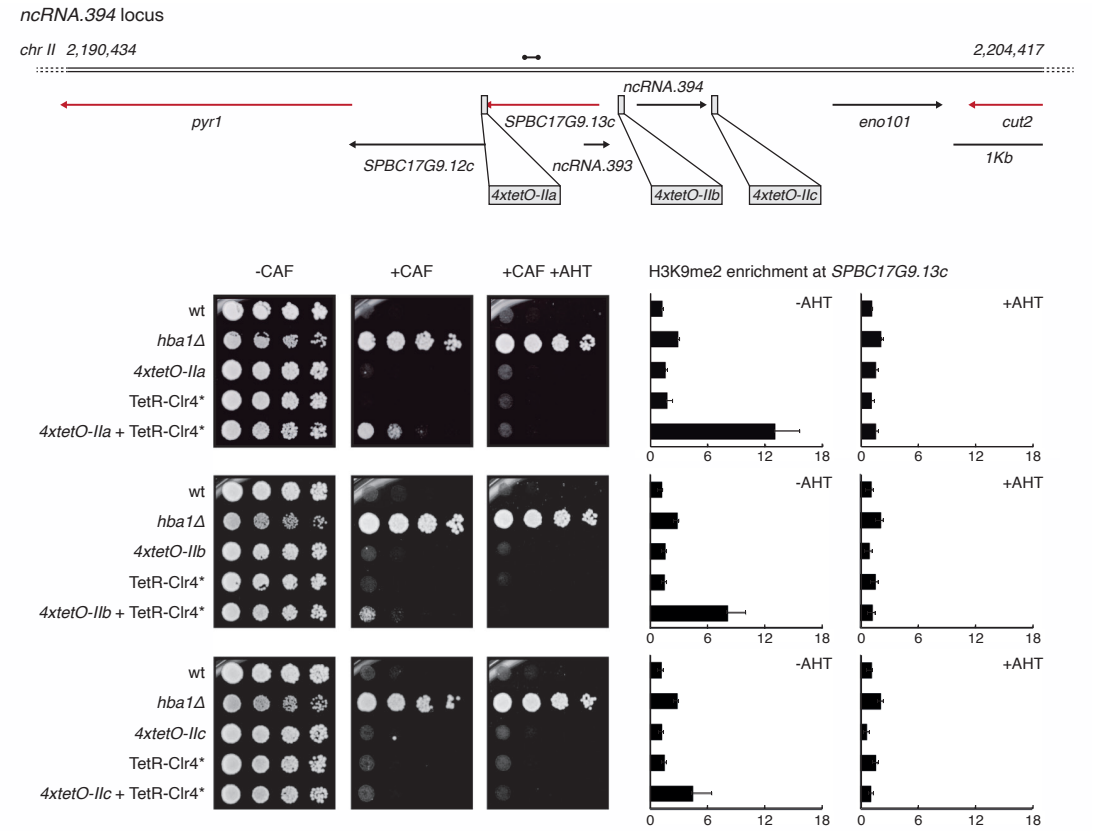

Figure 4.6. H3K9me2 levels over *SPBC17G9.13c* positively correlate with caffeine resistance. Wild-type cells harbouring *4xtetO* binding sites inserted at 3 different positions within the *ncRNA.394* locus and expressing TetR-Clr4* were assessed for caffeine resistance in the absence (-) or presence (+) of AHT. Quantitative chromatin immunoprecipitation (qChIP) of H3K9me2 levels on *SPBC17G9.13c. 4xtetO-IIa* was shown as *4xtetO-II* in Figure 4.1 and 4.2. Data are mean ± s.d. from three biological replicates. Dumbbell indicates oligonucleotides used. Red arrows indicate essential genes. *hba1Δ* cells served as positive control.

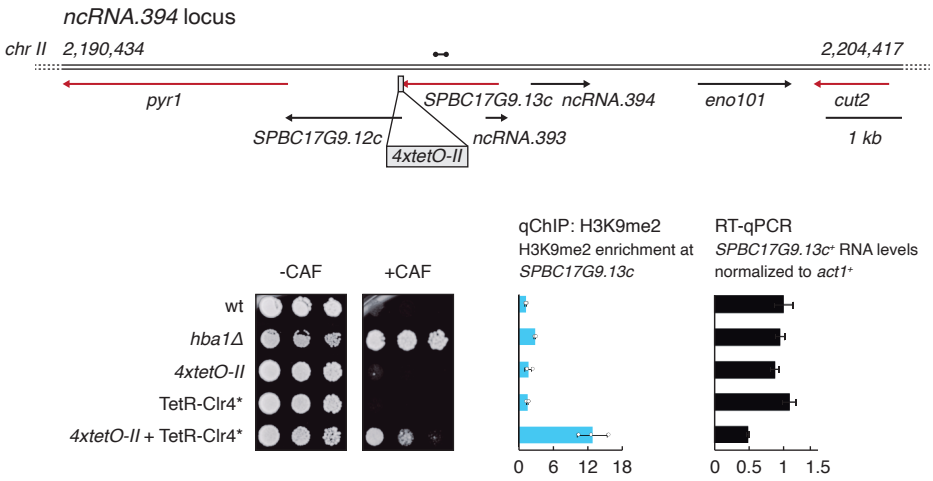

Figure 4.7. Transcriptional down-regulation of *SPBC17G9.13c*⁺ correlates with caffeine resistance. Wild-type cells harbouring *4xtetO* binding sites at *ncRNA.394* locus and expressing TetR-Clr4* were assessed for caffeine resistance in the absence of AHT as shown in Figure 4.1. Quantitative chromatin immunoprecipitation (qChIP) of H3K9me2 levels on *SPBC17G9.13c* as shown in Figure 4.1. RT-qPCR analysis of *SPBC17G9.13c*⁺ gene transcript levels in the same cells. Data are mean ± s.d. from three biological replicates. Dumbbell indicates oligonucleotides used. Red arrows indicate essential genes. *hba1Δ* cells served as positive control.

A direct test of *SPBC17G9.13c*⁺ imparting caffeine resistance would be to down-regulate its expression to mimic heterochromatin silencing. However, the promoter of *SPBC17G9.13c*⁺ does not include well-defined regulatory elements (Dreos et al. 2013; Li et al. 2015), and hence it is challenging to precisely tune the expression levels of this gene at its endogenous locus.

In *S. pombe,* a system that enables selective down-regulation of mRNAs has been described (Watson et al. 2013). Determinant of selective removal (DSR) motifs, usually located at the 3' end of meiosis-specific mRNAs, trigger the degradation of transcripts via recruitment of the nuclear exosome. This mechanism enables the selective removal of meiosis-specific transcripts in mitotic cells (Harigaya et al. 2006).

To investigate if reduced expression of *SPBC17G9.13c*⁺ (named here *cup1*⁺*, caffeine unstable phenotype 1*) is sufficient to drive caffeine resistance in wild-type cells, a copy of *cup1*⁺ with three downstream DSR motifs was expressed from an intergenic locus (*LocusPX:cup1-3xDSR*). Subsequent deletion of the

endogenous *cup1*$^{+}$ gene resulted in reduced *cup1-3xDSR* transcript levels and, importantly, cells displaying caffeine resistance (Figure 4.8A). In an alternative strategy, transcriptional attenuation of endogenous *cup1*$^{+}$ was achieved by replacement of part of its promoter with the 144-bp transcriptional terminator site from *ura4*$^{+}$ (*cup1-TT*). Cells expressing *cup1-TT* also exhibited caffeine resistance (Figure 4.8B, experiment performed by Dr. Alison Pidoux). Thus, it can be concluded that transcriptional down-regulation of *cup1*$^{+}$ (*SPBC17G9.13c*$^{+}$) at the *ncRNA.394* locus results in caffeine resistance.

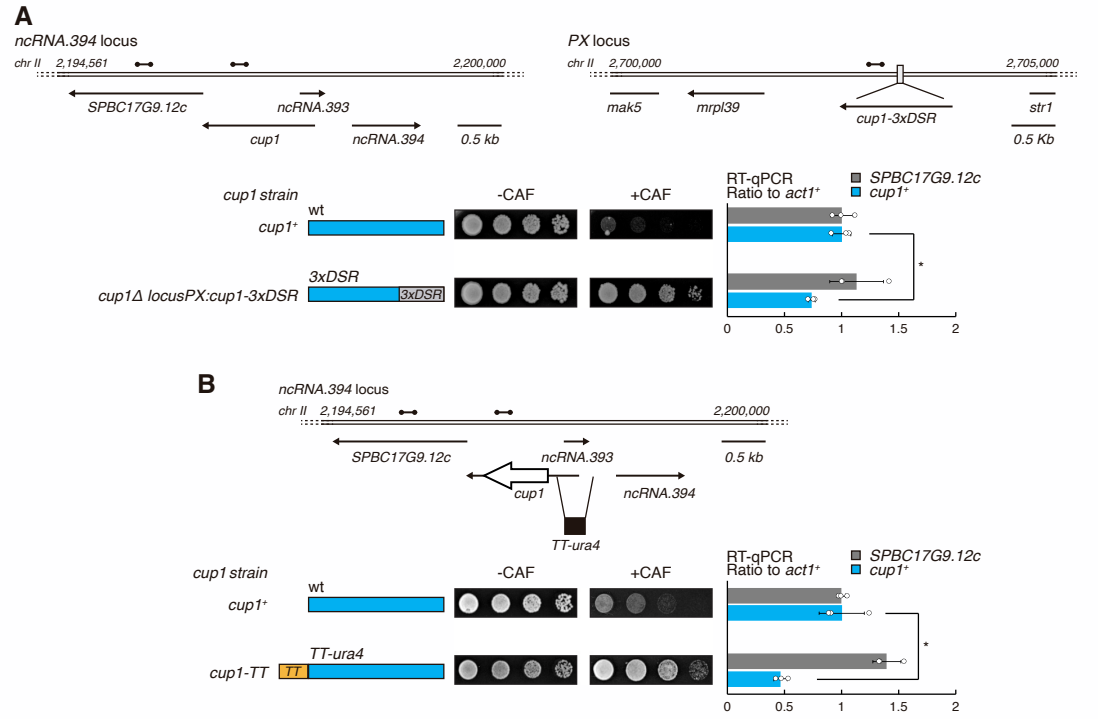

Figure 4.8. Reduced expression of *cup1*$^{+}$ results in caffeine resistance. A. An additional copy of *cup1*$^{+}$ with 3x determinant of selective removal (DSR) motifs fused to its 3' untranslated region was inserted at an intergenic region (*LocusPX:cup1-3xDSR*). After deletion of endogenous *cup1*$^{+}$, cells expressing only *cup1-3xDSR* were assessed for caffeine resistance. Right. Transcript levels of *cup1*$^{+}$ and *SPBC17G9.12c*$^{+}$ (as control) in *cup1Δ locusPX:cup1-3xDSR* cells compared to wild-type. Data are mean ± s.d. from three biological replicates. Dumbbells indicate oligonucleotides used. **P*<0.05 (two tailed Student's *t* test). *cup1-3xDSR* constructs were designed by Dr. Manu Shukla. **B.** Experiment performed by Dr. Alison Pidoux. The 144-bp transcriptional terminator site from *ura4*$^{+}$ was inserted in place of part of the putative *cup1*$^{+}$ promoter (*cup1-TT*) and cells were assessed for caffeine resistance. Right. Transcript levels of *cup1*$^{+}$ and *SPBC17G9.12c*$^{+}$ (as control) in *cup1-TT* cells compared to wild type. Data are mean ± s.d. from three biological replicates. Dumbbells indicate oligonucleotides used. **P*<0.05 (two tailed Student's *t* test).

Cup1 has been shown to localise to mitochondria when overexpressed from a plasmid (Matsuyama et al. 2006). Indeed, Cup1 contains an N-terminal leucine/tyrosine/arginine (LYR) domain often found in mitochondrial proteins (Angerer 2015). To confirm that Cup1 has mitochondrial localisation, endogenous Cup1 was C-terminally tagged with green fluorescent protein (GFP) (strain constructed in collaboration with Dr. Sharon White). Cytological analyses of Cup1-GFP using the mCherry-tagged mitochondrial protein Arg11 as control (Delerue et al. 2016), demonstrated that Cup1-GFP localizes to mitochondria (Figure 4.9, experiment performed by Dr. Alison Pidoux).

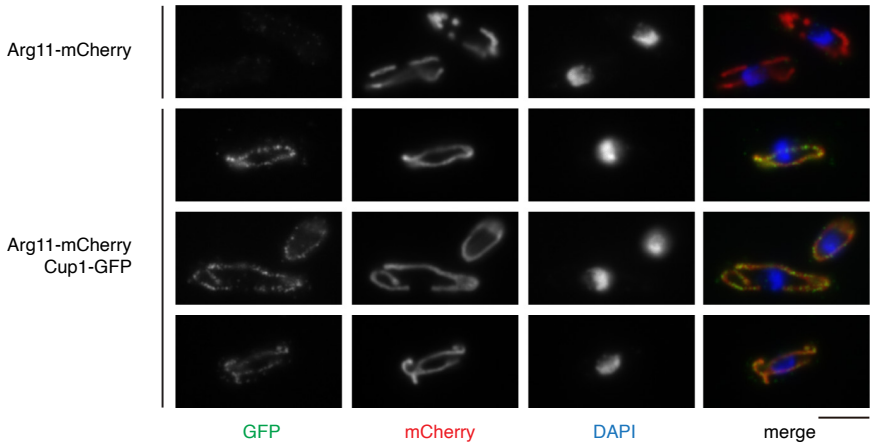

Figure 4.9. Cup1 localizes to mitochondria. Experiment performed by Dr. Alison Pidoux. Cells expressing either untagged Cup1 (top row) or Cup1-GFP (bottom three rows) were fixed and processed for immunofluorescence with anti-GFP antibody and Alexa-488 secondary antibody and DNA was stained with DAPI. The mitochondrial protein Arg11-mCherry served as a positive control for mitochondrial localisation. All images in the green channel (Cup1-GFP) are scaled relative to each other, as are those in the red channel (Arg11-mCherry); DAPI images are autoscaled. Bar, 5 mm. The strain harbouring Cup1-GFP was constructed in collaboration with Dr. Sharon White.

Several LYR domain-containing proteins have been associated with maintenance of mitochondrial homeostasis (Angerer et al. 2014; Angerer 2015), and LYR domain disruption has been shown to lead to phenotypic defects (Angerer et al. 2014). To determine whether disruption of the N-terminal LYR domain of Cup1 results in caffeine resistance, mutations

predicted to have a phenotypic effect by the *Phyre2* webtool (Kelley et al. 2015) were introduced into the endogenous *cup1*$^{+}$ gene (*cup1-L73G* and *cup1-F99G*) using the *SpEDIT* CRISPR/Cas9 genome editing system (see Methods section 2.2.10). Cells harbouring mutations in the N-terminal LYR domain of Cup1 (Cup1-L73G and Cup1-F99G) were found to exhibit resistance to caffeine (Figure 4.10, experiment performed in collaboration with Dr. Sharon White).

Figure 4.10. Cup1 LYR-domain mutation results in caffeine resistance. Experiment performed in collaboration with Dr. Sharon White. Point mutations (L73G and F99G) were introduced in the LYR domain of Cup1 and cells were assessed for caffeine resistance. Mutations were designed based on *Phyre2* webtool analysis (Kelley et al. 2015). *hba1Δ* cells were used as positive control.

Together, these analyses demonstrate that reduced levels or defective Cup1 (*SPBC17G9.13c*), a previously uncharacterized mitochondrial protein, result in caffeine resistance. It was therefore concluded that silencing of wild-type *cup1*$^{+}$ due to the formation of a heterochromatin island mediates caffeine resistance in unstable isolates.

4.2.3. Forced synthetic heterochromatin at the *hba1* or *ncRNA.394* loci is sufficient to drive antifungal drug resistance in wild-type cells

Deletion of *hba1*$^{+}$ confers resistance to caffeine, but also to additional drugs such as brefeldin A and staurosporine (Castillo et al. 2003). This multidrug-resistant phenotype is caused by the constitutive nuclear accumulation of Pap1 in *hba1Δ* cells (Toda et al. 1991; Turi et al. 1996; Kumada et al. 1996),

which leads to up-regulation of the major efflux transporter Bfr1 (Toone et al. 1998). Because *hba1Δ* cells display a multidrug resistance phenotype, it is possible that cells with ectopic heterochromatin islands at the *hba1* locus may also exhibit resistance to other compounds besides caffeine.

Azole drugs target ergosterol biosynthesis and are the most widely used class of fungicides (Parker et al. 2014). Furthermore, the emergence of azole resistance has been proposed to represent a threat to human health and food security (Fisher et al. 2018). Interestingly, mutation of several proteins with mitochondrial function has been shown to confer resistance to the azole drug clotrimazole (Fang et al. 2012), suggesting that reduced Cup1 levels due to ectopic heterochromatin formation at the *ncRNA.394-cup1* locus could lead to clotrimazole resistance.

To explore the possibility of multidrug resistance, strains with forced TetR-Clr4*-mediated synthetic heterochromatin tethering at the *hba1* or *ncRNA.394-cup1* loci were exposed to lethal concentrations of the azole drugs clotrimazole, tebuconazole and fluconazole. Clotrimazole and fluconazole are widely used to treat human infections, while tebuconazole is predominantly used in agricultural settings (Fisher et al. 2018). The formation of synthetic heterochromatin domains at the *hba1* or *ncRNA.394-cup1* loci was found to render cells resistant to all three tested azole compounds (Figure 4.11). In addition, unstable caffeine-resistant isolates that formed ectopic heterochromatin domains over *hba1* (UR-1) or *ncRNA.394-cup1* (UR-2) also exhibited cross-resistance to these fungicides (Figure 4.12). Together these results demonstrate that ectopic heterochromatin formation at the *hba1* or *ncRNA.394-cup1* loci is sufficient to drive resistance to commonly used azole fungicides.

4.3. Discussion

In this chapter, a synthetic tethering system was used to investigate whether the formation of ectopic heterochromatin islands previously identified in unstable caffeine-resistant isolates is sufficient to drive caffeine resistance in

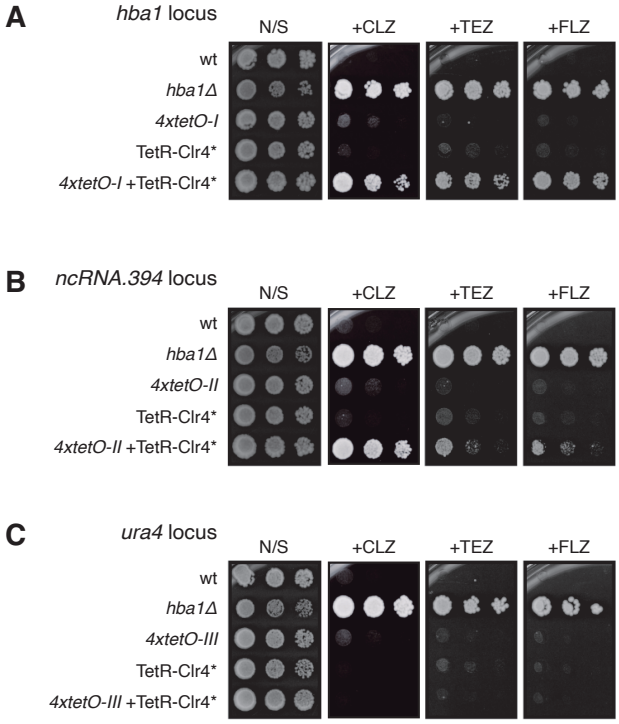

Figure 4.11. Forced assembly of synthetic heterochromatin at the *hba1* or *ncRNA.394* loci is sufficient to drive azole resistance in wild-type cells. A-C. Wild-type cells harbouring *4xtetO* binding sites at the *hba1* (**A**), *ncRNA.394* (**B**), or (control) *ura4* (**C**) loci and expressing TetR-Clr4***** were assessed for resistance to the drugs clotrimazole (+CLZ), tebuconazole (+TEZ) and fluconazole (+FLZ) in the absence of AHT. The exact position of *4xtetO* sites and H3K9me2 levels at the corresponding tethering sites are shown in Figure 4.2. *hba1Δ* cells were included to test whether deletion of *hba1*$^{+}$ leads to azole drug resistance. N/S, non-selective medium.

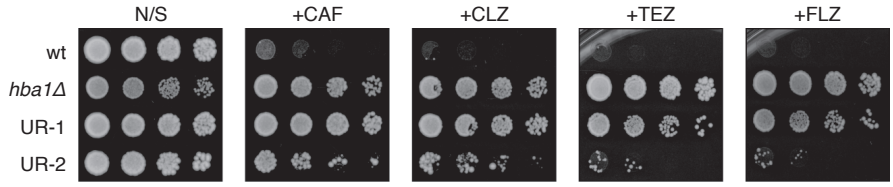

Figure 4.12. Unstable caffeine-resistant isolates show cross-resistance to fungicides. Unstable caffeine-resistant isolates UR-1 and UR-2 were serially diluted and spotted on non-selective (N/S), caffeine (+CAF), clotrimazole (+CLZ), tebuconazole (+TEZ) and fluconazole (+FLZ) media to assess resistance. *hba1Δ* cells were used as positive control.

wild-type cells. Targeting synthetic heterochromatin formation to the *hba1, ncRNA.394* or *mbx2* loci using tethered Clr4 H3K9 methyltransferase (TetR-Clr4*) resulted in cells displaying caffeine resistance (-AHT, Figure 4.1, 4.2 and 4.3). Notably, the caffeine-resistant phenotype could be reverted by the loss of H3K9me2 from tethering sites upon release of TetR-Clr4* (+AHT, Figure 4.1, 4.2 and 4.3), demonstrating that resistance is mediated by heterochromatin formation at these loci. Interestingly, heterochromatin domains that formed upon TetR-Clr4* tethering to the *hba1* or *ncRNA.394* loci showed lower H3K9me2 levels and spread over a smaller region than those formed at the control *ura4* locus, at least in non-selective conditions (Figure 4.2). These differences may be explained by the consequences of heterochromatin silencing at each locus on cellular fitness. In line with this hypothesis, silencing of endogenous *ura4* has no apparent consequence for cell growth (Audergon et al. 2015), whereas cells lacking the *hba1*$^{+}$ gene exhibit a marked growth defect (Figure 4.1B, compare *hba1Δ* to wt cells on non-selective medium). However, it is also possible that the observed variations in H3K9me2 levels among loci are due to differences in transcription across tethering sites, as previously reported (Audergon et al. 2015).

At the *hba1* locus, deletion of *hba1*$^{+}$ is known to confer caffeine resistance (Castillo et al. 2003), whereas deletion of the adjacent gene *ish1*$^{+}$ has no effect (Taricani et al. 2002). Hence, it was concluded that heterochromatin silencing of *hba1*$^{+}$ confers caffeine resistance at this locus.

Extensive functional dissection of the *ncRNA.394* locus revealed that silencing of *cup1*$^{+}$ (*SPBC17G9.13c*$^{+}$), a previously uncharacterized essential gene, mediates caffeine resistance. Deletion of *ncRNA.394* and other adjacent non-essential genes did not cause a resistant phenotype (Figure 4.4). Notably, growth in the presence of caffeine expanded the island of ectopic H3K9me2 heterochromatin at the *ncRNA.394* locus to cover *SPBC17G9.13c*$^{+}$ (Figure 4.5). Indeed, caffeine resistance correlated with H3K9me2 levels over *SPBC17G9.13c* (Figure 4.6), and reduced transcript levels of this gene were present in all analysed caffeine-resistant strains/isolates that exhibited

ncRNA.394 heterochromatin islands (Figure 4.7 and Chapter 3, Figure 3.9 and 3.10C). Importantly, strains with manipulations that increased the degradation of *cup1*$^{+}$ mRNA (*LocusPX:cup1–3xDSR*) or attenuated its transcription (*cup1–TT*) resulted in reduced *cup1*$^{+}$ transcript levels and caffeine resistance (Figure 4.8). Cup1 contains a LYR domain often found in mitochondrial proteins (Angerer 2015), and a Cup1-GFP fusion showed mitochondrial localisation (Figure 4.9). Mutation of the LYR domain led to caffeine resistance (Figure 4.10). Therefore, Cup1 (*SPBC17G9.13c*) is a mitochondrial protein whose mutation or reduced expression renders cells caffeine resistant. It was thus concluded that silencing of wild-type *cup1*$^{+}$ due to the formation of a heterochromatin island at the *ncRNA.394* locus mediates caffeine resistance in unstable isolates.

Further investigation is required to decipher the mechanism by which reduced Cup1 levels lead to caffeine resistance. Deletion of several genes encoding mitochondrial proteins has been shown to trigger a caffeine-resistant phenotype (Calvo et al. 2009; Paulo et al. 2014), but the function of these proteins is diverse. For example, loss of the thioredoxin reductase Trr1 leads to cellular hyper-oxidation (Jara et al. 2007), whereas cells lacking the p-hydroxybenzoate polyprenyl diphosphate transferase Ppt1 exhibit reduced levels of ubiquinone, an essential component of the electron transfer system (Uchida et al. 2000). One possible explanation is that related mechanisms involving the Pap1 pathway are responsible for caffeine resistance in cells lacking these functionally distinct mitochondrial factors. It is well known that disruption of Trr1 provokes caffeine resistance through the constitutive oxidation and subsequent nuclear localization of Pap1 (Benkö et al. 1997; Calvo et al. 2009; Calvo et al. 2012; Vivancos et al. 2004). Similarly, since ubiquinone has been shown to act as antioxidant in *S. pombe* (Suzuki et al. 1997; Uchida et al. 2000), it is plausible that loss of Ppt1 may also lead to Pap1 oxidation and the consequent activation of stress-response genes in the nucleus (see Figure 1.16 in Chapter 1 for an overview of the Pap1 pathway). A connection with ubiquinone metabolism may also underlie caffeine resistance in cells with reduced Cup1 levels. Indeed, LYR domain mutation of

the mitochondrial complex I subunit NMB4 in the yeast *Yarrowia lipolytica* leads to paralyzed ubiquinone reductase activity (and thus to less available ubiquinone with antioxidant activity) (Angerer et al. 2014). It is thus conceivable that reduced Cup1 levels might induce defects in mitochondrial function that ultimately drive resistance via a Pap1-dependent mechanism.

In addition, the data presented indicate that heterochromatin silencing at the *mbx2* locus is also sufficient to confer caffeine resistance in wild-type cells (Figure 4.3). However, the degree of resistance observed upon TetR-Clr4* recruitment to *mbx2* was less compared to that in strains that assembled synthetic heterochromatin at the *hba1* or *ncRNA.394-cup1* loci (Figure 4.1 and 4.3). Note that an extensive characterization of the TetR-Clr4*-mediated synthetic heterochromatin domain assembled at the *mbx2* locus was not performed. Thus, the weaker resistant phenotype exhibited by strains with forced heterochromatin at *mbx2* could be due to the formation of a smaller H3K9me2 domain surrounding the tethering site in these cells. Nevertheless, a functional dissection of this locus is required to identify the gene or genes responsible for resistance. In particular, an exhaustive examination of previously annotated Mbx2 targets (Kwon et al. 2012), might lead to the identification of suitable candidate genes.

Notably, strains with forced synthetic heterochromatin at either *hba1* or *ncRNA.394-cup1* displayed resistance to the widely-used antifungal agents clotrimazole, fluconazole and tebuconazole (Figure 4.11), and unstable isolates with heterochromatin islands at these loci (*hba1*, UR-1; *ncRNA.394-cup1,* UR-2) also showed cross-resistance to azoles. Deletion of *hba1*$^{+}$ is known to confer a multidrug resistance phenotype due to constitutive nuclear accumulation of Pap1 and subsequent expression of stress-response genes, including the major efflux transporter *bfr1*$^{+}$ (Toone et al. 1998). Indeed, overexpression of *pap1*$^{+}$ leads to resistance to clotrimazole (Liu et al. 2018). Thus, it is likely that Pap1-dependent up-regulation of *bfr1*$^{+}$ following heterochromatin-mediated silencing of *hba1*$^{+}$ is responsible for the multidrug resistance phenotype of these cells. In the case of *cup1*$^{+}$ silencing, insights

into how down-regulation of this gene leads to caffeine resistance will certainly shed light into potential mechanisms through which reduced levels of this novel mitochondrial protein cause resistance to other antifungal agents.

Taken together, the results presented here show that forced heterochromatin formation at the previously identified UR loci is sufficient to drive caffeine and azole resistance in wild-type cells. In the following chapter, the possibility that heterochromatin-mediated epimutations can act as stepping stones to subsequent genetic changes that augment resistance will be explored.

Chapter 5: Extrachromosomal circular DNA generation provides a supplementary mechanism for the evolution of caffeine resistance

5.1. Introduction

It has been proposed that epigenetic variation might have a role as a bridge towards genetic end points by facilitating genetic assimilation of characters (Waddington 1942). In fact, it was observed that when flies that exhibited an environmental stress-induced phenotypic change were manually selected for some generations, the displayed character eventually appeared in the absence of the stress (Waddington 1953 and 1956). More recently, theoretical studies have suggested that epigenetic variation has the potential to affect the outcomes of adaptation (Klironomos et al. 2013; Kronholm & Collins 2015). Indeed, simulations predict that adapted phenotypes driven by epimutations can appear long before stable genetic changes do (Klironomos et al. 2013). Thus, epigenetic changes have been conjectured to act as stepping stones to subsequent and permanent genetic changes (Klironomos et al. 2013; Nishikawa & Kinjo 2018).

However, not all genetic changes are irreversible. Copy number variations (CNVs) are alterations in number of copies of particular genes or other more extensive DNA sequences in a genome (McCarroll & Altshuler 2007). While CNVs caused by stable chromosomal amplifications and deletions are known to be an evolutionarily important source of genetic variation (Kidd et al. 2008), CNVs produced by extrachromosomal circular DNA (eccDNA) have been shown to facilitate adaptive evolution by allowing swift phenotypic responses to challenging conditions (Libuda & Winston 2006; Wu et al. 2019; Hull et al. 2019). Indeed, eccDNA structures are prone to rapid accumulation and loss and have been found in many organisms (Horowitz & Haber 1985; Schwedler et al. 1990; Navrátilová et al. 2008). In the budding yeast *S. cerevisiae*, eccDNA derived from all chromosomes has been detected (Møller et al. 2015).

Moreover, exposing *S. cerevisiae* to environmental copper has been shown to trigger the transcription-induced formation of eccDNAs containing a copper resistance gene that drive adaptation to copper-rich environments (Fogel & Welch 1982; Hull et al. 2017; Hull et al. 2019). In *S. pombe*, the extrachromosomal inheritance of nalidixic acid resistance has been reported (Massardo et al. 1982), as well as the existence of transient structural variations within clonal populations that affect gene expression and quantitative traits (Jeffares et al. 2017). However, whether these phenomena involve the formation of eccDNA in fission yeast is unknown.

It is possible that once an initial resistant phenotype is established by epigenetic changes, prolonged growth in the presence of the insult would induce the gain of supplementary adaptive genetic changes. In this chapter, I investigated whether unstable caffeine-resistant isolates harbouring ectopic heterochromatin-dependent epimutations can acquire subsequent genetic changes that augment resistance.

5.2. Results

5.2.1. Copy number variation analysis reveals a partial duplication of chromosome III in 12 of 30 unstable caffeine-resistant isolates

Detailed inspection of WGS data using *CNVkit* (Talevich et al. 2016) revealed that 12 of 30 independent unstable caffeine-resistant isolates, in addition to heterochromatin islands over euchromatic loci, also contained overlapping regions of chromosome III at increased copy number (Figure 5.1 and Table 5.1). Chromosome III CNVs were detected in isolates that exhibited ectopic heterochromatin islands at the *grt1* (UR-4), *fio1* (UR-5), *mbx2* (UR-6) and *ncRNA.394-cup1* (9 of 24 isolates) loci (Table 5.1), none of which are located on chromosome III. Interestingly, in 11 of 12 isolates displaying chromosome III CNVs, the minimal region of overlap (approximately 200 kb) contains the *cds1*$^{+}$ gene (Figure 5.1), overexpression of which is known to confer caffeine resistance (Wang et al. 1999). Although ectopic heterochromatin island formation at the *mbx2* or *ncRNA.394-cup1* loci was shown to be sufficient to

drive caffeine resistance in wild-type cells (Chapter 4), it is possible that amplification of the *cds1* locus constitutes an alternative or supplementary mechanism for the acquisition of caffeine resistance in these isolates. However, the majority of isolates (15 of 24) exhibiting a heterochromatin island at *ncRNA.394-cup1* do not harbour partial duplications of chromosome III (Table 5.1), suggesting that CNVs detected in a minority of these isolates (9 of 24) might have occurred after *ncRNA.394-cup1* island formation.

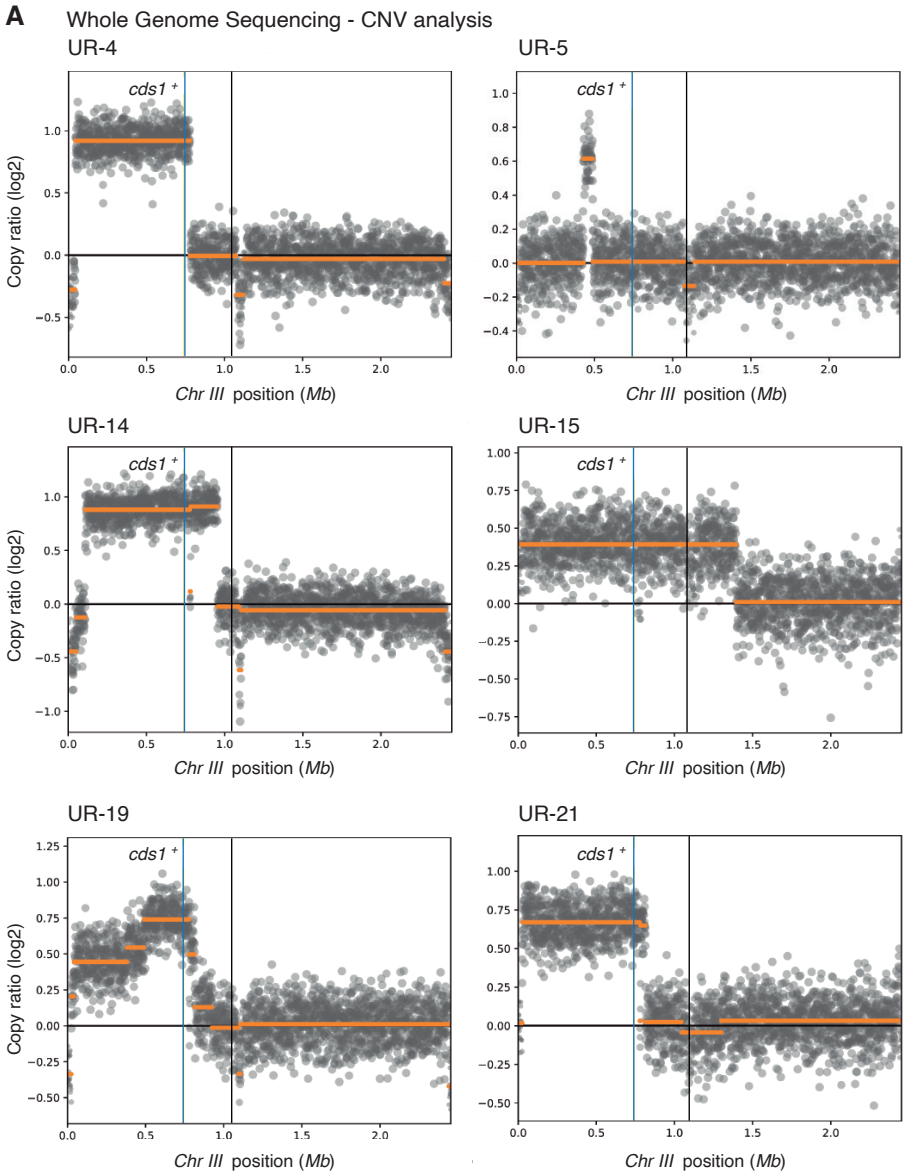

See next page for caption

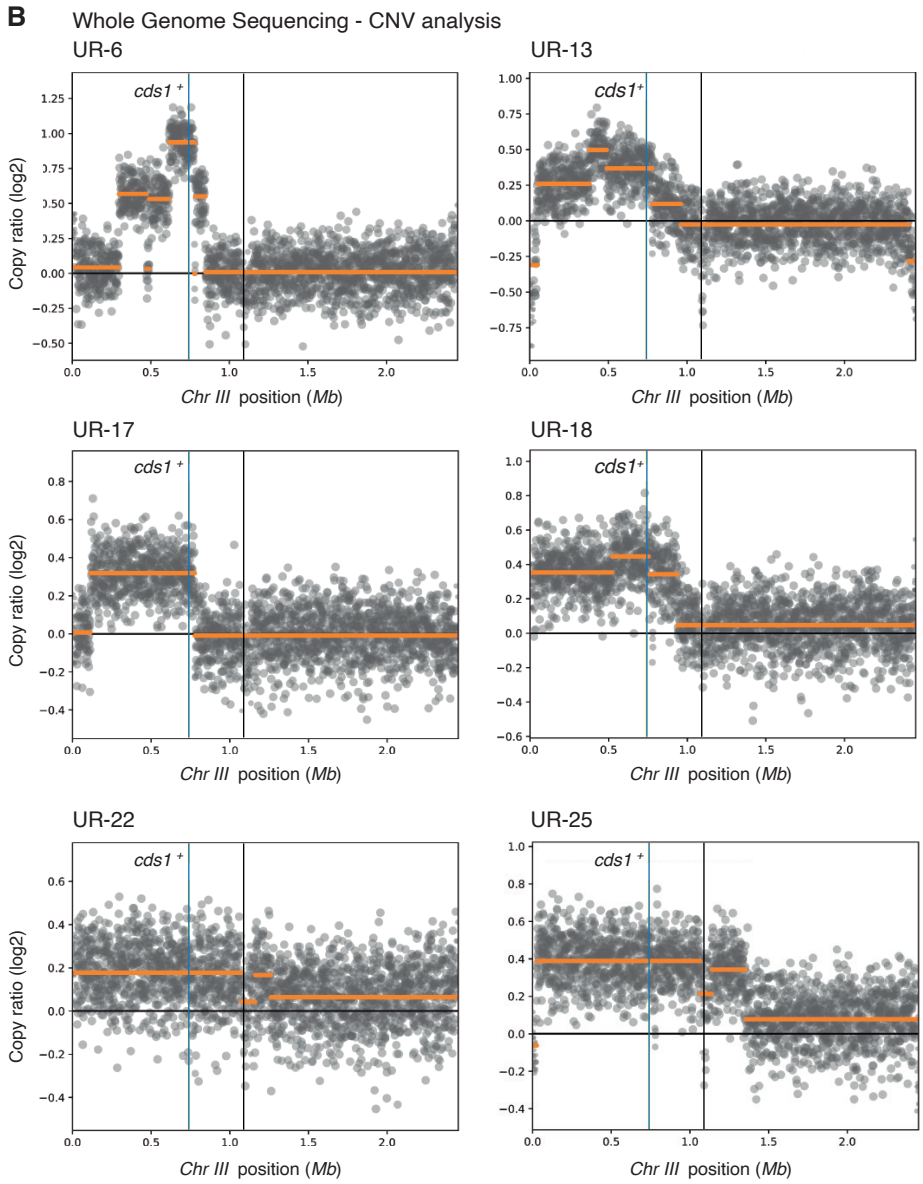

Figure 5.1. Copy number variation analysis reveals a partial duplication of chromosome III in 12 of 30 unstable caffeine-resistant isolates. A-B. Chromosome III coverage plots with overlaid segments in UR isolates showing partial duplication of chromosome III. Location of *cds1*$^{+}$ is highlighted in blue. Location of the centromere is highlighted in black. Wild-type ChIP-seq input data were used as the reference.

Table 5.1. Epigenetic (H3K9me2 islands) and genetic (SNPs, indels and copy number variation) changes found in unstable (UR) caffeine-resistant isolates. H3K9me2 islands, SNPs and indels as shown in Chapter 3 (Table 3.1 and 3.2). Data corresponds to isolates at their initial stage (4 days +CAF), as shown throughout this thesis, unless stated otherwise.

Isolate	Ectopic heterochromatin location		SNPs or indels in coding sequences	Partial duplication of Chr III?
	ncRNA.394	**other loci**		
UR-1		✓ (*hba1*)	Clr5-Q264STOP / Meu27-S100Y	
UR-2	✓		Sdo1-R11C	
UR-3		✓ (*ppr4*)	Clr5-Q264STOP / Meu27-S100Y	
UR-4		✓ (*grt1*)	-	✓
UR-5		✓ (*fio1*)	Clr5-Q264STOP / Meu27-S100Y	✓
UR-6		✓ (*mbx2*)	-	✓
UR-7		✓ (*ppr4*)	Clr5-Q264STOP / Meu27-S100Y	
UR-8	✓		-	
UR-9	✓		-	
UR-10	✓		Cob1-F318L	
UR-11	✓		-	
UR-12	✓		-	
UR-13	✓		-	✓
UR-14	✓		Npp-W300STOP / SPBC16H5.13-S1011L	✓
UR-15	✓		-	✓
UR-16	✓		-	
UR-17	✓		SPCC777.02-R120R	✓
UR-18	✓		SPCC777.02-R120R	✓
UR-19	✓		Sdo1-R11C	✓
UR-20	✓		-	
UR-21	✓		-	✓
UR-22	✓		-	✓
UR-23	✓		Pch1-Q234STOP	
UR-24	✓		-	
UR-25	✓		-	✓
UR-26	✓		SPBC1271.08c-A133A	
UR-27	✓		SPCC4B3.13-A229V	
UR-28	✓		Mug72-N116S	
UR-29	✓		Mug72-N116S	
UR-30	✓		-	

5.2.2. Epigenetic changes preceded genetic changes in the unstable caffeine-resistant isolate UR-2

To determine whether chromosome III CNVs (also referred to as *cds1* locus amplification) occurred before or after *ncRNA.394-cup1* heterochromatin island formation, samples frozen at earlier and later time points for the same isolate, UR-2, were analyzed. ChIP-seq and CNV analyses showed that in the initial caffeine-resistant isolate (at 4 days +CAF) the *ncRNA.394-cup1* H3K9me2 island was present (Figure 5.2A, as shown previously in Chapter 3), and chromosome III copy number levels were indistinguishable from wild-type (Figure 5.2A). However, prolonged growth in the presence of caffeine for 3 days (at 7 days +CAF) resulted in UR-2 cells exhibiting both the *ncRNA.394-cup1* H3K9me2 island and *cds1* locus amplification (Figure 5.2A). Furthermore, acquisition of chromosome III CNVs correlated with a slightly stronger caffeine-resistant phenotype (Figure 5.2B). Thus, in UR-2 a heterochromatin island arose before amplification of the *cds1* locus.

To test whether the acquisition of *cds1* locus amplification leads to heterochromatin not being required for resistance, *clr4*$^{+}$ was deleted in initial and subsequent UR-2 samples and cells were challenged with caffeine. Deletion of *clr4*$^{+}$ from the initial UR-2 isolate (at 4 days +CAF) resulted in loss of caffeine resistance in all transformants tested (6/6) (Figure 5.3). However, only half of the transformants (3/6 – transformants 1, 4 and 5) lost resistance to caffeine when *clr4*$^{+}$ was deleted from UR-2 cells displaying amplification of the *cds1* locus (at 7 days +CAF). In transformants that retained resistance after *clr4*$^{+}$ removal (3/6 – transformants 2, 3 and 6) a higher number of *cds1*$^{+}$ copies were present compared to *clr4Δ* transformants that lost resistance or to wild-type cells (Figure 5.3). It was thus concluded that once amplification of the *cds1* locus occurs heterochromatin is no longer required for caffeine resistance.

Because isolates exhibiting both a heterochromatin island and *cds1* locus amplification display unstable caffeine resistance (Table 5.1 and Chapter 3, Figure 3.3), causative epigenetic and genetic changes in these isolates are

expected to disappear following growth in the absence of caffeine. The *ncRNA.394-cup1* ectopic heterochromatin island was previously shown to disassemble following growth in non-selective medium (Chapter 4, Figure 4.5). To test whether chromosome III CNVs are also reversible, UR-2 cells displaying both the *ncRNA.394-cup1* H3K9me2 island and *cds1* locus amplification (at 7 days +CAF) were grown in non-selective medium for 14 days and then subjected to ChIP-seq and CNV analyses (Figure 5.4). Results confirmed that both events – the *ncRNA.394* heterochromatin island and *cds1* locus amplification – are unstable and lost following growth in the absence of caffeine (Figure 5.4).

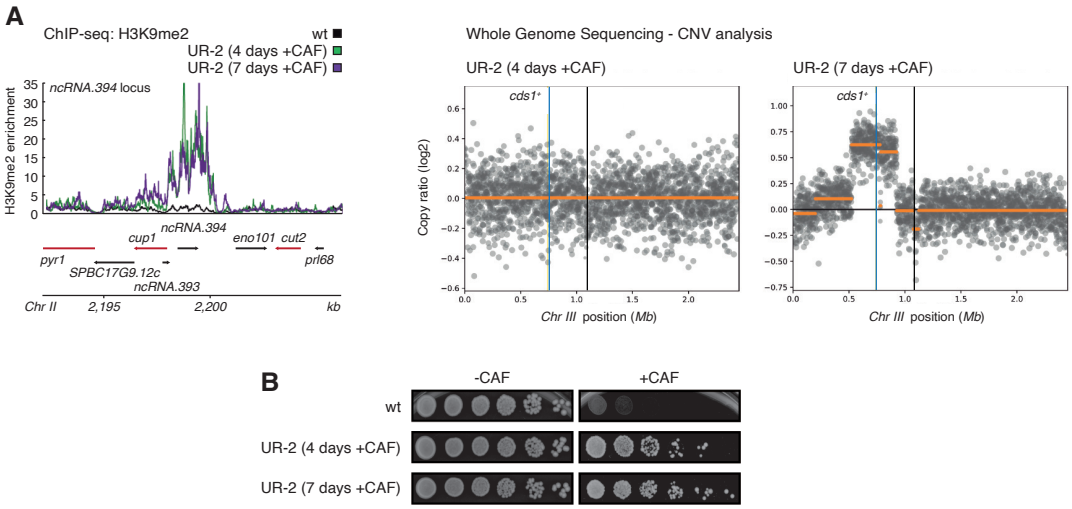

Figure 5.2. Epigenetic changes preceded genetic changes (CNVs) in the unstable caffeine-resistant isolate UR-2. A. H3K9me2 ChIP-seq enrichment at the *ncRNA.394-cup1* locus (left) and chromosome III coverage plots with overlaid segments (right) in UR-2 cells following prolonged growth on +CAF medium for 3 days (7 days +CAF). Location of *cds1*$^{+}$ is highlighted in blue. Location of the centromere is highlighted in black. Wild-type ChIP-seq input data were used as the reference for CNV analysis. **B.** UR-2 cells frozen at different stages (4 days +CAF and 7 days +CAF) were serially diluted and spotted on -CAF and +CAF plates to assess resistance to caffeine.

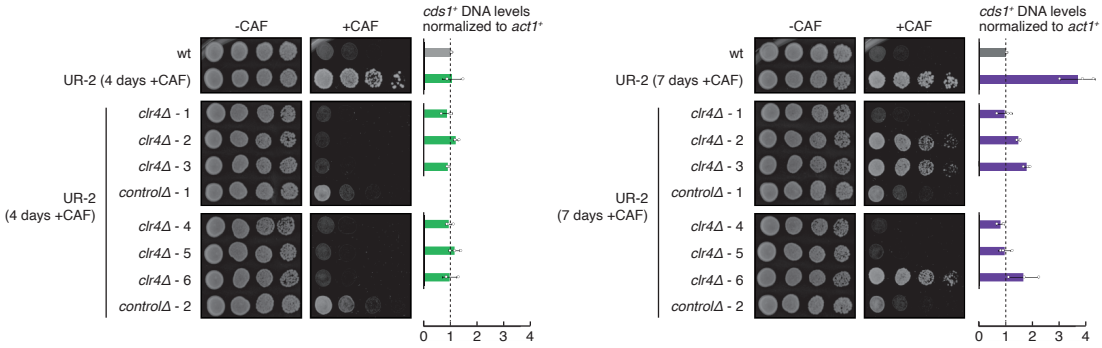

Figure 5.3. Cells displaying *cds1* locus amplification exhibit caffeine resistance in the absence of heterochromatin. *clr4*$^{+}$ (*clr4Δ*) or an unlinked intergenic region (control*Δ*) were deleted in UR-2 cells (4 days +CAF) and UR-2 cells after prolonged growth on +CAF medium for 3 days (7 days +CAF). All (6/6) UR-2 (4 days +CAF) *clr4Δ* transformants lost resistance to caffeine whereas only 50% (3/6, transformants 1, 4 and 5) UR-2 (7 days +CAF) lost resistance to caffeine. *cds1*$^{+}$ DNA levels in extracted genomic DNA were assessed by qPCR.

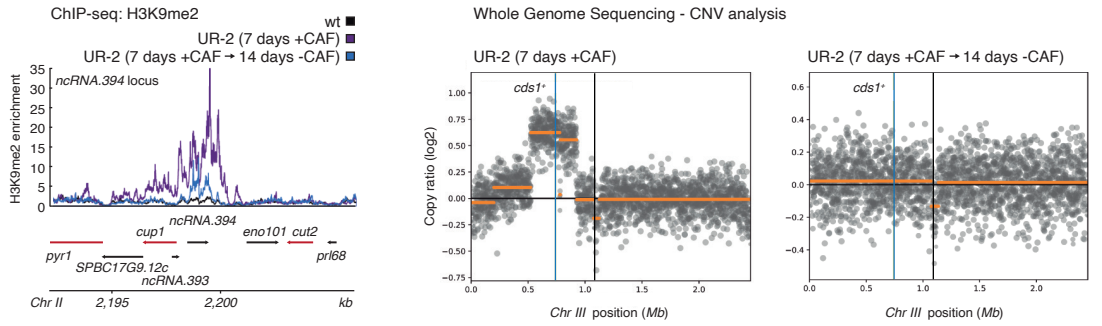

Figure 5.4. Both the *ncRNA.394-cup1* H3K9me2 island and *cds1* locus amplification are unstable. H3K9me2 ChIP-seq enrichment at the *ncRNA.394-cup1* locus (left) and chromosome III coverage plots with overlaid segments (right) in UR-2 cells following prolonged growth on non-selective medium for 14 days after prolonged growth on +CAF medium for 3 days (7 days +CAF → 14 days -CAF). Location of *cds1*$^{+}$ is highlighted in blue. Location of the centromere is highlighted in black. Wild-type ChIP-seq input data were used as the reference for CNV analysis.

5.2.3. Chromosome III CNVs correspond to extrachromosomal circular DNA

The instability displayed by the amplified *cds1* locus suggested that these CNVs may result from excision and formation of eccDNA, which can be rapidly accumulated and lost in eukaryotic cells (Libuda & Winston 2006; Wu et al. 2019; Hull et al. 2019). eccDNAs are usually generated through a recombination even between homologous sites on the same chromosome (Carroll et al. 1988; Paulsen et al. 2018). Inspection of CNV plots revealed the presence of repetitive elements at junctions of putative eccDNA (*5S rRNA.24/26* (403 kb apart) for UR-2 (at 7 days +CAF) and *LTR3/27* (743 kb apart) for UR-4) (Figure 5.5).

To test whether *cds1* locus amplification corresponds to eccDNA, primer pairs specific for putative circle junctions were designed and PCR analysis performed using extracted genomic DNA from UR-2 (at 7 days +CAF) and UR-4 isolates. Results confirmed the presence of eccDNA derived from chromosome III (Figure 5.5, experiment performed in collaboration with Dr. Alison Pidoux). These data indicate that repeat-mediated eccDNA generation provides a supplementary mechanism for the evolution of caffeine in fission yeast.

5.3. Discussion

In this chapter, the interplay between epigenetic and genetic changes in the evolution of caffeine resistance was investigated. CNV analysis indicated that 12 of the 30 unstable caffeine-resistant isolates that displayed an ectopic heterochromatin island also contained overlapping regions of chromosome III at increased copy number (Figure 5.1 and Table 5.1). Chromosome III CNVs exhibited very diverse sizes, ranging from 80 kb (UR-5) to 1.4 mb (UR-15 and UR-25). In 11 of 12 isolates, the minimal region of overlap contains the *cds1*$^{+}$ gene, known to drive caffeine resistance when overexpressed (Wang et al. 1999). *cds1*$^{+}$ encodes a protein kinase involved in the S-M (or replication) checkpoint, which prevents progression into mitosis until DNA replication is

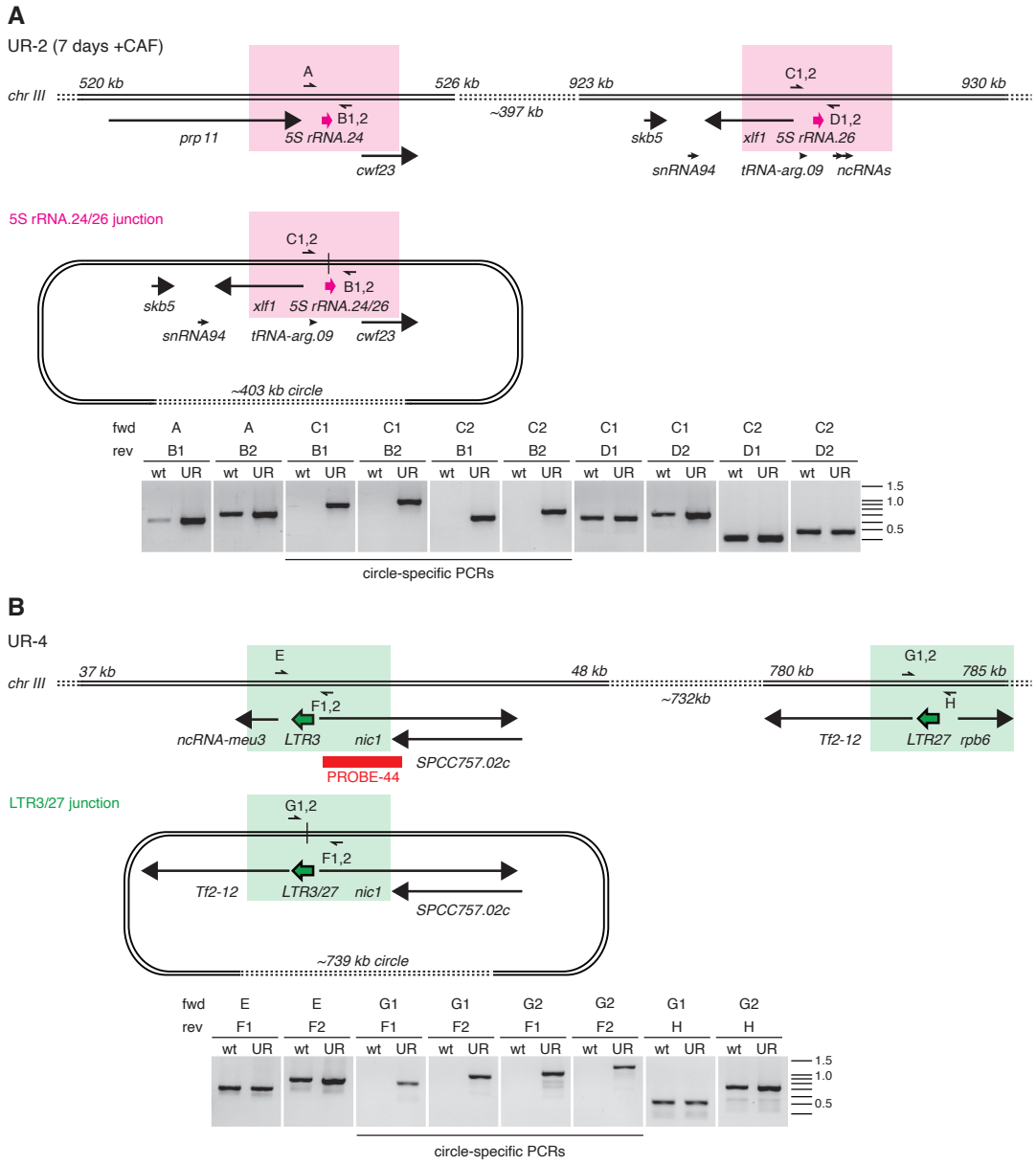

Figure 5.5. Chromosome III CNVs correspond to extrachromosomal circular DNA (eccDNA). Experiment performed in collaboration with Dr. Alison Pidoux. **A-B.** Junctions of putative extrachromosomal circles were identified at repetitive sequences by inspection of CNV plots for UR-2 (7 days +CAF) (**A**) and UR-4 (**B**). Positions of *5S rRNA.24* and *5S rRNA.26* (pink arrows), *LTR3* and *LTR27* (green arrows) and flanking genes are indicated. PCR primers (half arrows) flanking *5S rRNA.24* (A (forward); B1,2 (reverse)) and *5S rRNA.26* (C1,2; D1,2) were used to amplify products from wild-type (wt) and UR-2 (7 days +CAF) ChIP input samples, along with primer combinations (C1,2; B1,2) specific for the putative circle junctions (vertical black lines). Primers flanking *LTR3* (E; F1,2) and *LTR27* (G1,2; H) were used to amplify products from wild-type and UR-4 ChIP input samples, along with primer combinations (G1,2; F1,2) specific for the putative circle junction. Shaded boxes indicate primer locations and predicted circle junctions (pink: *5S rRNA.24/26*, green: *LTR3/27*). Positions of DNA markers are indicated in kb on right.

completed (Murakami & Okayama 1995). In wild-type cells, caffeine is known to override the S-M checkpoint, leading to septation in the absence of chromosome segregation and consequently cell death (Kumagai et al. 1998; Wang et al. 1999). Overexpression of *cds1*$^{+}$ has been proposed to suppress the detrimental effects of caffeine by preventing cells entering into mitosis until S phase is finalised, thus allowing correct cell cycle progression in the presence of the drug (Wang et al. 1999). Notably, chromosome III CNVs detected in UR-5 do not include *cds1*$^{+}$ (Figure 5.1). Because isolates were grown in non-selective medium prior to WGS and ChIP-seq experiments, it is possible that originally larger CNVs that included *cds1*$^{+}$ underwent rearrangement during growth of UR-5 cells in the absence of selective pressure. Alternatively, overexpression of one or many of the genes located within the detected amplified region might be responsible for driving or boosting the caffeine-resistant phenotype of these cells. However, database examination of the 35 genes located in this amplified 80 kb domain did not uncover any obvious candidate for resistance.

The initial UR-2 isolate, which only displayed a heterochromatin island at the *ncRNA.394-cup1* locus, was found to acquire increased copies of the *cds1* locus following prolonged growth in the presence of caffeine for 3 days (at 7 days +CAF), a change that correlated with a slight increase in caffeine resistance (Figure 5.2). Moreover, experiments performed on UR-2 cells frozen at the later time point (at 7 days +CAF) revealed that once amplification of the *cds1* locus occurs, heterochromatin is not a requirement for caffeine resistance (Figure 5.3). Notably, growth of UR-2 cells exhibiting both the *ncRNA.394-cup1* H3K9me2 island and *cds1* locus amplification in -CAF medium resulted in the loss of both adaptive events (Figure 5.4), a result consistent with the unstable caffeine-resistant phenotype observed in isolates harbouring both of these changes. It was thus concluded that in the UR-2 isolate, *cds1* locus amplification represents a subsequent yet unstable genetic change that supplements the caffeine-resistant phenotype driven by the *ncRNA.394-cup1* heterochromatin island. However, it is possible that these events are stochastic and occur in no fixed order. Refined screening strategies

in which isolates are examined at even earlier time points during the development of resistance would allow this hypothesis to be tested.

Notably, experiments performed after exhaustive inspection of CNV profiles revealed that amplifications of the *cds1* locus correspond to eccDNA generated through recombination between separate homologous repeats present on chromosome III (Figure 5.4). *S. pombe* has been shown to tolerate disomy for chromosome III (Niwa & Yanagida 1985; Niwa et al. 1986), and to stably maintain mini-chromosomes harbouring a functional centromere (Takahashi et al. 1992; Baum et al. 1994; Folco et al. 2008). However, the rapid loss of *cds1* locus amplification following non-selective growth, the diverse range of copies observed in individual isolates, and the fact that only 3 of the 12 observed CNV events harbour the centromere region of chromosome III, strongly suggest that eccDNAs are not maintained as additional chromosomes. Consistent with this hypothesis, *S. cerevisiae* eccDNAs have been shown to be generally acentric and to missegregate during cell division (Møller et al. 2015).

Importantly, it has been reported that reintegration of eccDNA provides an efficient pathway for gene amplification, with stable chromosomal changes being known or predicted to have emerged through eccDNA intermediates (Beverley et al. 1984; Galeote et al. 2011; Demeke et al. 2015). Comprehensive inspection of unstable isolates upon extensive growth in the presence of caffeine (e.g. at 20 days +CAF) could reveal whether eccDNAs act as intermediates to permanent genetic changes consisting of stably integrated amplifications of the *cds1* locus.

Together, the results presented here support the idea that development of resistance is a multistep process in which a combination of distinct epigenetic and genetic events allows cells to adapt to the insult. In the next chapter, the mechanism by which ectopic heterochromatin-mediated epimutations are generated following exposure to caffeine will be explored.

Chapter 6: Exposure to caffeine induces heterochromatin plasticity through regulation of key anti-silencing factors

6.1. Introduction

In *S. pombe*, the putative H3K9 demethylase Epe1 has been shown to prevent the epigenetic inheritance of synthetic heterochromatin domains (Audergon et al. 2015; Ragunathan et al. 2015). Loss of this JmjC domain-containing protein, for which *in vitro* demethylase activity has yet to be reported, has also been demonstrated to result in ectopic heterochromatin formation at euchromatic loci, as well as in increased H3K9me levels at facultative heterochromatin islands (Zofall et al. 2012; Wang et al. 2015; Parsa et al. 2018; Sorida et al. 2019). Thus, despite the lack of biochemical H3K9 demethylase activity, all phenotypic analyses are consistent with the *epe1*$^{+}$ gene encoding an H3K9 demethylase. Paradoxically, Epe1 localises to heterochromatin via interaction with the HP1-equivalent chromodomain protein Swi6 (Zofall & Grewal 2006; Trewick et al. 2007). Within constitutive heterochromatin domains, however, Epe1 is degraded through the action of the Cul4-Ddb1^{Cdt2} ubiquitin ligase, whose activity is limited to the interior of H3K9me domains and absent from their edges, thus restricting Epe1 activity to the boundaries of heterochromatin (Braun et al. 2011). Consistent with this idea, deletion of Epe1 leads to spreading of constitutive heterochromatin domains into neighbouring euchromatin (Zofall & Grewal 2006; Trewick et al. 2007).

In addition, the H3K14 acetyltransferase Mst2 has been reported to act in parallel to Epe1 to prevent the uncontrolled formation of heterochromatin (Wang et al. 2015). Indeed, cells lacking Mst2 exhibit increased H3K9me2 levels at facultative heterochromatin islands (Wang et al. 2015). Moreover, the combined loss of Epe1 and Mst2 has been shown to result in widespread

ectopic heterochromatin assembly at euchromatic loci, leading to severe growth defects (Wang et al. 2015).

Notably, 3 of the 6 distinctive ectopic heterochromatin domains detected in unstable caffeine-resistant isolates formed at loci previously described as facultative heterochromatin islands, which gain H3K9me2 in the absence of Epe1 (*ncRNA.394-cup1*, *ppr4* and *mbx2*; islands *14*, *4* and *16*, respectively, in Zofall et al. 2012). Indeed, H3K9me2 ChIP analyses performed here, as well as in other studies (Wang et al. 2015; Sorida et al. 2019), failed to detect H3K9me2 at these loci in untreated wild-type cells. The formation of ectopic heterochromatin islands at these and other loci in unstable resistant isolates suggests that the function of key anti-silencing regulators might be impaired upon caffeine treatment. In this chapter, I investigated the mechanism by which ectopic heterochromatin islands are generated following exposure to caffeine.

6.2. Results

6.2.1. Dynamic heterochromatin redistribution following short exposure to caffeine in wild-type cells

To investigate the dynamics of heterochromatin island formation in response to caffeine, wild-type cells were exposed to low (7 mM) or medium (14 mM) doses of caffeine for 18 hours. Cells in low caffeine accomplished ~8 doublings, whereas only ~3 population doublings occurred in medium caffeine (Figure 6.1). ChIP-seq for H3K9me2 detected the formation of several heterochromatin islands following exposure to low caffeine (Figure 6.2, top and 6.3). These caffeine-induced islands represent a subgroup of those known to accumulate H3K9me2 in the absence of Epe1 (facultative heterochromatin islands) (Zofall et al. 2012; Wang et al. 2015; Sorida et al. 2019), including *ncRNA.394-cup1* (Figure 6.2, top and 6.3), but did not overlap with the H3K9me2-heterochromatin domains that accumulate in the absence of nuclear exosome function (Yamanaka et al. 2013) or when cells are grown at 18°C (Gallagher et al. 2018) (Figure 6.3 – for a full list of genes and genomic

coordinates see Appendix V). Remarkably, following treatment with medium doses of caffeine, ectopic heterochromatin was restricted to *ncRNA.394-cup1*, and H3K9me2 levels at this locus were approximately four-fold greater after exposure to medium compared to low caffeine (Figure 6.2, bottom, 6.3 and 6.4). Together these data suggest that, when exposed to near-lethal doses of caffeine (medium, 14 mM), wild-type cells can rapidly develop resistance by forming heterochromatin at a locus (*ncRNA.394-cup1*) that confers resistance when silenced.

To determine if, in addition to caffeine, other insults also induce heterochromatin island formation, wild-type cells were exposed to oxidative stress by addition of hydrogen peroxide (1 mM) for 18 hours. ChIP-seq for H3K9me2 revealed the presence of heterochromatin islands at similar locations to those observed in low caffeine treatment, albeit H3K9me2 levels were lower (Figure 6.3 and 6.5).

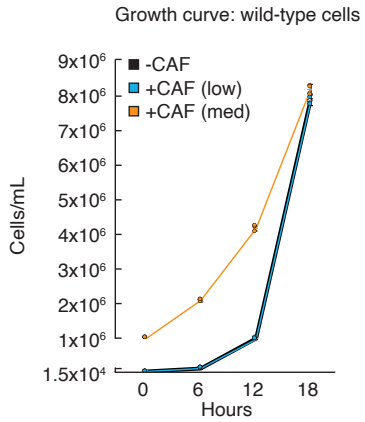

Figure 6.1. Growth of cells in caffeine. Wild-type cells were grown in the presence of low (7 mM) or medium (14 mM) doses of caffeine for 18 hours. Cell number was counted every 6 hours. Note that a larger inoculum was used for 14 mM caffeine culture in order to obtain the same final number of cells. Data are mean ± s.d. from three biological replicates. Cells from the 18-hr time point were used for experiment shown in Figure 6.4.

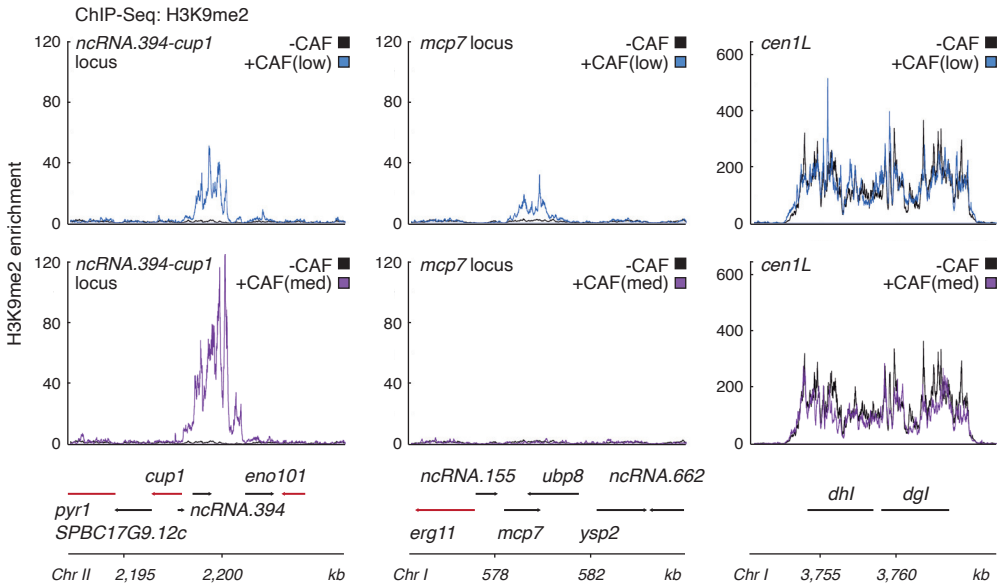

Figure 6.2. Dynamic heterochromatin redistribution following short exposure to caffeine in wild-type cells. H3K9me2 ChIP-seq enrichment at *ncRNA.394-cup1* and *mcp7* loci following 18 hr exposure to low (7 mM, top) or medium (14 mM, bottom) concentrations of caffeine. Data are represented as relative fold enrichment over input and compared to levels in untreated wild-type cells. Relevant genes within and flanking ectopic heterochromatin islands are indicated. Red arrows indicate essential genes. H3K9me2 enrichment on pericentromeric *dgl/dhl* repeats (*cen1L*) of chromosome I shown as control (note different scales). See Figure 6.3 for other loci.

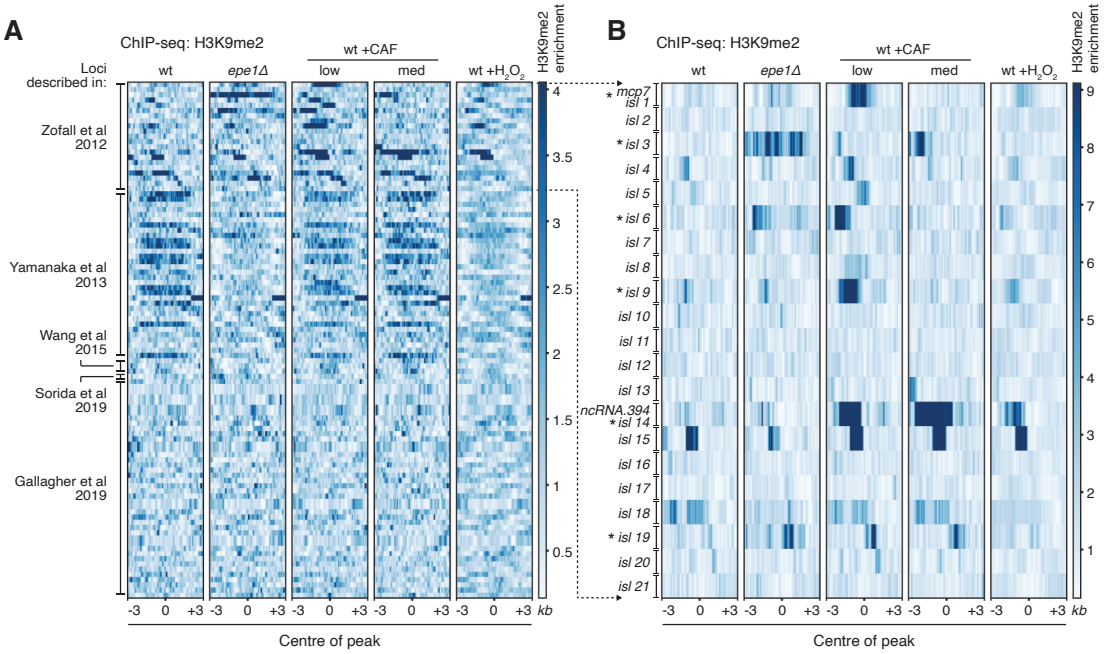

Figure 6.3. The heterochromatin profile of wild-type cells treated with low caffeine resembles that of untreated cells lacking Epe1. A-B. H3K9me2 ChIP-seq enrichment at previously-detected facultative heterochromatin loci (described in Zofall et al 2012 (**A** and **B**), Yamanaka et al 2013 (**A**), Wang et al 2015 (**A**), Sorida et al 2019 (**A**) and Gallagher et al 2019 (**A**)), in wild-type (wt) cells treated with caffeine (low dose, 7 mM or medium dose, 14 mM) or low dose of H_2O_2 (1 mM), compared to untreated *epe1Δ* and wt cells. Data are represented as relative fold enrichment over input. A subset of facultative heterochromatin islands detected in untreated *epe1Δ* cells (Zofall et al 2012, Wang et al 2015 and Sorida et al 2019) was detected in low caffeine-treated wild-type cells. Asterisks in **B** indicate loci with similar H3K9me2 patterns in low caffeine-treated wild-type cells and untreated *epe1Δ* cells, but not untreated wild-type cells. Facultative heterochromatin loci formed in the absence of the exosome (Yamanaka et al 2013) or in wild-type cells grown at 18°C (Gallagher et al 2019) were not detected in wild-type cells treated with caffeine (low dose, 7 mM or medium dose, 14 mM) or low dose of H_2O_2. For a full list of genes and genomic coordinates see Appendix V.

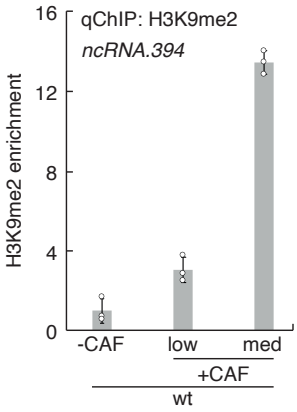

Figure 6.4. H3K9me2 accumulates at the *ncRNA.394-cup1* locus upon caffeine treatment. Quantitative ChIP (qChIP) of H3K9me2 levels on *ncRNA.394* in wild-type cells following 18 hr exposure to low (7 mM) or medium (14 mM) doses of caffeine. H3K9me2 levels were normalized to *S. octosporus* spike-in control. Data are mean ± s.d. from three biological replicates.

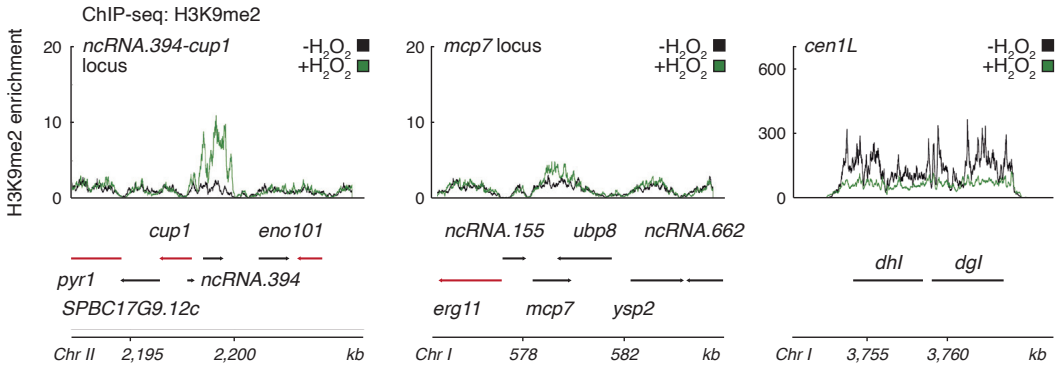

Figure 6.5. Dynamic heterochromatin redistribution following short exposure to hydrogen peroxide in wild-type cells. H3K9me2 ChIP-seq enrichment at *ncRNA.394-cup1* and *mcp7* loci following 18 hr exposure to a low concentration of H_2O_2 (1 mM). Data are represented as relative fold enrichment over input and compared to levels in untreated wild-type cells. Relevant genes within and flanking ectopic heterochromatin islands are indicated. Red arrows indicate essential genes. H3K9me2 enrichment on pericentromeric *dgl/dhl* repeats (*cen1L*) of chromosome I shown as control (note different scales). See Figure 6.3 for other loci.

6.2.2. The phenotype of wild-type cells treated with low caffeine resembles that of untreated cells lacking Epe1

The heterochromatin profile of wild-type cells treated with low caffeine partially resembles that of untreated cells lacking Epe1 (*epe1Δ*) (Figure 6.3B – assessed by visual inspection). It is possible that caffeine treatment might negatively regulate Epe1, thereby allowing ectopic heterochromatin islands to form in wild-type cells. TetR-Clr4*-mediated synthetic heterochromatin can be transmitted through cell division upon release of TetR-Clr4* from *tetO* binding sites only in the absence of Epe1 (Audergon et al. 2015; Ragunathan et al. 2015). To further test if caffeine treatment results in an *epe1Δ*-like phenotype, wild-type cells were treated with low caffeine and TetR-Clr4* was released from *tetO* binding sites placed upstream of *ura4*$^{+}$ (Figure 6.6, experiment performed in collaboration with Dr. Manu Shukla). qChIP for H3K9me2 showed that, like *epe1Δ*, caffeine treatment allowed synthetic heterochromatin retention at the tethering site for longer compared to untreated cells (Figure 6.6). These data strongly suggest that caffeine negatively regulates Epe1.

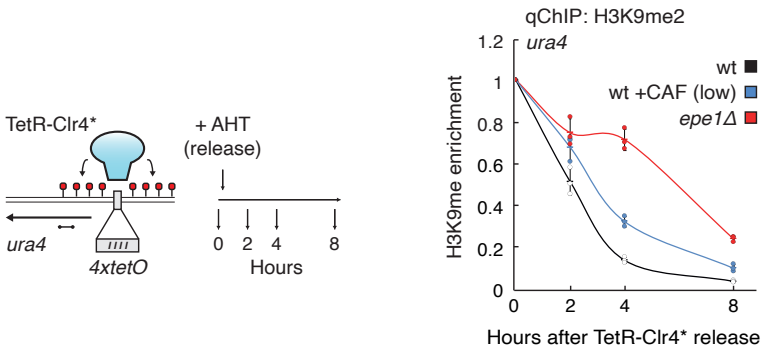

Figure 6.6. Caffeine treatment leads to prolonged retention of synthetic heterochromatin upon release of tethered Clr4 methyltransferase in wild-type cells. Experiment performed in collaboration with Dr. Manu Shukla. Quantitative chromatin immunoprecipitation (qChIP) of H3K9me2 levels on *4xtetO-ura4*$^{+}$ before and after TetR-Clr4* release in wild-type (wt) cells untreated or treated with low caffeine (7 mM). *epe1Δ* cells were used as positive control. Dumbbell indicates oligonucleotides used. H3K9me2 levels were normalized to *S. octosporus* spike-in control. Data are mean ± s.d. from three biological replicates.

6.2.3. Caffeine down-regulates Epe1 post-transcriptionally

To investigate whether caffeine treatment leads to reduced *epe1*$^{+}$ transcripts, wild-type cells were exposed to low caffeine (7 mM) for 18 hours and genome-wide transcriptome analysis (total RNA-seq) was performed. *epe1*$^{+}$ RNA levels were found not to be significantly altered by caffeine treatment (Figure 6.7). Similarly, transcript levels of genes encoding the anti-silencing histone acetyltransferase Mst2 or components of the Clr4 H3K9 methyltransferase CLRC complex were not substantially changed (Figure 6.7). To test if caffeine down-regulates Epe1 at the post-transcriptional level, cells harbouring 3x-FLAG-tagged Epe1 were subjected to western analysis after low caffeine treatment for 18 hours. Results revealed a 33% decrease in FLAG-Epe1 levels following exposure to caffeine (Figure 6.8, experiment performed in collaboration with Dr. Imtiyaz Yaseen). In addition, qChIP analysis of Epe1-GFP indicated that Epe1 association with various constitutive heterochromatin locations was reduced upon caffeine treatment (Figure 6.9).

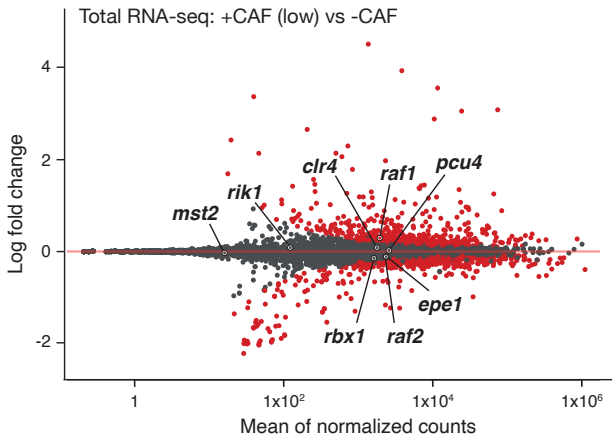

Figure 6.7. *epe1*$^{+}$ RNA levels do not change upon caffeine treatment. Total RNA-seq of wild-type cells treated with low caffeine (7 mM). Components of the CLRC complex (*clr4*$^{+}$, *rik1*$^{+}$, *raf1*$^{+}$, *raf2*$^{+}$, *pcu4*$^{+}$ *and rbx1*$^{+}$) and the anti-silencing factors *epe1*$^{+}$ *and mst2*$^{+}$ are highlighted.

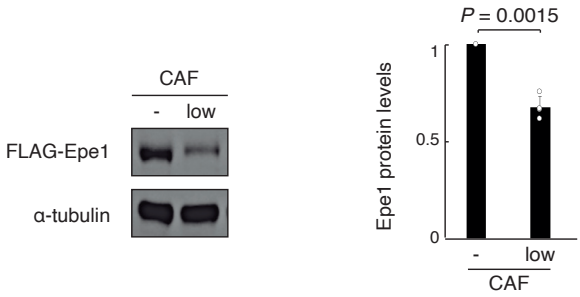

Figure 6.8. Epe1 protein levels decrease following caffeine treatment. Experiment performed in collaboration with Dr. Imtiyaz Yaseen. Left. Western analysis of 3xFLAG-Epe1 (expressed from its endogenous locus) before and after caffeine treatment (low concentration, 7 mM). Loading control: α-tubulin. Right. Quantification of 3xFLAG-Epe1 protein levels normalized to α-tubulin. Data are mean ± s.d. of four biological replicates. *P* value, two-tailed Student's *t*-test.

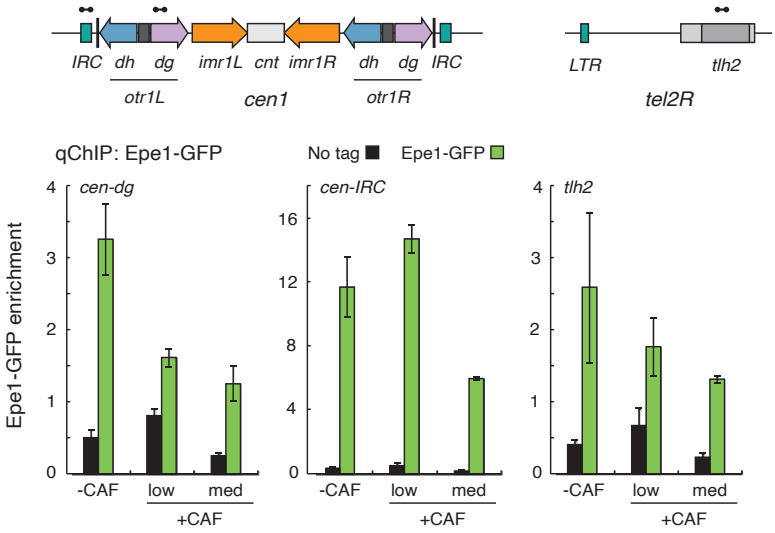

Figure 6.9. Epe1 loses association with chromatin upon caffeine treatment. qChIP analysis of Epe1-GFP levels at centromere 1 (*dg* repeats: cen-*dg*; outer boundary: *cen-IRC*), and at subtelomeric *tlh2* locus in wild-type cells treated with no, low (7 mM) or medium (14 mM) concentrations of caffeine. Dumbbells indicate oligonucleotides used. Epe1-GFP levels were normalized to spike-in control. Data are mean ± s.d. of three biological replicates.

Taken together, these data suggest that down-regulation of the protein levels of the likely H3K9 demethylase Epe1 plays a critical role in the response to external insults by allowing the formation of adaptive ectopic H3K9me-heterochromatin islands that, in turn, reduce expression of underlying genes to confer resistance. To further test this idea, *epe1Δ* cells were exposed to the lethal concentration of caffeine used previously to screen for unstable caffeine-resistant isolates (Chapter 3, Figure 3.2, +CAF medium). Consistent with the hypothesis above, *epe1Δ* cells were found to form more resistant colonies in the presence of caffeine than wild-type cells (Figure 6.10).

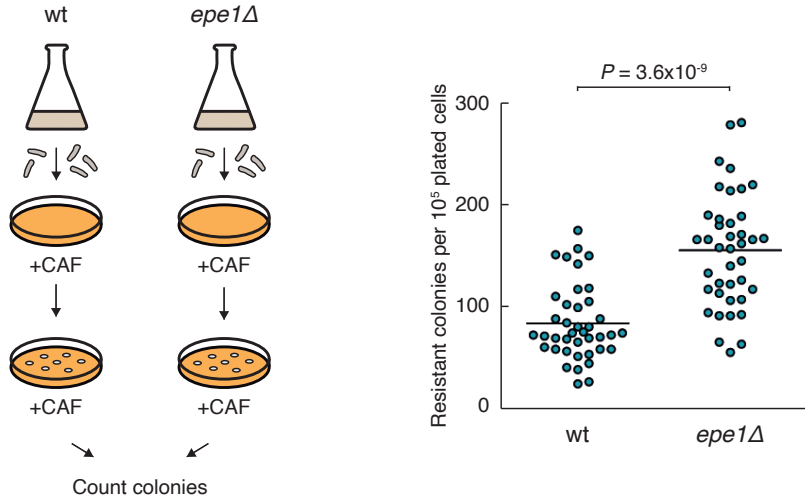

Figure 6.10. *epe1Δ* cells display increased resistance to caffeine. Left. Schematic of experiment. Wild-type (wt) and *epe1Δ* cells were plated on +CAF media (10^5 cells per plate, 40 plates per strain). Caffeine-resistant colonies were counted after 7 days. Right. *epe1Δ* cells forms more caffeine-resistant colonies than wild-type cells. Horizontal bars are mean from forty technical replicates. *P* value from a two-tailed Student's *t*-test is indicated.

6.2.4. Exposure to caffeine results in production of a shortened version of the anti-silencing factor Mst2

Although exposure to caffeine down-regulates Epe1 protein levels, higher levels of H3K9me2 accumulate at heterochromatin islands in the presence of caffeine than in untreated *epe1Δ* cells (Figure 6.3B). Thus, reduced Epe1

levels alone cannot account for the high levels of H3K9me2 observed at islands in the presence of caffeine. The histone acetyltransferase Mst2 has been shown to act synergistically with Epe1 to prevent heterochromatin island formation (Wang et al. 2015). Therefore, loss of function or decreased protein levels of Mst2 upon caffeine treatment could potentially explain the high H3K9me2 levels observed at islands.

Total *mst2*$^{+}$ transcript levels were not significantly altered upon caffeine treatment (Figure 6.7). However, detailed inspection of RNA-seq data revealed a potential change in the transcription start site (TSS) of *mst2*$^{+}$ following exposure to caffeine (Figure 6.11A). Notably, this alternative TSS has previously been detected upon exposure of fission yeast to other stresses (H_2O_2, heat shock and nitrogen starvation) (Thodberg et al. 2019). Indeed, western analysis of Mst2-13xMyc revealed the production of a shorter Mst2 protein (52 kDa rather than 62 kDa) upon exposure to caffeine (Figure 6.11B, experiment performed by Dr. Imtiyaz Yaseen). Importantly, this caffeine-induced shortened Mst2 isoform harbours a truncated MYST zinc finger domain, known to be required for *S. cerevisiae* Esa1 acetyltransferase activity (Yan et al. 2000). Thus, it is possible that this shortened version of Mst2 is unable to prevent heterochromatin island formation and, in combination with reduced Epe1 levels, allows accumulation of higher H3K9me2 levels at islands than that observed in untreated *epe1Δ* cells.

6.3. Discussion

In this chapter, the mechanism through which adaptive ectopic heterochromatin-mediated epimutations are generated upon exposure to caffeine was investigated. Treating wild-type cells with a low dose of caffeine overnight did not impact cell growth (Figure 6.1) yet resulted in the accumulation of H3K9me2 at diverse loci across the genome (Figure 6.2 and 6.3). These data indicate that although low caffeine treatment does not exert selective pressure on the cell population, it induces a plastic response leading to H3K9me2 accumulation at heterochromatin-prone loci, albeit at levels unlikely to have a phenotypic impact. Conversely, exposure to a near-lethal

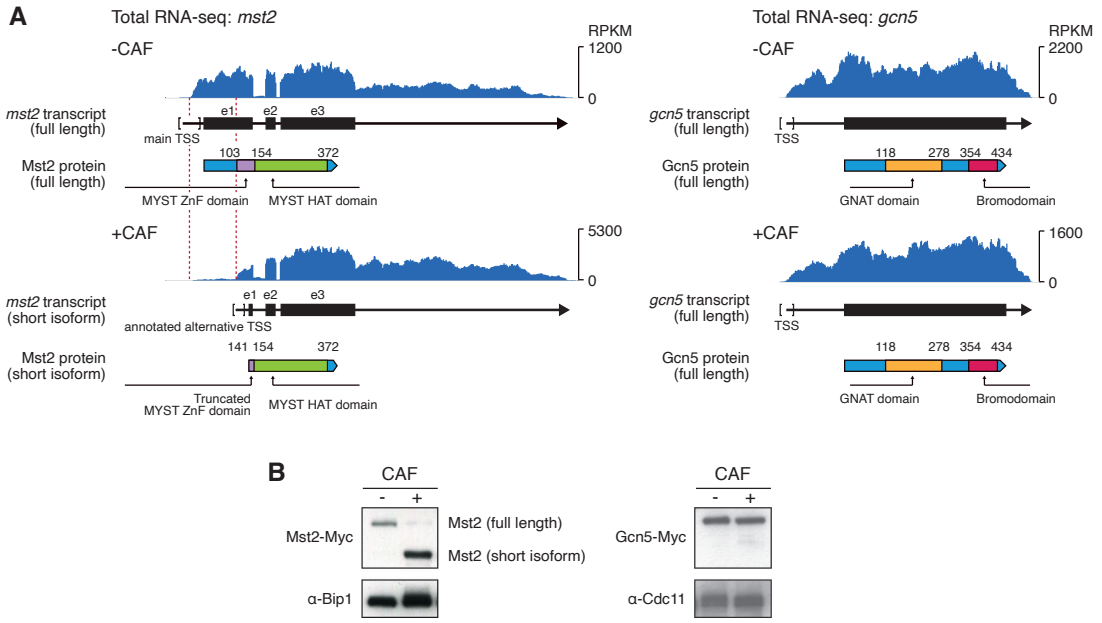

Figure 6.11. A shortened version of the anti-silencing factor Mst2 is produced upon exposure to caffeine. A. Total RNA-seq for *mst2* (left) and *gcn5* (as HAT control, right) of untreated wild-type cells (top) or wild-type cells treated with medium caffeine concentration (14 mM) (bottom). Diagrams illustrate *mst2* and *gcn5* transcripts and predicted protein domains. Reads are normalized to RPKM. Red dashed lines indicate the region of full length *mst2* transcript absent in the short isoform. The MYST zinc finger (ZnF) domain required for acetyltransferase activity (Yan et al. 2000) is truncated in the short isoform of Mst2. The alternative TSS potentially utilised for *mst2* in caffeine conditions was previously annotated (Thodberg et al. 2019). **B.** Experiment performed by Dr. Imtiyaz Yaseen. Western analysis of Mst2-13xMyc (left) and Gcn5-13xMyc (as HAT control, right) before and after caffeine treatment (medium concentration, 14 mM). Tagged proteins are expressed from their endogenous loci. Loading controls: left, Bip1; right, Cdc11. **A-B.** *gcn5* transcript and predicted protein are not altered upon exposure to caffeine.

(medium) dose of caffeine impaired the growth of wild-type cells (Figure 6.1), and resulted in the almost exclusive, dramatic accumulation of H3K9me2 at the *ncRNA.394-cup1* locus (Figure 6.2, 6.3 and 6.4). These data suggest that exposure to a toxic dose of caffeine initiates a selection process during which only cells harbouring an adaptive change that confers a fitness advantage – ectopic heterochromatin island formation over *ncRNA.394-cup1* – can prosper. Taken together, these results demonstrate that the *ncRNA.394-cup1* ectopic heterochromatin island is the predominant epimutation acquired following near-lethal or, as observed in unstable caffeine-resistant isolates, lethal caffeine exposure. Interestingly, facultative heterochromatin formation at

ncRNA.394-cup1 has been shown to depend on Taz1 (Zofall et al. 2016). Moreover, H3K9me2 accumulation at other Taz1-dependent facultative heterochromatin islands was proposed to require canonical Taz1 DNA-binding sequences, which can be found downstream of *ncRNA.394* (Zofall et al. 2016). Future experiments in which *taz1Δ* cells or strains harbouring deletions of Taz1-binding sequences at *ncRNA.394* are exposed to low and medium doses of caffeine will reveal whether Taz1 binding is required for adaptive heterochromatin island formation at this locus.

Note that the results presented here correspond to experiments performed at the population level. Therefore, it is not possible to discern if following low caffeine treatment all cells in the population assemble moderate levels of H3K9me2 at all the detected islands, or on the contrary distinct cell subpopulations accumulate high H3K9me2 levels at individual loci. Moreover, it is conceivable that many if not all of the observed caffeine-induced heterochromatin islands originate from low H3K9me2 levels already present at loci in a small fraction of untreated wild-type cells. Further investigation using suitable reporters coupled to single-cell technologies would allow testing of these hypotheses.

Exposing wild-type cells to a low dose of hydrogen peroxide caused the formation of ectopic heterochromatin at similar locations to those observed in low caffeine treatment, including *ncRNA.394-cup1* (Figure 6.3 and 6.5). However, H3K9me2 levels detected at heterochromatin islands following H_2O_2-induced oxidative stress were markedly lower compared to those after caffeine treatment. This difference could be due to distinct biological responses upon exposure to different stresses, but also to technical limitations related to the known instability of H_2O_2 (NCBI PubChem for CID-784, 2020). Notably, lower levels of H3K9me2 were observed at centromeres upon H_2O_2 treatment compared to untreated cells (shown for *cen1L* in Figure 6.5). This effect was not observed at other constitutive heterochromatin loci and may be explained by H_2O_2-specific regulation of limiting heterochromatin factors at centromeric repeats.

Low caffeine treatment resulted in an *epe1Δ*-like heterochromatin profile (Figure 6.2 and 6.3) but also in the prolonged retention of synthetic heterochromatin upon release of TetR-Clr4* from *tetO* sites at the neutral *ura4* locus (Figure 6.6). *epe1*$^{+}$ RNA levels were unaffected by caffeine (Figure 6.7). However, caffeine treatment resulted in a 33% reduction in FLAG-Epe1 protein levels and reduced association of Epe1-GFP with various heterochromatin loci (Figure 6.8 and 6.9), indicating that caffeine negatively regulates Epe1 at the post-transcriptional level. Furthermore, cells lacking Epe1 formed more caffeine-resistant colonies than wild-type cells on +CAF medium (Figure 6.10), demonstrating that loss of Epe1 alone is sufficient to increase the proportion of survivors upon lethal caffeine exposure. Unexpectedly, analyses presented here revealed that caffeine also regulates the anti-silencing factor Mst2, known to act in parallel to Epe1 to prevent the ectopic formation of heterochromatin (Wang et al. 2015). Interestingly, unlike the post-transcriptional regulative effect described for Epe1, caffeine exposure was found to trigger the production of a shortened, truncated version of Mst2 lacking part of its conserved MYST zinc finger domain (Figure 6.11). Although the functionality of this shorter Mst2 isoform remains to be determined, these results may explain the increased H3K9me2 levels observed at heterochromatin islands in low caffeine-treated wild-type cells compared to untreated *epe1Δ* cells (Figure 6.3). Thus, caffeine treatment of wild-type cells, both by lowering Epe1 levels and probably by disabling Mst2, allows the generation of adaptive heterochromatin islands with the potential to ultimately drive resistance.

Post-transcriptional and transcriptional effects observed here for Epe1 and Mst2, respectively, might be the downstream consequence of activation of known or still uncharacterized signalling pathways upon caffeine exposure. Components of the Sty1 and Pmk1 MAPK stress pathways are required for *S. pombe* tolerance to caffeine, and hyperactivation of either pathway has been shown to result in caffeine resistance (Calvo et al. 2009; see section 1.4.1.3 in Chapter 1 for an overview). The downstream target of the Sty1 and Pmk1 pathways is the transcription factor Atf1, activation of which is known to trigger a transcriptional stress response (Shiozaki & Russell 1996; Wilkinson et al.

1996). It is possible that caffeine-induced signalling cascades involving these MAPK pathways could cause the phosphorylation and subsequent poly-ubiquitylation-mediated degradation of Epe1, in a process similar to that described in other systems (Wu et al. 2006; Hunter 2007). Consistent with this idea, exposure to caffeine is known to activate the Sty1 kinase, leading to phosphorylation of Atf1, but also other cellular targets (Calvo et al. 2009; Papadakis & Workman 2015). Furthermore, poly-ubiquitylation-mediated degradation of Epe1 has been already reported to occur within constitutive heterochromatin domains through the action of the Cul4-Ddb1^{Cdt2} E3 complex (Braun et al. 2011), yet whether this mechanism requires Epe1 phosphorylation is unknown. Further experiments using mutants defective in the above-mentioned signalling cascades might reveal if these general pathways are directly involved in the regulatory mechanism that leads to reduced Epe1 protein levels upon caffeine exposure.

In addition to the transcriptional stress response triggered by Sty1- or Pmk1-mediated Atf1 activation, caffeine tolerance in wild-type cells has also been shown to require a specific gene expression program induced by the Pap1 transcription factor (Calvo et al. 2009; see section 1.4.1.3 in Chapter 1 for an overview). Indeed, overexpression or constitutive nuclear accumulation of Pap1 leads to caffeine resistance (Arioka et al. 1998; Castillo et al. 2003). The truncated Mst2 isoform observed after caffeine treatment appears to be produced through the use of an alternative TSS previously detected upon exposure to other stresses (Thodberg et al. 2019). It is possible that production of this Mst2 isoform might depend on binding of Atf1 or Pap1 to recognition sites within the coding sequence of *mst2*$^{+}$ upon caffeine treatment. However, preliminary inspection of the region immediately upstream of the alternative TSS in *mst2*$^{+}$ did not identify any of the consensus binding sequences for Atf1 or Pap1. Nevertheless, genome-wide or *mst2*$^{+}$-specific ChIP profiling experiments for Atf1 and Pap1 might reveal whether these factors are directly involved in the production of a shorter *mst2*$^{+}$ transcript. In addition, rapid amplification of cDNA ends (RACE) or cap analysis of gene expression (CAGE) experiments would confirm whether this truncated version of Mst2 is

indeed produced through the use of an alternative TSS upon caffeine treatment, as observed after exposure to other stresses (Thodberg et al. 2019).

Together, the findings presented in this chapter reveal an adaptive epigenetic response following exposure to caffeine that promotes phenotypic plasticity, and suggest that stress-response pathways may regulate activities that modulate heterochromatin formation, thereby ensuring cell survival in fluctuating environmental conditions.

Chapter 7: Discussion

7.1. An adaptive epigenetic response mediated by heterochromatin gene silencing upon exposure to a lethal insult

Epigenetic changes have been proposed to drive rapid phenotypic adaptation to fluctuating and challenging environments (Richards 2006; Heard & Martienssen 2014; Cavalli & Heard 2019). Indeed, epimutations, defined here as changes in gene expression that are independent of alterations in DNA sequence (Jeggo & Holliday 1986; Oey & Whitelaw 2014), have been predicted to mediate the formation of adaptive phenotypes before stable genetic changes do (Klironomos et al. 2013; Kronholm & Collins 2015). However, even though it has been extensively demonstrated that epigenetic variation exists in nature (Cubas et al. 1999; Jacobsen 1997; Morgan et al. 1999), and that it can respond to the environment and be inherited (Seong et al. 2011; Wibowo et al. 2016; Klosin et al. 2017), few convincing examples of real adaptive potential have been reported, and most of these are linked to the formation of small RNAs (Rechavi et al. 2011; Rechavi et al. 2014; Calo et al. 2014). In addition, although not usually considered in conventional definitions of epigenetics because they entail alterations in protein folding rather than changes in gene expression, prions have also been shown to reversibly drive phenotypic change. In fact, prion-based misfolded proteins possess the ability to robustly self-propagate and have been demonstrated to link environmental extremes with the acquisition and inheritance of new traits (Alberti et al. 2009; Jarosz, Brown et al. 2014; Jarosz, Lancaster et al. 2014; Harvey et al. 2020).

Thus, while advantageous phenotypic responses mediated by small RNAs or prions have been described previously, whether epigenetic changes at the chromatin level are also able to drive the formation of adaptive phenotypes has remained a long-standing question in the field (Wang et al. 2016; Allis & Jenuwein 2016; Sorida & Murakami 2020). Over recent years, however, a growing body of evidence has suggested that the generation of ectopic heterochromatin islands could provide a means of survival upon exposure to

external insults. The formation of *bona fide* heterochromatin domains, characterized by the presence of H3K9 methylation, leads to the acquisition of a repressed chromatin state and the transcriptional silencing of underlying genes (Rea et al. 2000; Bannister et al. 2001; Lachner et al. 2001; Nakayama et al. 2001). However, heterochromatin regions are highly dynamic structures, as illustrated by the existence of facultative heterochromatin domains packaged into a repressed state only in response to differentiation signals or environmental cues (Trojer & Reinberg 2007). It is important to mention that although H3K27me is widely considered the most prominent hallmark of facultative heterochromatin (Trojer & Reinberg 2007), H3K9me can also be found within these transiently repressive domains (Heard et al. 2001; Bastow et al. 2004). Moreover, facultative heterochromatin can also be exclusively mediated by H3K9me, as shown for cell type-specific chromatin domains in mammalian cells (Wen et al. 2009; Hawkins et al. 2010; Soufi et al. 2012; Zhu et al. 2013; Becker et al. 2016), or meiotic loci in fission yeast (Zofall et al. 2012).

Notably, H3K9me is an epigenetic mark that can be propagated through a *reader-writer* coupling mechanism, but only in cells lacking Epe1 (Audergon et al. 2015; Ragunathan et al. 2015), a likely H3K9 demethylase also shown to prevent the formation of ectopic heterochromatin at euchromatic loci (Trewick et al. 2007; Zofall et al. 2012; Wang et al. 2015; Parsa et al. 2018; Sorida et al. 2019). Together, these studies suggest that if the levels, location or function of key heterochromatin regulators were naturally modulated in wild-type cells, heterochromatin heritability might be employed to generate adaptive epimutations that ensure cell survival upon exposure to external insults.

In this thesis, I investigated whether wild-type fission yeast cells can form ectopic heterochromatin-mediated epimutations that drive resistance to a lethal insult. The purine analogue caffeine, a potent inhibitor of cAMP phosphodiesterase (Butcher & Sutherland 1962), was selected for this project because deletion of many *S. pombe* genes with a variety of cellular roles has been shown to confer caffeine resistance (Calvo et al. 2009). Since

heterochromatin silencing is expected to mimic the effect of null mutants, the comprehensive genome-wide deletion study performed by Calvo et al. (2009) provided an invaluable resource at the outset of this study. In addition, the molecular mechanisms that lead to the acquisition of caffeine resistance following mutation or loss of several genes have been well described (Benkö et al. 1997; Benkö et al. 1998; Benkö et al. 2004; Castillo et al. 2003), allowing the functional consequences of potential gene silencing events to be understood.

Chapter 3 described the identification of heterochromatin-dependent *S. pombe* epimutants resistant to the lowest dose of caffeine shown to inhibit the growth of wild-type cells. Indeed, caffeine concentration was kept to the minimum, approximately half of the dose previously used to screen for genetic caffeine-resistant mutants (Benkö et al. 1997), to maximize the chances of obtaining epimutations. Potential caffeine-resistant epimutants were identified based on their unstable phenotype, denoted by the loss of caffeine resistance after 14 days (approximately 140 cell divisions) of growth on non-selective medium. Note that the percentage of unstable caffeine-resistant isolates obtained (23%) was probably underestimated due to the strict selection criteria used, which also would explain the high (64%) percentage of isolates classified as 'unclear'. Because not all resistant isolates could be further analysed due to time and logistical constraints, only those exhibiting a clear resistance phenotype were selected. However, frozen stocks of all resistant isolates have been preserved, and thus unclear isolates could be subjected to further analyses to determine whether they can be ultimately classified as unstable or stable.

Importantly, deletion of *clr4*$^{+}$, encoding the only *S. pombe* H3K9 methyltransferase (Ivanova et al. 1998; Rea et al. 2000; Cam et al. 2005), resulted in loss of caffeine resistance in unstable, but not stable isolates, indicating that the caffeine-resistant phenotype of unstable isolates requires heterochromatin. *clr4*$^{+}$ deletions described here were carried out following a standard gene knock-out protocol, which proved to be an inefficient and non-

ideal method for this project as it entailed growing unstable isolates in the absence of caffeine for approximately 7 days. CRISPR/Cas9-mediated gene deletion using the *SpEDIT* system developed as part of this thesis does not constitute a more convenient alternative, as it would also require cells to be grown in non-selective conditions for a similar period of time. A plausible solution to this issue would be the implementation of a novel strategy by which rapid and controllable deletion of endogenous *clr4*$^{+}$ is achieved through recombination of flanking *loxP* sites after expression of a Cre-recombinase enzyme (Hamilton & Abremski 1984; Werler et al. 2003). Alternatively, inducible and swift Clr4 protein degradation could be attained by the use of an auxin-inducible depletion system (Kanke et al. 2011). These potential strategies would allow testing for heterochromatin dependence simultaneously in many unstable drug-resistant isolates and thus accelerating the identification of potential epimutants. Nevertheless, implementation of either strategy would require the comprehensive examination of heterochromatin integrity and dynamics in such genetic backgrounds to ensure that strains harbouring such manipulations are indistinguishable from wild-type.

Notably, while WGS analysis of a stable isolate uncovered a mutation in *pap1*$^{+}$ responsible for its caffeine-resistant phenotype, no mutations in genes known to cause caffeine resistance or to affect heterochromatin regulation were detected in any of the 30 unstable isolates examined. Moreover, the generation of DNA changes detected in 4 of 30 unstable isolates (Clr5-Q264STOP and Meu27-S100Y) in wild-type cells was shown to have no impact on the acquisition of caffeine resistance, nor to cause alterations of the heterochromatin profile. It is important to mention that other even rarer genetic changes (SNPs and indels) found in unstable isolates (described in Chapter 3, Table 3.1) were not investigated and thus a role of these *a priori* negligible genetic changes cannot be absolutely excluded. In addition, even though numerous genetic mutations that result in caffeine resistance have already been described (Benkö et al. 1998; Calvo et al. 2009), WGS analysis of additional stable isolates identified here might uncover novel alleles that drive a caffeine-resistant phenotype.

Genome-wide H3K9me2 profiling revealed the presence of ectopic heterochromatin islands in all 30 unstable caffeine-resistant isolates analysed. Ectopic islands of heterochromatin were detected at 6 distinct loci (*hba1*, *ncRNA.394-cup1*, *ppr4*, *grt1*, *fio1* and *mbx2*), with reduction in transcript levels of genes coated in ectopic H3K9me2. The assembly of an ectopic heterochromatin island over *hba1*$^{+}$, a gene known to confer caffeine resistance when deleted (Castillo et al. 2003), strongly suggested that ectopic heterochromatin islands formed in unstable isolates might be adaptive. Indeed, experiments presented in Chapter 4 demonstrated that synthetic heterochromatin tethering at the *hba1*, *ncRNA.394-cup1* or *mbx2* loci was sufficient to confer caffeine resistance in wild-type cells.

Notably, although synthetic heterochromatin tethering at *ncRNA.394-cup1* induced caffeine resistance, and 80% of unstable isolates displayed an ectopic heterochromatin island at this locus, none of the genes located within the *ncRNA.394-cup1* island had previously been implicated in caffeine resistance. Nevertheless, exhaustive functional dissection of this locus revealed that transcriptional down-regulation or LYR-domain mutation of the previously-uncharacterized gene *cup1*$^{+}$ (*SPBC17G9.13c*$^{+}$), encoding an essential mitochondrial protein, is sufficient to render wild-type cells resistant to caffeine. Note that the mechanism by which the reduction or mutation of Cup1 causes caffeine resistance remains to be uncovered. As proposed in Chapter 4, it is possible that defects in or reduction of Cup1 function might lead to mitochondrial deficiencies that could ultimately feed into and activate the Pap1 pathway, a mechanism previously shown to drive caffeine resistance (Benkö et al. 1998; Kudo et al. 1999; Castillo et al. 2003; Benkö et al. 2004). Interestingly, these findings suggest that other still uncharacterized essential genes whose transcriptional silencing confers drug resistance might exist. Since the function of such genes cannot be studied by simply deleting their coding sequence, the strategies presented here might allow the identification of additional loci at which epimutations confer resistance.

Further investigation will determine which gene at the *mbx2* locus drives caffeine resistance when silenced. Synthetic heterochromatin tethering immediately upstream of *mbx2*$^{+}$ led to wild-type cells displaying a caffeine-resistant phenotype, albeit resistance levels were reduced compared to those observed following tethering at two other loci. Therefore, the *mbx2*$^{+}$ MADS-box transcription factor, known to bind and activate the expression of several cellular targets (Matsuzawa et al. 2012; Kwon et al. 2012), constitutes the main candidate gene at this region. Furthermore, synthetic heterochromatin tethering at the *ppr4*, *grt1*, or *fio1* locus will allow testing whether heterochromatin formation at these loci is also sufficient to confer caffeine resistance in wild-type cells. Due to the large heterochromatin island size (60 kb) formed over the *grt1* locus, a modified TetR-Clr4*-based tethering strategy might be required. Insertion of multiple *4xtetO* cassettes at different locations within this locus or, alternatively, generation of larger *tetO* arrays similar to those previously described (*10xtetO,* Ragunathan et al. 2015) might allow the establishment of a large synthetic heterochromatin island that mimics that observed in natural conditions. Subsequently, a knock-out approach would allow the identification of specific genes responsible for resistance within these regions, as previously carried out for the *hba1* and *ncRNA.394-cup1* loci.

Taken together, the data presented in Chapters 3 and 4 demonstrate that ectopic heterochromatin-mediated epimutations that drive caffeine resistance can arise in wild-type fission yeast cells (Figure 7.1). As *S. pombe* lacks DNA methylation (Antequera et al. 1984; Wilkinson et al. 1995; Capuano et al. 2014), as well as PRC2-deposited H3K27me (Shaver et al. 2010; Dumesic et al. 2015), these epigenetic marks cannot be responsible for the epimutations described here. Instead, analyses performed in Chapters 3 and 4 indicate that these adaptive epimutations are transmitted in wild-type cells by the previously-identified Clr4/H3K9me *reader-writer* coupling mechanism (Zhang et al. 2008; Audergon et al. 2015; Ragunathan et al. 2015).

These findings might explain a phenomenon often experienced yet seldomly reported during phenotypic screens; the emergence of eccentric isolates that

lose resistance to a given drug once removed from selective medium (Stone et al. 2019). Indeed, phenotypic screens are generally very stringent and only the strongest mutants are retained for further investigation. Here, by applying the minimum inhibitory concentration of a drug that is at the threshold of preventing the growth of most cells, unstable isolates were purposely sought and further characterized. Such a strategy uncovered an adaptive epigenetic response mediated by heterochromatin gene silencing upon exposure to a lethal insult (Figure 7.1).

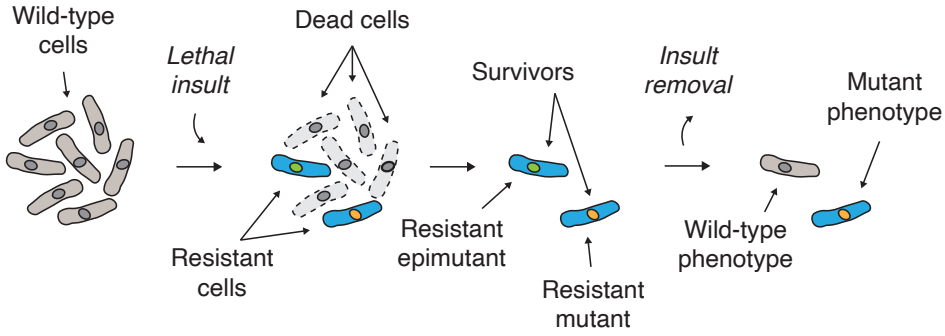

Figure 7.1. An adaptive epigenetic response mediated by heterochromatin gene silencing upon exposure to a lethal insult. Model. Resistant isolates arise following exposure to a lethal insult. Resistance could be mediated by permanent, DNA-based changes (resistant mutants) or reversible, heterochromatin-based epimutations (resistant epimutants). Upon insult removal, resistant epimutants can revert to wild-type (sensitive phenotype) by disassembling ectopic islands of heterochromatin, whereas resistant mutants continue displaying the mutant phenotype due to the genetic nature of DNA mutations.

7.2. Interplay between epigenetic and genetic changes in the evolution of drug resistance

Analyses presented in Chapter 5 revealed that 40% of unstable isolates, in addition to an ectopic heterochromatin island assembled over euchromatic loci, also harboured overlapping regions of chromosome III at increased copy number. Notably, most chromosome III CNVs include *cds1*$^{+}$, a gene shown to confer caffeine resistance when overexpressed (Wang et al. 1999), suggesting that amplification of the *cds1* locus might contribute to the caffeine-resistant phenotype of these isolates. The unstable isolate UR-2, which did not harbour

chromosome III CNVs at its initial stage (at 4 days +CAF) was found to acquire *cds1* locus amplification following prolonged growth in the presence of caffeine for 3 days (at 7 days +CAF). Importantly, once amplification of the *cds1* locus arose, heterochromatin was no longer required for resistance in this isolate. Thus, although *cds1* locus amplification can drive resistance in the absence of heterochromatin in UR-2 cells, this genetic change emerged after a resistant phenotype was already established by an adaptive ectopic heterochromatin island at *ncRNA.394-cup1*.

Experiments performed on UR-2 cells harbouring both epigenetic and genetic changes revealed that amplified copies of the *cds1* locus are also lost following growth on non-selective medium. This finding explained the unstable phenotype displayed by isolates harbouring chromosome III CNVs at their initial stage, which first appeared to be inconsistent with the supposed stability attributed to genetic changes. However, the further analysis presented in Chapter 5 demonstrated that chromosome III CNVs correspond to eccDNA generated through recombination between separate direct repeats present on chromosome III. Indeed, eccDNAs have been shown to ease adaptive evolution by enabling swift and extensive gene copy number variation in *S. cerevisiae* (Libuda & Winston 2006; Hull et al. 2019). eccDNAs are also a frequent feature of cancer cells (Turner et al. 2017; Verhaak et al. 2019), in which they enable overexpression of oncogenes residing on the extrachromosomal element as a result of both increased copy number and enhanced chromatin accessibility (Wu et al. 2019). Furthermore, eccDNAs are known to drive tumour heterogeneity through cell-to-cell fluctuations in copy number and unequal segregation of circular DNA from a parental cancer cell to offspring (Turner et al. 2017; deCarvalho et al. 2018). Consistent with this idea, the results presented here indicate that the amplified *cds1* locus is not homogeneously present in all cells of unstable isolates, since not all UR-2 cells harboured increased *cds1*$^{+}$ levels or became heterochromatin-independent following prolonged growth in the presence of caffeine (at 7 days +CAF). Because *cds1* amplification arose after the adaptive *ncRNA.394-cup1* heterochromatin island in UR-2 cells, and chromosome III CNVs were never

found in the absence of an ectopic heterochromatin island in other unstable isolates, it was concluded that eccDNA generation probably provides a supplementary mechanism for the evolution of caffeine resistance in fission yeast. Nevertheless, as discussed in Chapter 5, it is possible that these causative events might not always occur in the same order. Thus, examination of unstable caffeine-resistant isolates at earlier stages in the evolution of resistance might determine whether eccDNAs could also emerge before adaptive epigenetic changes do.

Importantly, it has been proposed that heterochromatic regions accumulate more mutations than euchromatic loci due to reduced DNA mismatch repair in heterochromatin (Schuster-Böckler & Lehner 2012; Supek & Lehner 2015). Therefore, it is tempting to speculate that ectopic heterochromatin islands formed over genes whose down-regulation drives resistance might also lead to increased mutagenesis at these loci, providing a novel molecular mechanism for what was originally proposed as genetic assimilation of characters (Waddington 1942, 1953 and 1956) (Figure 7.2). Indeed, a recent study proposed that induced histone deacetylation-mediated silencing in *S. cerevisiae* (that lacks H3K9me) leads to genetic assimilation of a silent phenotype (Stajic et al. 2019). However, silencing was found to have no impact on the local mutation rate and assimilation occurred through acquisition of novel alleles across the genome, many of which bolstered gene silencing to aid accelerated adaptation (Stajic et al. 2019).

It should also be noted that the establishment of stable caffeine resistance through multicopy eccDNA reintegration, as previously reported for other traits (Beverley et al. 1984; Galeote et al. 2011; Demeke et al. 2015), would also be considered, in theory, genetic assimilation (Waddington 1942). However, in a hypothetical case such as this the genetic fixation of an equally unstable initial phenotype would be mediated by eccDNA reintegration rather than by heterochromatin-driven mutagenesis. In fact, proposed mechanisms for genetic assimilation do not strictly require initial unstable phenotypes to be mediated by epigenetic variation (Rutherford & Lindquist 1998; Queitsch et al.

2002). For example, compromising the function of the heat-shock chaperone Hsp90 through mutation, pharmacological inhibition or environmental stress was shown to result in phenotypic variation in both *D. melanogaster* and *A. thaliana*. These morphological differences among nearly isogenic flies or plants were caused by manifestation of cryptic genetic variants (mutant misfolded proteins) which are, under normal conditions, silently buffered by Hsp90 function. Notably, when such traits were enriched by selection, they became rapidly independent of Hsp90 mutation or inhibition and continued to manifest even when Hsp90 function was restored (Rutherford & Lindquist 1998; Queitsch et al. 2002).

As proposed in Chapter 5, analysis of unstable isolates at further stages in the evolution of resistance might reveal whether stable genetic changes arise following extended growth in the presence of caffeine and, importantly, if the acquisition of these mutations is influenced by the type of unstable change that initially occurred.

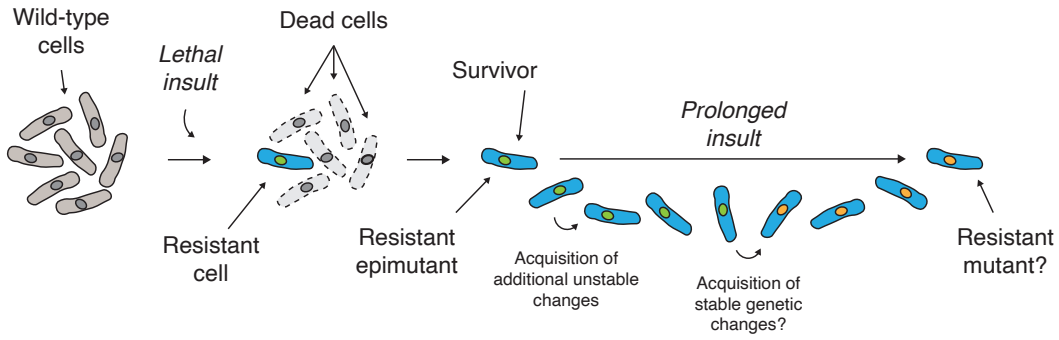

Figure 7.2. Interplay between epigenetic and genetic changes in the evolution of drug resistance. Model. Ectopic heterochromatin-mediated epimutations drive an unstable resistant phenotype upon exposure to a lethal insult (resistant epimutants). Prolonged insult exposure leads to the acquisition of supplementary unstable changes (e.g. eccDNAs) that boost resistance. Unstable changes present in resistant epimutants might facilitate the acquisition of adaptive mutations through genetic assimilation, leading to a stable resistant phenotype (resistant mutants).

7.3. Stress-induced heterochromatin redistribution through modulation of key anti-silencing factors

Results presented in Chapter 6 showed that exposing wild-type cells to sub-lethal caffeine concentrations results in a marked redistribution of the heterochromatin profile. Low caffeine treatment caused the assembly of H3K9me at a subset of previously described facultative heterochromatin islands known to gain H3K9me in the absence of Epe1, including *ncRNA.394-cup1* (Zofall et al. 2012). On the other hand, exposure to a near-lethal dose of caffeine led to the exclusive accumulation of H3K9me at the *ncRNA.394-cup1* locus. These findings prompt the question as to why resistant epimutants that formed ectopic heterochromatin islands at loci other than *ncRNA.394-cup1* were identified, given that this locus appears to be the preferential target of ectopic H3K9me2 upon exposure to a near-lethal dose of caffeine.

It is possible that *ncRNA.394-cup1* is the predominant caffeine-induced ectopic heterochromatin island because low levels of H3K9me exist at this locus in untreated wild-type cells, as previously proposed (Zofall et al. 2012). However, low levels of H3K9me were also reported in untreated wild-type cells at other facultative islands such as *mbx2* and *ppr4* (Zofall et al. 2012), which assembled high levels of H3K9me in some resistant epimutants. Still, neither *mbx2* nor *ppr4* accumulated H3K9me upon low caffeine treatment, suggesting that they are subjected to less plastic modulation than *ncRNA.394-cup1*, at least under caffeine conditions. Alternatively, the predominant formation of heterochromatin at *ncRNA.394-cup1*, over *mbx2* or *ppr4* might be due to the acquisition of a greater adaptive potential through silencing of *cup1*$^{+}$ than via down-regulation of genes located at *mbx2* or *ppr4*. Consistent with this idea, synthetic heterochromatin formation at *mbx2* results in weaker caffeine resistance than when synthetic heterochromatin is targeted to *ncRNA.394-cup1*, yet it is not known whether these differences are due to technical or biological reasons. A plausible experiment to test this idea directly would be to compare the caffeine-resistant phenotype of a strain expressing reduced levels of *cup1*$^{+}$ (*cup1-3xDSR* or *cup1-TT*, described in Chapter 4*)* to that of

strains carrying a similarly attenuated form of genes located at either the *mbx2* or *ppr4* loci. In addition, as discussed in Chapter 6, it is possible that the formation of H3K9me at *ncRNA.394-cup1* is facilitated by Taz1 binding to telomeric sequences downstream of *ncRNA.394,* as previously proposed for other Taz1-dependent facultative islands (Zofall et al. 2016). Of particular interest would be analyses in which strains harbouring an entire deletion of the *ncRNA.394-cup1* locus but preserving *cup1*$^{+}$ elsewhere are exposed to low and medium doses of caffeine. A prediction is that in such a situation one of the other ectopic heterochromatin islands found in resistant epimutants might become the preferred target of ectopic H3K9me. However, it is also conceivable that ectopic heterochromatin might still predominantly assemble over *cup1*$^{+}$ even at its novel location.

Exposing wild-type cells to a low dose of caffeine resulted in an *epe1Δ*-like phenotype, signified by the accumulation of H3K9me at facultative heterochromatin islands (Zofall et al. 2012; Wang et al. 2015; Sorida et al. 2019), and the prolonged retention of synthetic heterochromatin upon release of TetR-Clr4* from *tetO* sites placed upstream of *ura4* (Audergon et al. 2015; Ragunathan et al. 2015). Consistent with this phenotype, experiments performed in Chapter 6 revealed that although *epe1*$^{+}$ transcript levels did not change following caffeine treatment, both FLAG-Epe1 protein levels and Epe1-GFP association with chromatin were reduced, indicating that caffeine down-regulates Epe1 post-transcriptionally. Moreover, analyses also presented in Chapter 6 indicated that caffeine treatment leads to the production of a shortened version of the histone acetyltransferase Mst2, which lacks part of its conserved MYST zinc finger domain. Production of this Mst2 isoform appears to be achieved through the use of an alternative TSS previously detected upon exposure to other stresses (Thodberg et al. 2019). These data suggest that the combinatorial effect of reduced Epe1 and truncated Mst2 might be responsible for the increase in heterochromatin plasticity observed following caffeine treatment (Figure 7.3). Experiments in which an artificially shortened version of Mst2 is expressed from its endogenous locus in untreated cells would determine if the truncation of this

HAT increases H3K9me levels at facultative heterochromatin islands in a way similar to the observed in *mst2Δ* cells (Wang et al. 2015).

Together, these findings suggest that upon exposure to caffeine the levels or function of key heterochromatin regulators might be modulated through the action of known or still uncharacterized stress-response pathways. Indeed, it was discussed in Chapter 6 that the Sty1 MAPK, shown to be activated upon caffeine treatment (Calvo et al. 2009), might directly or indirectly induce the post-translational modification of Epe1 and ultimately its degradation. Furthermore, the expression of a shortened Mst2 transcript following caffeine exposure may be mediated by the activation of stress-responsive transcription factors such as Atf1 (the downstream component of the Sty1 pathway) or Pap1. Interestingly, both of these transcription factors are known to be required for caffeine tolerance (Calvo et al. 2009) (Figure 7.3).

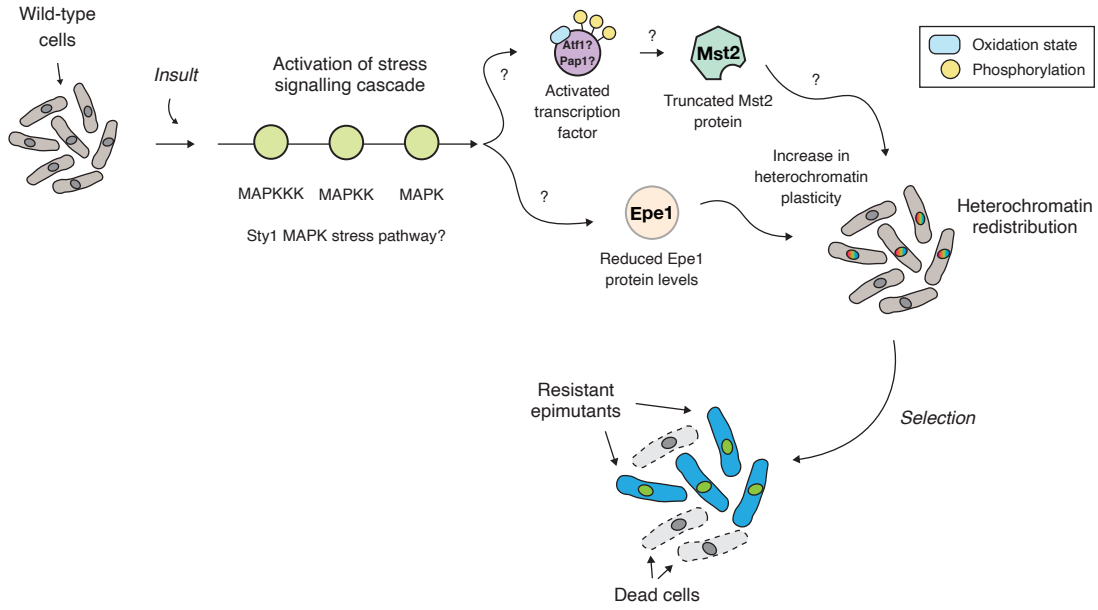

Figure 7.3. Stress-induced heterochromatin redistribution through modulation of key anti-silencing factors. Model. Exposure to an external insult leads to the activation of stress-response pathways which may in turn modulate the function or levels of key anti-silencing regulators to promote heterochromatin plasticity. Stress-induced heterochromatin redistribution might then facilitate the acquisition of adaptive epimutations that ultimately drive resistance.

7.4. Conclusions and final thoughts

The data presented in this thesis reveal that epigenetic processes promote phenotypic plasticity, allowing wild-type cells to adapt to a non-favorable environment without altering their genotype. Specifically, this work demonstrates that ectopic heterochromatin-mediated epimutations can drive resistance to caffeine in wild-type fission yeast cells, thereby providing foundational evidence for chromatin-based epialleles with adaptive impact.

Epimutations mostly occurred at loci not formerly implicated in caffeine resistance and led to the identification of a previously uncharacterized essential gene, *cup1*$^{+}$, whose transcriptional silencing was shown to render wild-type cells resistant to caffeine. Indeed, the fact that the predominant means to acquire unstable caffeine resistance in wild-type *S. pombe* involves heterochromatin silencing of an essential gene suggests that the formation of adaptive heterochromatin islands ought to be finely tuned to prevent deleterious consequences. Note that the estimated frequency of cells that assemble phenotypically relevant levels of H3K9me at *ncRNA.394-cup1* is relatively low; 1 unstable resistant cell with ectopic H3K9me at this locus per 10870 wild-type cells plated on +CAF medium (estimation based on analyses performed in Chapter 3). Thus, although it could be argued that ectopic heterochromatin formation over *ncRNA.394-cup1* constitutes a hardwired response, the fact that most cells in the population do not survive exposure to +CAF medium indicates that a truly fixed pathway cannot be assumed. Nevertheless, the results obtained illustrate the advantage of deploying reversible epimutations to mediate drug resistance. Cells lacking Hba1 or harbouring permanently reduced Cup1 function display moderate growth defects in non-selective conditions, indicating that if resistance was mediated by stable mutations in these factors the fitness cost for cells upon drug removal would be high. This idea needs to be taken into account when investigating the stability of ectopic heterochromatin islands such as those described here.

In some isolates, subsequent or co-occurring gene amplification events that involve the production of unstable eccDNA augment resistance. Moreover,

caffeine was found to reduce the levels of the Epe1 demethylase and probably the function of the Mst2 histone acetyltransferase, two key anti-silencing factors in *S. pombe*.

Taken together, these results indicate that heterochromatin-dependent epimutant formation provides a bet-hedging strategy that allows cells to remain genetically wild-type but adapt transiently to an external insult. Notably, the analyses presented suggest that this adaptive response might not only be limited to caffeine, as treatment with H_2O_2 also led to heterochromatin redistribution. Therefore, further investigation will determine whether similar epimutations arise when wild-type fission yeast cells are exposed to other toxic compounds.

Importantly, the unstable caffeine-resistant isolates identified here show cross-resistance to antifungal agents, suggesting that related heterochromatin-dependent processes may contribute to antifungal resistance in plant and human pathogenic fungi. Indeed, the findings presented in this thesis argue against the widespread use of related azole compounds to control fungus-mediated crop deterioration. Such control strategies may leave low fungicide levels in the soil and could lead to the inadvertent selection of resistant epimutants in fungi, similar to those described here, which may ultimately drive the emergence of antifungal resistance in both agricultural and clinical settings. Increasing evidence indicates that fungal infections are on the rise, especially in immunocompromised humans, who are particularly susceptible to opportunistic soil-borne fungi such as *Aspergillus* and *Cryptococcus* (Fisher et al. 2018). There are few effective antifungal agents and resistance is rendering them increasingly ineffective (Almeida et al. 2019). Monitoring of resistance in clinical isolates involves mutation identification by genome sequencing but resistance due to epimutations – similar to those described here – would be missed, leading to inaccurate diagnoses. The work presented in this thesis might provide fundamental insights into the management of fungal infections in plants and humans.

Appendix I

SpEDIT: A fast and efficient CRISPR/Cas9 method for fission yeast

The *SpEDIT* CRISPR/Cas9 genome editing system for *S. pombe* was developed as part of this thesis with the support of three MSc students: Baptiste Gaborieau, Lorenza di Pompeo and Luke Eivers.

Summary

The CRISPR/Cas9 system allows scarless, marker-free genome editing. Current CRISPR/Cas9 systems for the fission yeast *Schizosaccharomyces pombe* rely on tedious and time-consuming cloning procedures to introduce a specific sgRNA target sequence into a Cas9-expressing plasmid. In addition, Cas9 endonuclease has been reported to be toxic to fission yeast when constitutively overexpressed from the strong *adh1* promoter. To overcome these problems we have developed an improved system, *SpEDIT*, that uses a synthesised Cas9 sequence codon-optimised for *S. pombe* expressed from the medium strength *adh15* promoter. The *SpEDIT* system exhibits a flexible modular design where the sgRNA is fused to the 3' end of the self-cleaving hepatitis delta virus (HDV) ribozyme, allowing expression of the sgRNA cassette to be driven by RNA polymerase III from a tRNA gene sequence. Lastly, the inclusion of sites for the *Bsa*I type IIS restriction enzyme flanking a GFP placeholder enables one-step Golden Gate mediated replacement of GFP with synthesized sgRNAs for expression. The *SpEDIT* system allowed a 100% mutagenesis efficiency to be achieved when generating targeted point mutants in the *ade6*$^{+}$ or *ura4*$^{+}$ genes by transformation of cells from asynchronous cultures. *SpEDIT* also permitted insertion, tagging and deletion events to be obtained with minimal effort. Simultaneous editing of two independent non-homologous loci was also readily achieved. Importantly the *SpEDIT* system displayed reduced toxicity compared to currently available *S. pombe* editing systems. Thus, *SpEDIT* provides an effective and user-friendly CRISPR/Cas9 procedure that significantly improves the genome editing toolbox for fission yeast.

Introduction

The fission yeast *Schizosaccharomyces pombe* is a powerful model organism widely used in cellular and molecular biology (Fantes & Hoffman 2016). Traditionally, gene manipulation in *S. pombe* is achieved by transforming a DNA construct that includes the desired change alongside a selectable marker. The DNA construct integrates in the genome via flanking regions that target the genomic locus of interest. DNA constructs vary depending on the application but commonly consist of a sole PCR product that comprises an insertion, deletion or tagging cassette amplified from an existing plasmid (Bähler et al. 1998). Albeit convenient, this approach results in a selectable marker integrated at the target locus, consequently disrupting the local genomic context and limiting the availability of markers for subsequent manipulations.

The prokaryotic CRISPR/Cas9 system enables flexible and scarless genome editing without the necessity of selectable markers escorting the introduced DNA change and disturbing the local genomic environment (Jinek et al. 2012; Hsu et al. 2014). Adapted from a genome defence mechanism against invading DNA, the engineered minimal CRISPR/Cas9 system consists of a Cas9 endonuclease and a single-guide RNA (sgRNA) chimera that contains both the trans-activating CRISPR RNA and the targeting CRISPR RNA (Jinek et al. 2012). The sgRNA sequence targets the system to a defined genomic location where the Cas9 endonuclease binds to a protospacer adjacent motif (PAM). The Cas9 enzyme then creates a double-strand break (DSB) three base pairs upstream of the PAM site in the protospacer sequence (Jinek et al. 2012). Following DSB generation, repair is executed either through error-prone non-homologous end-joining (NHEJ), where strand end resection and subsequent repair frequently induce indels, or through high-fidelity homology-directed repair (HDR). HDR involves recombination via sequence homology and therefore can be exploited to generate precise mutations by providing a DNA editing template that contains the required DNA change and engages in homologous recombination (HR) with the cleaved region (Hsu et al. 2014).

Implementation of the CRISPR/Cas9 system in *S. pombe* has been previously described in several reports (Jacobs et al. 2014; Rodríguez-López et al. 2016; Fernandez & Berro 2016; Zhao & Boeke 2018; Zhang et al. 2018; Hayashi & Tanaka 2019). A useful web-tool, CRISPR4P, was also developed to support the design of sgRNAs and oligonucleotides required to perform CRISPR/Cas9-mediated gene deletions (Rodríguez-López et al. 2016).

To date, all CRISPR/Cas9 systems for *S. pombe* utilise the promoter/leader sequence of K RNA (*rrk1*) and a hammerhead ribozyme (HHR) for sgRNA cassette expression (Jacobs et al. 2014). A humanised Cas9 endonuclease expressed from the strong *adh1* promoter was used in the original *S. pombe* system (Jacobs et al. 2014). The resulting high levels of the Cas9 endonuclease were found to be detrimental for *S. pombe* growth. This Cas9 toxicity was partially bypassed by co-expression of the sgRNA and the Cas9 enzyme from a single plasmid (Jacobs et al. 2014).

Cloning of a sgRNA target into the single sgRNA/Cas9 plasmid was originally executed via *Csp*CI digestion (Jacobs et al. 2014). This procedure proved to be extremely inefficient due to the large plasmid size and the inconsistency in available commercial *Csp*CI preparations (Rodríguez-López et al. 2016). A subsequent study attempted to overcome this problem by implementing a PCR-based method in which a sgRNA target is introduced into a single sgRNA/Cas9 plasmid by using overlapping PCR primers that contain the sgRNA sequence (pMZ379 plasmid, (Rodríguez-López et al. 2016). Although an improvement over the initial system, this PCR-based method generated only a low frequency of bacterial colonies that contain correct and intact constructs. As a consequence, the required screening makes the entire process inefficient and time consuming.

To circumvent issues pertaining to Cas9 toxicity and inefficient sgRNA cloning procedures, here we report the development of *SpEDIT*, an improved CRISPR/Cas9 system for the efficient manipulation of the fission yeast genome. *SpEDIT* employs a highly effective one-step Golden Gate cloning strategy for the insertion of sgRNAs, that in combination with the use of a GFP

placeholder allows visual screening for identification of positive clones. The Cas9 endonuclease gene implemented in this system is codon-optimised for expression in *S. pombe* and driven by the medium strength promoter *adh15*, resulting in reduced toxicity associated with Cas9 levels. *SpEDIT* can generate targeted *ade6* and *ura4* point mutants in asynchronous cells with 100% mutagenesis efficiency. Moreover, *SpEDIT* allows simultaneous editing at two non-homologous genes at distinct locations in the *S. pombe* genome, as well as seamless insertion, deletion and tagging at *S. pombe* loci. *SpEDIT* provides an efficient and simple CRISPR/Cas9 method to easily manipulate the genome of the fission yeast.

Results

The *SpEDIT* system

The *SpEDIT* system has been developed to address the two main complications associated with existing CRISPR/Cas9 methods for *S. pombe*: toxicity associated with Cas9 overexpression, and laborious cloning procedures required to insert a specific sgRNA target sequence into a Cas9-containing plasmid. An overview of the *SpEDIT* system is provided (Appendix I Figure 1) along with a full protocol (see page 193).

High levels of human codon-optimised Cas9 endonuclease constitutively expressed from the exceptionally strong *adh1* promoter (400 RNA molecules/cell, PomBase, (Lock et al. 2019) lead to reduced cell growth in *S. pombe* (Jacobs et al. 2014). A recent report attempted to solve this toxicity problem by expressing the human codon-optimised Cas9 under control of the repressible *nmt41* promoter (Hayashi & Tanaka 2019). Although this approach does generate mutations, it requires the non-ideal use of minimal media and relies on auxotrophic (*ura4*$^{-}$ or *leu1*$^{-}$) strains to allow plasmid selection. Moreover, the mutagenesis efficiency obtained was dependent on the selectable marker employed.

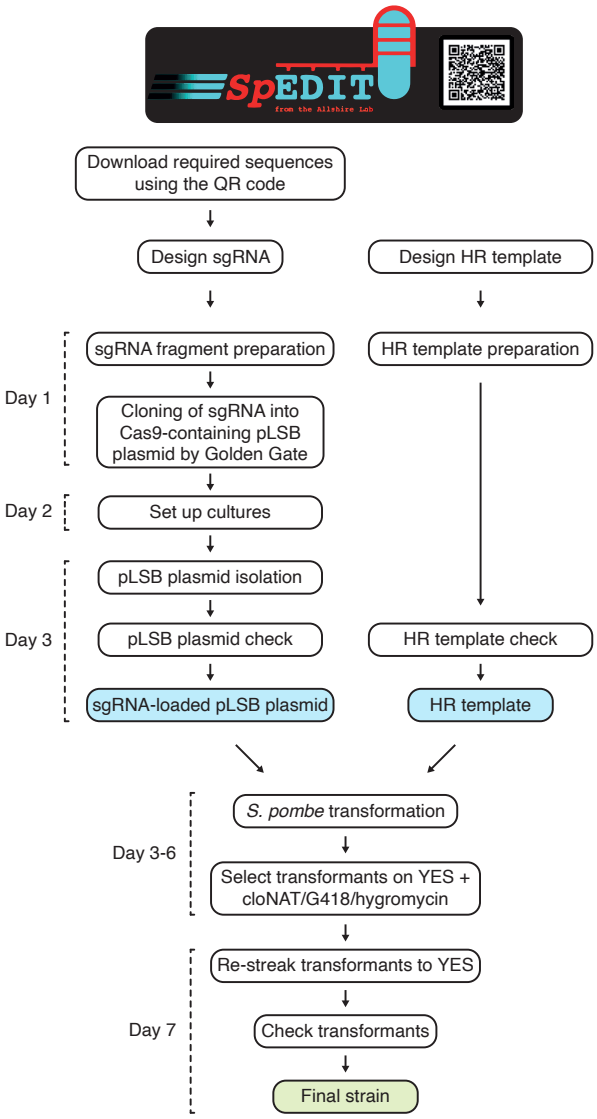

Appendix I Figure 1. *SpEDIT* provides a fast and effective CRISPR/Cas9 method to manipulate the genome of *Schizosaccharomyces pombe*. Diagram illustrating the required steps for *S. pombe* strain construction using *SpEDIT*. For a full protocol see page 193. sgRNA, single guide RNA. HR template, homologous recombination donor template.

To overcome the toxicity related to high levels of humanised Cas9, we synthesized a Cas9 gene codon-optimised for expression in *S. pombe* (SpCas9) that is transcribed from the medium strength *adh15* promoter (Yamagishi et al. 2008). This *adh15*-SpCas9 gene is carried on a new plasmid, pLSB, that contains a choice of dominant selectable markers. Versions bearing *natMX6, kanMX6* or *hphMX6* markers are available thereby allowing the

SpEDIT system to be employed on fission yeast strains that harbour various manipulations where other selectable markers are already present (Appendix I Figure 2A).

Eukaryotic CRISPR/Cas9 systems usually rely on snRNA or snoRNA RNA polymerase III (RNAPIII) promoters for transcription of the sgRNA cassette (Cong *et al.,* 2013). However, characterised *S. pombe* RNAPIII genes contain promoter elements within the transcribed region preventing their use for generating accurately positioned 5' ends, and RNA polymerase II (RNAPII) promoters generally do not generate transcripts with precise 5' and 3' ends. Consequently all sgRNA expression system for *S. pombe* so far utilise the *rrk1* promoter plus its downstream 5' untranslated region which generates a RNAPII transcript with a cleavable leader RNA (Jacobs et al. 2014). Insertion of sgRNA sequences targeting genomic regions of interest into the *rrk1* sgRNA expression cassette in current CRISPR/Cas9 systems for *S. pombe* relies on slow and arduous cloning procedures involving either traditional restriction digestion (Jacobs et al. 2014; Hayashi & Tanaka 2019) or PCR over a long template (Rodríguez-López et al. 2016). An alternative method that uses *in vivo* gap repair to assemble a gapped Cas9-encoding plasmid and a PCR-amplified sgRNA fragment into a single circular plasmid has been reported (Zhang et al. 2018). Although this method provided an advance, this system still utilises humanised Cas9 expressed from the very strong *adh1* promoter which consequently reduces cell growth due to Cas9-associated toxicity.

It has previously been shown that the upstream $tRNA^{Ser}$ gene of an *S. pombe* $tRNA^{Ser}$-$tRNA^{Met}$ gene pair drives RNAPIII expression of the downstream $tRNA^{Met}$ gene (Hottinger-Werlen et al. 1985). We therefore use this $tDNA^{Ser}$ to drive sgRNA expression in *S. pombe*. The resulting *SpEDIT* system employs a modular design where sgRNAs are expressed from this $tDNA^{Ser}$ sequence and fused to the hepatitis delta virus ribozyme (HDV), as previously described for *Saccharomyces cerevisiae* (Ryan et al. 2014). The $tDNA^{Ser}$ acts as a RNAPIII promoter and the self-cleaving ribozyme protects and defines the 5' end of the resulting sgRNA (Appendix I Figure 2A and B). The presence of the

HDV ribozyme was shown to result in a six-fold increase in sgRNA abundance and this correlated with high targeting efficiency in *S. cerevisiae* (Ryan et al. 2014). To facilitate cloning of sgRNA target sequences into this tDNA/HDV expression cassette, we placed sites for the *Bsa*I type IIS restriction enzyme on each side of a GFP placeholder thereby allowing one-step insertion of sgRNAs via Golden Gate cloning. Importantly, this strategy also permits visual screening to identify colonies that have lost the green GFP fluorescence signal indicating that the GFP has been successfully replaced with an incoming sgRNA (Appendix I Figure 2B and C).

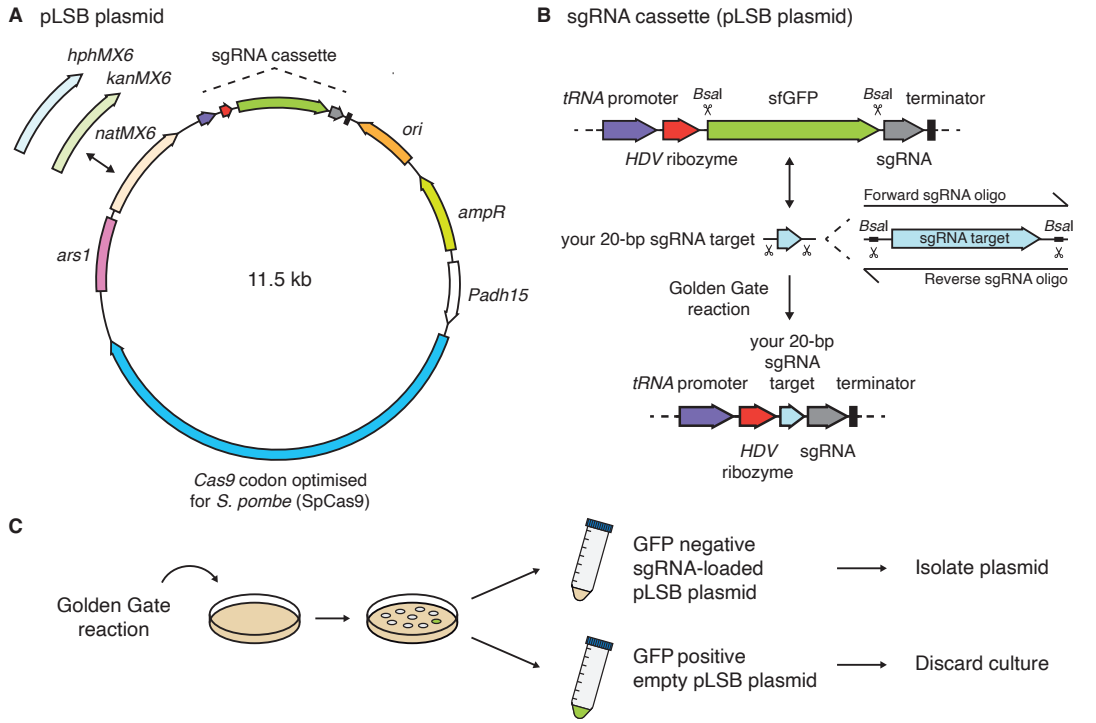

Appendix I Figure 2. The *SpEDIT* pLSB plasmid allows one-step insertion of sgRNAs via Golden Gate cloning. A. Map of pLSB plasmid. Full sequence is available scanning the QR code in Appendix I Figure 1 or at *allshirelab.com/spedit*. Versions with *natMX6* (cloNAT), *kanMX6* (G418) or *hphMX6* (hygromycin) *S. pombe* resistance markers are available. A Cas9 codon optimised for *S. pombe* (SpCas9) is expressed from the *adh15* promoter (*Padh15*). **B.** Diagram of sgRNA cassette and cloning procedure. sgRNA cassette expression is driven by a $tRNA^{Ser}$ Pol III promoter (purple block arrow). A self-cleaving hepatitis delta virus (HDV) ribozyme is located at the 5' end of the sgRNA cassette (red block arrow). A superfolder green fluorescent protein (sfGFP) is used as placeholder (green block arrow). *Bsa*I sites flanking sfGFP allow one-step insertion of a sgRNA target (light blue block arrow) into the sgRNA scaffold (grey block arrow) via Golden Gate cloning. The Pol III terminator sequence from *S. cerevisiae SUP4* ($tRNA^{Tyr}$) is present at the 3' end of the sgRNA cassette (black block). **C.** The sfGFP placeholder allows cultures carrying empty (green) pLSB plasmids to be distinguished from sgRNA-loaded (non-green) pLSB plasmids. sgRNA, single guide RNA.

SpEDIT can generate targeted *ade6* and *ura4* point mutants in asynchronous cells with 100% mutagenesis efficiency

To assess the performance of the *SpEDIT* system in comparison to the existing pMZ379 system (Rodríguez-López et al. 2016), we targeted the *ade6*$^{+}$ and *ura4*$^{+}$ genes and provided HR templates that disable the PAM (NGG) sequence downstream of the sgRNA target to generate premature STOP codon mutations (Appendix I Figure 3A). *ade6*$^{+}$ and *ura4*$^{+}$ mutations can be easily scored due to their characteristic phenotypes: *ade6* mutants, pink colonies develop on low (1/10) adenine-containing plates; *ura4* mutants, cannot grow in the absence of supplementing uracil (uracil auxotrophy) but can grow in the presence of counterselective 5-fluoroorotic acid (FOA resistant) (Appendix I Figure 3B). We scored cloNAT-resistant colonies after electroporation of asynchronous cultures with either *SpEDIT*/pLSB or pMZ379 plasmids expressing sgRNA designed to mediate cleavage within the *ade6*$^{+}$ or *ura4*$^{+}$ genes in the presence or absence of an HR template homologous to *ade6*$^{+}$ or *ura4*$^{+}$, respectively. The results revealed that both pLSB and pMZ379 plasmids can generate targeted mutations in *ade6*$^{+}$ and *ura4*$^{+}$ with 100% efficiency when a matching HR template was co-transformed (Appendix I Figure 3C). However, when an HR template targeting a different gene or no HR template was provided, the number of cloNAT-resistant colonies obtained was dramatically reduced. This decrease in transformant number in the absence of an HR template is consistent with futile cleavage-repair cycles where the persistence of a double strand break prevents cell division and thus colony formation (Appendix I Figure 3C).

Sequence analysis of the resulting *ade6* and *ura4* mutants showed that when a matching HR template was co-transformed, all clones analysed harboured the mutation provided by the HR template (Appendix I Figure 3E, left). However, a variety of mutations that disable the PAM sequence and ultimately disrupt the coding sequence of each gene were detected in mutants generated when a non-homologous HR template (targeting a different gene to the sgRNA) or no HR template was provided (Appendix I Figure 3E, left).

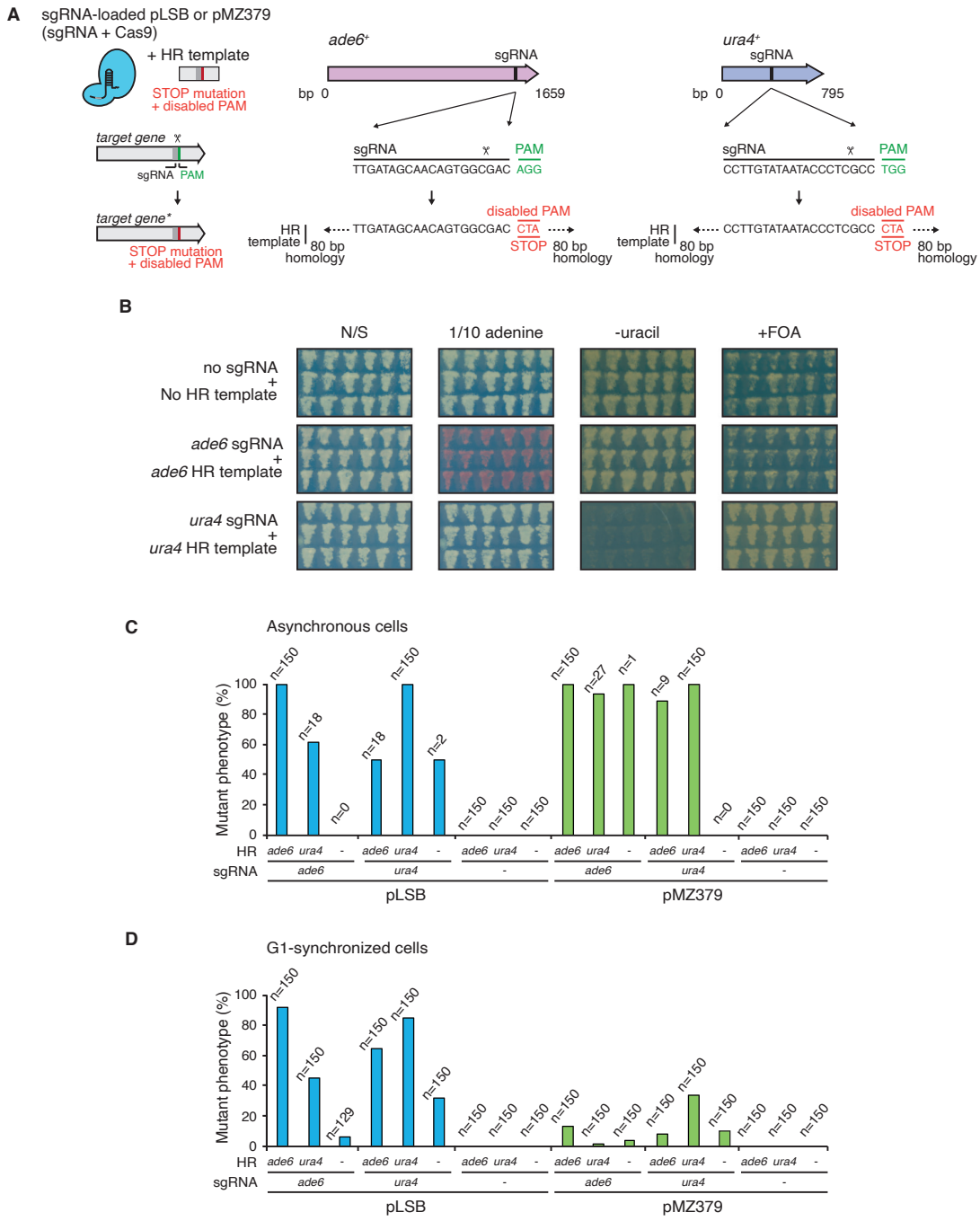

See next page for caption.

E

Asynchronous cells

	sgRNA	HR template	% Analysed colonies (n=5) Edited	Other mutation at PAM	No mutation
pLSB		*ade6*	100%		
	ade6	*ura4*		100%	
		-		*	
		ade6		100%	
	ura4	*ura4*	100%		
		-		100%	
		ade6			100%
	-	*ura4*			100%
		-			100%
pMZ379		*ade6*	100%		
	ade6	*ura4*		100%	
		-		100%	
		ade6		100%	
	ura4	*ura4*	100%		
		-		*	
		ade6			100%
	-	*ura4*			100%
		-			100%

G1-synchronized cells

	sgRNA	HR template	% Analysed colonies (n=5) Edited	Other mutation at PAM	No mutation
pLSB		*ade6*	100%		
	ade6	*ura4*		100%	
		-		100%	
		ade6		100%	
	ura4	*ura4*	80%	20%	
		-		100%	
		ade6			100%
	-	*ura4*			100%
		-			100%
pMZ379		*ade6*	80%	20%	
	ade6	*ura4*		100%	
		-		100%	
		ade6		100%	
	ura4	*ura4*	40%	60%	
		-		100%	
		ade6			100%
	-	*ura4*			100%
		-			100%

Appendix I Figure 3. *SpEDIT* can generate targeted *ade6* and *ura4* point mutants in asynchronous cells with 100% mutagenesis efficiency. A. Schematic of experiment to generate targeted *ade6* and *ura4* point mutants. A sgRNA-loaded pLSB or pMZ379 plasmid was co-transformed with an HR template that creates a premature STOP codon by disabling the PAM (NGG) sequence. sgRNA and HR template sequences for *ade6* and *ura4* are shown. Full HR template sequences can be found in Appendix IV. **B.** After transformation, cloNAT-resistant colonies were picked and re-streaked to non-selective YES plates. Cells were then replica-plated to indicated media to assess their phenotype. Representative plates from two independent experiments are shown. Quantification is shown in C-D. **C-D.** Percentage of cloNAT-resistant transformants displaying a mutant phenotype (pink cells, *ade6;* uracil auxotrophy and FOA resistance, *ura4*) after asynchronous (**C**) or G1-synchronized (**D**) wild-type cells were transformed with a sgRNA-loaded *SpEDIT/*pLSB (developed here, Appendix I Figure 2) or pMZ379 (Rodríguez-López et al. 2016) plasmid targeting *ade6*$^{+}$ or *ura4*$^{+}$ (or no sgRNA plasmid as control). An HR template targeting the same or a different gene was co-transformed as indicated. n = number of cloNAT-resistant colonies assayed. Note that when an HR template targeting a different gene or no HR template was co-transformed into asynchronous cells, the number of cloNAT-resistant colonies obtained was drastically reduced. Experiment was repeated twice with similar results. **E.** For each condition in **C**-**D**, five colonies displaying the mutant phenotype (or 5 cloNAT-resistant colonies for no sgRNA plasmids) were taken and the gene targeted by the sgRNA was sequenced to confirm changes in its DNA sequence. Both *ade6* and *ura4* were sequenced when no sgRNA was used. Edited clones harbour the change contained in the corresponding HR template. Other mutations at PAM disrupt the PAM (NGG) sequence and the corresponding gene coding sequence. For asynchronous cells transformed with pLSB-*ura4* (no HR template) and pMZ379-*ade6* (no HR template) only two and one colonies were respectively obtained and analysed. * No colonies were obtained for these conditions. sgRNA, single guide RNA. PAM, proto-spacer adjacent motif. HR, homologous recombination donor template. N/S, non-selective medium. FOA, 5-fluoroorotic acid.

A previous study suggested that G1 synchronization of *S. pombe* cultures by nitrogen starvation prior to CRISPR/Cas9-mediated genome editing enhances transformation and deletion efficiencies (Rodríguez-López et al. 2016). The rationale for this was that in G1 only one copy of a target locus would need to be modified as opposed to the two copies that are present in G2 cells. The remodelled transcriptional programme of G1 cells was also expected to render genomic regions more open (Mata et al. 2002), and thus increase accessibility to the editing machinery.

We therefore compared the performance of the *SpEDIT* system (pLSB plasmid) versus the existing pMZ379 system (pMZ379 plasmid) at generating *ade6* and *ura4* mutations using G1-synchronized *S. pombe* cells as previously described (Rodríguez-López et al. 2016). This comparison revealed that the pLSB plasmid is more efficient than the pMZ379 plasmid at generating mutations in G1-synchronized cells (Appendix I Figure 3D). However, even when a matching HR template was co-transformed, the mutagenesis efficiencies obtained with G1 cells were lower than that of asynchronous cells (pLSB-ade6, 92% G1 versus 100% Asynchronous; pLSB-ura4, 85% G1 versus 100% Asynchronous) (Appendix I Figure 3D).

Moreover, sequence analysis revealed that even when a matching HR template was co-transformed into G1 cells, not all mutant clones harboured the anticipated mutation that was presented by the HR template (Appendix I Figure 3E, right). This lack of accuracy is likely due to the suppression of the HR pathway that is known to occur in G1 cells (Trickey et al. 2008; Orthwein et al. 2015).

Taken together, our results show that the *SpEDIT* system can generate targeted mutations at *ade6*$^{+}$ and *ura4*$^{+}$ with 100% mutagenesis efficiency using asynchronous cell cultures. Notably, our experiments show that G1 synchronization of *S. pombe* cells prior transformation has a detrimental effect on mutagenesis efficiency regardless of the CRISPR/Cas9 system used.

SpEDIT shows reduced toxicity compared with the current pMZ379 CRISPR/Cas9 system in asynchronous cells

To determine if the *SpEDIT* system leads to reduced toxicity compared to the current pMZ379 system, we measured colony area on selection plates after transforming asynchronous or G1-synchronized cultures with pLSB or pMZ379 plasmids targeting *ade6*$^{+}$ or *ura4*$^{+}$ (or empty plasmid controls) in the presence of a matching HR template. The colony area (equivalent to colony size) was found to be greater when asynchronous cells were transformed with pLSB as opposed to pMZ379 (Appendix I Figure 4A). The resulting difference in colony size was independent of the presence of a sgRNA, indicating that excessive levels of Cas9 alone, and not Cas9 targeting to a genomic locus, are sufficient to cause the observed toxicity (Appendix I Figure 4A). Consistent with this, the toxicity of *adh1*-Cas9 has also been shown to be independent of Cas9 catalytic activity (Ciccaglione 2015).

In contrast, colony area measurements of pLSB and pMZ379 transformants obtained from G1-synchronized cells revealed no major difference in resulting colony size (Appendix I Figure 4B). This indicates that the toxicity related to high levels of catalytically active Cas9 is more prominent when transforming asynchronous cells. The lack of apparent toxicity in G1 cells is likely due to the known up-regulation of non-homologous end joining-mediated repair and the suppression of homologous recombination repair that is known to occur at this cell cycle stage (Orthwein et al. 2015).

SpEDIT allows simultaneous editing at two non-homologous genes at distinct locations in the *S. pombe* genome

The availability of pLSB versions bearing different dominant selectable markers presented the opportunity to test if the simultaneous editing of two different non-homologous loci by co-transformation with and selection of two distinct pLSB plasmids expressing different sgRNAs was possible.

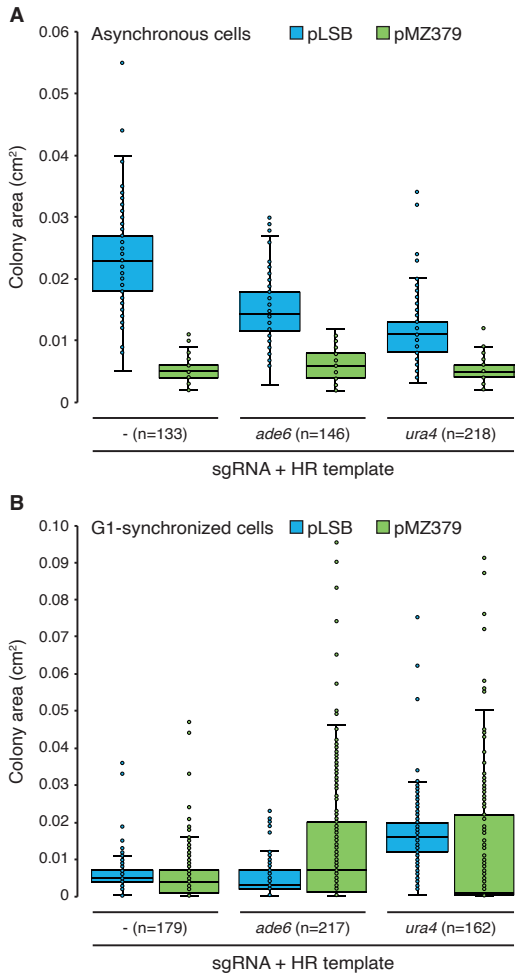

Appendix I Figure 4. *SpEDIT* shows reduced toxicity compared with the current pMZ379 *S. pombe* CRISPR/Cas9 system in asynchronous cells. A-B. Colony area measurements of asynchronous (**A**) or G1-synchronized (**B**) wild-type cells transformed with pLSB or pMZ379 plasmids and indicated HR templates growing on selective cloNAT-containing plates (same experiment as Appendix I Figure 3). Colony area was quantified (cm^2) using ImageJ. sgRNA, single guide RNA. HR, homologous recombination donor template.

To evaluate the possibility of simultaneous editing, we targeted two non-homologous genes, *clr5*$^+$ and *meu27*$^+$, located on different chromosomes (I and III, respectively) in wild-type cells using pLSB-cloNAT and pLSB-hygromycin plasmids that express sgRNAs designed to target *clr5*$^+$ and *meu27*$^+$, respectively. (Appendix I Figure 5A). We co-transformed two HR templates that generate point mutations in *clr5*$^+$ (*clr5-Q264STOP*) and *meu27*$^+$ (*meu27-S100Y*), and concomitantly disabled both corresponding PAM sequences (Appendix I Figure 5A and B). These mutations (*clr5-Q264STOP*

and *meu27-S100Y*) were identified in a proportion of heterochromatin-dependent epimutants resistant to caffeine (see Chapter 3). Sequencing of *clr5* and *meu27* in ten resulting cloNAT and hygromycin doubly resistant co-transformants revealed that two harboured both of the expected DNA changes. Five clones carried mutations in only one of the two targeted genes or bore mutations that uniquely affected the PAM sequence, and three clones displayed neither of the anticipated changes (Appendix I Figure 5C).

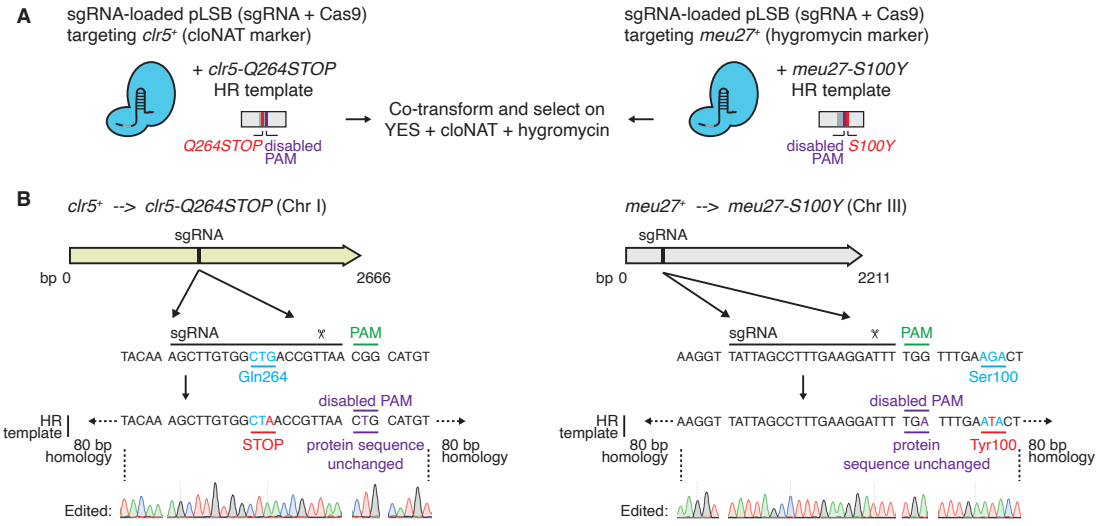

C

% Analysed transformants (n=10)	
clr5 and *meu27* edited	20%
clr5 or *meu27* edited	20%
Only PAM edited (in one gene or both)	30%
No change	30%

Appendix I Figure 5. *SpEDIT* allows simultaneous editing at two non-homologous genes at distinct locations in the *S. pombe* genome. A. Schematic of experiment to simultaneously generate targeted point mutations in *clr5*$^{+}$ and *meu27*$^{+}$. Two sgRNA-loaded pLSB plasmids (with different selection markers) were co-transformed with two HR templates that create the desired point mutations and disable the corresponding PAM (NGG) sequence. Transformed cells were then selected on selective plates containing both cloNAT and hygromycin. **B.** sgRNA and HR template sequences for *clr5* (left) and *meu27* (right) are shown, along with Sanger sequencing chromatograms for a successfully edited clone. Full HR template sequences can be found in Appendix IV. **C.** Percentage of cloNAT- and hygromycin-resistant transformants harbouring the targeted mutations in *clr5* and *meu27* as revealed by Sanger sequencing. sgRNA, single guide RNA. HR, homologous recombination donor template.

Importantly, whole-genome sequencing of one of the isolates that contained both expected gene editing events revealed no additional genetic changes (SNPs or indels) in coding regions of the genome (see Chapter 3; raw data accession number available in section 2.8 in Methods).

These results demonstrate that our improved system can be utilised to perform simultaneous gene editing at two distant, non-homologous *S. pombe* loci, albeit with reduced efficiency relative to the frequency of editing of a single locus.

Seamless insertion, deletion and tagging at *S. pombe* loci using *SpEDIT*

To assess the capabilities of *SpEDIT* in additional gene editing tasks we utilised it to perform insertion, deletion and tagging at single *S. pombe* loci. Specifically, using *SpEDIT*, we inserted *tetO* binding sites downstream of the *cup1*$^{+}$ (SPBC17G9.13c) gene (Appendix I Figure 6A). *tetO* binding sites allow tethering of proteins such as TetR-Clr4* and heterochromatin formation in the vicinity of the tethering site (see Chapter 4). A fusion-PCR construct containing *4xtetO* sites with 120-bp homology arms flanking the desired insertion site was used as the HR template (see Appendix IV for sgRNA and HR template sequences). Correct insertion of the *cup1:4xtetO* HR template resulted in ablation of the PAM sequence. Furthermore, we used *SpEDIT* to seamlessly fuse GFP in frame with the 3' end of the of *cup1*$^{+}$ gene to produce Cup1-GFP (Appendix I Figure 6B). To generate the *cup1-gfp* HR template, the *GFP* open reading frame was amplified with oligonucleotides that had long extensions homologous to sequence immediately up-stream and down-stream of the normal *cup1*$^{+}$ STOP codon. This HR template also carried a DNA change (in the 5' long oligo) designed to disable the PAM sequence without altering the Cup1 protein sequence. Resulting strains were confirmed to carry the planned *cup1:4xtetO* or Cup1-GFP insertions in the absence of any associated selectable marker and were utilised to show that heterochromatin-mediated silencing of *cup1*$^{+}$ is sufficient to drive caffeine resistance in wild-type cells and that Cup1-GFP localises to mitochondria (see Chapter 4, *cup1:4xtetO* = *4xtetO-II*).

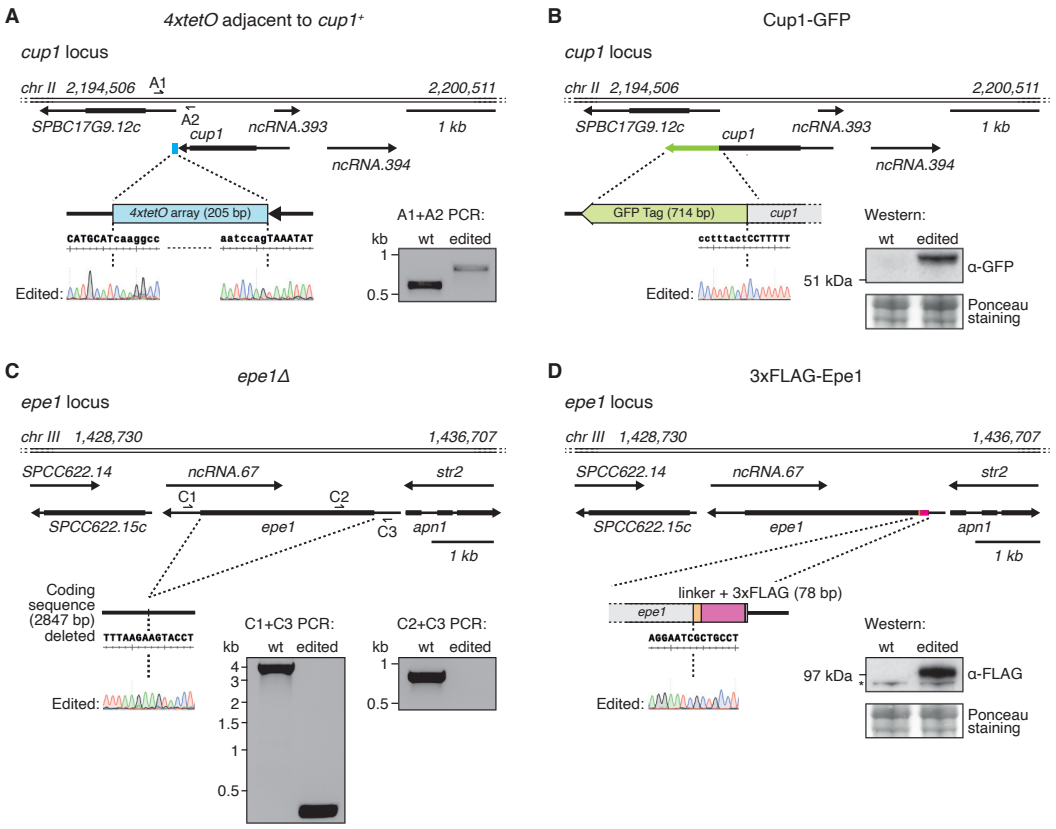

Appendix I Figure 6. *SpEDIT* allows seamless insertion, deletion and tagging at *S. pombe* loci. A. *4xtetO* binding sites were inserted downstream of *cup1*$^{+}$. Sanger sequencing chromatograms covering the insert junctions are shown for a successfully edited clone. PCR primers (half arrows) flanking the insert were used to amplify products from wild-type (wt) and edited strains. **B.** Cup1 was C-terminally tagged with a green fluorescent protein (GFP). Sanger sequencing chromatogram covering the gene-tag junction is shown for a successfully edited clone. Western blot using anti-GFP antibody was performed on wild-type (wt) and edited strains. **C.** The coding sequence of *epe1*$^{+}$ was deleted. Sanger sequencing chromatogram covering the deletion junction is shown for a successfully edited clone. PCR primers (half arrows) flanking the deletion (and within the *epe1*$^{+}$ coding sequence as control) were used to amplify products from wild-type (wt) and edited strains. **D.** Epe1 was N-terminally tagged with three FLAG epitopes. Sanger sequencing chromatogram covering the gene-tag junction is shown for a successfully edited clone. Western blot using anti-FLAG antibody was performed on wild-type (wt) and edited strains. For sgRNA and HR template sequences see Appendix IV.

Epe1 is a putative histone demethylase that acts to prevent heterochromatin island formation (Zofall et al. 2012; Wang et al. 2015; Sorida et al. 2019). Using *SpEDIT*, we deleted the *epe1*$^{+}$ coding sequence (Appendix I Figure 6C). The *epe1Δ* HR template employed contained 80-bp arms homologous to sequences immediately flanking the *epe1*$^{+}$ coding sequence as previously

used for the deletion of other sequences (Rodríguez-López et al. 2016). Correct deletion of the *epe1*$^{+}$ coding sequence results in loss of the sgRNA target and PAM sequences. In addition, we seamlessly inserted a sequence to encode a 3xFLAG epitope tag between the *epe1*$^{+}$ gene promoter and the 5' end of the *epe1*$^{+}$ coding sequence to allow the production of N-terminally 3xFLAG-tagged Epe1 without any associated selectable marker (Appendix I Figure 6D). To accomplish this, an in-frame *epe1-3xflag-epe1* HR template containing 50-bp arms homologous to the sequence immediately flanking the *epe1*$^{+}$ start codon was used. Correct insertion of the *epe1-3xflag-epe1 sequence* resulted in loss of both the sgRNA target and the PAM sequence. The resulting *epe1Δ* and 3xFLAG-Epe1 strains were utilised to study the role of Epe1 in ectopic heterochromatin island formation following caffeine exposure (see Chapter 6). Notably, whole-genome sequencing of the *epe1Δ* strain revealed no additional genetic changes (SNPs or indels) in coding regions of the genome (see Chapter 6; raw data accession number available in section 2.8 in Methods).

In the four distinct genome editing scenarios described above a maximum of eight primary transformants needed to be screened to obtain at least one that exhibited the desired sequence change. We therefore conclude that *SpEDIT* markedly speeds up the process of generating accurate insertion, deletion and tagging events at a variety of *S. pombe* loci.

Discussion

Here we report the development of *SpEDIT*, an optimized CRISPR/Cas9 editing system and method for the fission yeast, *S. pombe* (Appendix I Figure 1 and 2). *SpEDIT* makes use of Cas9 codon-optimised for expression in *S. pombe* that, coupled with the incorporation of a tDNA^{Ser}/HDV ribozyme sgRNA expression cassette (Ryan et al. 2014), achieves 100% efficiency in generating mutations at targeted *ade6*$^{+}$ or *ura4*$^{+}$ genes in asynchronous cells (Appendix I Figure 3). A high mutagenesis efficiency was also obtained with the pre-existing pMZ379 system in asynchronous cells (Jacobs et al. 2014; Rodríguez-López et al. 2016). However, *SpEDIT* displayed reduced toxicity by removing

the detrimental physiological effects associated with high humanised Cas9 endonuclease expression and consequently speeds up the genome editing process (Appendix I Figure 4). In addition, our analysis indicates that the use of G1-synchronized cell cultures for CRISPR/Cas9-mediated genome manipulation reduces the efficiency of targeted mutagenesis, with both the *SpEDIT* and pMZ379 systems, relative to asynchronous cultures (Appendix I Figure 3). G1 synchronization therefore represents an unnecessary time-consuming step in the genome editing process.

SpEDIT can be used to introduce simultaneous mutations at two non-homologous genes at distinct locations in the *S. pombe* genome (Appendix I Figure 5), and allows flexible engineering of seamless insertion, deletion and tagging events at *S. pombe* loci in the absence of linked selectable markers and without observed off-target sequence changes (Appendix I Figure 6). It is worth noting that many traditional *S. pombe* transformation protocols involve the use of carrier DNA. We advise against the use of carrier DNA as it has been shown to insert at many locations in resulting transformants causing unplanned off-target mutations (Longmuir et al. 2019).

Besides achieving high mutagenesis efficiency, the greatest advance of *SpEDIT* is a very simple cloning protocol allowing sgRNA target sequences to be inserted with minimal effort into the Cas9-bearing pLSB plasmid through a one-step Golden Gate reaction. Candidate sgRNA-bearing clones are easily visualized by loss of the GFP placeholder, negating the need for repetitive screening of numerous *E. coli* colonies by laborious plasmid purification and inspection.

Recently it was reported that homology arms of as short as 25-bp flanking each side of a cleavage site can be used to successfully introduce point mutations and epitope tags at *S. pombe* loci (Hayashi & Tanaka 2019). Further analyses will be required to determine whether HR templates with such short homology arms are as efficient as longer arms when combined with *SpEDIT.* In addition, the tDNA/HDV ribozyme sgRNA expression cassette that was originally developed for *S. cerevisiae* has been used to express up to three tandem

HDV-sgRNAs from a single tDNA RNAPIII promoter with 80% mutagenesis efficiency (Ryan et al. 2014). This suggests that a similar approach could be used with *SpEDIT* to simultaneously express multiple different sgRNAs that target a single locus or many distinct loci.

In summary, the combination of the CRISPR4P algorithm (Rodríguez-López et al. 2016), that conveniently aids the identification of suitable sgRNAs across the *S. pombe* genome, with *SpEDIT,* which provides a straightforward and user-friendly experimental method, markedly enhances the capabilities of CRISPR/Cas9-mediated genome editing in *S. pombe.* We anticipate *SpEDIT* will permit the broad application of genome editing procedures to fission yeast in order to explore diverse biological questions in this model fungal system.

***SpEDIT* protocol**

A convenient protocol card of this procedure can be found by visiting *allshirelab.com/spedit* or by scanning the QR code in Appendix I Figure 1.

Before you begin

- Download required DNA sequences at *allshirelab.com/spedit* or by scanning the QR code in Appendix I Figure 1

Required reagents

- pLSB vector (75 ng/µL) – Available on request
- NEB Golden Gate Assembly Kit (*Bsa*I-HF v2) – NEB #E1601S
- sgRNA fragment for Golden Gate assembly (1 ng/µL) – See below for design and preparation
- HR template (250-1000 ng) – See below for design and preparation

sgRNA design

- Find a suitable sgRNA targeting the gene of interest using CRISPR4P (Rodríguez-López et al. 2016)
- Copy the 20-bp sgRNA sequence in place of ‘your 20 bp targeting RNA’ in ‘GG_sgRNA_template.dna’ file
- Order 52-nt forward and reverse sgRNA oligonucleotides as indicated in the ‘GG_sgRNA_template.dna’ file

sgRNA fragment preparation

- Anneal sgRNA oligonucleotides
    - Mix 5 µL of 100 µM forward and reverse sgRNA oligonucleotides
    - Heat to 95°C for 3 min and cool down to room temperature slowly (e.g. -1°C/30 sec)
    - Add 1 µL of annealed mix to 1.5 mL of H_2O. This dilution corresponds to approximately 1 ng/µL annealed sgRNA fragment

Golden Gate reaction

- Mix the following components in a PCR tube:
    - pLSB plasmid (75 ng/µL) – 0.5 µL
    - Annealed sgRNA fragment (1 ng/µL) – 0.5 µL
    - T4 DNA Ligase Buffer (10x) – 1 µL
    - NEB Golden Gate Assembly Mix (*Bsa*I-HF v2) – 0.5 µL
    - H_2O – 7.5 µL
- Incubate at 37°C for 1 hr
- Incubate at 60°C for 5 min
- Transform into *Escherichia coli* by heat shock:
    - 1 µL of Golden Gate reaction to 25 µL of *DH5-alpha* or *10-Beta E. coli* cells
    - Place the mixture on ice for 30 min
    - Heat shock at exactly 42°C for exactly 30 sec
    - Place on ice for 5 min
    - Add 475 µL SOC media and recover cells at 37°C for 1 hr
    - Plate 200 µL / 100 µL / 50 µL / rest on LB plus ampicillin
- Select four *E. coli* colonies and set up liquid cultures in LB plus ampicillin
- Isolate plasmid (miniprep)
    - IMPORTANT: do not miniprep culture if green – these are GFP-containing clones where the Golden Gate reaction did not occur
    - One miniprep (approximately 200 ng/µL) should be sufficient for many *S. pombe* transformations (200 ng/transformation)

Plasmid check

- Digest plasmid using *Nco*I
    - This digest allows sgRNA-containing plasmids to be distinguished from those containing GFP
- Sequence sgRNA-containing plasmids using M13F oligonucleotide (see Appendix III) to confirm sgRNA insertion

HR template design and preparation

- The HR template should contain:
    - Your desired mutation: point mutation, insertion, deletion or tag
    - At least 80 bp homology on each side relative to the cleavage site (3 bp upstream of PAM sequence (NGG))
    - A mutation that disrupts the PAM sequence to avoid repeated DSBs
        - If the total size of the HR template is equal or smaller than 180 bp, we recommend generating HR templates by PCR using oligonucleotides with overlapping at their 3' end as described in Rodríguez-López et al. (2016)
        - If the total size of the HR template is larger than 180 bp, we recommend using a fusion PCR construct containing homology arms to the target site (see HR template for *cup1:4xtetO* in Appendix IV)

S. pombe transformation

- Transform *S. pombe* cells using your preferred method with sgRNA-loaded pLSB plasmid (200 ng) and HR template (500-1000 ng) (see section 2.1.2.2 in Chapter 2)
- Grow non-selectively o/n on YES plates or liquid
- Plate on YES plus cloNAT (or YES plus G418 or YES plus hygromycin depending on pLSB version used)
- Re-streak transformant colonies to non-selective media to allow loss of plasmid
- Amplify region of interest by colony PCR and sequence amplicon to confirm mutation

Appendix II

S. pombe strains used in this thesis

Strain number	Name	Description
143	wt	*h*- ED972 wild-type
B4411	SR-1	Stable 16 mM Caffeine Resistant Isolate – From wt – 1
B4412	SR-2	Stable 16 mM Caffeine Resistant Isolate – From wt – 2
B4413	UR-1	Unstable 16 mM Caffeine Resistant Isolate – From wt – 1
B4414	UR-2	Unstable 16 mM Caffeine Resistant Isolate – From wt – 2
B4415	UR-3	Unstable 16 mM Caffeine Resistant Isolate – From wt – 3
B4416	UR-4	Unstable 16 mM Caffeine Resistant Isolate – From wt – 4
B4417	UR-5	Unstable 16 mM Caffeine Resistant Isolate – From wt – 5
B4418	UR-6	Unstable 16 mM Caffeine Resistant Isolate – From wt – 6
B4419	UR-7	Unstable 16 mM Caffeine Resistant Isolate – From wt – 7
B4420	UR-8	Unstable 16 mM Caffeine Resistant Isolate – From wt – 8
B4421	UR-9	Unstable 16 mM Caffeine Resistant Isolate – From wt – 9
B4422	UR-10	Unstable 16 mM Caffeine Resistant Isolate – From wt – 10
B4423	UR-11	Unstable 16 mM Caffeine Resistant Isolate – From wt – 11
B4424	UR-12	Unstable 16 mM Caffeine Resistant Isolate – From wt – 12
B4425	UR-13	Unstable 16 mM Caffeine Resistant Isolate – From wt – 13
B4426	UR-14	Unstable 16 mM Caffeine Resistant Isolate – From wt – 14
B4427	UR-15	Unstable 16 mM Caffeine Resistant Isolate – From wt – 15
B4428	UR-16	Unstable 16 mM Caffeine Resistant Isolate – From wt – 16
B4429	UR-17	Unstable 16 mM Caffeine Resistant Isolate – From wt – 17
B4430	UR-18	Unstable 16 mM Caffeine Resistant Isolate – From wt – 18
B4431	UR-19	Unstable 16 mM Caffeine Resistant Isolate – From wt – 19
B4432	UR-20	Unstable 16 mM Caffeine Resistant Isolate – From wt – 20
B4433	UR-21	Unstable 16 mM Caffeine Resistant Isolate – From wt – 21
B4434	UR-22	Unstable 16 mM Caffeine Resistant Isolate – From wt – 22
B4435	UR-23	Unstable 16 mM Caffeine Resistant Isolate – From wt – 23
B4436	UR-24	Unstable 16 mM Caffeine Resistant Isolate – From wt – 24
B4437	UR-25	Unstable 16 mM Caffeine Resistant Isolate – From wt – 25
B4438	UR-26	Unstable 16 mM Caffeine Resistant Isolate – From wt – 26
B4439	UR-27	Unstable 16 mM Caffeine Resistant Isolate – From wt – 27
B4440	UR-28	Unstable 16 mM Caffeine Resistant Isolate – From wt – 28
B4441	UR-29	Unstable 16 mM Caffeine Resistant Isolate – From wt – 29
B4442	UR-30	Unstable 16 mM Caffeine Resistant Isolate – From wt – 30
B4443	SR-1 *clr4Δ* - 1	SR-1 *clr4Δ::NAT* - transformant 1
B4444	SR-1 *clr4Δ* - 2	SR-1 *clr4Δ::NAT* - transformant 2
B4445	SR-1 NAT control - 1	SR-1 *NAT:3' of ura4* - transformant 1
B4446	SR-1 NAT control - 2	SR-1 *NAT:3' of ura4* - transformant 2
B4447	SR-2 *clr4Δ* - 1	SR-2 *clr4Δ::NAT* - transformant 1
B4448	SR-2 *clr4Δ* - 2	SR-2 *clr4Δ::NAT* - transformant 2
B4449	SR-2 NAT control - 1	SR-2 *NAT:3' of ura4* - transformant 1
B4450	SR-2 NAT control - 2	SR-2 *NAT:3' of ura4* - transformant 2
B4451	UR-1 *clr4Δ* - 1	UR-1 *clr4Δ::NAT* - transformant 1
B4452	UR-1 *clr4Δ* - 2	UR-1 *clr4Δ::NAT* - transformant 2
B4453	UR-1 NAT control-1	UR-1 *NAT:3' of ura4* - transformant 1
B4454	UR-1 NAT control-2	UR-1 *NAT:3' of ura4* - transformant 2
B4455	UR-2 *clr4Δ* - 1	UR-2 *clr4Δ::NAT* - transformant 1
B4456	UR-2 *clr4Δ* - 2	UR-2 *clr4Δ::NAT* - transformant 2
B4457	UR-2 NAT control - 1	UR-2 *NAT:3' of ura4* - transformant 1
B4458	UR-2 NAT control - 2	UR-2 *NAT:3' of ura4* - transformant 2
B5022	UR-2 *dcr1Δ* - 1	UR-2 *dcr1Δ::NAT* - transformant 1
B5023	UR-2 *dcr1Δ* - 2	UR-2 *dcr1Δ::NAT* - transformant 2
B5024	UR-2 *ago1Δ* - 1	UR-2 *ago1Δ::NAT* - transformant 1
B5025	UR-2 *ago1Δ* - 2	UR-2 *ago1Δ::NAT* - transformant 2

B4352	Pap1-N424STOP	*h- pap1-N424STOP*
B4752	Clr5-Q264STOP Meu27-S100Y	*h- clr5-Q264STOP meu27-S100Y*
B4459	UR-2 +14 days -CAF	UR-2 after growth on -CAF media for 14 days
B4460	*hba1Δ*	*h- hba1Δ::NAT*
B4461	*SPBC17G9.12cc*	*h- SPBC17G9.12cΔ::NAT*
B4462	*ncRNA.393Δ*	*h- ncRNA.393Δ::NAT*
B4463	*ncRNA.394Δ*	*h- ncRNA.394Δ::NAT*
B4464	*eno101Δ*	*h- eno101Δ::NAT*
B3797	TetR-Clr4*	*h+ leu1+adh21-TetROFF-2xFLAG-Clr4-cdd*
B3808	*4xtetO-II (4xtetO-IIa) (cup1:4xtetO)*	*h- 4xtetO 3' of cup1 leu1-32 (cup1=SPBC17G9.13c)*
B3807	*4xtetO-IIb*	*h- 4xtetO 5' of cup1 leu1-32 (cup1=SPBC17G9.13c)*
B3810	*4xtetO-IIc*	*h- 4xtetO 3' of ncRNA.394 leu1-32*
B3813	*4xtetO-I*	*h- 4xtetO 5' of hba1 leu1-32*
B3820	*4xtetO-III*	*h- 4xtetO 5' of ura4 leu1-32*
B4707	*4xtetO-IV*	*h- 4xtetO 5' of mbx2*
B4465	*TetR-Clr4* + 4xtetO-II (4xtetO-IIa)*	*h+ leu1+adh21-TetROFF-2xFLAG-Clr4-cdd 4xtetO 3' of cup1 (cup1=SPBC17G9.13c)*
B5691	*TetR-Clr4* + 4xtetO-IIb*	*h+ leu1+adh21-TetROFF-2xFLAG-Clr4-cdd 4xtetO 5' of cup1 (cup1=SPBC17G9.13c)*
B4936	*TetR-Clr4* + 4xtetO-IIc*	*h+ leu1+adh21-TetROFF-2xFLAG-Clr4-cdd 4xtetO 3' of ncRNA.394*
B4466	*TetR-Clr4* + 4xtetO-I*	*h+ leu1+adh21-TetROFF-2xFLAG-Clr4-cdd 4xtetO 5' of hba1*
B4467	*TetR-Clr4* + 4xtetO-III*	*h+ leu1+adh21-TetROFF-2xFLAG-Clr4-cdd 4xtetO 5' of ura4*
B4807	*TetR-Clr4* + 4xtetO-IV*	*h+ leu1+adh21-TetROFF-2xFLAG-Clr4-cdd 4xtetO 5' of mbx2*
B4885	*cup1-3xDSR*	*h- cup1Δ LocusPX:cup1-3xDSR (cup1=SPBC17G9.13c)*
B5005	*cup1-TT*	*h- cup1-TT (cup1=SPBC17G9.13c)*
B4688	Cup1-L73G	*h- cup1-L73G (cup1=SPBC17G9.13c)*
B4690	Cup1-F99G	*h- cup1-F99G (cup1=SPBC17G9.13c)*
B4567	Cup1-GFP	*h- cup1-GFP (cup1=SPBC17G9.13c)*
B4909	Cup1-GFP Arg11-mCh	*h- cup1-GFP arg11-mCherry-NAT (cup1=SPBC17G9.13c)*
B4912	Arg11-mCherry	*h- arg11-mCherry-NAT*
B4468	UR-2 (7 days +CAF)	UR-2 after growth on +CAF media for 3 days
B4469	UR-2 (7 days +CAF →14 days -CAF)	UR-2 after growth on +CAF media for 3 days and then on -CAF media for 14 days
B4621	*epe1Δ*	*h- epe1Δ*
B2835	Epe1-GFP	*h- epe1-GFP-KAN*
B4958	3xFLAG-Epe1	*h- 3xFLAG-epe1*
B4767	*TetR-Clr4* + 4xtetO-III epe1Δ*	*h+ epe1Δ::NAT leu1+adh21-TetROFF-2xFLAG-Clr4-cdd 4xtetO 5' of ura4*
B1008	*clr4Δ*	*h- clr4Δ::NAT*
B3250	*S. cerevisiae* Sgo1-GFP	*S. cerevisiae SGO1-yeGFP::KanMX6 MATa, ade2-1, leu2-3, ura3, trp1-1, his3-11, 15, can1-100, GAL, psi+*
B3111	*S. octosporus* wt	*h90 S. octosporus* wild-type
B4108	Mst2-13xMyc	*h- mst2-13xMyc-NAT*
B0505	Gcn5-13xMyc	*h? gcn5-13xMyc-NAT cc2Δ6Kb:cc1 ade6-704-HYG*

Appendix III

Oligonucleotides used in this thesis

Name	Sequence	Description
qAct1-F	GGTTTCGCTGGAGATGATG	qPCR *act1*$^+$ - F
qAct1-R	ATACCACGCTTGCTTTGAG	qPCR *act1*$^+$ - R
qDg-F	AATTGTGGTGGTGTGGTAATAC	qPCR *dg* repeats - F
qDg-R	GGGTTCATCGTTTCCATTCAG	qPCR *dg* repeats - R
ST-52	GAATTGTGGAGCCATGTCCC	qPCR *slu7*$^+$ - F
ST-53	TCTTCTCCTGTCCAACGAGC	qPCR *slu7*$^+$ - R
ST-872	GAAACCCAGAAATTCGCAGGT	qPCR *kin17*$^+$ - F - primer pair 1 *hba1* locus
ST-873	ATGAGTTGCTTGGGCATCCA	qPCR *kin17*$^+$ - R - primer pair 1 *hba1* locus
ST-62	CAGCAAATTGGGGACTGTGT	qPCR *ish1*$^+$ - F - primer pair 2 *hba1* locus
ST-63	CTCAAGAAGCCTGGGAGTCA	qPCR *ish1*$^+$ - R - primer pair 2 *hba1* locus
ST-64	CGATGATCTGGTTGTATGGTGG	qPCR *hba1*$^+$ - F - primer pair 3 *hba1* locus
ST-65	TGCTCAGTACGCCATCTTGA	qPCR *hba1*$^+$ - R - primer pair 3 *hba1* locus
ST-66	GGGCTATCCTTAACGCTCTTC	qPCR *hba1*$^+$*cds* - F - primer pair 4 *hba1* locus
ST-67	CGCCTCCTCTGAACCAAAAG	qPCR *hba1*$^+$*cds* - R - primer pair 4 *hba1* locus
ST-58	CTTCCCACATCGCGTTCATT	qPCR *alp4*$^+$ - F - primer pair 5 *hba1* locus
ST-59	ACCTAAATCATCGCTGCTGG	qPCR *alp4*$^+$ - R - primer pair 5 *hba1* locus
ST-393	GGGCATGACAATCTCCGACT	qPCR *pyr1*$^+$ - F - primer pair 1 *ncRNA.394* locus
ST-394	GGCCTACCTCGGTGATCTTG	qPCR *pyr1*$^+$ - R - primer pair 1 *ncRNA.394* locus
ST-401	CCGTATGGTGAAGCAGGGTT	qPCR *SPBC17G9.12c*$^+$ - F - primer pair 2 *ncRNA.394* locus
ST-402	CCCGATCTCCGTGTAAGCAA	qPCR *SPBC17G9.12c*$^+$ - R - primer pair 2 *ncRNA.394* locus
ST-184	TTCGTCGTATGCCCTCTTGC	qPCR *SPBC17G9.13c*$^+$ - F - primer pair 3 *ncRNA.394* locus
ST-185	AAAATCCGCCATTTGCCCAG	qPCR *SPBC17G9.13c*$^+$ - R - primer pair 3 *ncRNA.394* locus
ST-251	TGCTGTAGTGATGCAGAGGAG	qPCR *ncRNA.393*$^+$ - F - primer pair 4 *ncRNA.394* locus
ST-252	GCGGCCATTTTGTTTACATTCC	qPCR *ncRNA.393*$^+$ - R - primer pair 4 *ncRNA.394* locus
ST-190	GAAAATTAGCGCGGCCGTTA	qPCR *ncRNA.394*$^+$ - F - primer pair 5 *ncRNA.394* locus
ST-191	TCAATCTGCTTGTCCCACCC	qPCR *ncRNA.394*$^+$ - R - primer pair 5 *ncRNA.394* locus
ST-263	GTGCTGCCCAAAAGAAGCTC	qPCR *eno101*$^+$ - F - primer pair 6 *ncRNA.394* locus
ST-264	TGGGAACCACCGTTCAAGAC	qPCR *eno101*$^+$ - R - primer pair 6 *ncRNA.394* locus
ST-249	AGCTTTCAAGGTAGCGGGTG	qPCR *cut2*$^+$ - F
ST-250	TTCCTCTGCTCAGCGTAGAC	qPCR *cut2*$^+$ - R
PA-354	CAGTTAGTTTCAGGTTTCCC	qPCR +2.5 kb *ura4*$^+$ - F - primer pair 1 *ura4* locus
PA-355	GCAGAGTAATGGTGATTGG	qPCR +2.5 kb *ura4*$^+$ - R - primer pair 1 *ura4* locus
ST-874	CACACAGTTTCAGAAGAAC	qPCR *tam14*$^+$ - F - primer pair 2 *ura4* locus
ST-875	GTTACGAGGAATCTTGGTAG	qPCR *tam14*$^+$ - R - primer pair 2 *ura4* locus
ST-796	CGCGACTGACAAGTTGCTTT	qPCR *ura4*$^+$ - F - primer pair 3 *ura4* locus
ST-797	AGCTAGAGCTGAGGGGATGA	qPCR *ura4*$^+$ - R - primer pair 3 *ura4* locus
ST-800	TGGTTTAAATCAAATCTTCCATGCG	qPCR 5' of *ura4*$^+$ - F - primer pair 4 *ura4* locus
ST-801	TGAGCAAACTGCTTTTGTGGT	qPCR 5' of *ura4*$^+$ - R - primer pair 4 *ura4* locus
ST-788	GGATGAAGCTGTCTCCCTGG	qPCR *new25*$^+$ - F - primer pair 5 *ura4* locus
ST-789	TATTGCTGCTTCTTCCCTGGC	qPCR *new25*$^+$ - R - primer pair 5 *ura4* locus
ST-876	GGAATCTATGTCGTTGCCG	qPCR *pmp20*$^+$ - F - primer pair 6 *ura4* locus
ST-877	GTAAACTCTCCGTTCCAGTC	qPCR *pmp20*$^+$ - R - primer pair 6 *ura4* locus
Clr4-KO-F	ATTTTTTAAATTCGTTCAGGCA TCATTTGGAGGGTTTGCTAAA AATCATCTCACCAAACAAGAG GTTATTAGTTTTGCGACGGAT CCCCGGGTTAATTAA	KO of *clr4*$^+$ with Bahler construct - F
Clr4-KO-R	AAATGAATGACCTTTTTCAGTT TAACAGTAATGGAGAAAAACA AATTGTAATTATTGGAGTCAAC CAGTAATAAATTAGCGAATTC GAGCTCGTTTAAAC	KO of *clr4*$^+$ with Bahler construct - R
ST-155	ATAGCTTAGGATTCATTATTTTTTAAGA GACAAATTTCTCGTCAATTGAATGAAA CCTTCCGCCTTTATTTTCTTTTTGACG GATCCCCGGGTTAATTAA	KO of *dcr1*$^+$ with Bahler construct - F
ST-156	GACTTGAAATATACAGTATTTCATTTTT TATGACCGCGGCCCTTGTAACTTTTCA AACTTTCAATTTGGGTCTCCAAAGCGA ATTCGAGCTCGTTTAAAC	KO of *dcr1*$^+$ with Bahler construct - R
ST-157	GGTTTGGTATATATAAGCTTCCAACCG CCAAAGCGAATTGTCTTCAGCCAACTC GTCCTTTATGATTCAGAGTGAGTAGGC GGATCCCCGGGTTAATTAA	KO of *ago1*$^+$ with Bahler construct - F

ST-158	TAAGGAAGTAAAAGTTGTGGGCAATC CAGTAGTCAATCGTATATCTATTTCATT ACTTATTGCATGCAATCCATCAAACAG AATTCGAGCTCGTTTAAAC	KO of *ago1*$^{+}$ with Bahler construct - R
ST-3	GTCCAACACCCAGTTGTTAAC TGCTTATAATGACGCGTATGAT TGCGATATTTTAAGACTCTGGC CATCCACCGCTTTATCCGACG GATCCCCGGGTTAATTAA	Inserting natMX6 marker 3' of *ura4*$^{+}$ (*controlΔ*) - F
ST-12	GCAGGTTCTAGTAATGCGCAT TCAATTTGTAGTATTCTTAAATA ATCATTAAACGACAAGGGCCTT CCGTGCTATAGTGTGAATTCGA GCTCGTTTAAAC	Inserting natMX6 marker 3' of *ura4*$^{+}$ (*controlΔ*) - R
ST-866	CtagaGGTCTCgGACTCTCCATTTTCGT TAGAATTAGTTTcGAGACCcttCC	Golden Gate cloning pap1-sgRNA-1-F
ST-867	GGaagGGTCTCgAAACTAATTCTAACG AAAATGGAGAGTCcGAGACCtctaG	Golden Gate cloning pap1-sgRNA-1-R
ST-868	AGCATGGCGCGAACCCGCTGAATCAT TGGACAAAGAATTCTTTAACGACGAGG GTGAAATAGATGATGTTTTTCATAATTA TTTTCATAATTCTAACGTC	Pap1-N424STOP - HR template - F
ST-869	GCTCAGGGAATGATTCGTTGGCATTCT CCAGAAAATCAAGACCATGCAATGAAT TAGTGATCAAGTCTCCATTTTCGTTAG ACGTTAGAATTATGAAAAT	Pap1-N424STOP - HR template - R
ST-284	CAGCTGTGTGTTTGATTGAATCCACAT TCGTCCTCATGTACTCATAGCTAGGTG AAATATATTAGGCTTTCAGTGATTCGC GGATCCCCGGGTTAATTAA	KO of *hba1*$^{+}$ with Bahler construct - F
ST-285	GAATGAATAAGAACCATAGTGAAGAG CTAAAAAAGAATCGAAAAGTACTTACT ATTTTACGAGTGGATCTTCTATCTCGC GAATTCGAGCTCGTTTAAAC	KO of *hba1*$^{+}$ with Bahler construct - R
ST-391	TCTTCTGCCTAACCATACTACTTCTTCT AGCCTTCAGACTTAAAAGCTTCGCCTT TAGAAAACATCTCTATTCCTTCAAACG GATCCCCGGGTTAATTAA	KO of *SPBC17G9.12c*$^{+}$ with Bahler construct - F
ST-392	CAAGAGAGATGGAAAACAGAGGA ATTGTGAACGTTCTCCTTATTCATATTT CCATAAAGCTTCTCCAATGACCTTTAT TGGAATTCGAGCTCGTTTAAAC	KO of *SPBC17G9.12c*$^{+}$ with Bahler construct - F
ST-307	GATAAAATCTTAGAGATTGTTGCTAAA TAAGCAAACAGTGTCTTTGCTGTAACT GGTGAGATATGTTTAAAATTAAATCAC GGATCCCCGGGTTAATTAA	KO of *ncRNA.393*$^{+}$ with Bahler construct - F
ST-308	TGATATAATATATTTTCCTTCTTTACTA TTACATTTCCTATTTTTTCACCATTTAC GATATGTGTAACACTATCTAACCCGAA TTCGAGCTCGTTTAAAC	KO of *ncRNA.393*$^{+}$ with Bahler construct - R
ST-95	TAATGAAAAAGGTTGCTAATTGGTTTG TTATATAAGAGTATGTCGCATTTGTTTA CGATAGGAGAGAGCGATTTTCCACAC GGATCCCCGGGTTAATTAA	KO of *ncRNA.394*$^{+}$ with Bahler construct - F
ST-96	TATTACTATGACTCTGGTTCTAGCTCG ACTCTGACCCTTGCCTGACATACAAAT ACTTTGCTCTTTTCAAAATGTACCGTG AATTCGAGCTCGTTTAAAC	KO of *ncRNA.394*$^{+}$ with Bahler construct - R
ST-305	ATATATAGAGTGGAAGGGCCGTCCGT TAGGACTTGTTTCAGTAAGAATCAATT AGTATTCTACAGTAAACATCGTTAATC CGGATCCCCGGGTTAATTAA	KO of *eno101*$^{+}$ with Bahler construct - F
ST-306	CTACTTCTACTACAACAACAGTTTACTT TAATACTAATAATAAATAAACACGCAA CCTGGCAAATTAATCCAAAACGCAAGA ATTCGAGCTCGTTTAAAC	KO of *eno101*$^{+}$ with Bahler construct - R
ST-756	CtagaGGTCTCgGACTGGTGCTTGACTT CTAATCTTGTTTcGAGACCcttCC	Golden Gate cloning *4xtetO-I*-sgRNA-F
ST-757	GGaagGGTCTCgAAACAAGATTAGAAG TCAAGCACCAGTCcGAGACCtctaG	Golden Gate cloning *4xtetO-I*-sgRNA-R
ST-732	AAACGCTAATCTAGCATGTCATGAAGG	Making *4tetO-I*-HR-template - 1F
ST-733	actagtaggccttgCCGTATTGAAATCAAAAT TATTAATAATGAGTAAGTGAATATATAC CA	Making *4tetO-I*-HR-template - 1R
ST-734	TGATTTCAATACGGcaaggcctactagtgcatg ca	Making *4tetO-I*-HR-template - 2F
ST-735	TCTATAACTTTTACGTTAGctggatttcgttta cctcaccac	Making *4tetO-I*-HR-template - 2R
ST-736	gaggtaaacgaaatccagCTAACGTAAAAGT TATAGACAGTATTATAACAAGTATTATT GTAAAA	Making *4tetO-I*-HR-template - 3F

ST-737	TTTAATTGTATTTTTTTATTCAAAGGTTCTACTTTGTCAATCATTTTCAA	Making *4tetO-I*-HR-template - 3R
ST-752	CtagaGGTCTCgGACTATTTCTTTTGCTTTACGGTCGTTTcGAGACCcttCC	Golden Gate cloning *4xtetO-II*-sgRNA-F (*4xtetO-IIa) (cup1:4xtetO)*
ST-753	GGaagGGTCTCgAAACGACCGTAAAGCAAAAGAAATAGTCcGAGACCctaG	Golden Gate cloning *4xtetO-II*-sgRNA-R (*4xtetO-IIa) (cup1:4xtetO)*
ST-720	TTGAATTAATTCATAGAGTATGATAAAAATTGATAGTAAATTCATTGG	Making *4tetO-II*-HR-template - 1F (*4xtetO-IIa) (cup1:4xtetO)*
ST-721	cactagtaggccttgATGCATGCTAATAAATCATCGTAACTCAAGTAG	Making *4tetO-II*-HR-template – 1R (*4xtetO-IIa) (cup1:4xtetO)*
ST-722	TTTATTAGCATGCATcaaggcctactagtgcatgca	Making *4tetO-II*-HR-template – 2F (*4xtetO-IIa) (cup1:4xtetO)*
ST-723	TTTTTTTTTTCATAAATATTTActggatttcgtttacctcaccacc	Making *4tetO-II*-HR-template – 2R (*4xtetO-IIa) (cup1:4xtetO)*
ST-724	tggtgaggtaaacgaaatccagTAAATATTTATGAAAAAAAAAATAAATGATTCATAACAAGCAGATGAAAA	Making *4tetO-II*-HR-template - 3F (*4xtetO-IIa) (cup1:4xtetO)*
ST-725	TTTGTAATGTATAATCTTCATTTATTTTGAAGAGTCCTAATTCGT	Making *4tetO-II*-HR-template – 3R (*4xtetO-IIa) (cup1:4xtetO)*
ST-750	CtagaGGTCTCgGACTGTGAAATTGCGCGCTTTAGAGTTTcGAGACCcttCC	Golden Gate cloning *4xtetO-IIb*-sgRNA-F
ST-751	GGaagGGTCTCgAAACTCTAAAGCGCGCAATTTCACAGTCcGAGACCctaG	Golden Gate cloning *4xtetO-IIb*-sgRNA-R
ST-714	CATCGAAAAACGAAAGGAGGGCT	Making *4tetO-IIb*-HR-template - 1F
ST-715	actagtaggccttgCACTATCTAACCCAGTTCATCAAGTTGTTCT	Making *4tetO-IIb*-HR-template – 1R
ST-716	GGGTTAGATAGTGcaaggcctactagtgcatgca	Making *4tetO-IIb*-HR-template – 2F
ST-717	TGGAAAAGAAAAAATTACctggatttcgtttactcaccacca	Making *4tetO-IIb*-HR-template – 2R
ST-718	gaggtaaacgaaatccagGTAATTTTTTCTTTTCCAAAACAAATTTTTAAAATGGTTTAAAG	Making *4tetO-IIb*-HR-template - 3F
ST-719	TAAACAAATGCGACATACTCTTATATAACAAACCAATTAGC	Making *4tetO-IIb*-HR-template – 3R
ST-754	CtagaGGTCTCgGACTTATGGACCAACTCGTGACACGTTTcGAGACCcttCC	Golden Gate cloning *4xtetO-IIc*-sgRNA-F
ST-755	GGaagGGTCTCgAAACGTGTCACGAGTTGGTCCATAAGTCcGAGACCctaG	Golden Gate cloning *4xtetO-IIc*-sgRNA-R
ST-726	ACGGTACATTTTGAAAAGAGCAAAGTATTTGT	Making *4tetO-IIc*-HR-template - 1F
ST-727	cactagtaggccttgTTGACTATGGATTTGGTTTGGCTATTGCTATGACTTT	Making *4tetO-IIc*-HR-template – 1R
ST-728	CAAATCCATAGTCAAcaaggcctactagtgcatgc	Making *4tetO-IIc*-HR-template – 2F
ST-729	TGTGCAAGCATCctggatttcgtttacctcaccacca	Making *4tetO-IIc*-HR-template – 2R
ST-730	acgaaatccagGATGCTTGCACATCACTACACT	Making *4tetO-IIc*-HR-template - 3F
ST-731	CGCTCGCTGTATCAGATTCACAG	Making *4tetO-IIc*-HR-template – 3R
ST-760	CtagaGGTCTCgGACTATATTTTAGATAGTTCTGTGGTTTcGAGACCcttCC	Golden Gate cloning *4xtetO-III*-sgRNA-F
ST-761	GGaagGGTCTCgAAACCACAGAACTATCTAAAATATAGTCcGAGACCctaG	Golden Gate cloning *4xtetO-III*-sgRNA-R
ST-744	CGGTAAGAAAACACGACATGTGCAG	Making *4tetO-III*-HR-template – 1F
ST-745	catgcactagtaggccttgTATAATTAAGATGTTTTAGAGACTTATACAATTTTGTCTTTATAAATTCT	Making *4tetO-III*-HR-template – 1R
ST-746	CTAAAACATCTTAATTATAcaaggcctactagtgcatgca	Making *4tetO-III*-HR-template – 2F
ST-747	TTTGCACTTTGTGAATctggatttcgtttacctcaccacca	Making *4tetO-III*-HR-template – 2R
ST-748	gtaaacgaaatccagATTCACAAAGTGCAAACATTATCATGAAAAAGAAC	Making *4tetO-III*-HR-template – 3F
ST-749	TGAAAAAGATAATCAGCCTTATAATCTTTACAAAAGTAAGAAATTCT	Making *4tetO-III*-HR-template – 3R
ST-858	CtagaGGTCTCgGACTGATTTGCCGTTCTACGACGGGTTTcGAGACCcttCC	Golden Gate cloning *4xtetO-IV*-sgRNA-F
ST-859	GGaagGGTCTCgAAACCCGTCGTAGAACGGCAAATCAGTCcGAGACCctaG	Golden Gate cloning *4xtetO-IV*-sgRNA-R
ST-836	CTCAACAAACCACTGGTTACATGGC	Making *4tetO-IV*-HR-template – 1F
ST-837	actagtaggccttgGATACTTCGCAAAATTCTAAGCATGGTGC	Making *4tetO-IV*-HR-template – 1R
ST-838	TTTGCGAAGTATCcaaggcctactagtgcatgca	Making *4tetO-IV*-HR-template – 2F
ST-839	TCGATACCACCTTTTActggatttcgtttacctcaccacc	Making *4tetO-IV*-HR-template – 2R

ST-840	gtaaacgaaatccagTAAAAGGTGGTATCGAGGAATGGCA	Making *4tetO-IV*-HR-template – 3F
ST-841	ATCCAATAGTTAATAAATCGATGCTTAATTTGGTGG	Making *4tetO-IV*-HR-template – 3R
ST-952	CtagaGGTCTCgGACTAGCTTGTGGCTGACCGTTAAGTTTcGAGACCcttCC	Golden Gate cloning clr5-sgRNA-F
ST-953	GGaagGGTCTCgAAACTTAACGGTCAGCCACAAGCTAGTCcGAGACCtctaG	Golden Gate cloning clr5-sgRNA-R
ST-954	CTTATTTGCAGCAGCCTTTCCAAATACCCTCTCAACGTTTCTCTCGACAGCAACAATCTCATCCATTCCCTGCTGCTCAACATGCAGTTAACGGTTAGCC	Making clr5-Q264STOP-HR-template – F
ST-955	CAGATTGGTTTGAAGAAGCAAACATGGTGGAGCCCATTGGGACATTTCTAGATTGGTAGATGAAAGGATACAAAGCTTGTGGCTAACCGTTAACTGCATG	Making clr5-Q264STOP-HR-template – R
ST-956	CtagaGGTCTCgGACTTATTAGCCTTTGAAGGATTTGTTTcGAGACCcttCC	Golden Gate cloning meu27-sgRNA-F
ST-957	GGaagGGTCTCgAAACAAATCCTTCAAAGGCTAATAAGTCcGAGACCtctaG	Golden Gate cloning meu27-sgRNA-R
ST-958	GCCAAAATCAATAGAGAACAATTATACTTTAAAAAAAAAAAAATGAAGAAGGCTTCTTAAGTCAACAGGAAAATAAGTATTCAAATCAAAATCCTTCAAAG	Making meu27-S100Y-HR-template – F
ST-959	GAGGTGCCGCCCAATTGCAGTATACAAGCTATGAATGTTATTGGCTTGCTTACGCCGAGCTTGTCGAAAAGGTTATTAGCCTTTGAAGGATTTTGATTTG	Making meu27-S100Y-HR-template – F
ST-1044	CCTTGGTTTTTATGTATTTACTAGTAAATCTATAATAATCATTAACT	Making cup1-3xDSR construct – 1F
ST-1045	TATATTTGAATAAgagaatggaaggaaggttcgttagcAAAAGGTAGGAGGAAGCAAGAAATGG	Making cup1-3xDSR construct – 1R
ST-1046	gctaacgaaccttccttccattctc	Making cup1-3xDSR construct – 2F
ST-1047	cAAGGGAGccAaGGatAttGgaaagtggatgaacaagatcatttggagc	Making cup1-3xDSR construct – 2R
ST-1048	tcCaaTatCCtTggCTCCCTTgtaacttatgactctcgtttacac	Making cup1-3xDSR construct – 3F
ST-1049	ttaatacggagtttaaagcacacgatttgctacc	Making cup1-3xDSR construct – 3R
ST-1050	caaatcgtgtgctttaaactccgtattaaacccattcttaaactaatcttcatttattttgaagagtcctaattcgtcatcatttttcatctgcttgttat	Making cup1-3xDSR construct – 4F
ST-1051	gttacgatgatttattagcatgcatccggaccgtaaagcaaaagaaattaaatatttatgaaaaaaaaaataaatgattcataacaagcagatgaaaatg	Making cup1-3xDSR construct – 4R
ST-1052	tccggatgcatgctaataaatcatcgtaacGTCATCTTTTGGCATATAGGGTAAAGGGG	Making cup1-3xDSR construct – 5F
ST-1053	AAATTTACTCTAACAGACGATATTGTCTCACTATCC	Making cup1-3xDSR construct – 5R
ST-1054	CtagaGGTCTCgGACTAGGCCTTAATATTAACCCCCGTTTcGAGACCcttCC	Golden Gate cloning LocusPX-sgRNA-F
ST-1055	GGaagGGTCTCgAAACGGGGGTTAATATTAAGGCCTAGTCcGAGACCtctaG	Golden Gate cloning LocusPX-sgRNA-R
ST-1056	CtagaGGTCTCgGACTttCGAACATTTTAGGTAGCCGTTTcGAGACCcttCC	Golden Gate cloning endogenous cup1-sgRNA-F
ST-1057	GGaagGGTCTCgAAACGGCTACCTAAAATGTTCGaaAGTCcGAGACCtctaG	Golden Gate cloning endogenous cup1-sgRNA-R
ST-989	GATGAAAATGATGACGAATTAGGACTCTTCAAAATAAATGAAGATTATACATTACAAACTTTGGTCTGACTTTTTAAAGCACACGATTTGTGAAGTATTT	Making endogenous *cup1Δ*-HR-template – F
ST-990	TGATTTAATTTTAAACATATCTCACCAGTTACAGCAAAGACACTGTTTGCTTATTTAGCAACAATCTCTAAGATTTTATCAAATACTTCACAAATCGTGT	Making endogenous *cup1Δ*-HR-template – R
TagJ-sgRNA-F	CTAGAGGTCTCGGACTGCTCAGGCTAAACGTCGGAAGTTTCGAGACCCTTCC	Golden Gate cloning of cup1-tag sgRNA-F
TagJ-sgRNA-R	GGAAGGGTCTCGAAACTTCCGACGTTTAGCCTGAGCAGTCCGAGACCTCTAG	Golden Gate cloning of cup1-tag sgRNA-R
JTHR-Sito-F	ATGACGAATTAGGACTCTTCAAAATAAATGAAGATTATACATTACAAACTTTGGTCTGACTTTTTAAAGCACACGATTTGCTATTTGTATAGTTCATCCA	Making HR template for C-terminal tagging of cup1 with GFP
JTHR-Sito-R	TTGTATCGTGGGACTCTTTGTCAGACATTCAGCTCAGGCTAAACGTCGGAAAAGTTCTTAAAAAGTCAGTCAAAAAAAGGAGTAAAGGAGAAGAACTTTT	Making HR template for C-terminal tagging of cup1 with GFP
lyrkosgRNA-F	CtagaGGTCTCgGACTCAAATCCTAATCCTCACAAGGTTTcGAGACCcttCC	Golden Gate cloning of cup1-LYR sgRNA-F

lyrkosgRNA-R	GGaagGGTCTCgAAACCTTGTGAGGATTAGGATTTGAGTCcGAGACCctaG	Golden Gate cloning of cup1-LYR sgRNA-R
HR-L73F	ACTCGAAGATTCTGGGATCCAATGGCATCCCAAATCGGAATCTCACATTTTCAAGCTTACGCCCGAAAAGCTCGCAAGTCAAATCCTAATCCTCACAAGCGAC	Making cup1-L73G-HR-template – F
HR-L73R	AGCTTGATGGTCGCCATCATTGGCGCGCTCAATACGACATGCAAAAGTTTTTAGGAGATTGCGAAACCGTTTTATGCGTCGCTTGTGAGGATTAGGATTT	Making cup1-L73G-HR-template – R
HR-F99F	CAATGGCATCCCAAATCCTAATCTCACATTTTCAAGCTTACGCCCGAAAAGCTCGCAAGTCAAATCCTAATCCTCACAAGCGACGCATAAAACGGGGTCG	Making cup1-F99G-HR-template – F
HR-F99R	TCGTAAAGTCTGCCATATAGCTTGATGGTCGCCATCATTGGCGCGCTCAATACGACATGCAAAAGTTTTTAGGAGATTGCGACCCCGTTTTATGCGTCGC	Making cup1-F99G-HR-template – R
WC258-sg-393-F	CtagaGGTCTCgGACTcaaatgctgtagtgatgcagGTTTcGAGACCcttCC	Golden Gate cloning of cup1/ncRNA393 region sgRNA-F
WC259-sg-393-R	GGaagGGTCTCgAAACctgcatcactacagcatttgAGTCcGAGACCctaG	Golden Gate cloning of cup1/ncRNA393 region sgRNA-R
WC279-cup1DP-uraTT-F	GATCATTTGGAGCTTGGAATGGTCTCCTTTTGGTAACTGTAGAAATAAATCTCATGAGTAAGGAATTTTGTATGAATGAAGCTTGTGATATTGACGAAAC	To amplify 144-bp ura4 transcriptional terminator to replace 697 bp of cup1 upstream/promoter region (to make cup1-TT)- F
WC280-cup1DP-uraTT-R	ATTACCGTCTAAAGCGCGCAATTTCACAGATGCCGCAAATTTGACATCTGGGTCTTTCAAGTCTTGTTAGAACATTGAATAACTATGTACAAAGCCAATG	To amplify 144-bp ura4 transcriptional terminator to replace 697 bp of cup1 upstream/promoter region (to make cup1-TT) - R
WC267-arg11-Ctag-F	TAAAGGTGCTGCTACTCAAGCTCTCCAGAATCTCAATCTGTCGTGTGGTTACGATGAATATGCCGGTATCCATTTGGATcggatccccgggttaattaa	C-terminal tagging of *arg11*$^{+}$ with mCherry using Bahler construct - F
WC268-arg11-Ctag-R	AATATTTGTAACAAAAAAATATCCAAATGGTACACAGAAAGAATAAAAATAACAAAAGAATGGGCTACAAAAAATATAAgaattcgagctcgtttaaac	C-terminal tagging of *arg11*$^{+}$ with mCherry using Bahler construct - R
WC301-UR2-C1-F	GGGAACCACATACAATGAATG	C1 primer upstream of 5S rRNA.26 – F ChrIII control PCR and putative circle junction in UR-2
WC305-UR2-C2-F	TAGTCAGTATATACTGAGCGG	C2 primer upstream of 5S rRNA.26 – F ChrIII control PCR and putative circle junction in UR-2
WC306-UR2-B1-R	TCGCTGCTTATTGACTTTGAG	B1 primer downstream of 5S rRNA.24 – R ChrIII control PCR and putative circle junction in UR-2
WC308-UR2-B2-R	AACTGCTCTACTACTATAACG	B2 primer downstream of 5S rRNA.24 – R ChrIII control PCR and putative circle junction in UR-2
WC310-CHR3-2-D1-R	ATCATCTCGATAAGTGCTTTC	D1 primer downstream of 5S rRNA.26 – R ChrIII control PCR
WC311-CHR3-2-A-F	TCCGACTATTTGCATAAGACC	A primer upstream of 5S rRNA.24 – F ChrIII control PCR
WC312-CHR3-2-D2-R	AGAACTTTGTTGTAGCCTGAG	D2 primer downstream of 5S rRNA.26 – R ChrIII control PCR
WC321-UR4-UR17-G1-F	TTCTCCTTTGAACCCAGAAGG	G1 primer upstream of LTR27 – F ChrIII control PCR and putative circle junction in UR-4
WC325-UR4-UR17-G2-F	AATTCCATCCAAATTCTCTGG	G2 primer upstream of LTR27 – F ChrIII control PCR and putative circle junction in UR-4
WC326-UR4-F1-R	TATCACAACAGTTCTGCAACG	F1 primer downstream of LTR3 – R ChrIII control PCR and putative circle junction in UR-4

WC328-UR4-F2-R	TGGAAGCTTTGATAGAAAGGG	F2 primer downstream of LTR3 – R ChrIII control PCR and putative circle junction in UR-4
WC329-CHR3-4-E-F	ACGAATACGGTGTTGTATGAC	E primer upstream of LTR3 – F ChrIII control PCR
WC330-CHR3-4-17-H-R	CGCATCGTTAATGAGTTCATC	H primer downstream of LTR27 – R ChrIII control PCR
ST-9	CCATAGAATCTCCTTAGTTTGCATCGC AATTTTATAGTTACCTTTTTGCTAGTAA GCAATTAATTTTTGGGACTTTTAAGCG GATCCCCGGGTTAATTAA	KO of *epe1*$^{+}$ with Bahler construct - F
ST-10	TGTGAACTACTCAAGAATCATAAGCAC GTGGGGATAAATATTCAATGGTAGCC GAAGGAAATAAAAAGTGCCGAGGTAC TGAATTCGAGCTCGTTTAAAC	KO of *epe1*$^{+}$ with Bahler construct - R
ST-1064	AAAATAACATTTATGATTTTGAAGATCA CTCTCCTGTTAGGGAAAAATGGGGGC ACAGGCTTCGGTCCAGAGGTGCTAGT CGGATCCCCGGGTTAATTAA	C-terminal tagging of *epe1*$^{+}$ with GFP using Bahler construct - F
ST-1065	CTTAATTATTTGATGAAACCTTCATGAT ATACTCATAAAATGTGAACTACTCAAG AATCATAAGCACGTGGGGATAAATAGA ATTCGAGCTCGTTTAAAC	C-terminal tagging of *epe1*$^{+}$ with GFP using Bahler construct - R
ST-1058	CtagaGGTCTCgGACTGGACTTTTAAGA TGGATTCCGTTTcGAGACCcttCC	Golden Gate cloning epe1-sgRNA-F
ST-1059	GGaagGGTCTCgAAACGGAATCCATCT TAAAAGTCCAGTCcGAGACCtctaG	Golden Gate cloning epe1-sgRNA-R
ST-1062	GTGAACTACTCAAGAATCATAAGCACG TGGGGATAAATATTCAATGGTAGCCGA AGGAAATAAAAAGTGCCGAGGTACTT CTTAAAAGTCCCAAAAATTA	Making *epe1Δ*-HR-template – F
ST-1063	CCATAGAATCTCCTTAGTTTGCATCGC AATTTTATAGTTACCTTTTTGCTAGTAA GCAATTAATTTTTGGGACTTTTAAGAA GTACCTCGGCACTTTTTA	Making *epe1Δ*-HR-template – R
ST-1060	TTTATAGTTACCTTTTTGCTAGTAAGCA ATTAATTTTTGGGACTTTTAAGATGGA CTACAAAGACCATGACGGTGATTATAA AGATCATGACATCGACTA	Making 3xFLAG-Epe1-HR-template – F
ST-1061	GAATATCAATGTCTTGATTTATAATGTC ATCGTATTCAAGCCAGGAATCGCTGC CTCCTCCCTTGTCATCGTCATCCTTGT AGTCGATGTCATGATCTTT	Making 3xFLAG-Epe1-HR-template – R
ST-36	CAGGAGTGTGTACAGGAGGT	qPCR *vps32*$^{+}$ - F
ST-37	AGATGAATTGGCCAACGAGTT	qPCR *vps32*$^{+}$ - R
ST-44	CTCGCCTGAAACTTGCTACA	qPCR *cgs1*$^{+}$ - F
ST-45	GCACGAGGTTGATTACGCAT	qPCR *cgs1*$^{+}$ - R
ST-48	GTCACGGGCGATTTTAGGAC	qPCR *ppr4*$^{+}$ - F
ST-49	TCCCTTGTCCGGCAGAATAA	qPCR *ppr4*$^{+}$ - R
ST-1012	TCTGCGTGACACTTGTTCGT	qPCR *grt1*$^{+}$ - F
ST-1013	TAGAGACTCCAGCGCATCCT	qPCR *grt1*$^{+}$ - R
ST-1010	GTCAGGTGCTCCTTGCAGAT	qPCR *eno102*$^{+}$ - F
ST-1011	GCGTTCCTGCATAGATTGCG	qPCR *eno102*$^{+}$ - R
ST-1006	ATTGGATAGGCGTCACCGTC	qPCR *aes1*$^{+}$ - F
ST-1007	AGCCGGATCCTCATTGACAT	qPCR *aes1*$^{+}$ - R
ST-1018	GATTGGGCCGAGTTGAAGGA	qPCR *cdc22*$^{+}$ - F
ST-1019	AAGCAGTAGGCATTGGTGCT	qPCR *cdc22*$^{+}$ - R
ST-1028	AAGCAGTAGGCATTGGTGCT	qPCR *fip1*$^{+}$ - F
ST-1029	CCCTTTTTCACCGTTCTGCG	qPCR *fip1*$^{+}$ - R
ST-1024	GCACCGGAGATGATACCCAG	qPCR *fio1*$^{+}$ - F
ST-1025	GCACCATTTCCGATCGTTGG	qPCR *fio1*$^{+}$ - R
ST-1022	TCACACATCGTGGCTATCCG	qPCR *cyp8*$^{+}$ - F
ST-1023	TCGTTCACGAGATCCCTCCA	qPCR *cyp8*$^{+}$ - R
ST-1040	CCTGCTGCCGAATTTCAACG	qPCR *pcn1*$^{+}$ - F
ST-1041	TGCAGCTAAAACGAACACCC	qPCR *pcn1*$^{+}$ - R
ST-1032	GTCTCCGGGTGCTACAGTTC	qPCR *mbx2*$^{+}$ - F
ST-1033	GTGCGTTTGCCTACGATGAC	qPCR *mbx2*$^{+}$ - R
ST-1038	CTCGTGTTCCTGAGACCACC	qPCR *nce103*$^{+}$ - F
ST-1039	AACGAGGAACGACATTGGCA	qPCR *nce103*$^{+}$ - R
ST-277	CATTTTGCGGGACAATGGGT	qPCR *cds1*$^{+}$ - F
ST-278	CCTCCGTCCAAGTTGACGTT	qPCR *cds1*$^{+}$ - R
ST-1068	tgctgaatgtaaccaacatca	qPCR *cen-IRC-L1*
ST-1069	gcctcaattgcctattagtgct	qPCR *cen-IRC-R1*
ST-1066	GGATAAGCCAATCATCGTTGAG	qPCR *tlh2* - F

ST-1067	GTAGTTGACGCTCCTTGGAAG	qPCR *tlh2* - R
ST-1070	CCGAGGCTTTCATAGCTTA	qPCR *S. cerevisiae CEN4* – F (for GFP spike-in qChIP)
ST-1071	ACCGGAAGGAAGAATAAGAA	qPCR *S. cerevisiae CEN4* – R (for GFP spike-in qChIP)
ST-161	CCCAATTGTTGTGATTGCTG	qPCR *S. octosporus* CEN3 heterochromatin – F (for H3K9me2 spike-in qChIP)
ST-162	GCGGATGCAGTATTTCGTTT	qPCR *S. octosporus* CEN3 heterochromatin – R (for H3K9me2 spike-in qChIP)
Mst2-C-Tag-F	ACCTTTTACTTAAAGAAAATATACTTAT TCCTCTACCTCAAAAGCGTCTATTAGA TAACTCTCATCATCTGGATTCCGTTCG GATCCCCGGGTTAATTAA	C-terminal tagging of *mst2*$^{+}$ with 13xMyc using Bahler construct - F
Mst2-C-Tag-R	TATAGAGCAACAACCAAGCCGTAGAT GATACAAATGCTTCACGACAAATATCG AAAGATTAAAATACTTATTTATTTGAAG AATTCGAGCTCGTTTAAAC	C-terminal tagging of *mst2*$^{+}$ with 13xMyc using Bahler construct - R
ST-493	CtagaGGTCTCgGACTTTGATAGCAACA GTGGCGACGTTTcGAGACCcttCC	Making *ade6* – sgRNA - F
ST-494	GGaagGGTCTCgAAACGTCGCCACTGT TGCTATCAAAGTCcGAGACCctaG	Making *ade6* – sgRNA - R
ST-495	CtagaGGTCTCgGACTCCTTGTATAATA CCCTCGCCGTTTcGAGACCcttCC	Making *ura4* – sgRNA - F
ST-496	GGaagGGTCTCgAAACGGCGAGGGTAT TATACAAGGAGTCcGAGACCctaG	Making *ura4* – sgRNA - R
ST-770	GCAATGACACCTCTTCCAGTAATCGG CGTTCCTGTAAAAGGAAGCACTCTTGA CGGAGTTGACTCTCTTTAGTCTATTGT TCAGATGCCTCGAGGTGTCT	Making *ade6* - HR template - F
ST-771	GGAGGGTTGAAATGTAGCAAGTATAC GACAGGCTAAAATACCGGCATTTTGG CTATTTATTGATAGCAACAGTGGCGAC CTAGACACCTCGAGGCATCTGA	Making *ade6* - HR template - R
ST-772	TTGGAAGACATTTCAGCCAAAAGCAAG AGACCACGTCCCAAAGGTAAACCAAC TTCTTTGAGGCCTTGTATAATACCCTC GCCCTACACTGTATGGCAAT	Making *ura4* - HR template - F
ST-773	ATTCGCAGACATTGGAAATACCGTCAA GCTACAATATGCATCTGGTGTGTACAA AATTTAGTCTTGGGCTCATATCACAAA TTGCCATACAGTGTAGGGC	Making *ura4* - HR template - R
ST-233	TTGTTTCAGCTCACCGCACA	Checking mutations *ade6* - F
ST-236	AAAGCAAGCAAAATCATTTAACAGT	Checking mutations *ade6* - R
ST-241	GCTCCATAGACTCCACGACC	Checking mutations *ura4* - F
ST-243	TTGTCAGTCGCGGTCGATTT	Checking mutations *ura4* - R
ST-34	AAATTTGCGCTCCTCTCTGC	Checking mutations *meu27* - F
ST-35	GTTTGGTATTTACGAGCTGCCA	Checking mutations *meu27* - R
ST-32	CACACAATGCGCACTCTTCT	Checking mutations *clr5* - F
ST-33	ACAGCAGTTGGTCCGTTAGA	Checking mutations *clr5* - R
ST-411	GGTTAGGCAGAAGACTTGAGCA	Checking *cup1:4xtetO* – F (A1)
ST-406	ATCATCACTTGCATTCACTTCTCT	Checking *cup1:4xtetO* – R (A2)
ST-409	GGCGAAGCTTTTAAGTCTGAAGG	Checking cup1-GFP - F
ST-408	GCTGTCCCACTCTTACCACA	Checking cup1-GFP - R
ST-1078	CAAATCTAACGAGTTTGCCTGC	Checking *epe1Δ* – F (C1)
ST-1079	GCAAACAACGAGTCAAAGTGGA	Checking *epe1Δ* – R (C3)
ST-1077	GGGCGAGCGGACAATCATAA	Checking *epe1 cds* – F (C2)
ST-1076	AGTGAGGCTGTGCAAAGGAA	Checking *3xFLAG-epe1* - F
ST-1073	TCTAACGAGTTTGCCTGCTT	Checking *3xFLAG-epe1* - R
M13F	GTAAAACGACGGCCAGT	Checking successful cloning of sgRNAs into pLSB

Appendix IV

sgRNA and HR template sequences used in this thesis. All sgRNA sequences were obtained using CRISPR4P (Rodríguez-López et al. 2016)

Name	Sequence
pap1 - sgRNA	CTCCATTTTCGTTAGAATTA
pap1-N424STOP - HR template	AGCATGGCGCGAACCCGCTGAATCATTGGACAAAGAATTCTTTAAC GACGAGGGTGAAATAGATGATGTTTTTCATAATTATTTTCATAATTCT AACGTCTAACGAAAATGGAGACTTGATCACTAATTCATTGCATGGTC TTGATTTTCTGGAGAATGCCAACGAATCATTCCCTGAGC
4xtetO-I - sgRNA	GGTGCTTGACTTCTAATCTT
4xtetO-I - HR template	AAACGCTAATCTAGCATGTCATGAAGTGCAAATCTCATAACTGTCTA TTTAAAAAGTTAAAAAACATTCAACCTTGGTATATATTCACTTACTCA TTATTAATAATTTTGATTTCAATACGGcaaggcctactagtgcatgcatcgatagat cctctatcactgatagggagatctccctatcagtgatagagaggatctccctatcagtgatagagagg atctccctatcagtgatagagaggatctccctatcagtgatagagaggatcctctctatcactgatagg gagatcttcaacttggtggtgaggtaaacgaaatccagCTAACGTAAAAGTTATAGAC AGTATTATAACAAGTATTATTGTAAAATCTAAGCTATATCGAAATAGG AATTGAAAATGATTGACAAAGTAGAACCTTTGAATAAAAAAATACAAT TAAA
4xtetO-II - sgRNA *(4xtetO-IIa) (cup1:4xtetO)*	ATTTCTTTTGCTTTACGGTC
4xtetO-II - HR template *(4xtetO-IIa) (cup1:4xtetO)*	TTGAATTAATTCATAGAGTATGATAAAAATTGATAGTAAATTCATTGG TATACTAAAGTGATGTAGAAAATTAAGAAATCACATAGACTACTTGA GTTACGATGATTTATTAGCATGCATcaaggcctactagtgcatgcatcgatagatcc tctatcactgatagggagatctccctatcagtgatagagaggatctccctatcagtgatagagaggat ctccctatcagtgatagagaggatctccctatcagtgatagagaggatcctctctatcactgataggg agatcttcaacttggtggtgaggtaaacgaaatccagTAAATATTTATGAAAAAAAAAA TAAATGATTCATAACAAGCAGATGAAAATGATGACGAATTAGGACTC TTCAAAATAAATGAAGATTATACATTACAAA
4xtetO-IIb - sgRNA	GTGAAATTGCGCGCTTTAGA
4xtetO-IIb - HR template	CATCGAAAAACGAAAGGAGGGCTTTTTTCTGGGGGAAGAGGGTGAT TATGGGAATCACTGTGAAATGGAAATTCTTCGGTTGGGCGAAGAGA ACAACTTGATGAACTGGGTTAGATAGTGcaaggcctactagtgcatgcatcgata gatcctctatcactgatagggagatctccctatcagtgatagagaggatctccctatcagtgatagag aggatctccctatcagtgatagagaggatctccctatcagtgatagagaggatcctctctatcactgat agggagatcttcaacttggtggtgaggtaaacgaaatccagGTAATTTTTTCTTTTCCAA AACAAATTTTTAAAATGGTTTAAAGTATTATAAAAGCATTTTTAAGGT AATGAAAAAGGTTGCTAATTGGTTTGTTATATAAGAGTATGTCGCAT TTGTTTA
4xtetO-IIc - sgRNA	TATGGACCAACTCGTGACAC
4xtetO-IIc - HR template	ACGGTACATTTTGAAAAGAGCAAAGTATTTGTATGTCAGGCAAGGG TCAGAGTCGAGCTAGAACCAGAGTCATAGTAATAACGAAAGTCATA GCAATAGCCAAACCAAATCCATAGTCAAcaaggcctactagtgcatgcatcgata gatcctctatcactgatagggagatctccctatcagtgatagagaggatctccctatcagtgatagag aggatctccctatcagtgatagagaggatctccctatcagtgatagagaggatcctctctatcactgat agggagatcttcaacttggtggtgaggtaaacgaaatccagGATGCTTGCACATCACTA CACTTGTGTTTGCTGGTCCGCGTTAACCTTGTAGTGAATAGCATGCT GAGTTTCGCTAACGCGCTGCTCCGTGTCGCTGCTGTGAATCTGATA CAGCGAGCG
4xtetO-III - sgRNA	ATATTTTAGATAGTTCTGTG
4xtetO-III - HR template	CGGTAAGAAAACACGACATGTGCAGAGATGCCGACGAAGCATAGTT AAACTGGGATGGTAAAATCAATTAAGAATTTATAAAGACAAAATTGT ATAAGTCTCTAAAACATCTTAATTATAcaaggcctactagtgcatgcatcgatagat cctctatcactgatagggagatctccctatcagtgatagagaggatctccctatcagtgatagagagg atctccctatcagtgatagagaggatctccctatcagtgatagagaggatcctctctatcactgatagg gagatcttcaacttggtggtgaggtaaacgaaatccagATTCACAAAGTGCAAACATT ATCATGAAAAAGAACCATTTTAATTTAAAGCAAGGGCATTAAGGCTT ATTTACAGAATTTCTTACTTTTGTAAAGATTATAAGGCTGATTATCTT TTTCA
4xtetO-IV - sgRNA	GATTTGCCGTTCTACGACGG
4xtetO-IV - HR template	CTCAACAAACCACTGGTTACATGGCTAATATTTAGTAAAAAAAAATA ACATTTAATGAAGATCCCTTATAAAGAGCCTAAGTTATTTCGTAATG GAGATGGAAATTCATTTGCACCATGCTTAGAATTTTGCGAAGTATCc aaggcctactagtgcatgcatcgatagatcctctatcactgatagggagatctccctatcagtgatag agaggatctccctatcagtgatagagaggatctccctatcagtgatagagaggatctccctatcagtg

	atagagaggatcctctctatcactgatagggagatcttcaacttggtggtgaggtaaacgaaatcca gTAAAAGGTGGTATCGAGGAATGGCATATTTAGTTTAAAAGTAATTA CGATTCCGTTTAATGTCTCTTACAGTAATTTCATACAATTGTGTTAAA CCATTCTTCTCCACCAAATTAAGCATCGATTTATTAACTATTGGAT
clr5 - sgRNA	AGCTTGTGGCTGACCGTTAA
clr5-Q264STOP - HR template	CTTATTTGCAGCAGCCTTTCCAAATACCCTCTCAACGTTTCTCTCGA CAGCAACAATCTCATCCATTCCCTGCTGCTCAACATGCAGTTAACG GTTAGCCACAAGCTTTGTATCCTTTCATCTACCAATCTAGAAATGTC CCAATGGGCTCCACCATGTTTGCTTCTTCAAACCAATCTG
meu27 - sgRNA	TATTAGCCTTTGAAGGATTT
meu27-S100Y - HR template	GCCAAAATCAATAGAGAACAATTATACTTTAAAAAAAAAAAATGAAG AAGGCTTCTTAAGTCAACAGGAAAATAAGTATTCAAATCAAAATCCT TCAAAGGCTAATAACCTTTTCGACAAGCTCGGCGTAAGCAAGCCAA TAACATTCATAGCTTGTATACTGCAATTGGGCGGCACCTC
Locus *PX* - sgRNA	AGGCCTTAATATTAACCCCC
cup1-3xDSR - HR template	CCTTGGTTTTTATGTATTTACTAGTAAATCTATAATAATCATTAACTTT AATAACTTTCTTCAACTGATCAATTTCCCAACCAAAATGCTTTGTTAT TTGTTCTTTAAGCTTGCTATGTTCTTTAGCTGCGTGTCTATCATCTCT TCTTGTTTGGCTTGGCACGTGCCATTTTACCATTTCTTGCTTCCTCC TACCTTTTgctaacgaaccttccttccattctcTTATTCAAATATACTCCTCTGCAT CACTACAGCATTTGCTTGAATTTTCGCAAGTCTAAAAAAAAAAAACT AGTACAAAAACTCATTCTTTTACAAATGAAATTATCTTTTTGAAAAAA ATAACTATTCGAAAACTCATGTACAAAACTTCACTTTTGATATTGCTT TTTATTGTGCGTCGTGAACTGCCTTTCTGCGTAATAACGTTACACTG ATTTAATTTTAAACATATCTCACCAGTTACAGCAAAGACACTGTTTGC TTATTTAGCAACAATCTCTAAGATTTTATCAAATACTTCATTTCTTTGT CCCTTCATCTTGGCCCTTGGTTTTAATTTTTATATTTGGTTTTTCTTTT TTTTTTTTTTTTTTTTTTGCATTGTTTCACTTAACTTTCATGTTTCATTC ATACAAAATTCCTTACTCATGAGATTTATTTCTACAGTTACCAAAAGG AGACCATTCCAAgctccaaatgatcttgttcatccactttcCaaTatCCtTggCTCCCTT gtaacttatgactctcgtttacacTTACCTCAACCAAAGGACAGGCAGTGCTCGA CTCTAGTCCCTCTTTATCGAAGACTATTAAAGGCAACTCGAAGATTC TGGGATCCAATGGCATCCCAAATCCTAATCTCACATTTTCAAGCTTA CGCCCGAAAAGCTCGCAAGTCAAATCCTAATCCTCACAAGCGGCGC ATAAAACGGTTTCGCAATCTCCTAAAAACTTTTGCATGTCGTATTGA GCGCGCCAATGATGGCGACCATCAAGCTATATGGCAGACTTTACGA TACGCTTATTCACAAACAGGTCCTCTTCGTCATAGGCGTCTTCATTA TTTACAAGATAATAAAATTCGACCTTCAAAGATACCCAAAAGTTTACC ATCTAATTCACCAGTTCGTCTTCCTTACATTTCATCCCTATTATCGGC CGTTTTTGAGATAAATATGGAAAATGCAAAAATCCGCCATTTGCCCA GCGTCATATTTGACGGTTTAATAGAGAAAAACAAAGATCGCCCTTAC CATATTAACCTTAGTTGCAAGAGGGCATACGACGAACTTTTGCCTC GTATTGCTGTCCCACTCTTACCACATGAATATCATCACTTGCATTCA CTTCTCTTAGATGTCACACTTCGAAATCCACAAATTTCGCGACCACC GTTTGCACCACTGAACCCCAGAAAGGGGTTCTGTCGTATCTTACAG AGATCGCTCATAACCTTTTTGAGTGCCGTTTGCTATTTGCCTTATAA TCCTCACCCTACCTCCAAACCTGTTGTATCGTGGGACTCTTTGTCAG ACATTCAGCTCAGGCTAAACGTCGGAAAGGTTCTTAAAAAGTCAGT CAAAAAAAggtagcaaatcgtgtgctttaaactccgtattaaacccattcttaaactaatcttcattt attttgaagagtcctaattcgtcatcattttcatctgcttgttatgaatcatttatttttttttcataaatatttaatt tcttttgctttacggtccggatgcatgctaataaatcatcgtaacGTCATCTTTTGGCATATA GGGTAAAGGGGCCAAACTCACTATCCAAGATAAGTCTAAGTATGCA ACTGTTAACATTTCAGTTAAGCACGTTGTCTCCTATAAGCAAGTATA ACGTAGTTTAAAAAGAACGTTAAGTTAATTAGTCTGCACATAATACA AACATGGGATAGTGAGACAATATCGTCTGTTAGAGTAAATTT
cup1 - sgRNA	ttCGAACATTTTAGGTAGCC
cup1Δ - HR template	GATGAAAATGATGACGAATTAGGACTCTTCAAAATAAATGAAGATTA TACATTACAAACTTTGGTCTGACTTTTTAAAGCACACGATTTGTGAA GTATTTGATAAAATCTTAGAGATTGTTGCTAAATAAGCAAACAGTGT CTTTGCTGTAACTGGTGAGATATGTTTAAAATTAAATCA
cup1 tagging - sgRNA	GCTCAGGCTAAACGTCGGAA
cup1-GFP - HR template	ATGACGAATTAGGACTCTTCAAAATAAATGAAGATTATACATTACAAA CTTTGGTCTGACTTTTTAAAGCACACGATTTGctatttgtatagttcatccatgcc atgtgtaatcccagcagctgttacaaactcaagaaggaccatgtggtctctcttttcgttgggatctttcg aaagggcagattgtgtggacaggtaatggttgtctggtaaaaggacagggccatcgccaattggag tattttgttgataatggtctgctagttgaacgcttccatcttcaatgttgtgtctaattttgaagttaactttgatt ccattcttttgtttgtctgccatgatgtatacattgtgtgagttatagttgtattccaatttgtgtccaagaatgt ttccatcttctttaaaatcaatacctttttaactcgattctattaacaagggtatcaccttcaaacttgacttc agcacgtgtcttgtagttcccgtcatctttgaaaaatatagttctttcctgtacataaccttcgggcatggc actcttgaaaaagtcatgccgtttcatatgatctgggtatcttgaaaagcattgaacaccataagtgaa agtagtgacaagtgttggccatggaacaggtagttttccagtagtgcaaataaatttaagggtaagttt tccgtatgttgcatcaccttcaccctctccactgacagaaaatttgtgcccattaacatcaccatctaatt

	caacaagaattgggacaactccagtgaaaagttcttctcctttactCCTTTTTTTGACTGAC TTTTTAAGAACCTTTCCGACGTTTAGCCTGAGCTGAATGTCTGACAA AGAGTCCCACGATACAA
cup1-LYR - sgRNA	CAAATCCTAATCCTCACAAG
cup1-L73G - HR template	ACTCGAAGATTCTGGGATCCAATGGCATCCCAAATCGGAATCTCAC ATTTTCAAGCTTACGCCCGAAAAGCTCGCAAGTCAAATCCTAATCCT CACAAGCGACGCATAAAACGGTTTCGCAATCTCCTAAAAACTTTTGC ATGTCGTATTGAGCGCGCCAATGATGGCGACCATCAAGCT
cup1-F99G - HR template	CAATGGCATCCCAAATCCTAATCTCACATTTTCAAGCTTACGCCCGA AAAGCTCGCAAGTCAAATCCTAATCCTCACAAGCGACGCATAAAAC GGGGTCGCAATCTCCTAAAAACTTTTGCATGTCGTATTGAGCGCGC CAATGATGGCGACCATCAAGCTATATGGCAGACTTTACGA
cup1 promoter - sgRNA	caaatgctgtagtgatgcag
cup1-TT - HR template	GATCATTTGGAGCTTGGAATGGTCTCCTTTTGGTAACTGTAGAAATA AATCTCATGAGTAAGGAATTTTGTATGAATGAAGCTTGTGATATTGA CGAAACTTTTTGACATCTAATTTATTCTGTTCCAACACCAATGTTTAT AACCAAGTTTTATCTTGTTTGTCTACATGGTATTTTACATTCATCTAC ATACATCTTTCATTGGCTTTGTACATAGTTATTCAATGTTCTAACAAG ACTTGAAAGACCCAGATGTCAAATTTGCGGCATCTGTGAAATTGCG CGCTTTAGACGGTAAT
epe1 - sgRNA	GGACTTTTAAGATGGATTCC
epe1Δ - HR template	GTGAACTACTCAAGAATCATAAGCACGTGGGGATAAATATTCAATG GTAGCCGAAGGAAATAAAAAGTGCCGAGGTACTTCTTAAAAGTCCC AAAAATTA
3xFLAG-epe1 - HR template	GAATATCAATGTCTTGATTTATAATGTCATCGTATTCAAGCCAGGAA TCGCTGCCTCCTCCCTTGTCATCGTCATCCTTGTAGTCGATGTCATG ATCTTTATAATCACCGTCATGGTCTTTGTAGTCCATCTTAAAAGTCC CAAAAATTAATTGCTTACTAGCAAAAAGGTAACTATAAA
ade6 - sgRNA	TTGATAGCAACAGTGGCGAC
ade6 - HR template	GCAATGACACCTCTTCCAGTAATCGGCGTTCCTGTAAAAGGAAGCA CTCTTGACGGAGTTGACTCTCTTTAGTCTATTGTTCAGATGCCTCGA GGTGTCTAGGTCGCCACTGTTGCTATCAATAATAGCCAAAATGCCG GTATTTTAGCCTGTCGTATACTTGCTACATTTCAACCCTCC
ura4 - sgRNA	CCTTGTATAATACCCTCGCC
ura4 - HR template	TTGGAAGACATTTCAGCCAAAAGCAAGAGACCACGTCCCAAAGGTA AACCAACTTCTTTGAGGCCTTGTATAATACCCTCGCCCTACACTGTA TGGCAATTTGTGATATGAGCCCAAGACTAAATTTTGTACACACCAGA TGCATATTGTAGCTTGACGGTATTTCCAATGTCTGCGAAT

Appendix V

Genomic coordinates used to generate heatmaps for heterochromatin islands. Loci that accumulate H3K9me upon caffeine treatment are indicated (low or medium concentration, experiments described in Chapter 6)

					Increased H3K9me levels upon caffeine treatment? (performed here, compared to untreated)	
Chromosome	**Start**	**End**	**Name**	**First described in**	Low caffeine	Medium caffeine
I	578000	582000	*Island 1 - mcp7*	Zofall et al. 2012	✓	-
I	2447000	2449000	*Island 2 - mug8*	Zofall et al. 2012	-	-
I	2521000	2525000	*Island 3 - avl9*	Zofall et al. 2012	✓	✓
I	3647000	3651000	*Island 4 - dtd1*	Zofall et al. 2012	-	-
I	3727000	3730000	*Island 5 - vps29*	Zofall et al. 2012	✓	-
I	4534000	4540000	*Island 6 - ssm4*	Zofall et al. 2012	✓	-
I	4653000	4656000	*Island 7 - iec1*	Zofall et al. 2012	-	-
II	898000	903000	*Island 8 - mcp5*	Zofall et al. 2012	✓	-
II	1472000	1479000	*Island 9 - mei4*	Zofall et al. 2012	✓	-
II	1551000	1554000	*Island 10 - isp4*	Zofall et al. 2012	-	-
II	1670000	1680000	*Island 11 - cdc28*	Zofall et al. 2012	-	-
II	1692000	1698000	*Island 12 - sre1*	Zofall et al. 2012	-	-
II	1869000	1873000	*Island 13 - mug142*	Zofall et al. 2012	-	-
II	2199000	2202000	*Island 14 - ncRNA.394*	Zofall et al. 2012	✓✓	✓✓✓
II	2338000	2342000	*Island 15 - SPBC24C6.09c*	Zofall et al. 2012	-	-
II	3628000	3631000	*Island 16 - pvg4*	Zofall et al. 2012	-	-
II	3640000	3642000	*Island 17 - mug45*	Zofall et al. 2012	-	-
III	958000	968000	*Island 18 - gsf2*	Zofall et al. 2012	-	-
III	1036000	1040000	*Island 19 - rpa12*	Zofall et al. 2012	✓	✓
III	2369000	2371000	*Island 20 - mug9*	Zofall et al. 2012	-	-
III	2422000	2424000	*Island 21 - SPCC569.06*	Zofall et al. 2012	-	-
I	1465847	1469848	*HOOD 1 - tf2-1*	Yamanaka et al. 2013	-	-
I	1564163	1568414	*HOOD 2 - tf2-2*	Yamanaka et al. 2013	-	-
I	2544835	2561773	*HOOD 3 - myp2*	Yamanaka et al. 2013	-	-
I	2927156	2941954	*HOOD 4 - tf2-3*	Yamanaka et al. 2013	-	-
I	2977013	2988899	*HOOD 5 - mfc1*	Yamanaka et al. 2013	-	-
I	2994807	3009469	*HOOD 6 - dni1*	Yamanaka et al. 2013	-	-
I	3361499	3365727	*HOOD 7 - tf2-4*	Yamanaka et al. 2013	-	-
I	3736902	3743575	*HOOD 8 - SPAP7G5.03*	Yamanaka et al. 2013	-	-
I	3791825	3796114	*HOOD 9 - rad50*	Yamanaka et al. 2013	-	-
I	3996353	4000615	*HOOD 10 - tf2-5*	Yamanaka et al. 2013	-	-
I	4022326	4026545	*HOOD 11 - tf2-6*	Yamanaka et al. 2013	-	-
I	5069824	5083205	*HOOD 12 - mcp3*	Yamanaka et al. 2013	-	-
I	5191103	5195325	*HOOD 13 - tf2-7*	Yamanaka et al. 2013	-	-
I	5195656	5199909	*HOOD 14 - tf2-8*	Yamanaka et al. 2013	-	-
I	5234000	5250176	*HOOD 15 - mug5*	Yamanaka et al. 2013	-	-

II	91600	101684	*HOOD 16 - SPBPB10D8.05c*	Yamanaka et al. 2013	-	-
II	347505	354250	*HOOD 17 - SPBC1271.09*	Yamanaka et al. 2013	-	-
II	898107	902233	*HOOD 18 - mcp5*	Yamanaka et al. 2013	-	-
II	1812684	1816937	*HOOD 19 - tf2-9*	Yamanaka et al. 2013	-	-
II	1965175	1969519	*HOOD 20 - tf2-10*	Yamanaka et al. 2013	-	-
II	2126590	2128479	*HOOD 21 - rpp202*	Yamanaka et al. 2013	-	-
II	4414469	4418768	*HOOD 22 - tf2-11*	Yamanaka et al. 2013	-	-
II	4442538	4449562	*HOOD 23 - SPBC8E4.01c*	Yamanaka et al. 2013	-	-
III	173841	176400	*HOOD 24 - SPCC1235.01*	Yamanaka et al. 2013	-	-
III	254411	256353	*HOOD 25 - tf2-ORF*	Yamanaka et al. 2013	-	-
III	778123	782331	*HOOD 26 - tf2-12*	Yamanaka et al. 2013	-	-
III	1047657	1056145	*HOOD 27 - SPCC1259.08*	Yamanaka et al. 2013	-	-
III	1168500	1176000	*HOOD 28 - SPCC4B3.03c*	Yamanaka et al. 2013	-	-
III	1179500	1182650	*HOOD 29 - rhp26*	Yamanaka et al. 2013	-	-
III	1196050	1196500	*HOOD 30 - tf2-ORF*	Yamanaka et al. 2013	-	-
III	1763512	1775613	*HOOD 31 - ste6*	Yamanaka et al. 2013	-	-
III	2320230	2324503	*HOOD 32 - tf2-13-pseudo*	Yamanaka et al. 2013	-	-
I	239913	249656	*SPAC806.04c & SPAC806.05*	Wang et al. 2015	-	-
I	4527389	4533031	*LTR & SPAC27D7.11c*	Wang et al. 2015	-	-
III	273261	279340	*mae2*	Wang et al. 2015	-	-
II	2301681	2308661	*pfk1/sad1*	Sorida et al. 2019	-	-
I	94000	97000	*SPAC1F8.05*	Gallagher et al. 2019	-	-
I	125000	129000	*SPAC11D3.11c*	Gallagher et al. 2019	-	-
I	125000	129000	*SPAC11D3.10*	Gallagher et al. 2019	-	-
I	1036000	1042000	*SPAC23C4.05c*	Gallagher et al. 2019	-	-
I	1036000	1042000	*SPAC23C4.06c*	Gallagher et al. 2019	-	-
I	1513000	1517000	*SPAC57A7.13*	Gallagher et al. 2019	-	-
I	1513000	1517000	*SPAC57A7.12*	Gallagher et al. 2019	-	-
I	2147000	2150000	*SPAC23C11.09*	Gallagher et al. 2019	-	-
I	2174000	2179000	*SPAC13F5.03c*	Gallagher et al. 2019	-	-
I	2395000	2398500	*SPAC15F9.01c*	Gallagher et al. 2019	-	-
I	2977500	2985500	*SPAPB1A11.02*	Gallagher et al. 2019	-	-
I	3476500	3481000	*SPAC328.03*	Gallagher et al. 2019	-	-
I	5309000	5311500	*SPNCRNA.1068*	Gallagher et al. 2019	-	-
I	5309000	5311500	*SPNCRNA.1069*	Gallagher et al. 2019	-	-
I	5390000	5396000	*SPAC3G6.07*	Gallagher et al. 2019	-	-
II	102000	105000	*SPBC359.01*	Gallagher et al. 2019	-	-
II	167500	170500	*SPBC1683.12*	Gallagher et al. 2019	-	-
II	200500	203000	*SPBC660.05*	Gallagher et al. 2019	-	-
II	221500	224000	*SPBC660.14*	Gallagher et al. 2019	-	-
II	337500	340500	*SPNCRNA.103*	Gallagher et al. 2019	-	-
II	459500	464000	*SPBC428.10*	Gallagher et al. 2019	-	-
II	538000	541000	*SPBC649.04*	Gallagher et al. 2019	-	-
II	919500	922500	*SPBC216.07c*	Gallagher et al. 2019	-	-
II	948000	951000	*SPNCRNA.334*	Gallagher et al. 2019	-	-
II	948000	951000	*SPNCRNA.335*	Gallagher et al. 2019	-	-

II	1223500	1226000	*SPBC725.10*	Gallagher et al. 2019	-	-
II	1309000	1312000	*SPBC30B4.04c*	Gallagher et al. 2019	-	-
II	1495000	1499000	*SPBC11B10.07c*	Gallagher et al. 2019	-	-
II	2184000	2186500	*SPBC17G9.08c*	Gallagher et al. 2019	-	-
II	3344629	3348817	*SPBC17D1.17*	Gallagher et al. 2019	-	-
II	3530000	3532500	*SPBC1105.12*	Gallagher et al. 2019	-	-
II	3530000	3532500	*SPBC1105.13c*	Gallagher et al. 2019	-	-
II	4103000	4108500	*SPBC56F2.06*	Gallagher et al. 2019	-	-
II	4409500	4414500	*SPBC1289.14*	Gallagher et al. 2019	-	-
III	31500	34500	*SPCP20C8.03*	Gallagher et al. 2019	-	-
III	34500	39000	*SPCC1884.01*	Gallagher et al. 2019	-	-
III	739000	742000	*SPCC18B5.11c*	Gallagher et al. 2019	-	-
III	1265500	1268000	*SPCC23B6.01c*	Gallagher et al. 2019	-	-
III	2072000	2075000	*SPCPB1C11.02*	Gallagher et al. 2019	-	-
III	2286000	2289500	*SPCC965.04c*	Gallagher et al. 2019	-	-
III	2410325	2415970	*SPCC569.08c*	Gallagher et al. 2019	-	-
III	2429000	2433000	*SPCC569.03*	Gallagher et al. 2019	-	-

References

Adam, M., Robert, F., Larochelle, M. & Gaudreau, L. (2001) H2A.Z is required for global chromatin integrity and for recruitment of RNA polymerase II under specific conditions. *Molecular and cellular biology*. 21 (18), 6270–6279.

Akhtar, A. & Becker, P.B. (2000) Activation of transcription through histone H4 acetylation by MOF, an acetyltransferase essential for dosage compensation in Drosophila. *Molecular cell*. 5 (2), 367–375.

Al-Sady, B., Madhani, H.D. & Narlikar, G.J. (2013) Division of labor between the chromodomains of HP1 and Suv39 methylase enables coordination of heterochromatin spread. *Molecular cell*. 51 (1), 80–91.

Alberti, S., Halfmann, R., King, O., Kapila, A. & Lindquist, S. (2009) A systematic survey identifies prions and illuminates sequence features of prionogenic proteins. *Cell*. 137 (1), 146–158.

Allfrey, V.G., Faulkner, R. & Mirsky, A.E. (1964) Acetylation and methylation of histones and their possible role in the regulation of RNA synthesis. *Proc Natl Acad Sci USA*. 51(5), 786–794.

Allis, C.D. & Jenuwein, T. (2016) The molecular hallmarks of epigenetic control. *Nature reviews. Genetics*. 17 (8), 487–500.

Allis, C.D., Bowen, J.K., Abraham, G.N., Glover, C.V. & Gorovsky, M.A. (1980) Proteolytic processing of histone H3 in chromatin: a physiologically regulated event in Tetrahymena micronuclei. *Cell*. 20 (1), 55–64.

Allshire, R.C. & Ekwall, K. (2015) Epigenetic regulation of chromatin states in *Schizosaccharomyces pombe*. *Cold Spring Harbor perspectives in biology*. 7 (7), a018770.

Allshire, R.C. & Karpen, G.H. (2008) Epigenetic regulation of centromeric chromatin: old dogs, new tricks? *Nature reviews. Genetics*. 9 (12), 923–937.

Allshire, R.C. & Madhani, H.D. (2018) Ten principles of heterochromatin formation and function. *Nature reviews. Molecular cell biology*. 19 (4), 229–244.

Allshire, R.C., Javerzat, J.P., Redhead, N.J. & Cranston, G. (1994) Position effect variegation at fission yeast centromeres. *Cell*. 76 (1), 157–169.

Allshire, R.C., Nimmo, E.R., Ekwall, K., Javerzat, J.P. & Cranston, G. (1995) Mutations derepressing silent centromeric domains in fission yeast disrupt chromosome segregation. *Genes & development*. 9 (2), 218–233.

Almeida, F., Rodrigues, M.L. & Coelho, C. (2019) The still underestimated problem of fungal diseases worldwide. *Frontiers in microbiology*. 10, 214.

Almeida, M., Pintacuda, G., Masui, O., Koseki, Y., Gdula, M., Cerase, A., Brown, D., Mould, A., Innocent, C., Nakayama, M., Schermelleh, L., Nesterova, T.B., Koseki, H. & Brockdorff, N. (2017) PCGF3/5-PRC1 initiates Polycomb recruitment in X chromosome inactivation. *Science*. 356 (6342), 1081–1084.

Alper, B.J., Job, G., Yadav, R.K., Shanker, S., Lowe, B.R. & Partridge, J.F. (2013) Sir2 is required for Clr4 to initiate centromeric heterochromatin assembly in fission yeast. *The EMBO journal*. 32 (17), 2321–2335.

Amabile, A., Migliara, A., Capasso, P., Biffi, M., Cittaro, D., Naldini, L. & Lombardo, A. (2016) Inheritable silencing of endogenous genes by Hit-and-Run targeted epigenetic editing. *Cell*. 167 (1), 219–232.e14.

Andrulis, E.D., Neiman, A.M., Zappulla, D.C. & Sternglanz, R. (1998) Perinuclear localization of chromatin facilitates transcriptional silencing. *Nature*. 394 (6693), 592–595.

Angel, A., Song, J., Dean, C. & Howard, M. (2011) A Polycomb-based switch underlying quantitative epigenetic memory. *Nature*. 476 (7358), 105–108.

Angerer, H. (2015) Eukaryotic LYR proteins interact with mitochondrial protein complexes. *Biology*. 4 (1), 133–150.

Angerer, H., Radermacher, M., Mańkowska, M., Steger, M., Zwicker, K., Heide, H., Wittig, I., Brandt, U. & Zickermann, V. (2014) The LYR protein subunit NB4M/NDUFA6 of mitochondrial complex I anchors an acyl carrier protein and is essential for catalytic activity. *Proc Natl Acad Sci USA*. 111 (14), 5207–5212.

Annunziato, A.T., Eason, M.B. & Perry, C.A. (1995) Relationship between methylation and acetylation of arginine-rich histones in cycling and arrested HeLa cells. *Biochemistry*. 34 (9), 2916–2924.

Antequera, F., Tamame, M., Villanueva, J.R. & Santos, T. (1984) DNA methylation in the fungi. *The Journal of biological chemistry*. 259 (13), 8033–8036.

Aravin, A.A., Sachidanandam, R., Bourc'his, D., Schaefer, C., Pezic, D., Toth, K.F., Bestor, T. & Hannon, G.J. (2008) A piRNA pathway primed by individual transposons is linked to de novo DNA methylation in mice. *Molecular cell*. 31 (6), 785–799.

Aravin, A.A., Sachidanandam, R., Girard, A., Fejes-Toth, K. & Hannon, G.J. (2007) Developmentally regulated piRNA clusters implicate MILI in transposon control. *Science*. 316 (5825), 744.

Ard, R., Tong, P. & Allshire, R.C. (2014) Long non-coding RNA-mediated transcriptional interference of a permease gene confers drug tolerance in fission yeast. *Nature communications*. 5 (1), 5576.

Arioka, M., Kouhashi, M., Yoda, K., Takatsuki, A., Yamasaki, M. & Kitamoto, K. (1998) Multidrug resistance phenotype conferred by overexpressing *bfr2*$^{+}$/*pad1*$^{+}$/*sks1*$^{+}$ or *pap1*$^{+}$ genes and mediated by *bfr1*$^{+}$ gene product, a structural and functional homologue of P-glycoprotein in *Schizosaccharomyces pombe*. *Bioscience, biotechnology, and biochemistry*. 62 (2), 390–392.

Ashe, A., Sapetschnig, A., Weick, E.-M., Mitchell, J., Bagijn, M.P., Cording, A.C., Doebley, A.-L., Goldstein, L.D., Lehrbach, N.J., Le Pen, J., Pintacuda, G., Sakaguchi, A., Sarkies, P., Ahmed, S. & Miska, E.A. (2012) piRNAs can trigger a multigenerational epigenetic memory in the germline of *C. elegans*. *Cell*. 150 (1), 88–99.

Askwith, C. & Kaplan, J. (1997) An oxidase-permease-based iron transport system in *Schizosaccharomyces pombe* and its expression in *Saccharomyces cerevisiae*. *The Journal of biological chemistry*. 272 (1), 401–405.

Audergon, P.N.C.B., Catania, S., Kagansky, A., Tong, P., Shukla, M., Pidoux, A.L. & Allshire, R.C. (2015) Restricted epigenetic inheritance of H3K9 methylation. *Science*. 348 (6230), 132–135.

Aygün, O., Mehta, S. & Grewal, S.I.S. (2013) HDAC-mediated suppression of histone turnover promotes epigenetic stability of heterochromatin. *Nature structural & molecular biology*. 20 (5), 547–554.

Ayoub, N., Noma, K.-I., Isaac, S., Kahan, T., Grewal, S.I.S. & Cohen, A. (2003) A novel jmjC domain protein modulates heterochromatization in fission yeast. *Molecular and cellular biology*. 23 (12), 4356–4370.

Bannister, A.J. & Kouzarides, T. (2011) Regulation of chromatin by histone modifications. *Nature Publishing Group*. 21 (3), 381–395.

Bannister, A.J., Schneider, R. & Kouzarides, T. (2002) Histone methylation: dynamic or static? *Cell*. 109 (7), 801–806.

Bannister, A.J., Zegerman, P., Partridge, J.F., Miska, E.A., Thomas, J.O., Allshire, R.C. & Kouzarides, T. (2001) Selective recognition of methylated lysine 9 on histone H3 by the HP1 chromo domain. *Nature*. 410 (6824), 120–124.

Barr, M.L. & Bertram, E.G. (1949) A morphological distinction between neurones of the male and female, and the behaviour of the nucleolar satellite during accelerated nucleoprotein synthesis. *Nature*. 163 (4148), 676–677.

Barski, A., Cuddapah, S., Cui, K., Roh, T.-Y., Schones, D.E., Wang, Z., Wei, G., Chepelev, I. & Zhao, K. (2007) High-resolution profiling of histone methylations in the human genome. *Cell*. 129 (4), 823–837.

Bastow, R., Mylne, J.S., Lister, C., Lippman, Z., Martienssen, R.A. & Dean, C. (2004) Vernalization requires epigenetic silencing of *FLC* by histone methylation. *Nature*. 427 (6970), 164–167.

Baulcombe, D.C. & Dean, C. (2014) Epigenetic regulation in plant responses to the environment. *Cold Spring Harbor perspectives in biology*. 6 (9), a019471.

Baum, M., Ngan, V.K. & Clarke, L. (1994) The centromeric K-type repeat and the central core are together sufficient to establish a functional *Schizosaccharomyces pombe* centromere. *Molecular biology of the cell*. 5 (7), 747–761.

Baumbusch, L.O., Thorstensen, T., Krauss, V., Fischer, A., Naumann, K., Assalkhou, R., Schulz, I., Reuter, G. & Aalen, R.B. (2001) The *Arabidopsis thaliana* genome contains at least 29 active genes encoding SET domain proteins that can be assigned to four evolutionarily conserved classes. *Nucleic acids research*. 29 (21), 4319–4333.

Bayne, E.H., Portoso, M., Kagansky, A., Kos-Braun, I.C., Urano, T., Ekwall, K., Alves, F., Rappsilber, J. & Allshire, R.C. (2008) Splicing factors facilitate RNAi-directed silencing in fission yeast. *Science*. 322 (5901), 602–606.

Bayne, E.H., White, S.A., Kagansky, A., Bijos, D.A., Sanchez-Pulido, L., Hoe, K.-L., Kim, D.-U., Park, H.-O., Ponting, C.P., Rappsilber, J. & Allshire, R.C. (2010) Stc1: a critical link between RNAi and chromatin modification required for heterochromatin integrity. *Cell*. 140 (5), 666–677.

Bähler, J., Wu, J.Q., Longtine, M.S., Shah, N.G., McKenzie, A., Steever, A.B., Wach, A., Philippsen, P. & Pringle, J.R. (1998) Heterologous modules for efficient and versatile PCR-based gene targeting in *Schizosaccharomyces pombe*. *Yeast*. 14 (10), 943–951.

Becker, J.S., Nicetto, D. & Zaret, K.S. (2016) H3K9me3-dependent heterochromatin: barrier to cell fate changes. *Trends in genetics*. 32 (1), 29–41.

Benkö, Z., Fenyvesvolgyi, C., Pesti, M. & Sipiczki, M. (2004) The transcription factor Pap1/Caf3 plays a central role in the determination of caffeine resistance in *Schizosaccharomyces pombe*. *Molecular genetics and genomics*. 271 (2), 161–170.

Benkö, Z., Miklos, I., Carr, A.M. & Sipiczki, M. (1997) Caffeine-resistance in *S. pombe*: mutations in three novel *caf* genes increase caffeine tolerance and affect radiation sensitivity, fertility, and cell cycle. *Current genetics*. 31 (6), 481–487.

Benkö, Z., Sipiczki, M. & Carr, A.M. (1998) Cloning of *caf1*$^{+}$, *caf2*$^{+}$ and *caf4*$^{+}$ from *Schizosaccharomyces pombe*: their involvement in multidrug resistance, UV and pH sensitivity. *Molecular & general genetics*. 260 (5), 434–443.

Bernard, P., Maure, J.F., Partridge, J.F., Genier, S., Javerzat, J.P. & Allshire, R.C. (2001) Requirement of heterochromatin for cohesion at centromeres. *Science*. 294 (5551), 2539–2542.

Bernstein, E., Caudy, A.A., Hammond, S.M. & Hannon, G.J. (2001) Role for a bidentate ribonuclease in the initiation step of RNA interference. *Nature*. 409 (6818), 363–366.

Berry, S., Hartley, M., Olsson, T.S.G., Dean, C. & Howard, M. (2015) Local chromatin environment of a Polycomb target gene instructs its own epigenetic inheritance. *eLife*. 4, e07205.

Bertani, G. (1951) Studies on lysogenesis. I. The mode of phage liberation by lysogenic *Escherichia coli*. *Journal of bacteriology*. 62 (3), 293–300.

Beverley, S.M., Coderre, J.A., Santi, D.V. & Schimke, R.T. (1984) Unstable DNA amplifications in methotrexate-resistant Leishmania consist of extrachromosomal circles which relocalize during stabilization. *Cell*. 38 (2), 431–439.

Bickmore, W.A. & van Steensel, B. (2013) Genome architecture: domain organization of interphase chromosomes. *Cell*. 152 (6), 1270–1284.

Bintu, L., Yong, J., Antebi, Y.E., McCue, K., Kazuki, Y., Uno, N., Oshimura, M. & Elowitz, M.B. (2016) Dynamics of epigenetic regulation at the single-cell level. *Science*. 351 (6274), 720–724.

Bird, A. (2007) Perceptions of epigenetics. *Nature*. 447 (7143), 396–398.

Bird, A., Taggart, M., Frommer, M., Miller, O.J. & Macleod, D. (1985) A fraction of the mouse genome that is derived from islands of nonmethylated, CpG-rich DNA. *Cell*. 40 (1), 91–99.

Blackledge, N.P., Farcas, A.M., Kondo, T., King, H.W., McGouran, J.F., Hanssen, L.L.P., Ito, S., Cooper, S., Kondo, K., Koseki, Y., Ishikura, T., Long, H.K., Sheahan, T.W., Brockdorff, N., Kessler, B.M., Koseki, H. & Klose, R.J. (2014) Variant PRC1 complex-dependent H2A ubiquitylation drives PRC2 recruitment and polycomb domain formation. *Cell*. 157 (6), 1445–1459.

Bolger, A.M., Lohse, M. & Usadel, B. (2014) Trimmomatic: a flexible trimmer for Illumina sequence data. *Bioinformatics*. 30 (15), 2114–2120.

Bonev, B. & Cavalli, G. (2016) Organization and function of the 3D genome. *Nature reviews. Genetics*. 17 (11), 661–678.

Borun, T.W., Pearson, D. & Paik, W.K. (1972) Studies of histone methylation during the HeLa S-3 cell cycle. *The Journal of biological chemistry*. 247 (13), 4288–4298.

Brasher, S.V., Smith, B.O., Fogh, R.H., Nietlispach, D., Thiru, A., Nielsen, P.R., Broadhurst, R.W., Ball, L.J., Murzina, N.V. & Laue, E.D. (2000) The structure of mouse HP1 suggests a unique mode of single peptide recognition by the shadow chromo domain dimer. *The EMBO journal*. 19 (7), 1587–1597.

Braun, S., Garcia, J.F., Rowley, M., Rougemaille, M., Shankar, S. & Madhani, H.D. (2011) The Cul4-Ddb1(Cdt)² ubiquitin ligase inhibits invasion of a

boundary-associated antisilencing factor into heterochromatin. *Cell*. 144 (1), 41–54.

Brennecke, J., Aravin, A.A., Stark, A., Dus, M., Kellis, M., Sachidanandam, R. & Hannon, G.J. (2007) Discrete small RNA-generating loci as master regulators of transposon activity in Drosophila. *Cell*. 128 (6), 1089–1103.

Brown, G.D., Denning, D.W., Gow, N.A.R., Levitz, S.M., Netea, M.G. & White, T.C. (2012) Hidden killers: human fungal infections. *Science translational medicine*. 4 (165), 165rv13.

Brownell, J.E., Zhou, J., Ranalli, T., Kobayashi, R., Edmondson, D.G., Roth, S.Y. & Allis, C.D. (1996) Tetrahymena histone acetyltransferase A: a homolog to yeast Gcn5p linking histone acetylation to gene activation. *Cell*. 84 (6), 843–851.

Buker, S.M., Iida, T., Bühler, M., Villén, J., Gygi, S.P., Nakayama, J.-I. & Moazed, D. (2007) Two different Argonaute complexes are required for siRNA generation and heterochromatin assembly in fission yeast. *Nature structural & molecular biology*. 14 (3), 200–207.

Burgess, R.J. & Zhang, Z. (2013) Histone chaperones in nucleosome assembly and human disease. *Nature structural & molecular biology*. 20 (1), 14–22.

Buscaino, A., Lejeune, E., Audergon, P., Hamilton, G., Pidoux, A. & Allshire, R.C. (2013) Distinct roles for Sir2 and RNAi in centromeric heterochromatin nucleation, spreading and maintenance. *The EMBO journal*. 32 (9), 1250–1264.

Buscaino, A., White, S.A., Houston, D.R., Lejeune, E., Simmer, F., de Lima Alves, F., Diyora, P.T., Urano, T., Bayne, E.H., Rappsilber, J. & Allshire, R.C. (2012) Raf1 is a DCAF for the Rik1 DDB1-like protein and has separable roles in siRNA generation and chromatin modification. *PLoS genetics*. 8 (2), e1002499.

Butcher, R.W. & Sutherland, E.W. (1962) Adenosine 3',5'-phosphate in biological materials. I. Purification and properties of cyclic 3',5'-nucleotide phosphodiesterase and use of this enzyme to characterize adenosine 3‘,5’-phosphate in human urine. *The Journal of biological chemistry*. 237, 1244–1250.

Bühler, M., Verdel, A. & Moazed, D. (2006) Tethering RITS to a nascent transcript initiates RNAi- and heterochromatin-dependent gene silencing. *Cell*. 125 (5), 873–886.

Byvoet, P., Shepherd, G.R., Hardin, J.M. & Noland, B.J. (1972) The distribution and turnover of labeled methyl groups in histone fractions of cultured mammalian cells. *Archives of biochemistry and biophysics*. 148 (2), 558–567.

Calo, S., Nicolás, F.E., Lee, S.C., Vila, A., Cervantes, M., Torres-Martínez, S., Ruiz-Vázquez, R.M., Cardenas, M.E. & Heitman, J. (2017) A non-canonical RNA degradation pathway suppresses RNAi-dependent epimutations in the human fungal pathogen Mucor circinelloides. *PLoS genetics*. 13 (3), e1006686.

Calo, S., Shertz-Wall, C., Lee, S.C., Bastidas, R.J., Nicolás, F.E., Granek, J.A., Mieczkowski, P., Torres-Martínez, S., Ruiz-Vázquez, R.M., Cardenas, M.E. & Heitman, J. (2014) Antifungal drug resistance evoked via RNAi-dependent epimutations. *Nature*. 513 (7519), 555–558.

Calvo, I.A., Gabrielli, N., Iglesias-Baena, I., García-Santamarina, S., Hoe, K.-L., Kim, D.-U., Sansó, M., Zuin, A., Pérez, P., Ayté, J. & Hidalgo, E. (2009) Genome-wide screen of genes required for caffeine tolerance in fission yeast. *PloS one*. 4 (8), e6619.

Calvo, I.A., García, P., Ayté, J. & Hidalgo, E. (2012) The transcription factors Pap1 and Prr1 collaborate to activate antioxidant, but not drug tolerance, genes in response to H2O2. *Nucleic acids research*. 40 (11), 4816–4824.

Cam, H.P., Sugiyama, T., Chen, E.S., Chen, X., FitzGerald, P.C. & Grewal, S.I.S. (2005) Comprehensive analysis of heterochromatin- and RNAi-mediated epigenetic control of the fission yeast genome. *Nature Genetics*. 37 (8), 809–819.

Campos, E.I., Fillingham, J., Li, G., Zheng, H., Voigt, P., Kuo, W.-H.W., Seepany, H., Gao, Z., Day, L.A., Greenblatt, J.F. & Reinberg, D. (2010) The program for processing newly synthesized histones H3.1 and H4. *Nature structural & molecular biology*. 17 (11), 1343–1351.

Canzio, D., Chang, E.Y., Shankar, S., Kuchenbecker, K.M., Simon, M.D., Madhani, H.D., Narlikar, G.J. & Al-Sady, B. (2011) Chromodomain-mediated oligomerization of HP1 suggests a nucleosome-bridging mechanism for heterochromatin assembly. *Molecular cell*. 41 (1), 67–81.

Canzio, D., Liao, M., Naber, N., Pate, E., Larson, A., Wu, S., Marina, D.B., Garcia, J.F., Madhani, H.D., Cooke, R., Schuck, P., Cheng, Y. & Narlikar, G.J. (2013) A conformational switch in HP1 releases auto-inhibition to drive heterochromatin assembly. *Nature*. 496 (7445), 377–381.

Cao, R., Wang, L., Wang, H., Xia, L., Erdjument-Bromage, H., Tempst, P., Jones, R.S. & Zhang, Y. (2002) Role of histone H3 lysine 27 methylation in Polycomb-group silencing. *Science*. 298 (5595), 1039–1043.

Capuano, F., Mülleder, M., Kok, R., Blom, H.J. & Ralser, M. (2014) Cytosine DNA methylation is found in *Drosophila melanogaster* but absent in *Saccharomyces cerevisiae*, *Schizosaccharomyces pombe*, and other yeast species. *Analytical chemistry*. 86 (8), 3697–3702.

Carobbio, S., Realini, C., Norbury, C.J., Toda, T., Cavalli, F. & Spataro, V. (2001) Sequence of Crm1/exportin 1 mutant alleles reveals critical sites associated with multidrug resistance. *Current genetics*. 39 (1), 2–9.

Carroll, S.M., DeRose, M.L., Gaudray, P., Moore, C.M., Needham-Vandevanter, D.R., Hoff, Von, D.D. & Wahl, G.M. (1988) Double minute chromosomes can be produced from precursors derived from a chromosomal deletion. *Molecular and cellular biology*. 8 (4), 1525–1533.

Casadio, F., Lu, X., Pollock, S.B., LeRoy, G., Garcia, B.A., Muir, T.W., Roeder, R.G. & Allis, C.D. (2013) H3R42me2a is a histone modification with positive transcriptional effects. *Proc Natl Acad Sci USA*. 110 (37), 14894–14899.

Castel, S.E. & Martienssen, R.A. (2013) RNA interference in the nucleus: roles for small RNAs in transcription, epigenetics and beyond. *Nature reviews. Genetics*. 14 (2), 100–112.

Castillo, E.A., Vivancos, A.P., Jones, N., Ayté, J. & Hidalgo, E. (2003) *Schizosaccharomyces pombe* cells lacking the Ran-binding protein Hba1 show a multidrug resistance phenotype due to constitutive nuclear accumulation of Pap1. *The Journal of biological chemistry*. 278 (42), 40565–40572.

Cavalli, G. & Heard, E. (2019) Advances in epigenetics link genetics to the environment and disease. *Nature*. 571 (7766), 489–499.

Chen, D., Toone, W.M., Mata, J., Lyne, R., Burns, G., Kivinen, K., Brazma, A., Jones, N. & Bähler, J. (2003) Global transcriptional responses of fission

yeast to environmental stress. *Molecular biology of the cell*. 14 (1), 214–229.

Chen, E.S., Zhang, K., Nicolas, E., Cam, H.P., Zofall, M. & Grewal, S.I.S. (2008) Cell cycle control of centromeric repeat transcription and heterochromatin assembly. *Nature*. 451 (7179), 734–737.

Choi, J., Hyun, Y., Kang, M.-J., In Yun, H., Yun, J.-Y., Lister, C., Dean, C., Amasino, R.M., Noh, B., Noh, Y.-S. & Choi, Y. (2009) Resetting and regulation of Flowering Locus C expression during Arabidopsis reproductive development. *The Plant journal*. 57 (5), 918–931.

Chu, C., Zhang, Q.C., da Rocha, S.T., Flynn, R.A., Bharadwaj, M., Calabrese, J.M., Magnuson, T., Heard, E. & Chang, H.Y. (2015) Systematic discovery of *Xist* RNA binding proteins. *Cell*. 161 (2), 404–416.

Clapier, C.R., Iwasa, J., Cairns, B.R. & Peterson, C.L. (2017) Mechanisms of action and regulation of ATP-dependent chromatin-remodelling complexes. *Nature reviews. Molecular cell biology*. 18 (7), 407–422.

Clements, A., Poux, A.N., Lo, W.-S., Pillus, L., Berger, S.L. & Marmorstein, R. (2003) Structural basis for histone and phosphohistone binding by the GCN5 histone acetyltransferase. *Molecular cell*. 12 (2), 461–473.

Coleman, R.T. & Struhl, G. (2017) Causal role for inheritance of H3K27me3 in maintaining the OFF state of a Drosophila HOX gene. *Science*. 356 (6333).

Colmenares, S.U., Buker, S.M., Bühler, M., Dlakić, M. & Moazed, D. (2007) Coupling of double-stranded RNA synthesis and siRNA generation in fission yeast RNAi. *Molecular cell*. 27 (3), 449–461.

Cook, A.J.L., Gurard-Levin, Z.A., Vassias, I. & Almouzni, G. (2011) A specific function for the histone chaperone NASP to fine-tune a reservoir of soluble H3-H4 in the histone supply chain. *Molecular cell*. 44 (6), 918–927.

Cooper, J.P., Nimmo, E.R., Allshire, R.C. & Cech, T.R. (1997) Regulation of telomere length and function by a Myb-domain protein in fission yeast. *Nature*. 385 (6618), 744–747.

Cooper, J.P., Watanabe, Y. & Nurse, P. (1998) Fission yeast Taz1 protein is required for meiotic telomere clustering and recombination. *Nature*. 392 (6678), 828–831.

Cooper, S., Dienstbier, M., Hassan, R., Schermelleh, L., Sharif, J., Blackledge, N.P., De Marco, V., Elderkin, S., Koseki, H., Klose, R., Heger, A. &

Brockdorff, N. (2014) Targeting polycomb to pericentric heterochromatin in embryonic stem cells reveals a role for H2AK119u1 in PRC2 recruitment. *Cell reports*. 7 (5), 1456–1470.

Cooper, S., Grijzenhout, A., Underwood, E., Ancelin, K., Zhang, T., Nesterova, T.B., Anil-Kirmizitas, B., Bassett, A., Kooistra, S.M., Agger, K., Helin, K., Heard, E. & Brockdorff, N. (2016) Jarid2 binds mono-ubiquitylated H2A lysine 119 to mediate crosstalk between Polycomb complexes PRC1 and PRC2. *Nature communications*. 713661.

Cornelis, M.C. (2019) The impact of caffeine and coffee on human health. *Nutrients*. 11 (2), 416.

Costigan, C., Gehrung, S. & Snyder, M. (1992) A synthetic lethal screen identifies SLK1, a novel protein kinase homolog implicated in yeast cell morphogenesis and cell growth. *Molecular and cellular biology*. 12 (3), 1162–1178.

Cowieson, N.P., Partridge, J.F., Allshire, R.C. & McLaughlin, P.J. (2000) Dimerisation of a chromo shadow domain and distinctions from the chromodomain as revealed by structural analysis. *Current Biology*. 10 (9), 517–525.

Crevillén, P., Yang, H., Cui, X., Greeff, C., Trick, M., Qiu, Q., Cao, X. & Dean, C. (2014) Epigenetic reprogramming that prevents transgenerational inheritance of the vernalized state. *Nature*. 515 (7528), 587–590.

Csorba, T., Qüesta, J.I., Sun, Q. & Dean, C. (2014) Antisense COOLAIR mediates the coordinated switching of chromatin states at *FLC* during vernalization. *Proc Natl Acad Sci USA*. 111 (45), 16160–16165.

Cubas, P., Vincent, C. & Coen, E. (1999) An epigenetic mutation responsible for natural variation in floral symmetry. *Nature*. 401 (6749), 157–161.

Czermin, B., Melfi, R., McCabe, D., Seitz, V., Imhof, A. & Pirrotta, V. (2002) Drosophila enhancer of Zeste/ESC complexes have a histone H3 methyltransferase activity that marks chromosomal Polycomb sites. *Cell*. 111 (2), 185–196.

da Rocha, S.T., Boeva, V., Escamilla-Del-Arenal, M., Ancelin, K., Granier, C., Matias, N.R., Sanulli, S., Chow, J., Schulz, E., Picard, C., Kaneko, S., Helin, K., Reinberg, D., Stewart, A.F., Wutz, A., Margueron, R. & Heard, E. (2014) Jarid2 is implicated in the initial *Xist*-induced targeting of PRC2 to the inactive X chromosome. *Molecular cell*. 53 (2), 301–316.

Das, P.P., Bagijn, M.P., Goldstein, L.D., Woolford, J.R., Lehrbach, N.J., Sapetschnig, A., Buhecha, H.R., Gilchrist, M.J., Howe, K.L., Stark, R., Matthews, N., Berezikov, E., Ketting, R.F., Tavaré, S. & Miska, E.A. (2008) Piwi and piRNAs act upstream of an endogenous siRNA pathway to suppress Tc3 transposon mobility in the *Caenorhabditis elegans* germline. *Molecular cell*. 31 (1), 79–90.

Davey, C.A., Sargent, D.F., Luger, K., Maeder, A.W. & Richmond, T.J. (2002) Solvent mediated interactions in the structure of the nucleosome core particle at 1.9 a resolution. *Journal of molecular biology*. 319 (5), 1097–1113.

de Jong, I.G., Haccou, P. & Kuipers, O.P. (2011) Bet hedging or not? A guide to proper classification of microbial survival strategies. *BioEssays*. 33 (3), 215–223.

de Napoles, M., Mermoud, J.E., Wakao, R., Tang, Y.A., Endoh, M., Appanah, R., Nesterova, T.B., Silva, J., Otte, A.P., Vidal, M., Koseki, H. & Brockdorff, N. (2004) Polycomb group proteins Ring1A/B link ubiquitylation of histone H2A to heritable gene silencing and X inactivation. *Developmental Cell*. 7 (5), 663–676.

deCarvalho, A.C., Kim, H., Poisson, L.M., Winn, M.E., Mueller, C., Cherba, D., Koeman, J., Seth, S., Protopopov, A., Felicella, M., Zheng, S., Multani, A., Jiang, Y., Zhang, J., Nam, D.-H., Petricoin, E.F., Chin, L., Mikkelsen, T. & Verhaak, R.G.W. (2018) Discordant inheritance of chromosomal and extrachromosomal DNA elements contributes to dynamic disease evolution in glioblastoma. *Nature Genetics*. 50 (5), 708–717.

Delerue, T., Khosrobakhsh, F., Daloyau, M., Emorine, L.J., Dedieu, A., Herbert, C.J., Bonnefoy, N., Arnauné-Pelloquin, L. & Belenguer, P. (2016) Loss of Msp1p in *Schizosaccharomyces pombe* induces a ROS-dependent nuclear mutator phenotype that affects mitochondrial fission genes. *FEBS letters*. 590 (20), 3544–3558.

Demeke, M.M., Foulquié-Moreno, M.R., Dumortier, F. & Thevelein, J.M. (2015) Rapid evolution of recombinant *Saccharomyces cerevisiae* for Xylose fermentation through formation of extra-chromosomal circular DNA. *PLoS genetics*. 11 (3), e1005010.

DeVoti, J., Seydoux, G., Beach, D. & McLeod, M. (1991) Interaction between *ran1*$^{+}$ protein kinase and cAMP dependent protein kinase as negative regulators of fission yeast meiosis. *The EMBO journal*. 10 (12), 3759–3768.

Dhalluin, C., Carlson, J.E., Zeng, L., He, C., Aggarwal, A.K. & Zhou, M.M. (1999) Structure and ligand of a histone acetyltransferase bromodomain. *Nature*. 399 (6735), 491–496.

Dias, B.G. & Ressler, K.J. (2014) Parental olfactory experience influences behavior and neural structure in subsequent generations. *Nature Neuroscience*. 17 (1), 89–96.

Diaz, A., Park, K., Lim, D.A. & Song, J.S. (2012) Normalization, bias correction, and peak calling for ChIP-seq. *Statistical applications in genetics and molecular biology*. 11 (3), 9.

Dillon, S.C., Zhang, X., Trievel, R.C. & Cheng, X. (2005) The SET-domain protein superfamily: protein lysine methyltransferases. *Genome biology*. 6 (8), 227.

Djupedal, I., Portoso, M., Spåhr, H., Bonilla, C., Gustafsson, C.M., Allshire, R.C. & Ekwall, K. (2005) RNA Pol II subunit Rpb7 promotes centromeric transcription and RNAi-directed chromatin silencing. *Genes & development*. 19 (19), 2301–2306.

Dobin, A., Davis, C.A., Schlesinger, F., Drenkow, J., Zaleski, C., Jha, S., Batut, P., Chaisson, M. & Gingeras, T.R. (2013) STAR: ultrafast universal RNA-seq aligner. *Bioinformatics*. 29 (1), 15–21.

Donze, D., Adams, C.R., Rine, J. & Kamakaka, R.T. (1999) The boundaries of the silenced HMR domain in *Saccharomyces cerevisiae*. *Genes & development*. 13 (6), 698–708.

Dossin, F., Pinheiro, I., Żylicz, J.J., Roensch, J., Collombet, S., Le Saux, A., Chelmicki, T., Attia, M., Kapoor, V., Zhan, Y., Dingli, F., Loew, D., Mercher, T., Dekker, J. & Heard, E. (2020) SPEN integrates transcriptional and epigenetic control of X-inactivation. *Nature*. 578 (7795), 455–460.

Dreos, R., Ambrosini, G., Cavin Périer, R. & Bucher, P. (2013) EPD and EPDnew, high-quality promoter resources in the next-generation sequencing era. *Nucleic acids research*. 41 (Database issue), D157–64.

Duempelmann, L., Mohn, F., Shimada, Y., Oberti, D., Andriollo, A., Lochs, S. & Bühler, M. (2019) Inheritance of a phenotypically neutral epimutation evokes gene silencing in later generations. *Molecular cell*. 74 (3), 534–541.e4.

Duerre, J.A. & Lee, C.T. (1974) In vivo methylation and turnover of rat brain histones. *Journal of neurochemistry*. 23 (3), 541–547.

Dumesic, P.A., Homer, C.M., Moresco, J.J., Pack, L.R., Shanle, E.K., Coyle, S.M., Strahl, B.D., Fujimori, D.G., Yates, J.R. & Madhani, H.D. (2015) Product binding enforces the genomic specificity of a yeast polycomb repressive complex. *Cell*. 160 (1-2), 204–218.

Earnshaw, W.C. (2015) Discovering centromere proteins: from cold white hands to the A, B, C of CENPs. *Nature reviews. Molecular cell biology*. 16 (7), 443–449.

Earnshaw, W.C. & Rothfield, N. (1985) Identification of a family of human centromere proteins using autoimmune sera from patients with scleroderma. *Chromosoma*. 91 (3), 313–321.

Egan, E.D., Braun, C.R., Gygi, S.P. & Moazed, D. (2014) Post-transcriptional regulation of meiotic genes by a nuclear RNA silencing complex. *RNA*. 20 (6), 867–881.

Eissenberg, J.C., James, T.C., Foster-Hartnett, D.M., Hartnett, T., Ngan, V. & Elgin, S.C. (1990) Mutation in a heterochromatin-specific chromosomal protein is associated with suppression of position-effect variegation in *Drosophila melanogaster*. *Proc Natl Acad Sci USA*. 87 (24), 9923–9927.

Elgin, S.C.R. & Reuter, G. (2013) Position-effect variegation, heterochromatin formation, and gene silencing in Drosophila. *Cold Spring Harbor perspectives in biology*. 5 (8), a017780.

Erler, A., Maresca, M., Fu, J. & Stewart, A.F. (2006) Recombineering reagents for improved inducible expression and selection marker re-use in *Schizosaccharomyces pombe*. *Yeast*. 23 (11), 813–823.

Fabre, F. (1972) Relation between repair mechanisms and induced mitotic recombination after UV irradiation, in the yeast *Schizosaccharomyces pombe*. Effects of caffeine. *Molecular & general genetics*. 117 (2), 153–166.

Fang, Y., Hu, L., Zhou, X., Jaiseng, W., Zhang, B., Takami, T. & Kuno, T. (2012) A genome-wide screen in *Schizosaccharomyces pombe* for genes affecting the sensitivity of antifungal drugs that target ergosterol biosynthesis. *Antimicrobial agents and chemotherapy*. 56 (4), 1949–1959.

Fantes, P.A. & Hoffman, C.S. (2016) A brief history of *Schizosaccharomyces pombe* research: a perspective over the past 70 years. *Genetics*. 203 (2), 621–629.

Farcas, A.M., Blackledge, N.P., Sudbery, I., Long, H.K., McGouran, J.F., Rose, N.R., Lee, S., Sims, D., Cerase, A., Sheahan, T.W., Koseki, H., Brockdorff, N., Ponting, C.P., Kessler, B.M. & Klose, R.J. (2012) KDM2B links the Polycomb Repressive Complex 1 (PRC1) to recognition of CpG islands. *eLife*. 1, e00205.

Feng, S., Jacobsen, S.E. & Reik, W. (2010) Epigenetic reprogramming in plant and animal development. *Science*. 330 (6004), 622–627.

Fernandez, R. & Berro, J. (2016) Use of a fluoride channel as a new selection marker for fission yeast plasmids and application to fast genome editing with CRISPR/Cas9. *Yeast*. 33 (10), 549–557.

Ferrari, K.J., Scelfo, A., Jammula, S., Cuomo, A., Barozzi, I., Stützer, A., Fischle, W., Bonaldi, T. & Pasini, D. (2014) Polycomb-dependent H3K27me1 and H3K27me2 regulate active transcription and enhancer fidelity. *Molecular cell*. 53 (1), 49–62.

Fire, A., Xu, S., Montgomery, M.K., Kostas, S.A., Driver, S.E. & Mello, C.C. (1998) Potent and specific genetic interference by double-stranded RNA in *Caenorhabditis elegans*. *Nature*. 391 (6669), 806–811.

Fischer, T., Cui, B., Dhakshnamoorthy, J., Zhou, M., Rubin, C., Zofall, M., Veenstra, T.D. & Grewal, S.I.S. (2009) Diverse roles of HP1 proteins in heterochromatin assembly and functions in fission yeast. *Proc Natl Acad Sci USA*. 106 (22), 8998–9003.

Fischle, W., Wang, Y., Jacobs, S.A., Kim, Y., Allis, C.D. & Khorasanizadeh, S. (2003) Molecular basis for the discrimination of repressive methyl-lysine marks in histone H3 by Polycomb and HP1 chromodomains. *Genes & development*. 17 (15), 1870–1881.

Fisher, M.C., Hawkins, N.J., Sanglard, D. & Gurr, S.J. (2018) Worldwide emergence of resistance to antifungal drugs challenges human health and food security. *Science*. 360 (6390), 739–742.

Flamm, W.G., Walker, P.M.B. & McCallum, M. (1969) Some properties of the single strands isolated from the DNA of the nuclear satellite of the mouse (*Mus musculus*). *Journal of molecular biology*. 40 (3), 423–443.

Flaus, A., Martin, D.M.A., Barton, G.J. & Owen-Hughes, T. (2006) Identification of multiple distinct Snf2 subfamilies with conserved structural motifs. *Nucleic acids research*. 34 (10), 2887–2905.

Fletcher, S.J., Boden, M., Mitter, N. & Carroll, B.J. (2018) SCRAM: a pipeline for fast index-free small RNA read alignment and visualization. *Bioinformatics*. 34 (15), 2670–2672.

Fogel, S. & Welch, J.W. (1982) Tandem gene amplification mediates copper resistance in yeast. *Proc Natl Acad Sci USA*. 79 (17), 5342.

Folco, H.D., Pidoux, A.L., Urano, T. & Allshire, R.C. (2008) Heterochromatin and RNAi are required to establish CENP-A chromatin at centromeres. *Science*. 319 (5859), 94–97.

Fornerod, M., Ohno, M., Yoshida, M. & Mattaj, I.W. (1997) CRM1 is an export receptor for leucine-rich nuclear export signals. *Cell*. 90 (6), 1051–1060.

Freitag, M., Hickey, P.C., Khlafallah, T.K., Read, N.D. & Selker, E.U. (2004) HP1 is essential for DNA methylation in neurospora. *Molecular cell*. 13 (3), 427–434.

Fulton, J.L., Dinas, P.C., Carrillo, A.E., Edsall, J.R., Ryan, E.J. & Ryan, E.J. (2018) Impact of genetic variability on physiological responses to caffeine in humans: a systematic review. *Nutrients*. 10 (10).

Galeote, V., Bigey, F., Beyne, E., Novo, M., Legras, J.-L., Casaregola, S. & Dequin, S. (2011) Amplification of a *Zygosaccharomyces bailii* DNA segment in wine yeast genomes by extrachromosomal circular DNA formation. *PloS one*. 6 (3), e17872.

Gallagher, P.S., Larkin, M., Thillainadesan, G., Dhakshnamoorthy, J., Balachandran, V., Xiao, H., Wellman, C., Chatterjee, R., Wheeler, D. & Grewal, S.I.S. (2018) Iron homeostasis regulates facultative heterochromatin assembly in adaptive genome control. *Nature structural & molecular biology*. 25 (5), 372–383.

Galupa, R. & Heard, E. (2018) X-chromosome inactivation: a crossroads between chromosome architecture and gene regulation. *Annu. Rev. Genet.* 52 (1), 535–566.

Garcia, J.F., Al-Sady, B. & Madhani, H.D. (2015) Intrinsic toxicity of unchecked heterochromatin spread is suppressed by redundant chromatin boundary runctions in *Schizosacchromyces pombe*. *G3*. 5 (7), 1453–1461.

Gendall, A.R., Levy, Y.Y., Wilson, A. & Dean, C. (2001) The VERNALIZATION 2 gene mediates the epigenetic regulation of vernalization in Arabidopsis. *Cell*. 107 (4), 525–535.

Gentner, N.E. & Werner, M.M. (1975) Repair in *Schizosaccharomyces pombe* as measured by recovery from caffeine enhancement of radiation-induced lethality. *Molecular & general genetics*. 142 (3), 171–183.

Gerace, E.L., Halic, M. & Moazed, D. (2010) The methyltransferase activity of $Clr4^{Suv39h}$ triggers RNAi independently of histone H3K9 methylation. *Molecular cell*. 39 (3), 360–372.

Goldberg, A.D., Allis, C.D. & Bernstein, E. (2007) Epigenetics: a landscape takes shape. *Cell*. 128 (4), 635–638.

Goll, M.G. & Bestor, T.H. (2005) Eukaryotic cytosine methyltransferases. *Annual review of biochemistry*. 74 (1), 481–514.

Gossen, M., Freundlieb, S., Bender, G., Muller, G., Hillen, W. & Bujard, H. (1995) Transcriptional activation by tetracyclines in mammalian cells. *Science*. 268 (5218), 1766.

Grewal, S.I. & Klar, A.J. (1997) A recombinationally repressed region between mat2 and mat3 loci shares homology to centromeric repeats and regulates directionality of mating-type switching in fission yeast. *Genetics*. 146 (4), 1221–1238.

Grewal, S.I., Bonaduce, M.J. & Klar, A.J. (1998) Histone deacetylase homologs regulate epigenetic inheritance of transcriptional silencing and chromosome segregation in fission yeast. *Genetics*. 150 (2), 563–576.

Grewal, S.I.S. & Jia, S. (2007) Heterochromatin revisited. *Nature reviews. Genetics*. 8 (1), 35–46.

Groth, A., Corpet, A., Cook, A.J.L., Roche, D., Bartek, J., Lukas, J. & Almouzni, G. (2007) Regulation of replication fork progression through histone supply and demand. *Science*. 318 (5858), 1928–1931.

Groth, A., Rocha, W., Verreault, A. & Almouzni, G. (2007) Chromatin challenges during DNA replication and repair. *Cell*. 128 (4), 721–733.

Gu, T. & Elgin, S.C.R. (2013) Maternal depletion of Piwi, a component of the RNAi system, impacts heterochromatin formation in Drosophila. *PLoS genetics*. 9 (9), e1003780.

Gunawardane, L.S., Saito, K., Nishida, K.M., Miyoshi, K., Kawamura, Y., Nagami, T., Siomi, H. & Siomi, M.C. (2007) A slicer-mediated mechanism for repeat-associated siRNA 5' end formation in Drosophila. *Science*. 315 (5818), 1587–1590.

Gurard-Levin, Z.A., Quivy, J.-P. & Almouzni, G. (2014) Histone chaperones: assisting histone traffic and nucleosome dynamics. *Annual review of biochemistry*. 83 (1), 487–517.

Haldar, S., Saini, A., Nanda, J.S., Saini, S. & Singh, J. (2011) Role of Swi6/HP1 self-association-mediated recruitment of Clr4/Suv39 in establishment and maintenance of heterochromatin in fission yeast. *The Journal of biological chemistry*. 286 (11), 9308–9320.

Halic, M. & Moazed, D. (2010) Dicer-independent primal RNAs trigger RNAi and heterochromatin formation. *Cell*. 140 (4), 504–516.

Hall, I.M., Shankaranarayana, G.D., Noma, K.-I., Ayoub, N., Cohen, A. & Grewal, S.I.S. (2002) Establishment and maintenance of a heterochromatin domain. *Science*. 297 (5590), 2232–2237.

Hamamoto, H., Hasegawa, K., Nakaune, R., Lee, Y.J., Makizumi, Y., Akutsu, K. & Hibi, T. (2000) Tandem repeat of a transcriptional enhancer upstream of the sterol 14alpha-demethylase gene (CYP51) in *Penicillium digitatum*. *Applied and environmental microbiology*. 66 (8), 3421–3426.

Hamilton, A.J. & Baulcombe, D.C. (1999) A species of small antisense RNA in posttranscriptional gene silencing in plants. *Science*. 286 (5441), 950–952.

Hamilton, D.L. & Abremski, K. (1984) Site-specific recombination by the bacteriophage P1 lox-Cre system. Cre-mediated synapsis of two lox sites. *Journal of molecular biology*. 178 (2), 481–486.

Hansen, K.H., Bracken, A.P., Pasini, D., Dietrich, N., Gehani, S.S., Monrad, A., Rappsilber, J., Lerdrup, M. & Helin, K. (2008) A model for transmission of the H3K27me3 epigenetic mark. *Nature cell biology*. 10 (11), 1291–1300.

Hansen, K.R., Hazan, I., Shanker, S., Watt, S., Verhein-Hansen, J., Bähler, J., Martienssen, R.A., Partridge, J.F., Cohen, A. & Thon, G. (2011) H3K9me-independent gene silencing in fission yeast heterochromatin by Clr5 and histone deacetylases. *PLoS genetics*. 7 (1), e1001268.

Hanson, S.J. & Wolfe, K.H. (2017) An evolutionary perspective on yeast mating-type switching. *Genetics*. 206 (1), 9–32.

Harigaya, Y., Tanaka, H., Yamanaka, S., Tanaka, K., Watanabe, Y., Tsutsumi, C., Chikashige, Y., Hiraoka, Y., Yamashita, A. & Yamamoto, M. (2006) Selective elimination of messenger RNA prevents an incidence of untimely meiosis. *Nature*. 442 (7098), 45–50.

Harvey, Z.H., Chakravarty, A.K., Futia, R.A. & Jarosz, D.F. (2020) A prion epigenetic switch establishes an active chromatin state. *Cell*. 180 (5), 928–940.e14.

Hathaway, N.A., Bell, O., Hodges, C., Miller, E.L., Neel, D.S. & Crabtree, G.R. (2012) Dynamics and memory of heterochromatin in living cells. *Cell*. 149 (7), 1447–1460.

Hawkins, R.D., Hon, G.C., Lee, L.K., Ngo, Q., Lister, R., Pelizzola, M., Edsall, L.E., Kuan, S., Luu, Y., Klugman, S., Antosiewicz-Bourget, J., Ye, Z., Espinoza, C., Agarwahl, S., Shen, L., Ruotti, V., Wang, W., Stewart, R., Thomson, J.A., et al. (2010) Distinct epigenomic landscapes of pluripotent and lineage-committed human cells. *Cell stem cell*. 6 (5), 479–491.

Hayashi, A. & Tanaka, K. (2019) Short-homology-mediated CRISPR/Cas9-based method for genome editing in fission yeast. *G3.* 9 (4), 1153–1163.

Hayles, J., Wood, V., Jeffery, L., Hoe, K.-L., Kim, D.-U., Park, H.-O., Salas-Pino, S., Heichinger, C. & Nurse, P. (2013) A genome-wide resource of cell cycle and cell shape genes of fission yeast. *Open biology*. 3 (5), 130053.

Heard, E. & Martienssen, R.A. (2014) Transgenerational epigenetic inheritance: myths and mechanisms. *Cell*. 157 (1), 95–109.

Heard, E., Rougeulle, C., Arnaud, D., Avner, P., Allis, C.D. & Spector, D.L. (2001) Methylation of histone H3 at Lys-9 is an early mark on the X chromosome during X inactivation. *Cell*. 107 (6), 727–738.

Hecht, A., Strahl-Bolsinger, S. & Grunstein, M. (1996) Spreading of transcriptional repressor SIR3 from telomeric heterochromatin. *Nature*. 383 (6595), 92–96.

Heitz, E. (1928) Das heterochromatin der moose. I. *Jahrb Wiss Bot.* 69, 762–818.

Hentges, P., Van Driessche, B., Tafforeau, L., Vandenhaute, J. & Carr, A.M. (2005) Three novel antibiotic marker cassettes for gene disruption and marker switching in *Schizosaccharomyces pombe*. *Yeast*. 22 (13), 1013–1019.

Hepworth, J., Antoniou-Kourounioti, R.L., Berggren, K., Selga, C., Tudor, E.H., Yates, B., Cox, D., Collier Harris, B.R., Irwin, J.A., Howard, M., Säll, T., Holm, S. & Dean, C. (2020) Natural variation in autumn expression is the major adaptive determinant distinguishing Arabidopsis *FLC* haplotypes. *eLife*. 9, e57671

Holla, S., Dhakshnamoorthy, J., Folco, H.D., Balachandran, V., Xiao, H., Sun, L.-L., Wheeler, D., Zofall, M. & Grewal, S.I.S. (2020) Positioning heterochromatin at the nuclear periphery suppresses histone turnover to promote epigenetic inheritance. *Cell*. 180 (1), 150–164.e15.

Holliday, R. (2006) Epigenetics: a historical overview. *Epigenetics*. 1 (2), 76–80.

Holliday, R. & Pugh, J.E. (1975) DNA modification mechanisms and gene activity during development. *Science*. 187 (4173), 226–232.

Holoch, D. & Moazed, D. (2015) RNA-mediated epigenetic regulation of gene expression. *Nature reviews. Genetics*. 16 (2), 71–84.

Hong, E.-J.E., Villén, J., Gerace, E.L., Gygi, S.P. & Moazed, D. (2005) A cullin E3 ubiquitin ligase complex associates with Rik1 and the Clr4 histone H3-K9 methyltransferase and is required for RNAi-mediated heterochromatin formation. *RNA biology*. 2 (3), 106–111.

Horn, P.J., Bastie, J.-N. & Peterson, C.L. (2005) A Rik1-associated, cullin-dependent E3 ubiquitin ligase is essential for heterochromatin formation. *Genes & development*. 19 (14), 1705–1714.

Horowitz, H. & Haber, J.E. (1985) Identification of autonomously replicating circular subtelomeric Y' elements in *Saccharomyces cerevisiae*. *Molecular and cellular biology*. 5 (9), 2369–2380.

Hottinger-Werlen, A., Schaack, J., Lapointe, J., Mao, J., Nichols, M. & Söll, D. (1985) Dimeric tRNA gene arrangement in *Schizosaccharomyces pombe* allows increased expression of the downstream gene. *Nucleic acids research*. 13 (24), 8739–8747.

Houseley, J., LaCava, J. & Tollervey, D. (2006) RNA-quality control by the exosome. *Nature reviews. Molecular cell biology*. 7 (7), 529–539.

Hsu, P.D., Lander, E.S. & Zhang, F. (2014) Development and applications of CRISPR-Cas9 for genome engineering. *Cell*. 157 (6), 1262–1278.

Hu, L., Fang, Y., Hayafuji, T., Ma, Y. & Furuyashiki, T. (2015) Azoles activate Atf1-mediated transcription through MAP kinase pathway for antifungal effects in fission yeast. *Genes to cells.* 20 (9), 695–705.

Hull, R.M., Cruz, C., Jack, C.V. & Houseley, J. (2017) Environmental change drives accelerated adaptation through stimulated copy number variation. *PLoS biology*. 15 (6), e2001333.

Hull, R.M., King, M., Pizza, G., Krueger, F., Vergara, X. & Houseley, J. (2019) Transcription-induced formation of extrachromosomal DNA during yeast ageing. *PLoS biology*. 17 (12), e3000471.

Hunter, T. (2007) The age of crosstalk: phosphorylation, ubiquitination, and beyond. *Molecular cell*. 28 (5), 730–738.

Hyland, E.M., Molina, H., Poorey, K., Jie, C., Xie, Z., Dai, J., Qian, J., Bekiranov, S., Auble, D.T., Pandey, A. & Boeke, J.D. (2011) An evolutionarily 'young' lysine residue in histone H3 attenuates transcriptional output in *Saccharomyces cerevisiae*. *Genes & development*. 25 (12), 1306–1319.

Irvine, D.V., Zaratiegui, M., Tolia, N.H., Goto, D.B., Chitwood, D.H., Vaughn, M.W., Joshua-Tor, L. & Martienssen, R.A. (2006) Argonaute slicing is required for heterochromatic silencing and spreading. *Science*. 313 (5790), 1134–1137.

Ito, T., Bulger, M., Pazin, M.J., Kobayashi, R. & Kadonaga, J.T. (1997) ACF, an ISWI-containing and ATP-utilizing chromatin assembly and remodeling factor. *Cell*. 90 (1), 145–155.

Ivanova, A.V., Bonaduce, M.J., Ivanov, S.V. & Klar, A.J. (1998) The chromo and SET domains of the Clr4 protein are essential for silencing in fission yeast. *Nature Genetics*. 19 (2), 192–195.

Jackson, J.P., Lindroth, A.M., Cao, X. & Jacobsen, S.E. (2002) Control of CpNpG DNA methylation by the KRYPTONITE histone H3 methyltransferase. *Nature*. 416 (6880), 556–560.

Jacobs, J.J.L., Kieboom, K., Marino, S., DePinho, R.A. & van Lohuizen, M. (1999) The oncogene and Polycomb-group gene *bmi-1* regulates cell proliferation and senescence through the *ink4a* locus. *Nature*. 397 (6715), 164–168.

Jacobs, J.Z., Ciccaglione, K.M., Tournier, V. & Zaratiegui, M. (2014) Implementation of the CRISPR-Cas9 system in fission yeast. *Nature communications*. 55344.

Jacobsen, S.E. (1997) Hypermethylated SUPERMAN epigenetic alleles in Arabidopsis. *Science*. 277 (5329), 1100–1103.

Jara, M., Vivancos, A.P., Calvo, I.A., Moldón, A., Sansó, M. & Hidalgo, E. (2007) The peroxiredoxin Tpx1 is essential as a H2O2 scavenger during aerobic growth in fission yeast. *Molecular biology of the cell*. 18 (6), 2288–2295.

Jarosz, D.F., Brown, J.C.S., Walker, G.A., Datta, M.S., Ung, W.L., Lancaster, A.K., Rotem, A., Chang, A., Newby, G.A., Weitz, D.A., Bisson, L.F. & Lindquist, S. (2014) Cross-kingdom chemical communication drives a heritable, mutually beneficial prion-based transformation of metabolism. *Cell*. 158 (5), 1083–1093.

Jarosz, D.F., Lancaster, A.K., Brown, J.C.S. & Lindquist, S. (2014) An evolutionarily conserved prion-like element converts wild fungi from metabolic specialists to generalists. *Cell*. 158 (5), 1072–1082.

Jeffares, D.C., Jolly, C., Hoti, M., Speed, D., Shaw, L., Rallis, C., Balloux, F., Dessimoz, C., Bähler, J. & Sedlazeck, F.J. (2017) Transient structural variations have strong effects on quantitative traits and reproductive isolation in fission yeast. *Nature communications*. 8 (1), 1–11.

Jeffares, D.C., Rallis, C., Rieux, A., Speed, D., Převorovský, M., Mourier, T., Marsellach, F.X., Iqbal, Z., Lau, W., Cheng, T.M.K., Pracana, R., Mülleder, M., Lawson, J.L.D., Chessel, A., Bala, S., Hellenthal, G., O'Fallon, B., Keane, T., Simpson, J.T., et al. (2015) The genomic and phenotypic diversity of *Schizosaccharomyces pombe*. *Nature Genetics*. 47 (3), 235–241.

Jeggo, P.A. & Holliday, R. (1986) Azacytidine-induced reactivation of a DNA repair gene in Chinese hamster ovary cells. *Molecular and cellular biology*. 6 (8), 2944–2949.

Jenuwein, T. & Allis, C.D. (2001) Translating the histone code. *Science*. 293 (5532), 1074–1080.

Jia, S., Kobayashi, R. & Grewal, S.I.S. (2005) Ubiquitin ligase component Cul4 associates with Clr4 histone methyltransferase to assemble heterochromatin. *Nature cell biology*. 7 (10), 1007–1013.

Jia, S., Noma, K.-I. & Grewal, S.I.S. (2004) RNAi-independent heterochromatin nucleation by the stress-activated ATF/CREB family proteins. *Science*. 304 (5679), 1971–1976.

Jih, G., Iglesias, N., Currie, M.A., Bhanu, N.V., Paulo, J.A., Gygi, S.P., Garcia, B.A. & Moazed, D. (2017) Unique roles for histone H3K9me states in RNAi and heritable silencing of transcription. *Nature*. 547 (7664), 463–467.

Jinek, M., Chylinski, K., Fonfara, I., Hauer, M., Doudna, J.A. & Charpentier, E. (2012) A programmable dual-RNA-guided DNA endonuclease in adaptive bacterial immunity. *Science*. 337 (6096), 816–821.

Joh, R.I., Khanduja, J.S., Calvo, I.A., Mistry, M., Palmieri, C.M., Savol, A.J., Ho Sui, S.J., Sadreyev, R.I., Aryee, M.J. & Motamedi, M. (2016) Survival in quiescence requires the euchromatic deployment of Clr4/Suv39h by Argonaute-associated small RNAs. *Molecular cell*. 64 (6), 1088–1101.

Kagansky, A., Folco, H.D., Almeida, R., Pidoux, A.L., Boukaba, A., Simmer, F., Urano, T., Hamilton, G.L. & Allshire, R.C. (2009) Synthetic heterochromatin bypasses RNAi and centromeric repeats to establish functional centromeres. *Science*. 324 (5935), 1716–1719.

Kanke, M., Nishimura, K., Kanemaki, M., Kakimoto, T., Takahashi, T.S., Nakagawa, T. & Masukata, H. (2011) Auxin-inducible protein depletion system in fission yeast. *BMC cell biology*. 12 (1), 8.

Kanoh, J., Sadaie, M., Urano, T. & Ishikawa, F. (2005) Telomere binding protein Taz1 establishes Swi6 heterochromatin independently of RNAi at telomeres. *Current Biology*. 15 (20), 1808–1819.

Kato, H., Goto, D.B., Martienssen, R.A., Urano, T., Furukawa, K. & Murakami, Y. (2005) RNA polymerase II is required for RNAi-dependent heterochromatin assembly. *Science*. 309 (5733), 467–469.

Kelley, L.A., Mezulis, S., Yates, C.M., Wass, M.N. & Sternberg, M.J.E. (2015) The Phyre2 web portal for protein modeling, prediction and analysis. *Nature protocols*. 10 (6), 845–858.

Kidd, J.M., Cooper, G.M., Donahue, W.F., Hayden, H.S., Sampas, N., Graves, T., Hansen, N., Teague, B., Alkan, C., Antonacci, F., Haugen, E., Zerr, T., Yamada, N.A., Tsang, P., Newman, T.L., Tüzün, E., Cheng, Z., Ebling, H.M., Tusneem, N., et al. (2008) Mapping and sequencing of structural variation from eight human genomes. *Nature*. 453 (7191), 56–64.

Kim, D.-H. & Sung, S. (2014) Polycomb-mediated gene silencing in *Arabidopsis thaliana*. *Molecules and cells*. 37 (12), 841–850.

Kim, D.-U., Hayles, J., Kim, D., Wood, V., Park, H.-O., Won, M., Yoo, H.-S., Duhig, T., Nam, M., Palmer, G., Han, S., Jeffery, L., Baek, S.-T., Lee, H., Shim, Y.S., Lee, M., Kim, L., Heo, K.-S., Noh, E.J., et al. (2010) Analysis of a genome-wide set of gene deletions in the fission yeast *Schizosaccharomyces pombe*. *Nature biotechnology*. 28 (6), 617–623.

Kit, S. (1961) Equilibrium sedimentation in density gradients of DNA preparations from animal tissues. *Journal of molecular biology*. 3 (6), 711–IN2.

Klar, A.J. & Bonaduce, M.J. (1991) *swi6*$^{+}$, a gene required for mating-type switching, prohibits meiotic recombination in the mat2-mat3 ‘cold spot’ of fission yeast. *Genetics*. 129 (4), 1033–1042.

Klironomos, F.D., Berg, J. & Collins, S. (2013) How epigenetic mutations can affect genetic evolution: model and mechanism. *BioEssays.* 35 (6), 571–578.

Kloc, A., Zaratiegui, M., Nora, E. & Martienssen, R. (2008) RNA interference guides histone modification during the S phase of chromosomal replication. *Current Biology*. 18 (7), 490–495.

Klose, R.J. & Zhang, Y. (2007) Regulation of histone methylation by demethylimination and demethylation. *Nature reviews. Molecular cell biology*. 8 (4), 307–318.

Klosin, A., Casas, E., Hidalgo-Carcedo, C., Vavouri, T. & Lehner, B. (2017) Transgenerational transmission of environmental information in *C. elegans*. *Science*. 356 (6335), 320–323.

Kornberg, R.D. (1974) Chromatin structure: a repeating unit of histones and DNA. *Science*. 184 (4139), 868–871.

Kornberg, R.D. & Lorch, Y. (1999) Twenty-five years of the nucleosome, fundamental particle of the eukaryote chromosome. *Cell*. 98 (3), 285–294.

Kornberg, R.D. & Thomas, J.O. (1974) Chromatin structure; oligomers of the histones. *Science*. 184 (4139), 865–868.

Kouzarides, T. (2007) Chromatin modifications and their function. *Cell*. 128 (4), 693–705.

Kowalik, K.M., Shimada, Y., Flury, V., Stadler, M.B., Batki, J. & Bühler, M. (2015) The Paf1 complex represses small-RNA-mediated epigenetic gene silencing. *Nature*. 520 (7546), 248–252.

Kronholm, I. & Collins, S. (2015) Epigenetic mutations can both help and hinder adaptive evolution. *Molecular ecology*. 25 (8), 1856–1868.

Kudo, N., Taoka, H., Toda, T., Yoshida, M. & Horinouchi, S. (1999) A novel nuclear export signal sensitive to oxidative stress in the fission yeast transcription factor Pap1. *The Journal of biological chemistry*. 274 (21), 15151–15158.

Kueng, S., Oppikofer, M. & Gasser, S.M. (2013) SIR proteins and the assembly of silent chromatin in budding yeast. *Annu. Rev. Genet.* 47 (1), 275–306.

Kumada, K., Yanagida, M. & Toda, T. (1996) Caffeine-resistance in fission yeast is caused by mutations in a single essential gene, *crm1*$^{+}$. *Molecular & general genetics*. 250 (1), 59–68.

Kumagai, A., Guo, Z., Emami, K.H., Wang, S.X. & Dunphy, W.G. (1998) The Xenopus Chk1 protein kinase mediates a caffeine-sensitive pathway of checkpoint control in cell-free extracts. *The Journal of cell biology*. 142 (6), 1559–1569.

Kühl, I., Dujeancourt, L., Gaisne, M., Herbert, C.J. & Bonnefoy, N. (2011) A genome wide study in fission yeast reveals nine PPR proteins that regulate mitochondrial gene expression. *Nucleic acids research*. 39 (18), 8029–8041.

Kwon, E.-J.G., Laderoute, A., Chatfield-Reed, K., Vachon, L., Karagiannis, J. & Chua, G. (2012) Deciphering the transcriptional-regulatory network of flocculation in *Schizosaccharomyces pombe*. *PLoS genetics*. 8 (12), e1003104.

Labbe, S., Peña, M.M., Fernandes, A.R. & Thiele, D.J. (1999) A copper-sensing transcription factor regulates iron uptake genes in

Schizosaccharomyces pombe. *The Journal of biological chemistry*. 274 (51), 36252–36260.

Lachner, M., O'Carroll, D., Rea, S., Mechtler, K. & Jenuwein, T. (2001) Methylation of histone H3 lysine 9 creates a binding site for HP1 proteins. *Nature*. 410 (6824), 116–120.

Langmead, B. & Salzberg, S.L. (2012) Fast gapped-read alignment with Bowtie 2. *Nature methods*. 9 (4), 357–359.

Laprell, F., Finkl, K. & Müller, J. (2017) Propagation of Polycomb-repressed chromatin requires sequence-specific recruitment to DNA. *Science*. 356 (6333), 85–88.

Larson, A.G., Elnatan, D., Keenen, M.M., Trnka, M.J., Johnston, J.B., Burlingame, A.L., Agard, D.A., Redding, S. & Narlikar, G.J. (2017) Liquid droplet formation by HP1α suggests a role for phase separation in heterochromatin. *Nature*. 547 (7662), 236–240.

Law, J.A. & Jacobsen, S.E. (2010) Establishing, maintaining and modifying DNA methylation patterns in plants and animals. *Nature reviews. Genetics*. 11 (3), 204–220.

Lawrence, Michael, Huber, W., Pagès, H., Aboyoun, P., Carlson, M., Gentleman, R., Morgan, M.T. & Carey, V.J. (2013) Software for computing and annotating genomic ranges. *PLoS computational biology*. 9 (8), e1003118.

Lawrence, Moyra, Daujat, S. & Schneider, R. (2016) Lateral thinking: how histone modifications regulate gene expression. *Trends in genetics*. 32 (1), 42–56.

Lee, H.-G., Kahn, T.G., Simcox, A., Schwartz, Y.B. & Pirrotta, V. (2015) Genome-wide activities of Polycomb complexes control pervasive transcription. *Genome research*. 25 (8), 1170–1181.

Lee, N.N., Chalamcharla, V.R., Reyes-Turcu, F., Mehta, S., Zofall, M., Balachandran, V., Dhakshnamoorthy, J., Taneja, N., Yamanaka, S., Zhou, M. & Grewal, S.I.S. (2013) Mtr4-like protein coordinates nuclear RNA processing for heterochromatin assembly and for telomere maintenance. *Cell*. 155 (5), 1061–1074.

Lehnertz, B., Ueda, Y., Derijck, A.A.H.A., Braunschweig, U., Perez-Burgos, L., Kubicek, S., Chen, T., Li, E., Jenuwein, T. & Peters, A.H.F.M. (2003)

Suv39h-mediated histone H3 lysine 9 methylation directs DNA methylation to major satellite repeats at pericentric heterochromatin. *Current Biology*. 13 (14), 1192–1200.

Leroux, P., Albertini, C., Gautier, A., Gredt, M. & Walker, A.-S. (2007) Mutations in the CYP51 gene correlated with changes in sensitivity to sterol 14 alpha-demethylation inhibitors in field isolates of *Mycosphaerella graminicola*. *Pest management science*. 63 (7), 688–698.

Leupold, U. (1949) Die vererbung von homothallie und heterothallie bei *Schizosaccharomyces pombe*. *Compt. Rend. Trav. Lab. Carlsberg. Ser. Physiol*. 24, 381–480

Lewis, E.B. (1978) A gene complex controlling segmentation in Drosophila. *Nature*. 276 (5688), 565–570.

Li, Heng, Handsaker, B., Wysoker, A., Fennell, T., Ruan, J., Homer, N., Marth, G., Abecasis, G., Durbin, R. 1000 Genome Project Data Processing Subgroup (2009) The Sequence Alignment/Map format and SAMtools. *Bioinformatics*. 25 (16), 2078–2079.

Li, Hua, Hou, J., Bai, L., Hu, C., Tong, P., Kang, Y., Zhao, X. & Shao, Z. (2015) Genome-wide analysis of core promoter structures in *Schizosaccharomyces pombe* with DeepCAGE. *RNA biology*. 12 (5), 525–537.

Libuda, D.E. & Winston, F. (2006) Amplification of histone genes by circular chromosome formation in *Saccharomyces cerevisiae*. *Nature*. 443 (7114), 1003–1007.

Liu, J., Carmell, M.A., Rivas, F.V., Marsden, C.G., Thomson, J.M., Song, J.-J., Hammond, S.M., Joshua-Tor, L. & Hannon, G.J. (2004) Argonaute2 is the catalytic engine of mammalian RNAi. *Science*. 305 (5689), 1437–1441.

Liu, Q., Yao, F., Jiang, G., Xu, M., Chen, S., Zhou, L., Sakamoto, N., Kuno, T. & Fang, Y. (2018) Dysfunction of Prohibitin 2 results in reduced susceptibility to multiple antifungal drugs via activation of the oxidative stress-responsive transcription factor Pap1 in fission yeast. *Antimicrobial agents and chemotherapy*. 62 (11).

Lock, A., Rutherford, K., Harris, M.A., Hayles, J., Oliver, S.G., Bähler, J. & Wood, V. (2019) PomBase 2018: user-driven reimplementation of the fission yeast database provides rapid and intuitive access to diverse, interconnected information. *Nucleic acids research*. 47 (D1), D821–D827.

Longmuir, S., Akhtar, N. & MacNeill, S.A. (2019) Unexpected insertion of carrier DNA sequences into the fission yeast genome during CRISPR-Cas9 mediated gene deletion. *BMC research notes*. 12 (1), 191.

Loprieno, N., Barale, R. & Baroncelli, S. (1974) Genetic effects of caffeine. *Mutation research*. 26 (2), 83–87.

Lorentz, A., Ostermann, K., Fleck, O. & Schmidt, H. (1994) Switching gene *swi6*$^{+}$, involved in repression of silent mating-type loci in fission yeast, encodes a homologue of chromatin-associated proteins from Drosophila and mammals. *Gene*. 143 (1), 139–143.

Love, M.I., Huber, W. & Anders, S. (2014) Moderated estimation of fold change and dispersion for RNA-seq data with DESeq2. *Genome biology*. 15 (12), 550.

Lu, J. & Gilbert, D.M. (2007) Proliferation-dependent and cell cycle regulated transcription of mouse pericentric heterochromatin. *The Journal of cell biology*. 179 (3), 411–421.

Lu, X., Simon, M.D., Chodaparambil, J.V., Hansen, J.C., Shokat, K.M. & Luger, K. (2008) The effect of H3K79 dimethylation and H4K20 trimethylation on nucleosome and chromatin structure. *Nature structural & molecular biology*. 15 (10), 1122–1124.

Luger, K., Mäder, A.W., Richmond, R.K., Sargent, D.F. & Richmond, T.J. (1997) Crystal structure of the nucleosome core particle at 2.8 A resolution. *Nature*. 389 (6648), 251–260.

Lustig, A.J., Liu, C., Zhang, C. & Hanish, J.P. (1996) Tethered Sir3p nucleates silencing at telomeres and internal loci in *Saccharomyces cerevisiae*. *Molecular and cellular biology*. 16 (5), 2483.

Malone, C.D., Brennecke, J., Dus, M., Stark, A., McCombie, W.R., Sachidanandam, R. & Hannon, G.J. (2009) Specialized piRNA pathways act in germline and somatic tissues of the Drosophila ovary. *Cell*. 137 (3), 522–535.

Marguerat, S., Schmidt, A., Codlin, S., Chen, W., Aebersold, R. & Bähler, J. (2012) Quantitative analysis of fission yeast transcriptomes and proteomes in proliferating and quiescent cells. *Cell*. 151 (3), 671–683.

Margueron, R., Justin, N., Ohno, K., Sharpe, M.L., Son, J., Drury, W.J., Voigt, P., Martin, S.R., Taylor, W.R., De Marco, V., Pirrotta, V., Reinberg, D. &

Gamblin, S.J. (2009) Role of the polycomb protein EED in the propagation of repressive histone marks. *Nature*. 461 (7265), 762–767.

Martienssen, R. & Moazed, D. (2015) RNAi and heterochromatin assembly. *Cold Spring Harbor perspectives in biology*. 7 (8), a019323.

Martire, S. & Banaszynski, L.A. (2020) The roles of histone variants in fine-tuning chromatin organization and function. *Nature reviews. Molecular cell biology*. 21 (9), 522–541.

Massardo, D.R., Del Giudice, L., Manna, F. & Wolf, K. (1982) Extrachromosomal inheritance of nalidixic acid resistance in the petite negative yeast *Schizosaccharomyces pombe*. *Molecular & general genetics.* 187 (1), 96–100.

Masumoto, H., Hawke, D., Kobayashi, R. & Verreault, A. (2005) A role for cell-cycle-regulated histone H3 lysine 56 acetylation in the DNA damage response. *Nature*. 436 (7048), 294–298.

Mata, J., Lyne, R., Burns, G. & Bähler, J. (2002) The transcriptional program of meiosis and sporulation in fission yeast. *Nature Genetics*. 32 (1), 143–147.

Matsui, T., Leung, D., Miyashita, H., Maksakova, I.A., Miyachi, H., Kimura, H., Tachibana, M., Lorincz, M.C. & Shinkai, Y. (2010) Proviral silencing in embryonic stem cells requires the histone methyltransferase ESET. *Nature*. 464 (7290), 927–931.

Matsuo, Y. & Kawamukai, M. (2017) cAMP-dependent protein kinase involves calcium tolerance through the regulation of Prz1 in *Schizosaccharomyces pombe. Bioscience, biotechnology, and biochemistry*. 81 (2), 231–241.

Matsuyama, A., Arai, R., Yashiroda, Y., Shirai, A., Kamata, A., Sekido, S., Kobayashi, Y., Hashimoto, A., Hamamoto, M., Hiraoka, Y., Horinouchi, S. & Yoshida, M. (2006) ORFeome cloning and global analysis of protein localization in the fission yeast *Schizosaccharomyces pombe*. *Nature biotechnology*. 24 (7), 841–847.

Matsuzawa, T., Yoritsune, K.-I. & Takegawa, K. (2012) MADS box transcription factor Mbx2/Pvg4 regulates invasive growth and flocculation by inducing *gsf2*$^{+}$ expression in fission yeast. *Eukaryotic Cell*. 11 (2), 151–158.

Mayer, W., Niveleau, A., Walter, J., Fundele, R. & Haaf, T. (2000) Demethylation of the zygotic paternal genome. *Nature*. 403 (6769), 501–502.

McCarroll, S.A. & Altshuler, D.M. (2007) Copy-number variation and association studies of human disease. *Nature Genetics*. 39 (7 Suppl), S37–42.

McKenna, A., Hanna, M., Banks, E., Sivachenko, A., Cibulskis, K., Kernytsky, A., Garimella, K., Altshuler, D., Gabriel, S., Daly, M. & DePristo, M.A. (2010) The Genome Analysis Toolkit: a MapReduce framework for analyzing next-generation DNA sequencing data. *Genome research*. 20 (9), 1297–1303.

McLaren, W., Gil, L., Hunt, S.E., Riat, H.S., Ritchie, G.R.S., Thormann, A., Flicek, P. & Cunningham, F. (2016) The Ensembl variant effect predictor. *Genome biology*. 17 (1), 122.

Mizuguchi, G., Shen, X., Landry, J., Wu, W.-H., Sen, S. & Wu, C. (2004) ATP-driven exchange of histone H2AZ variant catalyzed by SWR1 chromatin remodeling complex. *Science*. 303 (5656), 343–348.

Morgan, H.D., Sutherland, H.G., Martin, D.I. & Whitelaw, E. (1999) Epigenetic inheritance at the agouti locus in the mouse. *Nature Genetics*. 23 (3), 314–318.

Morrison, D.K. (2012) MAP kinase pathways. *Cold Spring Harbor perspectives in biology*. 4 (11), a011254.

Motamedi, M.R., Hong, E.-J.E., Li, X., Gerber, S., Denison, C., Gygi, S. & Moazed, D. (2008) HP1 proteins form distinct complexes and mediate heterochromatic gene silencing by nonoverlapping mechanisms. *Molecular cell*. 32 (6), 778–790.

Motamedi, M.R., Verdel, A., Colmenares, S.U., Gerber, S.A., Gygi, S.P. & Moazed, D. (2004) Two RNAi complexes, RITS and RDRC, physically interact and localize to noncoding centromeric RNAs. *Cell*. 119 (6), 789–802.

Muller, H.J. (1930) Types of visible variations induced by X-rays inDrosophila. *Journal of Genetics*. 22 (3), 299–334.

Murakami, H. & Okayama, H. (1995) A kinase from fission yeast responsible for blocking mitosis in S phase. *Nature*. 374 (6525), 817–819.

Müller, J. & Verrijzer, P. (2009) Biochemical mechanisms of gene regulation by polycomb group protein complexes. *Current opinion in genetics & development*. 19 (2), 150–158.

Müller, J., Hart, C.M., Francis, N.J., Vargas, M.L., Sengupta, A., Wild, B., Miller, E.L., O'Connor, M.B., Kingston, R.E. & Simon, J.A. (2002) Histone methyltransferase activity of a Drosophila Polycomb group repressor complex. *Cell*. 111 (2), 197–208.

Mylne, J.S., Barrett, L., Tessadori, F., Mesnage, S., Johnson, L., Bernatavichute, Y.V., Jacobsen, S.E., Fransz, P. & Dean, C. (2006) LHP1, the Arabidopsis homologue of HETEROCHROMATIN PROTEIN1, is required for epigenetic silencing of *FLC*. *Proc Natl Acad Sci USA*. 103 (13), 5012–5017.

Møller, H.D., Parsons, L., Jørgensen, T.S., Botstein, D. & Regenberg, B. (2015) Extrachromosomal circular DNA is common in yeast. *Proc Natl Acad Sci USA*. 112 (24), E3114–22.

Nagao, K., Taguchi, Y., Arioka, M., Kadokura, H., Takatsuki, A., Yoda, K. & Yamasaki, M. (1995) *bfr1*$^{+}$, a novel gene of *Schizosaccharomyces pombe* which confers brefeldin A resistance, is structurally related to the ATP-binding cassette superfamily. *Journal of bacteriology*. 177 (6), 1536–1543.

Nakayama, J., Rice, J.C., Strahl, B.D., Allis, C.D. & Grewal, S.I. (2001) Role of histone H3 lysine 9 methylation in epigenetic control of heterochromatin assembly. *Science*. 292 (5514), 110–113.

Nakayama, J.-I., Xiao, G., Noma, K.-I., Malikzay, A., Bjerling, P., Ekwall, K., Kobayashi, R. & Grewal, S.I.S. (2003) Alp13, an MRG family protein, is a component of fission yeast Clr6 histone deacetylase required for genomic integrity. *The EMBO journal*. 22 (11), 2776–2787.

Navrátilová, A., Koblízková, A. & Macas, J. (2008) Survey of extrachromosomal circular DNA derived from plant satellite repeats. *BMC plant biology*. 8 (1), 90–13.

National Center for Biotechnology Information. PubChem compound summary for CID 784, hydrogen peroxide. *PubChem*. Accessed 26 October 2020.

Ng, H.H., Ciccone, D.N., Morshead, K.B., Oettinger, M.A. & Struhl, K. (2003) Lysine-79 of histone H3 is hypomethylated at silenced loci in yeast and mammalian cells: a potential mechanism for position-effect variegation. *Proc Natl Acad Sci USA*. 100 (4), 1820–1825.

Ng, H.H., Feng, Q., Wang, H., Erdjument-Bromage, H., Tempst, P., Zhang, Y. & Struhl, K. (2002) Lysine methylation within the globular domain of histone H3 by Dot1 is important for telomeric silencing and Sir protein association. *Genes & development*. 16 (12), 1518–1527.

Ng, S.-F., Lin, R.C.Y., Laybutt, D.R., Barres, R., Owens, J.A. & Morris, M.J. (2010) Chronic high-fat diet in fathers programs β-cell dysfunction in female rat offspring. *Nature*. 467 (7318), 963–966.

Nicolas, E., Yamada, T., Cam, H.P., FitzGerald, P.C., Kobayashi, R. & Grewal, S.I.S. (2007) Distinct roles of HDAC complexes in promoter silencing, antisense suppression and DNA damage protection. *Nature structural & molecular biology*. 14 (5), 372–380.

Nimmo, E.R., Pidoux, A.L., Perry, P.E. & Allshire, R.C. (1998) Defective meiosis in telomere-silencing mutants of *Schizosaccharomyces pombe*. *Nature*. 392 (6678), 825–828.

Nishikawa, K. & Kinjo, A.R. (2018) Mechanism of evolution by genetic assimilation. *Biophysical reviews*. 10 (2), 667–676.

Niwa, O. & Yanagida, M. (1985) Triploid meiosis and aneuploidy in *Schizosaccharomyces pombe*: an unstable aneuploid disomic for chromosome III. *Current genetics*. 9 (6), 463–470.

Niwa, O., Matsumoto, T. & Yanagida, M. (1986) Construction of a mini-chromosome by deletion and its mitotic and meiotic behaviour in fission yeast. *Molecular & general genetics*. 203 (3), 397–405.

Noma, K.-I., Cam, H.P., Maraia, R.J. & Grewal, S.I.S. (2006) A role for TFIIIC transcription factor complex in genome organization. *Cell*. 125 (5), 859–872.

Obersriebnig, M.J., Pallesen, E.M.H., Sneppen, K., Trusina, A. & Thon, G. (2016) Nucleation and spreading of a heterochromatic domain in fission yeast. *Nature communications*. 7 (1), 11518.

Oey, H. & Whitelaw, E. (2014) On the meaning of the word 'epimutation'. *Trends in genetics*. 30 (12), 519–520.

Ohno, S., Kaplan, W.D. & Kinosita, R. (1959) Formation of the sex chromatin by a single X-chromosome in liver cells of *Rattus norvegicus*. *Experimental Cell Research*. 18 (2), 415–418.

Olins, A.L. & Olins, D.E. (1974) Spheroid chromatin units (v bodies). *Science*. 183 (4122), 330–332.

Olins, D.E. & Olins, A.L. (2003) Chromatin history: our view from the bridge. *Nature reviews. Molecular cell biology*. 4 (10), 809–814.

Onishi, M., Liou, G.-G., Buchberger, J.R., Walz, T. & Moazed, D. (2007) Role of the conserved Sir3-BAH domain in nucleosome binding and silent chromatin assembly. *Molecular cell*. 28 (6), 1015–1028.

Orthwein, A., Noordermeer, S.M., Wilson, M.D., Landry, S., Enchev, R.I., Sherker, A., Munro, M., Pinder, J., Salsman, J., Dellaire, G., Xia, B., Peter, M. & Durocher, D. (2015) A mechanism for the suppression of homologous recombination in G1 cells. *Nature*. 528 (7582), 422–426.

Osman, F. & McCready, S. (1998) Differential effects of caffeine on DNA damage and replication cell cycle checkpoints in the fission yeast *Schizosaccharomyces pombe*. *Molecular & general genetics*. 260 (4), 319–334.

Oya, E., Nakagawa, R., Yoshimura, Y., Tanaka, M., Nishibuchi, G., Machida, S., Shirai, A., Ekwall, K., Kurumizaka, H., Tagami, H. & Nakayama, J.-I. (2019) H3K14 ubiquitylation promotes H3K9 methylation for heterochromatin assembly. *EMBO reports*. 20 (10), e48111.

Papadakis, M.A. & Workman, C.T. (2015) Oxidative stress response pathways: Fission yeast as archetype. *Critical reviews in microbiology*. 41 (4), 520–535.

Pardee, A.B. (1974) A restriction point for control of normal animal cell proliferation. *Proc Natl Acad Sci USA*. 71 (4), 1286–1290.

Parker, J.E., Warrilow, A.G.S., Price, C.L., Mullins, J.G.L., Kelly, D.E. & Kelly, S.L. (2014) Resistance to antifungals that target CYP51. *Journal of chemical biology*. 7 (4), 143–161.

Parsa, J.-Y., Boudoukha, S., Burke, J., Homer, C. & Madhani, H.D. (2018) Polymerase pausing induced by sequence-specific RNA-binding protein drives heterochromatin assembly. *Genes & development*. 32 (13-14), 953–964.

Partridge, J.F., Borgstrøm, B. & Allshire, R.C. (2000) Distinct protein interaction domains and protein spreading in a complex centromere. *Genes & development*. 14 (7), 783–791.

Partridge, J.F., Scott, K.S.C., Bannister, A.J., Kouzarides, T. & Allshire, R.C. (2002) cis-acting DNA from fission yeast centromeres mediates histone H3 methylation and recruitment of silencing factors and cohesin to an ectopic site. *Current Biology*. 12 (19), 1652–1660.

Patel, D.J. (2016) A structural perspective on readout of epigenetic histone and DNA methylation marks. *Cold Spring Harbor perspectives in biology*. 8 (3), a018754.

Patino, M.M., Liu, J.J., Glover, J.R. & Lindquist, S. (1996) Support for the prion hypothesis for inheritance of a phenotypic trait in yeast. *Science*. 273 (5275), 622–626.

Paulo, E., García-Santamarina, S., Calvo, I.A., Carmona, M., Boronat, S., Domènech, A., Ayté, J. & Hidalgo, E. (2014) A genetic approach to study H2O2 scavenging in fission yeast--distinct roles of peroxiredoxin and catalase. *Molecular microbiology*. 92 (2), 246–257.

Paulsen, T., Kumar, P., Koseoglu, M.M. & Dutta, A. (2018) Discoveries of extrachromosomal circles of DNA in normal and tumor Cells. *Trends in genetics*. 34 (4), 270–278.

Petryk, N., Dalby, M., Wenger, A., Stromme, C.B., Strandsby, A., Andersson, R. & Groth, A. (2018) MCM2 promotes symmetric inheritance of modified histones during DNA replication. *Science*. 361 (6409), 1389–1392.

Phanstiel, D.H., Boyle, A.P., Araya, C.L. & Snyder, M.P. (2014) Sushi.R: flexible, quantitative and integrative genomic visualizations for publication-quality multi-panel figures. *Bioinformatics*. 30 (19), 2808–2810.

Pidoux, A.L. & Armstrong, J. (1993) The BiP protein and the endoplasmic reticulum of *Schizosaccharomyces pombe*: fate of the nuclear envelope during cell division. *Journal of cell science*. 105 (Pt 4), 1115–1120.

Pintacuda, G., Wei, G., Roustan, C., Kirmizitas, B.A., Solcan, N., Cerase, A., Castello, A., Mohammed, S., Moindrot, B., Nesterova, T.B. & Brockdorff, N. (2017) hnRNPK recruits PCGF3/5-PRC1 to the *Xist* RNA B-Repeat to establish Polycomb-mediated chromosomal silencing. *Molecular cell*. 68 (5), 955–969.e10.

Plath, K., Fang, J., Mlynarczyk-Evans, S.K., Cao, R., Worringer, K.A., Wang, H., la Cruz, de, C.C., Otte, A.P., Panning, B. & Zhang, Y. (2003) Role of histone H3 lysine 27 methylation in X inactivation. *Science*. 300 (5616), 131–135.

Pokholok, D.K., Harbison, C.T., Levine, S., Cole, M., Hannett, N.M., Lee, T.I., Bell, G.W., Walker, K., Rolfe, P.A., Herbolsheimer, E., Zeitlinger, J., Lewitter, F., Gifford, D.K. & Young, R.A. (2005) Genome-wide map of nucleosome acetylation and methylation in yeast. *Cell*. 122 (4), 517–527.

Ptashne, M. (2007) On the use of the word 'epigenetic'. *Current Biology*. 17 (7), R233–236.

Qian, C. & Zhou, M.M. (2006) SET domain protein lysine methyltransferases: Structure, specificity and catalysis. *Cellular and molecular life sciences*. 63 (23), 2755–2763.

Queitsch, C., Sangster, T.A. & Lindquist, S. (2002) Hsp90 as a capacitor of phenotypic variation. *Nature*. 417 (6889), 618–624.

Quinn, J., Findlay, V.J., Dawson, K., Millar, J.B.A., Jones, N., Morgan, B.A. & Toone, W.M. (2002) Distinct regulatory proteins control the graded transcriptional response to increasing H2O2 levels in fission yeast *Schizosaccharomyces pombe*. *Molecular biology of the cell*. 13 (3), 805–816.

Quivy, J.-P., Gérard, A., Cook, A.J.L., Roche, D. & Almouzni, G. (2008) The HP1-p150/CAF-1 interaction is required for pericentric heterochromatin replication and S-phase progression in mouse cells. *Nature structural & molecular biology*. 15 (9), 972–979.

Qüesta, J.I., Song, J., Geraldo, N., An, H. & Dean, C. (2016) Arabidopsis transcriptional repressor VAL1 triggers Polycomb silencing at *FLC* during vernalization. *Science*. 353 (6298), 485–488.

Raab, J.R., Chiu, J., Zhu, J., Katzman, S., Kurukuti, S., Wade, P.A., Haussler, D. & Kamakaka, R.T. (2012) Human tRNA genes function as chromatin insulators. *The EMBO journal*. 31 (2), 330–350.

Rae, P.M.M. & Franke, W.W. (1972) The interphase distribution of satellite DNA-containing heterochromatin in mouse nuclei. *Chromosoma*. 39 (4), 443–456.

Ragunathan, K., Jih, G. & Moazed, D. (2015) Epigenetic inheritance uncoupled from sequence-specific recruitment. *Science*. 348 (6230), 1258699.

Ramírez, F., Ryan, D.P., Grüning, B., Bhardwaj, V., Kilpert, F., Richter, A.S., Heyne, S., Dündar, F. & Manke, T. (2016) deepTools2: a next generation

web server for deep-sequencing data analysis. *Nucleic acids research*. 44 (W1), W160–165.

Ratnakumar, K., Duarte, L.F., LeRoy, G., Hasson, D., Smeets, D., Vardabasso, C., Bönisch, C., Zeng, T., Xiang, B., Zhang, D.Y., Li, H., Wang, X., Hake, S.B., Schermelleh, L., Garcia, B.A. & Bernstein, E. (2012) ATRX-mediated chromatin association of histone variant macroH2A1 regulates α-globin expression. *Genes & development*. 26 (5), 433–438.

Rea, S., Eisenhaber, F., O'Carroll, D., Strahl, B.D., Sun, Z.W., Schmid, M., Opravil, S., Mechtler, K., Ponting, C.P., Allis, C.D. & Jenuwein, T. (2000) Regulation of chromatin structure by site-specific histone H3 methyltransferases. *Nature*. 406 (6796), 593–599.

Rechavi, O., Houri-Ze'evi, L., Anava, S., Goh, W.S.S., Kerk, S.Y., Hannon, G.J. & Hobert, O. (2014) Starvation-induced transgenerational inheritance of small RNAs in *C. elegans*. *Cell*. 158 (2), 277–287.

Rechavi, O., Minevich, G. & Hobert, O. (2011) Transgenerational inheritance of an acquired small RNA-based antiviral response in *C. elegans*. *Cell*. 147 (6), 1248–1256.

Reyes-Turcu, F.E., Zhang, K., Zofall, M., Chen, E. & Grewal, S.I.S. (2011) Defects in RNA quality control factors reveal RNAi-independent nucleation of heterochromatin. *Nature structural & molecular biology*. 18 (10), 1132–1138.

Rhind, N., Chen, Z., Yassour, M., Thompson, D.A., Haas, B.J., Habib, N., Wapinski, I., Roy, S., Lin, M.F., Heiman, D.I., Young, S.K., Furuya, K., Guo, Y., Pidoux, A., Chen, H.M., Robbertse, B., Goldberg, J.M., Aoki, K., Bayne, E.H., et al. (2011) Comparative functional genomics of the fission yeasts. *Science*. 332 (6032), 930–936.

Richards, E.J. (2006) Inherited epigenetic variation--revisiting soft inheritance. *Nature reviews. Genetics*. 7 (5), 395–401.

Richart, A.N., Brunner, C.I.W., Stott, K., Murzina, N.V. & Thomas, J.O. (2012) Characterization of chromoshadow domain-mediated binding of heterochromatin protein 1α (HP1α) to histone H3. *The Journal of biological chemistry*. 287 (22), 18730–18737.

Robson, M.I., Las Heras, de, J.I., Czapiewski, R., Lê Thành, P., Booth, D.G., Kelly, D.A., Webb, S., Kerr, A.R.W. & Schirmer, E.C. (2016) Tissue-specific gene repositioning by muscle nuclear membrane proteins

enhances repression of critical developmental genes during myogenesis. *Molecular cell*. 62 (6), 834–847.

Roche, B., Arcangioli, B. & Martienssen, R.A. (2016) RNA interference is essential for cellular quiescence. *Science*. 354 (6313), aah5651.

Rodríguez-López, M., Cotobal, C., Fernández-Sánchez, O., Borbarán Bravo, N., Oktriani, R., Abendroth, H., Uka, D., Hoti, M., Wang, J., Zaratiegui, M. & Bähler, J. (2016) A CRISPR/Cas9-based method and primer design tool for seamless genome editing in fission yeast. *Wellcome open research*. 1, 19.

Rougemaille, M., Shankar, S., Braun, S., Rowley, M. & Madhani, H.D. (2008) Ers1, a rapidly diverging protein essential for RNA interference-dependent heterochromatic silencing in *Schizosaccharomyces pombe*. *The Journal of biological chemistry*. 283 (38), 25770–25773.

Ruby, J.G., Jan, C., Player, C., Axtell, M.J., Lee, W., Nusbaum, C., Ge, H. & Bartel, D.P. (2006) Large-scale sequencing reveals 21U-RNAs and additional microRNAs and endogenous siRNAs in *C. elegans*. *Cell*. 127 (6), 1193–1207.

Rutherford, S.L. & Lindquist, S. (1998) Hsp90 as a capacitor for morphological evolution. *Nature*. 396 (6709), 336–342.

Ryan, O.W., Skerker, J.M., Maurer, M.J., Li, X., Tsai, J.C., Poddar, S., Lee, M.E., DeLoache, W., Dueber, J.E., Arkin, A.P. & Cate, J.H.D. (2014) Selection of chromosomal DNA libraries using a multiplex CRISPR system. *eLife*. 3, e03703.

Sabatinos, S.A. & Forsburg, S.L. (2010) Molecular genetics of *Schizosaccharomyces pombe*. *Methods in enzymology*. 470759–795.

Sadaie, M., Iida, T., Urano, T. & Nakayama, J.-I. (2004) A chromodomain protein, Chp1, is required for the establishment of heterochromatin in fission yeast. *The EMBO journal*. 23 (19), 3825–3835.

Santos-Rosa, H., Kirmizis, A., Nelson, C., Bartke, T., Saksouk, N., Côté, J. & Kouzarides, T. (2009) Histone H3 tail clipping regulates gene expression. *Nature structural & molecular biology*. 16 (1), 17–22.

Sanulli, S., Trnka, M.J., Dharmarajan, V., Tibble, R.W., Pascal, B.D., Burlingame, A.L., Griffin, P.R., Gross, J.D. & Narlikar, G.J. (2019) HP1

reshapes nucleosome core to promote phase separation of heterochromatin. *Nature*. 575 (7782), 390–394.

Schalch, T., Duda, S., Sargent, D.F. & Richmond, T.J. (2005) X-ray structure of a tetranucleosome and its implications for the chromatin fibre. *Nature*. 436 (7047), 138–141.

Schotta, G., Ebert, A., Krauss, V., Fischer, A., Hoffmann, J., Rea, S., Jenuwein, T., Dorn, R. & Reuter, G. (2002) Central role of Drosophila Su(var)3-9 in histone H3-K9 methylation and heterochromatic gene silencing. *The EMBO journal*. 21 (5), 1121–1131.

Schuettengruber, B., Bourbon, H.-M., Di Croce, L. & Cavalli, G. (2017) Genome regulation by Polycomb and Trithorax: 70 years and counting. *Cell*. 171 (1), 34–57.

Schultz, J. (1936) Variegation in Drosophila and the inert chromosome regions. *Proc Natl Acad Sci USA*. 22 (1), 27.

Schuster-Böckler, B. & Lehner, B. (2012) Chromatin organization is a major influence on regional mutation rates in human cancer cells. *Nature*. 488 (7412), 504–507.

Schwedler, von, U., Jäck, H.M. & Wabl, M. (1990) Circular DNA is a product of the immunoglobulin class switch rearrangement. *Nature*. 345 (6274), 452–456.

Scott, K.C., White, C.V. & Willard, H.F. (2007) An RNA polymerase III-dependent heterochromatin barrier at fission yeast centromere 1. *PloS one*. 2 (10), e1099.

Selmecki, A., Forche, A. & Berman, J. (2006) Aneuploidy and isochromosome formation in drug-resistant *Candida albicans*. *Science*. 313 (5785), 367–370.

Seong, K.-H., Li, D., Shimizu, H., Nakamura, R. & Ishii, S. (2011) Inheritance of stress-induced, ATF-2-dependent epigenetic change. *Cell*. 145 (7), 1049–1061.

Shankaranarayana, G.D., Motamedi, M.R., Moazed, D. & Grewal, S.I.S. (2003) Sir2 regulates histone H3 lysine 9 methylation and heterochromatin assembly in fission yeast. *Current Biology*. 13 (14), 1240–1246.

Shaver, S., Casas-Mollano, J.A., Cerny, R.L. & Cerutti, H. (2010) Origin of the polycomb repressive complex 2 and gene silencing by an E(z) homolog in the unicellular alga Chlamydomonas. *Epigenetics*. 5 (4), 301–312.

Shi, Y., Lan, F., Matson, C., Mulligan, P., Whetstine, J.R., Cole, P.A., Casero, R.A. & Shi, Y. (2004) Histone demethylation mediated by the nuclear amine oxidase homolog LSD1. *Cell*. 119 (7), 941–953.

Shiozaki, K. & Russell, P. (1995) Cell-cycle control linked to extracellular environment by MAP kinase pathway in fission yeast. *Nature*. 378 (6558), 739–743.

Shiozaki, K. & Russell, P. (1996) Conjugation, meiosis, and the osmotic stress response are regulated by Spc1 kinase through Atf1 transcription factor in fission yeast. *Genes & development*. 10 (18), 2276–2288.

Shogren-Knaak, M., Ishii, H., Sun, J.-M., Pazin, M.J., Davie, J.R. & Peterson, C.L. (2006) Histone H4-K16 acetylation controls chromatin structure and protein interactions. *Science*. 311 (5762), 844–847.

Silva, J., Mak, W., Zvetkova, I., Appanah, R., Nesterova, T.B., Webster, Z., Peters, A.H.F.M., Jenuwein, T., Otte, A.P. & Brockdorff, N. (2003) Establishment of histone H3 methylation on the inactive X chromosome requires transient recruitment of Eed-Enx1 Polycomb group complexes. *Developmental Cell*. 4 (4), 481–495.

Simon, J., Chiang, A., Bender, W., Shimell, M.J. & O'Connor, M. (1993) Elements of the Drosophila bithorax complex that mediate repression by Polycomb group products. *Developmental biology*. 158 (1), 131–144.

Simon, M., North, J.A., Shimko, J.C., Forties, R.A., Ferdinand, M.B., Manohar, M., Zhang, M., Fishel, R., Ottesen, J.J. & Poirier, M.G. (2011) Histone fold modifications control nucleosome unwrapping and disassembly. *Proc Natl Acad Sci USA*. 108 (31), 12711–12716.

Smith, Z.D., Chan, M.M., Humm, K.C., Karnik, R., Mekhoubad, S., Regev, A., Eggan, K. & Meissner, A. (2014) DNA methylation dynamics of the human preimplantation embryo. *Nature*. 511 (7511), 611–615.

Smothers, J.F. & Henikoff, S. (2000) The HP1 chromo shadow domain binds a consensus peptide pentamer. *Current Biology*. 10 (1), 27–30.

Soboleva, T.A., Nekrasov, M., Pahwa, A., Williams, R., Huttley, G.A. & Tremethick, D.J. (2011) A unique H2A histone variant occupies the

transcriptional start site of active genes. *Nature structural & molecular biology*. 19 (1), 25–30.

Sorida, M. & Murakami, Y. (2020) Unprogrammed epigenetic variation mediated by stochastic formation of ectopic heterochromatin. *Current genetics*. 66 (2), 319–325.

Sorida, M., Hirauchi, T., Ishizaki, H., Kaito, W., Shimada, A., Mori, C., Chikashige, Y., Hiraoka, Y., Suzuki, Y., Ohkawa, Y., Kato, H., Takahata, S. & Murakami, Y. (2019) Regulation of ectopic heterochromatin-mediated epigenetic diversification by the JmjC family protein Epe1. *PLoS genetics*. 15 (6), e1008129.

Soufi, A., Donahue, G. & Zaret, K.S. (2012) Facilitators and impediments of the pluripotency reprogramming factors' initial engagement with the genome. *Cell*. 151 (5), 994–1004.

Stajic, D., Perfeito, L. & Jansen, L.E.T. (2019) Epigenetic gene silencing alters the mechanisms and rate of evolutionary adaptation. *Nature ecology & evolution*. 3 (3), 491–498.

Steger, D.J., Lefterova, M.I., Ying, L., Stonestrom, A.J., Schupp, M., Zhuo, D., Vakoc, A.L., Kim, J.-E., Chen, J., Lazar, M.A., Blobel, G.A. & Vakoc, C.R. (2008) DOT1L/KMT4 recruitment and H3K79 methylation are ubiquitously coupled with gene transcription in mammalian cells. *Molecular and cellular biology*. 28 (8), 2825–2839.

Stone, N.R., Rhodes, J., Fisher, M.C., Mfinanga, S., Kivuyo, S., Rugemalila, J., Segal, E.S., Needleman, L., Molloy, S.F., Kwon-Chung, J., Harrison, T.S., Hope, W., Berman, J. & Bicanic, T. (2019) Dynamic ploidy changes drive fluconazole resistance in human cryptococcal meningitis. *The Journal of clinical investigation*. 129 (3), 999–1014.

Strahl, B.D. & Allis, C.D. (2000) The language of covalent histone modifications. *Nature*. 403 (6765), 41–45.

Strom, A.R., Emelyanov, A.V., Mir, M., Fyodorov, D.V., Darzacq, X. & Karpen, G.H. (2017) Phase separation drives heterochromatin domain formation. *Nature*. 547 (7662), 241–245.

Sugiyama, T. & Sugioka-Sugiyama, R. (2011) Red1 promotes the elimination of meiosis-specific mRNAs in vegetatively growing fission yeast. *The EMBO journal*. 30 (6), 1027–1039.

Sugiyama, T., Cam, H., Verdel, A., Moazed, D. & Grewal, S.I.S. (2005) RNA-dependent RNA polymerase is an essential component of a self-enforcing loop coupling heterochromatin assembly to siRNA production. *Proc Natl Acad Sci USA*. 102 (1), 152–157.

Sugiyama, T., Cam, H.P., Sugiyama, R., Noma, K.-I., Zofall, M., Kobayashi, R. & Grewal, S.I.S. (2007) SHREC, an effector complex for heterochromatic transcriptional silencing. *Cell*. 128 (3), 491–504.

Sugiyama, T., Thillainadesan, G., Chalamcharla, V.R., Meng, Z., Balachandran, V., Dhakshnamoorthy, J., Zhou, M. & Grewal, S.I.S. (2016) Enhancer of rudimentary cooperates with conserved RNA-processing factors to promote meiotic mRNA decay and facultative heterochromatin assembly. *Molecular cell*. 61 (5), 747–759.

Sung, S. & Amasino, R.M. (2004) Vernalization in *Arabidopsis thaliana* is mediated by the PHD finger protein VIN3. *Nature*. 427 (6970), 159–164.

Sung, S., He, Y., Eshoo, T.W., Tamada, Y., Johnson, L., Nakahigashi, K., Goto, K., Jacobsen, S.E. & Amasino, R.M. (2006) Epigenetic maintenance of the vernalized state in *Arabidopsis thaliana* requires LIKE HETEROCHROMATIN PROTEIN 1. *Nature Genetics*. 38 (6), 706–710.

Supek, F. & Lehner, B. (2015) Differential DNA mismatch repair underlies mutation rate variation across the human genome. *Nature*. 521 (7550), 81–84.

Surani, M.A., Hayashi, K. & Hajkova, P. (2007) Genetic and epigenetic regulators of pluripotency. *Cell*. 128 (4), 747–762.

Sutton, A., Immanuel, D. & Arndt, K.T. (1991) The SIT4 protein phosphatase functions in late G1 for progression into S phase. *Molecular and cellular biology*. 11 (4), 2133–2148.

Suzuki, K., Okada, K., Kamiya, Y., Zhu, X.F., Nakagawa, T., Kawamukai, M. & Matsuda, H. (1997) Analysis of the decaprenyl diphosphate synthase (dps) gene in fission yeast suggests a role of ubiquinone as an antioxidant. *Journal of biochemistry*. 121 (3), 496–505.

Svensson, J.P., Shukla, M., Menendez-Benito, V., Norman-Axelsson, U., Audergon, P., Sinha, I., Tanny, J.C., Allshire, R.C. & Ekwall, K. (2015) A nucleosome turnover map reveals that the stability of histone H4 Lys20 methylation depends on histone recycling in transcribed chromatin. *Genome research*. 25 (6), 872–883.

Swiezewski, S., Liu, F., Magusin, A. & Dean, C. (2009) Cold-induced silencing by long antisense transcripts of an Arabidopsis Polycomb target. *Nature*. 462 (7274), 799–802.

Tachibana, M., Sugimoto, K., Fukushima, T. & Shinkai, Y. (2001) Set domain-containing protein, G9a, is a novel lysine-preferring mammalian histone methyltransferase with hyperactivity and specific selectivity to lysines 9 and 27 of histone H3. *The Journal of biological chemistry*. 276 (27), 25309–25317.

Tachibana, M., Ueda, J., Fukuda, M., Takeda, N., Ohta, T., Iwanari, H., Sakihama, T., Kodama, T., Hamakubo, T. & Shinkai, Y. (2005) Histone methyltransferases G9a and GLP form heteromeric complexes and are both crucial for methylation of euchromatin at H3-K9. *Genes & development*. 19 (7), 815–826.

Tagami, H., Ray-Gallet, D., Almouzni, G. & Nakatani, Y. (2004) Histone H3.1 and H3.3 complexes mediate nucleosome assembly pathways dependent or independent of DNA synthesis. *Cell*. 116 (1), 51–61.

Takahashi, K., Murakami, S., Chikashige, Y., Funabiki, H., Niwa, O. & Yanagida, M. (1992) A low copy number central sequence with strict symmetry and unusual chromatin structure in fission yeast centromere. *Molecular biology of the cell*. 3 (7), 819–835.

Takeda, T., Toda, T., Kominami, K., Kohnosu, A., Yanagida, M. & Jones, N. (1995) *Schizosaccharomyces pombe atf1*$^{+}$ encodes a transcription factor required for sexual development and entry into stationary phase. *The EMBO journal*. 14 (24), 6193–6208.

Talbert, P.B. & Henikoff, S. (2017) Histone variants on the move: substrates for chromatin dynamics. *Nature reviews. Molecular cell biology*. 18 (2), 115–126.

Talevich, E., Shain, A.H., Botton, T. & Bastian, B.C. (2016) CNVkit: genome-wide copy number detection and visualization from targeted DNA sequencing. *PLoS computational biology*. 12 (4), e1004873.

Tamaru, H. & Selker, E.U. (2001) A histone H3 methyltransferase controls DNA methylation in *Neurospora crassa*. *Nature*. 414 (6861), 277–283.

Tan, M., Luo, H., Lee, S., Jin, F., Yang, J.S., Montellier, E., Buchou, T., Cheng, Z., Rousseaux, S., Rajagopal, N., Lu, Z., Ye, Z., Zhu, Q., Wysocka, J., Ye, Y., Khochbin, S., Ren, B. & Zhao, Y. (2011) Identification of 67 histone

marks and histone lysine crotonylation as a new type of histone modification. *Cell*. 146 (6), 1016–1028.

Taricani, L., Tejada, M.L. & Young, P.G. (2002) The fission yeast ES2 homologue, Bis1, interacts with the Ish1 stress-responsive nuclear envelope protein. *The Journal of biological chemistry*. 277 (12), 10562–10572.

Tartof, K.D., Hobbs, C. & Jones, M. (1984) A structural basis for variegating position effects. *Cell*. 37 (3), 869–878.

Tashiro, S., Nishihara, Y., Kugou, K., Ohta, K. & Kanoh, J. (2017) Subtelomeres constitute a safeguard for gene expression and chromosome homeostasis. *Nucleic acids research*. 45 (18), 10333–10349.

Taunton, J., Hassig, C.A. & Schreiber, S.L. (1996) A mammalian histone deacetylase related to the yeast transcriptional regulator Rpd3p. *Science*. 272 (5260), 408–411.

Tessarz, P. & Kouzarides, T. (2014) Histone core modifications regulating nucleosome structure and dynamics. *Nature reviews. Molecular cell biology*. 15 (11), 703–708.

Thodberg, M., Thieffry, A., Bornholdt, J., Boyd, M., Holmberg, C., Azad, A., Workman, C.T., Chen, Y., Ekwall, K., Nielsen, O. & Sandelin, A. (2019) Comprehensive profiling of the fission yeast transcription start site activity during stress and media response. *Nucleic acids research*. 47 (4), 1671–1691.

Thon, G. & Verhein-Hansen, J. (2000) Four chromo-domain proteins of *Schizosaccharomyces pombe* differentially repress transcription at various chromosomal locations. *Genetics*. 155 (2), 551–568.

Toda, T., Dhut, S., Superti-Furga, G., Gotoh, Y., Nishida, E., Sugiura, R. & Kuno, T. (1996) The fission yeast *pmk1*$^{+}$ gene encodes a novel mitogen-activated protein kinase homolog which regulates cell integrity and functions coordinately with the protein kinase C pathway. *Molecular and cellular biology*. 16 (12), 6752–6764.

Toda, T., Shimanuki, M. & Yanagida, M. (1991) Fission yeast genes that confer resistance to staurosporine encode an AP-1-like transcription factor and a protein kinase related to the mammalian ERK1/MAP2 and budding yeast FUS3 and KSS1 kinases. *Genes & development*. 5 (1), 60–73.

Tompa, R. & Madhani, H.D. (2007) Histone H3 lysine 36 methylation antagonizes silencing in *Saccharomyces cerevisiae* independently of the Rpd3S histone deacetylase complex. *Genetics*. 175 (2), 585–593.

Tong, P., Pidoux, A.L., Toda, N.R.T., Ard, R., Berger, H., Shukla, M., Torres-Garcia, J., Müller, C.A., Nieduszynski, C.A. & Allshire, R.C. (2019) Interspecies conservation of organisation and function between nonhomologous regional centromeres. *Nature communications*. 10 (1), 2343.

Toone, W.M., Kuge, S., Samuels, M., Morgan, B.A., Toda, T. & Jones, N. (1998) Regulation of the fission yeast transcription factor Pap1 by oxidative stress: requirement for the nuclear export factor Crm1 (Exportin) and the stress-activated MAP kinase Sty1/Spc1. *Genes & development*. 12 (10), 1453–1463.

Trewick, S.C., McLaughlin, P.J. & Allshire, R.C. (2005) Methylation: lost in hydroxylation? *EMBO reports*. 6 (4), 315–320.

Trewick, S.C., Minc, E., Antonelli, R., Urano, T. & Allshire, R.C. (2007) The JmjC domain protein Epe1 prevents unregulated assembly and disassembly of heterochromatin. *The EMBO journal*. 26 (22), 4670–4682.

Trickey, M., Grimaldi, M. & Yamano, H. (2008) The anaphase-promoting complex/cyclosome controls repair and recombination by ubiquitylating Rhp54 in fission yeast. *Molecular and cellular biology*. 28 (12), 3905–3916.

Trojer, P. & Reinberg, D. (2007) Facultative heterochromatin: is there a distinctive molecular signature? *Molecular cell*. 28 (1), 1–13.

Tschiersch, B., Hofmann, A., Krauss, V., Dorn, R., Korge, G. & Reuter, G. (1994) The protein encoded by the Drosophila position-effect variegation suppressor gene Su(var)3-9 combines domains of antagonistic regulators of homeotic gene complexes. *The EMBO journal*. 13 (16), 3822–3831.

Tsukada, Y.-I., Fang, J., Erdjument-Bromage, H., Warren, M.E., Borchers, C.H., Tempst, P. & Zhang, Y. (2006) Histone demethylation by a family of JmjC domain-containing proteins. *Nature*. 439 (7078), 811–816.

Tsukiyama, T., Becker, P.B. & Wu, C. (1994) ATP-dependent nucleosome disruption at a heat-shock promoter mediated by binding of GAGA transcription factor. *Nature*. 367 (6463), 525–532.

Turi, T.G., Mueller, U.W., Sazer, S. & Rose, J.K. (1996) Characterization of a nuclear protein conferring brefeldin A resistance in *Schizosaccharomyces pombe*. *The Journal of biological chemistry*. 271 (15), 9166–9171.

Turner, B.M. (1993) Decoding the nucleosome. *Cell*. 75 (1), 5–8.

Turner, K.M., Deshpande, V., Beyter, D., Koga, T., Rusert, J., Lee, C., Li, B., Arden, K., Ren, B., Nathanson, D.A., Kornblum, H.I., Taylor, M.D., Kaushal, S., Cavenee, W.K., Wechsler-Reya, R., Furnari, F.B., Vandenberg, S.R., Rao, P.N., Wahl, G.M., et al. (2017) Extrachromosomal oncogene amplification drives tumour evolution and genetic heterogeneity. *Nature*. 543 (7643), 122–125.

Uchida, N., Suzuki, K., Saiki, R., Kainou, T., Tanaka, K., Matsuda, H. & Kawamukai, M. (2000) Phenotypes of fission yeast defective in ubiquinone production due to disruption of the gene for p-hydroxybenzoate polyprenyl diphosphate transferase. *Journal of bacteriology*. 182 (24), 6933–6939.

Urlinger, S., Baron, U., Thellmann, M., Hasan, M.T., Bujard, H. & Hillen, W. (2000) Exploring the sequence space for tetracycline-dependent transcriptional activators: novel mutations yield expanded range and sensitivity. *Proc Natl Acad Sci USA*. 97 (14), 7963–7968.

Vakoc, C.R., Mandat, S.A., Olenchock, B.A. & Blobel, G.A. (2005) Histone H3 lysine 9 methylation and HP1gamma are associated with transcription elongation through mammalian chromatin. *Molecular cell*. 19 (3), 381–391.

Valencia, A.M. & Kadoch, C. (2019) Chromatin regulatory mechanisms and therapeutic opportunities in cancer. *Nature cell biology*. 21 (2), 152–161.

Van der Auwera, G.A., Carneiro, M.O., Hartl, C., Poplin, R., Del Angel, G., Levy-Moonshine, A., Jordan, T., Shakir, K., Roazen, D., Thibault, J., Banks, E., Garimella, K.V., Altshuler, D., Gabriel, S. & DePristo, M.A. (2013) From FastQ data to high confidence variant calls: the Genome Analysis Toolkit best practices pipeline. *Current protocols in bioinformatics*. 43 (1), 11.10.1–33.

van Lohuizen, M., Frasch, M., Wientjens, E. & Berns, A. (1991) Sequence similarity between the mammalian *bmi-1* proto-oncogene and the Drosophila regulatory genes *Psc* and *Su(z)2*. *Nature*. 353 (6342), 353–355.

van Steensel, B. & Belmont, A.S. (2017) Lamina-associated domains: links with chromosome architecture, heterochromatin, and gene repression. *Cell*. 169 (5), 780–791.

Verdel, A., Jia, S., Gerber, S., Sugiyama, T., Gygi, S., Grewal, S.I.S. & Moazed, D. (2004) RNAi-mediated targeting of heterochromatin by the RITS complex. *Science*. 303 (5658), 672–676.

Verhaak, R.G.W., Bafna, V. & Mischel, P.S. (2019) Extrachromosomal oncogene amplification in tumour pathogenesis and evolution. *Nature reviews. Cancer*. 19 (5), 283–288.

Vivancos, A.P., Castillo, E.A., Jones, N., Ayté, J. & Hidalgo, E. (2004) Activation of the redox sensor Pap1 by hydrogen peroxide requires modulation of the intracellular oxidant concentration. *Molecular microbiology*. 52 (5), 1427–1435.

Volpe, T.A., Kidner, C., Hall, I.M., Teng, G., Grewal, S.I.S. & Martienssen, R.A. (2002) Regulation of heterochromatic silencing and histone H3 lysine-9 methylation by RNAi. *Science*. 297 (5588), 1833–1837.

Waddington, C.H. (1942) The epigenotype. *Endeavour*. 1, 18–20

Waddington, C.H. (1942) Canalization of development and the inheritance of acquired characters. *Nature*. 150 (3811), 563–565.

Waddington, C.H. (1953) Genetic assimilation of an acquired character. *Evolution*. 7 (2), 118–126.

Waddington, C.H. (1956) Genetic assimilation of the bithorax phenotype. *Evolution*. 10 (1), 1–13.

Wang, J., Cohen, A.L., Letian, A., Tadeo, X., Moresco, J.J., Liu, J., Yates, J.R., Qiao, F. & Jia, S. (2016) The proper connection between shelterin components is required for telomeric heterochromatin assembly. *Genes & development*. 30 (7), 827–839.

Wang, J., Jia, S.T. & Jia, S. (2016) New insights into the regulation of heterochromatin. *Trends in genetics*. 32 (5), 284–294.

Wang, J., Reddy, B.D. & Jia, S. (2015) Rapid epigenetic adaptation to uncontrolled heterochromatin spreading. *eLife*. 4, e06179.

Wang, S.H. & Elgin, S.C.R. (2011) Drosophila Piwi functions downstream of piRNA production mediating a chromatin-based transposon silencing

mechanism in female germ line. *Proc Natl Acad Sci USA*. 108 (52), 21164–21169.

Wang, S.W., Norbury, C., Harris, A.L. & Toda, T. (1999) Caffeine can override the S-M checkpoint in fission yeast. *Journal of cell science*. 112 (Pt 6), 927–937.

Wang, X. & Moazed, D. (2017) DNA sequence-dependent epigenetic inheritance of gene silencing and histone H3K9 methylation. *Science*. 356 (6333), 88–91.

Watanabe, T., Tomizawa, S.-I., Mitsuya, K., Totoki, Y., Yamamoto, Y., Kuramochi-Miyagawa, S., Iida, N., Hoki, Y., Murphy, P.J., Toyoda, A., Gotoh, K., Hiura, H., Arima, T., Fujiyama, A., Sado, T., Shibata, T., Nakano, T., Lin, H., Ichiyanagi, K., et al. (2011) Role for piRNAs and noncoding RNA in de novo DNA methylation of the imprinted mouse *Rasgrf1* locus. *Science*. 332 (6031), 848–852.

Watanabe, Y. & Yamamoto, M. (1996) *Schizosaccharomyces pombe pcr1*$^{+}$ encodes a CREB/ATF protein involved in regulation of gene expression for sexual development. *Molecular and cellular biology*. 16 (2), 704–711.

Watson, A.T., Daigaku, Y., Mohebi, S., Etheridge, T.J., Chahwan, C., Murray, J.M. & Carr, A.M. (2013) Optimisation of the *Schizosaccharomyces pombe* urg1 expression system. *PloS one*. 8 (12), e83800.

Wen, B., Wu, H., Shinkai, Y., Irizarry, R.A. & Feinberg, A.P. (2009) Large histone H3 lysine 9 dimethylated chromatin blocks distinguish differentiated from embryonic stem cells. *Nature Genetics*. 41 (2), 246–250.

Werler, P.J.H., Hartsuiker, E. & Carr, A.M. (2003) A simple Cre-loxP method for chromosomal N-terminal tagging of essential and non-essential *Schizosaccharomyces pombe* genes. *Gene*. 304133–141.

White, S.A. & Allshire, R.C. (2008) RNAi-mediated chromatin silencing in fission yeast. *Current topics in microbiology and immunology*. 320157–183.

White, S.A., Buscaino, A., Sanchez-Pulido, L., Ponting, C.P., Nowicki, M.W. & Allshire, R.C. (2014) The RFTS domain of Raf2 is required for Cul4 interaction and heterochromatin integrity in fission yeast. *PloS one*. 9 (8), e104161.

Wibowo, A., Becker, C., Marconi, G., Durr, J., Price, J., Hagmann, J., Papareddy, R., Putra, H., Kageyama, J., Becker, J., Weigel, D. & Gutierrez-Marcos, J. (2016) Hyperosmotic stress memory in Arabidopsis is mediated by distinct epigenetically labile sites in the genome and is restricted in the male germline by DNA glycosylase activity. *eLife*. 5, e13546.

Wiedemann, S.M., Mildner, S.N., Bönisch, C., Israel, L., Maiser, A., Matheisl, S., Straub, T., Merkl, R., Leonhardt, H., Kremmer, E., Schermelleh, L. & Hake, S.B. (2010) Identification and characterization of two novel primate-specific histone H3 variants, H3.X and H3.Y. *The Journal of cell biology*. 190 (5), 777–791.

Wilkinson, C.R., Bartlett, R., Nurse, P. & Bird, A.P. (1995) The fission yeast gene *pmt1*$^{+}$ encodes a DNA methyltransferase homologue. *Nucleic acids research*. 23 (2), 203–210.

Wilkinson, M.G., Samuels, M., Takeda, T., Toone, W.M., Shieh, J.C., Toda, T., Millar, J.B. & Jones, N. (1996) The Atf1 transcription factor is a target for the Sty1 stress-activated MAP kinase pathway in fission yeast. *Genes & development*. 10 (18), 2289–2301.

Wood, V., Gwilliam, R., Rajandream, M.A., Lyne, M., Lyne, R., Stewart, A., Sgouros, J., Peat, N., Hayles, J., Baker, S., Basham, D., Bowman, S., Brooks, K., Brown, D., Brown, S., Chillingworth, T., Churcher, C., Collins, M., Connor, R., et al. (2002) The genome sequence of *Schizosaccharomyces pombe*. *Nature*. 415 (6874), 871–880.

Woods, A., Sherwin, T., Sasse, R., MacRae, T.H., Baines, A.J. & Gull, K. (1989) Definition of individual components within the cytoskeleton of *Trypanosoma brucei* by a library of monoclonal antibodies. *Journal of cell science*. 93 (Pt 3), 491–500.

Woudstra, E.C., Gilbert, C., Fellows, J., Jansen, L., Brouwer, J., Erdjument-Bromage, H., Tempst, P. & Svejstrup, J.Q. (2002) A Rad26–Def1 complex coordinates repair and RNA pol II proteolysis in response to DNA damage. *Nature*. 415 (6874), 929–933.

Wu, S., Turner, K.M., Nguyen, N., Raviram, R., Erb, M., Santini, J., Luebeck, J., Rajkumar, U., Diao, Y., Li, B., Zhang, W., Jameson, N., Corces, M.R., Granja, J.M., Chen, X., Coruh, C., Abnousi, A., Houston, J., Ye, Z., et al. (2019) Circular ecDNA promotes accessible chromatin and high oncogene expression. *Nature*. 575 (7784), 699–703.

Wu, Z.-H., Shi, Y., Tibbetts, R.S. & Miyamoto, S. (2006) Molecular linkage between the kinase ATM and NF-kB signaling in response to genotoxic stimuli. *Science*. 311 (5764), 1141–1146.

Wysocka, J., Swigut, T., Xiao, H., Milne, T.A., Kwon, S.Y., Landry, J., Kauer, M., Tackett, A.J., Chait, B.T., Badenhorst, P., Wu, C. & Allis, C.D. (2006) A PHD finger of NURF couples histone H3 lysine 4 trimethylation with chromatin remodelling. *Nature*. 442 (7098), 86–90.

Xu, F., Zhang, K. & Grunstein, M. (2005) Acetylation in histone H3 globular domain regulates gene expression in yeast. *Cell*. 121 (3), 375–385.

Yamada, H.Y., Matsumoto, S. & Matsumoto, T. (2000) High dosage expression of a zinc finger protein, Grt1, suppresses a mutant of fission yeast *slp1*$^{+}$, a homolog of CDC20/p55CDC/Fizzy. *Journal of cell science*. 113 (Pt 22), 3989–3999.

Yamada, T., Fischle, W., Sugiyama, T., Allis, C.D. & Grewal, S.I.S. (2005) The nucleation and maintenance of heterochromatin by a histone deacetylase in fission yeast. *Molecular cell*. 20 (2), 173–185.

Yamagishi, Y., Sakuno, T., Shimura, M. & Watanabe, Y. (2008) Heterochromatin links to centromeric protection by recruiting shugoshin. *Nature*. 455 (7210), 251–255.

Yamamoto, K. & Sonoda, M. (2003) Self-interaction of heterochromatin protein 1 is required for direct binding to histone methyltransferase, SUV39H1. *Biochemical and biophysical research communications*. 301 (2), 287–292.

Yamanaka, S., Mehta, S., Reyes-Turcu, F.E., Zhuang, F., Fuchs, R.T., Rong, Y., Robb, G.B. & Grewal, S.I.S. (2013) RNAi triggered by specialized machinery silences developmental genes and retrotransposons. *Nature*. 493 (7433), 557–560.

Yamanaka, S., Yamashita, A., Harigaya, Y., Iwata, R. & Yamamoto, M. (2010) Importance of polyadenylation in the selective elimination of meiotic mRNAs in growing *S. pombe* cells. *The EMBO journal*. 29 (13), 2173–2181.

Yan, Y., Barlev, N.A., Haley, R.H., Berger, S.L. & Marmorstein, R. (2000) Crystal structure of yeast Esa1 suggests a unified mechanism for catalysis and substrate binding by histone acetyltransferases. *Molecular cell*. 6 (5), 1195–1205.

Yang, H., Berry, S., Olsson, T.S.G., Hartley, M., Howard, M. & Dean, C. (2017) Distinct phases of Polycomb silencing to hold epigenetic memory of cold in Arabidopsis. *Science*. 357 (6356), 1142–1145.

Yasmineh, W.G. & Yunis, J.J. (1970) Localization of mouse satellite DNA in constitutive heterochromatin. *Experimental Cell Research*. 59 (1), 69–75.

Yasuhara, J.C. & Wakimoto, B.T. (2008) Molecular landscape of modified histones in Drosophila heterochromatic genes and euchromatin-heterochromatin transition zones. *PLoS genetics*. 4 (1), e16.

Ye, J., Ai, X., Eugeni, E.E., Zhang, L., Carpenter, L.R., Jelinek, M.A., Freitas, M.A. & Parthun, M.R. (2005) Histone H4 lysine 91 acetylation a core domain modification associated with chromatin assembly. *Molecular cell*. 18 (1), 123–130.

Yelagandula, R., Stroud, H., Holec, S., Zhou, K., Feng, S., Zhong, X., Muthurajan, U.M., Nie, X., Kawashima, T., Groth, M., Luger, K., Jacobsen, S.E. & Berger, F. (2014) The histone variant H2A.W defines heterochromatin and promotes chromatin condensation in Arabidopsis. *Cell*. 158 (1), 98–109.

Yu, G., Li, J. & Young, D. (1994) The *Schizosaccharomyces pombe pka1*$^{+}$ gene, encoding a homolog of cAMP-dependent protein kinase. *Gene*. 151 (1-2), 215–220.

Zaratiegui, M., Castel, S.E., Irvine, D.V., Kloc, A., Ren, J., Li, F., de Castro, E., Marín, L., Chang, A.-Y., Goto, D., Cande, W.Z., Antequera, F., Arcangioli, B. & Martienssen, R.A. (2011) RNAi promotes heterochromatic silencing through replication-coupled release of RNA Pol II. *Nature*. 479 (7371), 135–138.

Zaratiegui, M., Irvine, D.V. & Martienssen, R.A. (2007) Noncoding RNAs and gene silencing. *Cell*. 128 (4), 763–776.

Zhang, H., Lang, Z. & Zhu, J.-K. (2018) Dynamics and function of DNA methylation in plants. *Nature reviews. Molecular cell biology*. 19 (8), 489–506.

Zhang, K., Fischer, T., Porter, R.L., Dhakshnamoorthy, J., Zofall, M., Zhou, M., Veenstra, T. & Grewal, S.I.S. (2011) Clr4/Suv39 and RNA quality control factors cooperate to trigger RNAi and suppress antisense RNA. *Science*. 331 (6024), 1624–1627.

Zhang, K., Mosch, K., Fischle, W. & Grewal, S.I.S. (2008) Roles of the Clr4 methyltransferase complex in nucleation, spreading and maintenance of heterochromatin. *Nature structural & molecular biology*. 15 (4), 381–388.

Zhang, X.-R., He, J.-B., Wang, Y.-Z. & Du, L.-L. (2018) A cloning-free method for CRISPR/Cas9-mediated genome editing in fission yeast. *G3.* 8 (6), 2067–2077.

Zhang, Xiaoyu, Yazaki, J., Sundaresan, A., Cokus, S., Chan, S.W.L., Chen, H., Henderson, I.R., Shinn, P., Pellegrini, M., Jacobsen, S.E. & Ecker, J.R. (2006) Genome-wide high-resolution mapping and functional analysis of DNA methylation in Arabidopsis. *Cell*. 126 (6), 1189–1201.

Zhang, Xibo, Fang, Y., Jaiseng, W., Hu, L., Lu, Y., Ma, Y. & Furuyashiki, T. (2015) Characterization of tamoxifen as an antifungal agent using the yeast *Schizosaccharomyces pombe* model organism. *The Kobe journal of medical sciences*. 61 (2), E54–63.

Zhang, Y. & Reinberg, D. (2001) Transcription regulation by histone methylation: interplay between different covalent modifications of the core histone tails. *Genes & development*. 15 (18), 2343–2360.

Zhang, Y., Liu, T., Meyer, C.A., Eeckhoute, J., Johnson, D.S., Bernstein, B.E., Nusbaum, C., Myers, R.M., Brown, M., Li, W. & Liu, X.S. (2008) Model-based analysis of ChIP-Seq (MACS). *Genome biology*. 9 (9), R137.

Zhao, Y. & Boeke, J.D. (2018) Construction of designer selectable marker deletions with a CRISPR-Cas9 Toolbox in *Schizosaccharomyces pombe* and new design of common entry vectors. *G3.* 8 (3), 789–796.

Zheng, H. & Xie, W. (2019) The role of 3D genome organization in development and cell differentiation. *Nature reviews. Molecular cell biology*. 20 (9), 535–550.

Zhou, K., Gaullier, G. & Luger, K. (2019) Nucleosome structure and dynamics are coming of age. *Nature structural & molecular biology*. 26 (1), 3–13.

Zhu, A., Ibrahim, J.G. & Love, M.I. (2019) Heavy-tailed prior distributions for sequence count data: removing the noise and preserving large differences. *Bioinformatics*. 35 (12), 2084–2092.

Zhu, J., Adli, M., Zou, J.Y., Verstappen, G., Coyne, M., Zhang, X., Durham, T., Miri, M., Deshpande, V., De Jager, P.L., Bennett, D.A., Houmard, J.A., Muoio, D.M., Onder, T.T., Camahort, R., Cowan, C.A., Meissner, A.,

Epstein, C.B., Shoresh, N., et al. (2013) Genome-wide chromatin state transitions associated with developmental and environmental cues. *Cell*. 152 (3), 642–654.

Zoch, A., Auchynnikava, T., Berrens, R.V., Kabayama, Y., Schöpp, T., Heep, M., Vasiliauskaitė, L., Pérez-Rico, Y.A., Cook, A.G., Shkumatava, A., Rappsilber, J., Allshire, R.C. & O'Carroll, D. (2020) SPOCD1 is an essential executor of piRNA-directed de novo DNA methylation. *Nature*. 584 (7822), 635–639.

Zofall, M. & Grewal, S.I.S. (2006) Swi6/HP1 recruits a JmjC domain protein to facilitate transcription of heterochromatic repeats. *Molecular cell*. 22 (5), 681–692.

Zofall, M., Smith, D.R., Mizuguchi, T., Dhakshnamoorthy, J. & Grewal, S.I.S. (2016) Taz1-Shelterin promotes facultative heterochromatin assembly at chromosome-internal sites containing late replication origins. *Molecular cell*. 62 (6), 862–874.

Zofall, M., Yamanaka, S., Reyes-Turcu, F.E., Zhang, K., Rubin, C. & Grewal, S.I.S. (2012) RNA elimination machinery targeting meiotic mRNAs promotes facultative heterochromatin formation. *Science*. 335 (6064), 96–100.